EXPERIMENTAL PROBES OF GAS PHASE IONS AND MOLECULES:

I.

PRODUCT KINETIC ENERGY RELEASE MEASUREMENTS AS A PROBE OF REACTION THERMOCHEMISTRY, DYNAMICS, AND CHEMICAL STRUCTURE IN SYSTEMS CONTAINING TRANSITION METAL IONS

II.

PHOTOELECTRON AND OPTICAL STUDIES OF ORGANIC TRANSIENT SPECIES

Thesis by

David Vernell Dearden

In Partial Fulfillment of the Requirements

for the Degree of

Doctor of Philosophy

California Institute of Technology

Pasadena, California

1989

(Submitted May 11, 1989)

With gratitude for a rich heritage,

to Melvin O. and Marion G. Dearden;

with a twinkling eye forward,

to Denise, Danielle, and the future

ACKNOWLEDGEMENTS

I would like to thank my advisor, Jack Beauchamp, for his financial, intellectual, and psychological support during my stay at Caltech. His endless supply of creative research ideas has been a great inspiration as well as a seed for much of what appears in this thesis. I also want to thank Jack for letting me serve as "copilot" on several occasions. It has been wonderful fun seeing science, computers, and flying mix with Jack.

I am grateful to the members of the Beauchamp group, past and present, for being my primary teachers during graduate school. Their many helpful suggestions are thankfully acknowledged, as are the companionship and fun they have shared with me.

I also owe great thanks to Mike Bowers, Petra van Koppen, and the rest of the Bowers group at UCSB. They have made me welcome in their labs and in their homes, and have provided most of the foundation for the kinetic energy release studies.

The expert help of the Caltech technical staff, especially Tom Dunn and Tony Stark, was indispensable.

Financial support from the National Science Foundation (1983-1986) and the Shell Foundation (1987-1988), in the form of a graduate fellowships, is gratefully acknowledged.

I would never have become a chemist without the support and encouragement of the Chemistry faculty at Brigham Young University. Reed

Izatt deserves special thanks for serving as my advisor and mentor, and for giving me some of my most significant lessons in scientific thinking and writing.

The spiritual and social support lent me throughout graduate school by many friends in the Pasadena I, Pasadena III, and East Pasadena wards of the Church of Jesus Christ of Latter-Day Saints has been a sustaining influence which I appreciate.

Finally, I reserve my greatest thanks for my family. My parents have been my greatest teachers and shapers, and I thank them for raising me in an environment of love and mutual support. I appreciate Denise's love, companionship, and zest for life, which have given my life real meaning. Thanks for hanging in there patiently as the months rolled by, at the same time urging me forward.

ABSTRACT

The release of kinetic energy in the decomposition of a metastable ion is a reflection of both the overall energetics and the potential energy surface on which the process takes place. Chapter 1 applies measurements of the kinetic energy release distributions (KERDs) for decomposition of metastable $Mn(CO)_x^+$ to the dynamics and energetics of exchange processes for the CO ligands. All the dissociations can be described by statistical phase space theory, in agreement with efficient CO exchange rates indicating that conservation of electronic spin is not important to the dynamics. A general method is presented and used whereby Mn^+-CO bond energies are obtained from the KERDs. Chapter 2 deals with reactions of Fe^+ and Co^+ with alkanes to eliminate methane, which have KERDs narrower than predicted by statistical theory. Restriction of the angular momentum (or, equivalently, the impact parameter) to values less than those anticipated by simple ion-molecule collision theory can account for the narrowed distributions. The restrictions result from barriers in the effective potential energy surfaces and from limitations in our measurement techniques. In Chapter 3, KERDs are used to demonstrate the existence of cobaltacyclobutane$^+$, (hydrido)(cyclopropyl)Co^+, and $Co(propene)^+$ structures which do not interconvert on the μs time scale in the gas phase. Chapter 4 deals with the dehydrogenations of cyclic alkanes by Fe^+ and Co^+, and shows that, contrary to previous

assumptions, statistical energy partitioning occurs in these processes.

Chapters 5 and 6 deal with studies of transient organic species. Chapter 5 presents preliminary work on charge-reversed, resonance enhanced multiphoton ionization (CRREMPI), a potentially powerful new method which exploits the special characteristics of the ion cyclotron resonance spectrometer to obtain optical spectra of a wide variety of transient species. In Chapter 6 photoelectron spectroscopy is used to observe the rearrangements of primary alkyl radicals, produced by flash vacuum pyrolysis of nitrites, to the thermodynamically more stable secondary isomers. Decomposition processes are also observed.

TABLE OF CONTENTS

LIST OF FIGURES

CHAPTER 1

CHAPTER 2

CHAPTER 6

LIST OF TABLES

CHAPTER 1

CHAPTER 2

CHAPTER 4

CHAPTER 6

LIST OF SCHEMES

CHAPTER 2

CHAPTER 4

CHAPTER 1

FUNDAMENTAL STUDIES OF THE ENERGETICS AND DYNAMICS OF LIGAND DISSOCIATION AND EXCHANGE PROCESSES AT TRANSITION METAL CENTERS IN THE GAS PHASE: $Mn(CO)_x^+$, x = 1 - 6.

FUNDAMENTAL STUDIES OF THE ENERGETICS AND DYNAMICS OF LIGAND DISSOCIATION AND EXCHANGE PROCESSES AT TRANSITION METAL CENTERS IN THE GAS PHASE: $Mn(CO)_x^+$, x = 1 - 6.

David V. Dearden, Kathleen Hayashibara, and J. L. Beauchamp*

Contribution number 7850 from the Arthur Amos Noyes Laboratory of Chemical Physics, California Institute of Technology, Pasadena, CA 91125.

Nicholas J. Kirchner, Petra A. M. van Koppen, and Michael T. Bowers*

Department of Chemistry, University of California, Santa Barbara, CA 93106.

*Authors to whom correspondence should be addressed.

Abstract

A significant change in spin multiplicity results from sequential addition of CO to $Mn^+(^7S)$ to form $Mn(CO)_6^+(^1A_{1g})$. To explore the possible effects of changes in spin multiplicity on the dynamics of ligand dissociation and exchange processes at transition metal centers in the gas phase, we have measured labeled CO exchange rates (x = 1-6) and kinetic energy release distributions (KERDs) for metastable decomposition by loss of CO (x = 2-6) for $Mn(CO)_x^+$. With the exception of the coordinatively saturated species $Mn(CO)_6^+$, for which no ligand exchange is observed, the CO exchange rates are within an order of magnitude of collision-limited in all cases. All KERDs were statistical, indicating no barrier in the CO-loss exit channel. These results are discussed in terms of the requirements for spin conservation in ligand exchange reactions. Quantitative analysis of statistical KERDs requires a knowledge of the internal energy of the decomposing species, which in the present experiment are formed by electron impact with a broad range of internal energies. We demonstrate that the temporal constraints of the experiment select metastables with a particular range of internal energies which can be bracketed using RRKM theory, enabling the KERDs to be modeled using phase space theory. Individual $D_o^\circ(Mn(CO)_{x-1}^+\text{-CO})$ (kcal/mol) values were determined by fitting the phase space calculations to the experimental KERDs: x = 6, 32 ± 5; x = 5, 16 ± 3; x = 4, 20 ± 3; x = 3, 31 ± 6; x = 2, <25; x = 1, >7.

Introduction

In a recent series of studies on the addition rates of CO to coordinatively unsaturated, neutral metal carbonyls, spin conservation was used to explain the large variations in the rates for reaction 1 among members of the $Fe(CO)_x$ system.

$$M(CO)_x + CO \rightarrow M(CO)_{x+1} \quad (1)$$

For x = 4, the rate was 2.5 orders of magnitude slower than for x = 3 or x = 2, which have rates within an order of magnitude of the collision rate.[1,2] Since $Fe(CO)_5$ has a singlet ground state while the ground state of $Fe(CO)_4$ is known from magnetic circular dichroism studies to be a triplet[3], the recombination rates were taken to be a reflection of the spin-forbidden nature of CO addition to $Fe(CO)_4$, while it was assumed that CO addition to $Fe(CO)_2$ and to $Fe(CO)_3$ are spin-allowed processes. Subsequent studies on $Cr(CO)_x$ (x = 5, 4, 3, 2)[4,5] and $Co(CO)_x$ (x = 1, 2, 3)[6] found that the CO recombination rates were all fast, leading to the suggestion that all of these recombination reactions proceed with spin conservation. A natural question arising from this work is whether or not the spin conservation requirement for rapid reaction is general.

An equally interesting area is that of bond energetics for metal carbonyls, especially where the potential exists for determining individual, rather than average M-CO bond energies. Despite the fact that stable

transition metal carbonyl compounds have been known for the better part of a century, the bonding in these compounds remains a subject of discussion. Such interest is understandable in light of such facts as that the basic structures of simple metal carbonyl fragments serve as building blocks for assembling large, polynuclear compounds, that metal carbonyl species are potentially important in a number of catalytic processes, and that the theoretical description of bonding in such species remains a challenge. Considerable data exist for coordinatively saturated metal carbonyls, but relatively little is available for the coordinatively unsaturated fragments. Photochemical and kinetic[7] methods, as well as photodetachment from anions,[8,9] have been used to obtain information on neutral species, while appearance potentials have been measured for a few series of metal carbonyl fragment ions.[10,11] Further information in this area is valuable for understanding bonding trends in homologous series as well as periodic relationships.

The $Mn(CO)_x^+$ (x = 0 - 6) system presents an opportunity to study both the role of spin conservation in "simple" ligand exchange processes and bond energetics. Since this is a d^6 system, a variety of spin states are possible. Mn^+ has a ^7S ground state[12] while the $Mn(CO)_6^+$ ground state is $^1A_{1g}$.[13,14] Although the ground spin states for intermediate members of the series are unknown, it is likely that more than one spin state is exhibited among the ground states of the $Mn(CO)_x^+$ series, leading to the anticipation of slow rates for reactions involving changes in spin

multiplicity at the metal center. These ions are isoelectronic with the well-studied $Cr(CO)_x$ system[4,5], offering a chance to compare bonding in an ionic system with that of a series of coordinatively unsaturated neutrals.

To probe the energetics and ligand dissociation dynamics of the $Mn(CO)_x^+$ system, we report the results of two different experiments. In the first, CO exchange rates are examined by observing the incorporation of ^{13}CO into the $Mn(CO)_x^+$ ions. This experiment is closely analogous to the CO recombination experiments with coordinatively unsaturated, neutral metal carbonyls noted above, since in order to exchange CO the $Mn(CO)_x^+$ must undergo CO addition. In the neutral case the recombination product is collisionally stabilized, while in the exchange experiments, carried out at low pressure, the adduct is not stabilized and loss of any CO but the label results in exchange. The aim of these experiments is to detect spin-forbidden processes in a manner analogous to that used for the neutral studies noted above.

In the second experiment, the potential surfaces for ligand loss are probed by measuring the kinetic energy released when metastable $[Mn(CO)_x^+]^*$ decomposes through CO loss. If decomposition occurs on a "Type I" surface (where there is no barrier to the reverse CO addition reaction), the kinetic energy release is expected to be in accord with the predictions of statistical theory. If a "Type II" surface is involved, with a barrier in the exit channel, a broad range of kinetic energies peaking away from zero is expected.[15]

A major advantage of the kinetic energy release experiments is the possibility of extracting quantitative information on the energetics of the decomposition, even when the metastable ions are not prepared with well-defined internal energies. A method for obtaining this information by modeling the experimental results using statistical theory, is described, and the technique is applied to determine individual Mn^+-CO bond energies for members of the $Mn(CO)_x^+$ system.

Experimental Section

Exchange experiments using ^{13}CO were performed with a fourier transform ion cyclotron resonance spectrometer equipped with a 1-inch cubic cell and a data acquisition system supplied by Ion Spec Corporation. $Mn(CO)_x^+$ ions were produced by 15-35 eV electron impact on either $Mn(CO)_5COCH_3$ (x = 1-5) or $Mn(CO)_5COCF_3$ (x = 1-6). Typical fragment intensities 150 msec after the end of the electron beam pulse are given for these compounds in Table I. Electron energies were adjusted to maximize the intensity of the ion of interest. In some cases collision-induced dissociation was performed using ^{13}CO as the collision gas, in order to enhance the population of fragment ions. With these methods of ion production, it is expected that the resulting species are produced with a broad range of internal energies. The $Mn(CO)_x^+$ ions were isolated using sweep-out pulses and allowed to react with 0.5-1.3 x 10^{-6} torr ^{13}CO for up to 1 sec.

Table I. Typical Fragment Intensities 150 msec After Ionization

$Mn(CO)_5COCF_3$ Electron Energy: 15 eV		$Mn(CO)_5COCH_3$ Electron Energy: 22 eV	
m/z	Relative Intensity	m/z	Relative Intensity
111.5	5.0	55.	5.9
124.	8.3	70.	36.5
139.	6.0	83.	14.1
152.	6.9	98.	19.7
154.	3.3	111.	21.9
167.	7.2	126.	13.7
180.	5.1	137.	6.5
182.	8.7	139.	30.8
195.	20.3	144.	5.6
210.	3.2	154.	16.6
223.	100.0	164.5	10.0
224.	7.1	167.	59.8
264.	7.3	179.	5.8
		182.	73.3
		191.5	8.8
		195.	39.7
		196.	7.5
		206.5	6.8
		210.	100.0
		211.	7.8
		224.	45.0
		232.5	11.8
		237.	86.1

Decay of the $Mn(CO)_x^+$ signal, as well as growth of signal due to singly- and multiply-^{13}CO substituted products, was followed as a function of time. Pressures were measured using a Schultz-Phelps ionization gauge calibrated against an MKS Baratron capacitance manometer.

Rate constants for ^{13}CO exchange reactions were determined by analysis of the decay of $Mn(CO)_x^+$ in cases where side reactions (primarily charge transfer) were not important. Where side reactions were significant, the constants were determined by plotting $\ln(I/I_0)$ versus time, where I and I_0 are the absolute signal intensities in the presence and absence of ^{13}CO, respectively.[16] The reported rate constants are the average and standard deviation of several measurements. It is important to note that the same results, within experimental error, were obtained using $Mn(CO)_5COCH_3$ to generate $Mn(CO)_x^+$ ions, as were obtained using $Mn(CO)_5COCF_3$, and that the same results were obtained both in the presence and absence of side reactions.

Kinetic energy release experiments for metastable decomposition, photodissociation, and CID experiments were performed on a VG Industries ZAB-2F double focusing, reverse geometry mass spectrometer with a home built temperature and pressure variable electron impact source. The techniques used in metastable decomposition[17] and photodissociation studies[18] have been described in detail elsewhere. Briefly, samples of $Mn(CO)_5COCH_3$ or $Mn(CO)_5COCF_3$ were heated to approximately 50° C and introduced into the source through a leak valve, with pressures in the

source of approximately 10 mtorr as determined by a Baratron capacitance manometer. Typically, $Mn(CO)_x^+$ (x = 1-6) ions were produced at electron energies of approximately 300 eV, with the energy varied to maximize ion beam intensity. Again, the resulting ions are expected to exhibit a broad range of internal energies. In metastable studies, the energy resolution of the beam was always better than 2 eV FWHM, and typically was better than 1 eV, while for photodissociation studies the resolution was approximately 6 eV FWHM. The identity of the $Mn(CO)_x^+$ ions was verified by CID. The ions were extracted from the source and accelerated to 8 keV, after which they passed through a magnetic sector for mass analysis where the ion of interest was selected. Next the ions entered the second field-free region, where metastable decomposition (or collision with He for CID experiments) took place. Photodissociation was performed by crossing the mass-selected ion beam at its secondary focal point in the second field-free region with the output of an Ar^+ ion laser (Coherent, Innova 20) operating on the 514-nm line, after passage of the laser beam through a polarization rotator (Spectra Physics, 310A). Fragment ions produced in the second field-free region were energy analyzed in an electric sector and detected using pulse counting techniques. The background pressure in the second field-free region was less than 1×10^{-9} torr for metastable and photodissociation studies. For CID experiments He was added to the collision cell until an indicated pressure of $2\text{-}3 \times 10^{-8}$ torr was obtained. This resulted in attenuation of the ion beam by approximately 30%.

Kinetic energy release distributions were obtained from the shapes of the metastable peaks by using equation 2.

$$P(E) = dI/dE \qquad (2)$$

P(E) is the probability of a given translational energy, and dI/dE is the derivative of peak intensity with respect to energy.[18a,19] For x = 3-6 metastables, the peaks were fitted to a polynomial before the derivative was taken, while for x = 1,2 the unprocessed data were numerically differentiated. The effect of fitting the curve before differentiation is simply to smooth the resulting kinetic energy release distribution, with no quantitative effects on the results.

$Mn(CO)_5COCH_3$ and $Mn(CO)_5COCF_3$ were synthesized following published procedures.[20] The 99% purity of the ^{13}CO was verified by FTICR.

Results

CO Exchange Studies. As an example of the results of the exchange experiments, signal intensities due to $Mn(CO)_{5-n}(^{13}CO)_n^+$, n = 0-5 in the presence of ^{13}CO are shown as a function of time in Figure 1. Incorporation of the label into the metal carbonyl ion is clearly evident. The semilog plot of the unsubstituted $Mn(CO)_5^+$ signal versus time (Figure 2) is linear.

Figure 1. Results of FTICR ^{13}CO exchange experiment for $Mn(CO)_5^+$. $Mn(CO)_5^+$ was generated by collision-induced dissociation (CID) of $Mn(CO)_6^+$ produced from electron impact on $Mn(CO)_5COCF_3$. $P_{CO} = 1 \times 10^{-5}$ torr. Signal intensities are normalized such that $\Sigma\, I(Mn(CO)_{5-n}(^{13}CO)_n^+) = 1$ for n = 0-5. The zero on the time scale corresponds to the end of the excitation pulse used for CID.

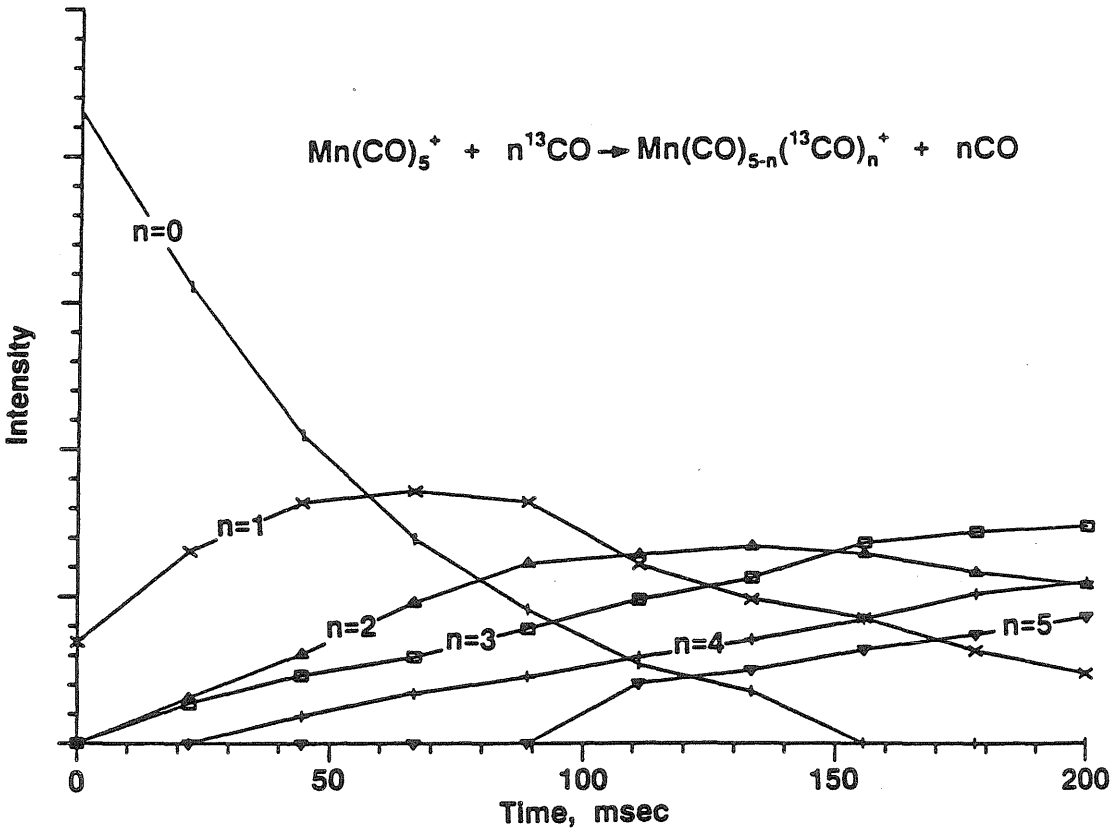
$Mn(CO)_5^+ + n^{13}CO \rightarrow Mn(CO)_{5-n}(^{13}CO)_n^+ + nCO$
n=0
n=1
n=2
n=3
n=4
n=5
Intensity
0
50
100
150
200
Time, msec

Figure 2. Plot of $\log[I(Mn(CO)_5^+)/(\Sigma\ I(Mn(CO)_{5-n}(^{13}CO)_n^+))$, n = 0-5, versus time, using the data of figure 1.

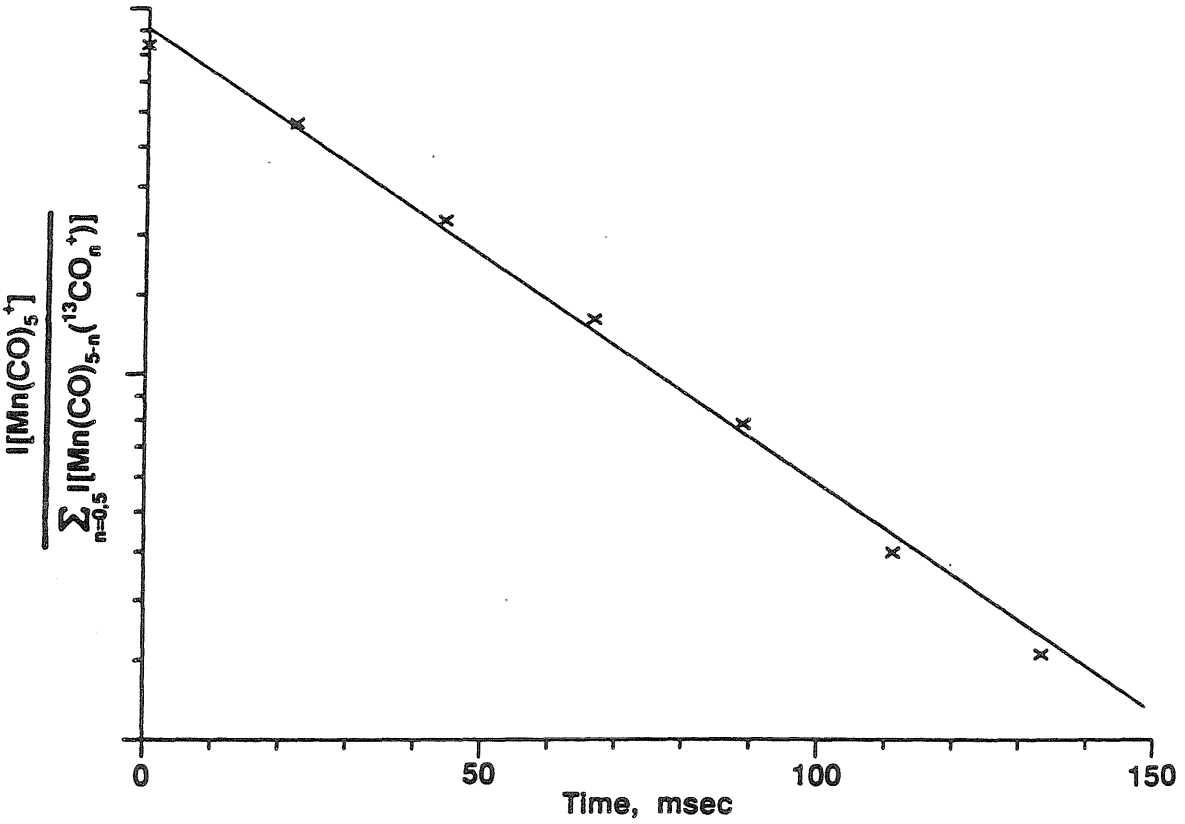
I[Mn(CO)5+]
Σ n=0,5 I[Mn(CO)5-n(13COn+)]
0
50
100
150
Time, msec

Rate constants determined for reaction 3 are listed in Table II, along with reaction efficiencies calculated by dividing the measured rate constant by the Langevin collision rate, statistically adjusted for the number of CO's present (assuming all the ligands in the collision complex are equivalent).

$$Mn(CO)_x^+ + {}^{13}CO \rightarrow [Mn(CO)_x{}^{13}CO]^+ \rightarrow Mn(CO)_{x-1}{}^{13}CO^+ + CO \quad (3)$$

For x = 1-5, the CO exchange rates are similar, with reaction efficiencies in the range 9-36%. No exchange is observed for x = 6.

Kinetic Energy Release Distributions. In these experiments, metastable ions produced by electron impact fragmentation of the precursor dissociated in the second field-free region of the double-sector instrument according to reaction 4.

$$[Mn(CO)_x^+]^* \rightarrow Mn(CO)_{x-1}^+ + CO \quad (4)$$

Kinetic energy release distributions measured for the loss of CO from $Mn(CO)_x^+$ (x = 2-6) metastables are plotted in Figure 3.

The smaller metastable members of the $Mn(CO)_x^+$ series decompose quickly. Consequently, most decomposition occurs in the ion source rather than in the second field-free region, and metastables are therefore difficult to detect. For x = 1, an added complication is the difficulty of distinguishing

Table II. CO Exchange Rates $Mn(CO)^{+}_{x}$ + ^{13}CO → $Mn(CO)_{x-1}{}^{13}COB^{+}$ + CO.

x	k [b]	$k_{Langevin}$*x/(x+1) [b]	Efficiency (%)
6	No Reaction	58	0
5	6.3±0.7	57	11
4	4.8±1.7	55	9
3	13.1±3.3	52	25
2	17.5±2.6	48	36
1	8.2±1.8	37	22

[b] Units of 10^{-11} cm^{-3} $molecule^{-1}$ s^{-1}

Figure 3. Kinetic energy release distributions for metastable $[Mn(CO)_x^+]^*$ decomposition. Data for x = 1 (dashed line) reflect collision-induced dissociation rather than metastable decomposition.

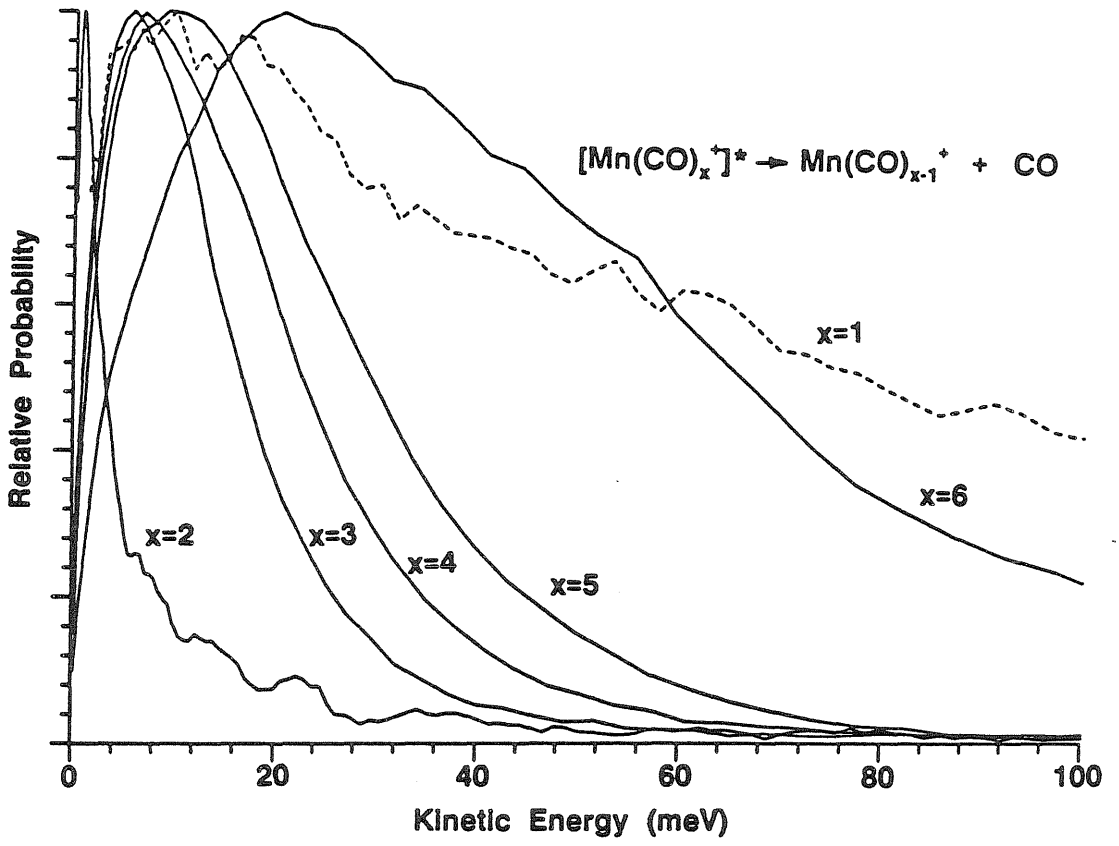
[Mn(CO)x+]* → Mn(CO)x-1+ + CO
x=1
x=2
x=3
x=4
x=5
x=6
Relative Probability
0
20
40
60
80
100
Kinetic Energy (meV)

between metastable decomposition and CID resulting from collision with residual gas in the second field-free region. Examination of the variation in intensity of the $MnCO^+$ dissociation signal as the background pressure of He in the second field-free region was increased showed that for $MnCO^+$ the signal is primarily due to CID; it increases linearly with added He. The distribution obtained for x = 2 is too narrow to be due to CID; distributions measured with He added to the collision cell are much broader. For x > 2, decomposition rates are slower and this problem does not occur.

Photodissociation Studies. Kinetic energy release distributions were obtained for the photodissociation reactions (5).

$$Mn(CO)_x^+ + h\nu \rightarrow Mn(CO)_{x-2}^+ + 2CO \qquad (x = 2, 5) \qquad (5)$$

The details will be published elsewhere.[21] For both the x = 2 and the x = 5 cases the product kinetic energy distributions are peaked near zero and fall off essentially exponentially to higher energy. The average energies for the two systems are $\langle E_t(Mn(CO)_5^+)\rangle$ = 0.11 eV and $\langle E_t(Mn(CO)_2^+)\rangle$ = 0.29 eV, and the maximum kinetic energies are 0.42 ± 0.05 eV and 1.0 ± 0.1 eV for $Mn(CO)_5^+$ and $Mn(CO)_2^+$ respectively. Photodissociation of $MnCO^+$, as well as loss of a single CO from $Mn(CO)_2^+$, was not observed at 514 nm.

Discussion

Spin Conservation and CO Exchange Studies. As was expected, no exchange was observed for $Mn(CO)_6^+$, since this is a stable, coordinatively saturated 18-electron ion, and exchange would involve a crowded 20-electron intermediate. This same behavior is found in solution; at ambient temperature, no exchange of CO was observed for $Mn(CO)_6^+$ after 15 hours.[22] Likewise, the isoelectronic $Cr(CO)_6$ is unreactive toward ligand exchange.[23]

If spin conservation is important in reactivity, then large variations in CO exchange rates are expected. It was therefore surprising to find that the CO exchange rates are similar for x = 1-5. There was some small variation in exchange rates, but certainly the differences were much less than the 2.5 orders of magnitude observed for the neutral $Fe(CO)_x$ system.[2] Why $Fe(CO)_x$ and $Mn(CO)_x^+$ are so different warrants speculation.

One possibility is that $Mn(CO)_x^+$, x = 1-6, all have singlet ground states, and that the transition from septet to singlet takes place upon the addition of one CO. Comparison with the isoelectronic $Cr(CO)_x$ species yields some support for this idea: all CO addition reactions of $Cr(CO)_x$, x = 2-5, were found to be rapid, leading to the prediction that all members of this series have singlet ground states.[5,24] However, it seems inconceivable that $MnCO^+$ has a singlet ground state: the lowest known singlet state of Mn^+ lies 4.8 eV above the septet ground state[25]. Assuming the existence of lower-lying singlet Mn^+ states, the minimum energy required

to produce a singlet from septet Mn^+ can be estimated to be at least 60 kcal/mol.[26] In either event, this is more energy than could reasonably be recovered through formation of the Mn^+-CO bond.

Another alternative is that the exchange reactions lead to excited products, conserving spin. This idea has several problems. First, it requires that the spins of the $Mn(CO)_x^+$ ground state, the $Mn(CO)_{x+1}^+$ complex leading to exchange, and the first $Mn(CO)_x^+$ excited state all be the same. Further, $Mn(CO)_{x+1}^+$ must dissociate to excited $Mn(CO)_x^+$, while being produced from ground state $Mn(CO)_x^+$. This process is clearly endoergic and would not be expected to occur efficiently.

It is also possible that the reactants are in excited states. This is a common problem when using electron impact ionization.[27] While the possibility cannot be completely eliminated, several factors argue against it. First, the same results were obtained using $Mn(CO)_5COCH_3$ and $Mn(CO)_5COCF_3$ to generate the $Mn(CO)_x^+$. It seems improbable that both should lead to the same population of excited states. Further, the results showed no dependence on the 15-35 eV electron energy used for ionization. In addition, failure to observe metastable $MnCO^+$ implies that predissociation from a long-lived excited electronic state is not important in the x = 1 case.[28] Finally, no curvature was apparent in any of the plots of log(signal intensity) versus time, arguing strongly that excited ions are absent. An example of such a plot, for the x = 5 case, is given in Figure 2.

A more likely possibility is that the $Mn(CO)_x^+$ exchange reactions do not always probe the $Mn(CO)_{x+1}^+$ ground state potential energy wells. For CO addition to neutral, coordinatively unsaturated metal carbonyls, the reactions occur at rates approximately one order of magnitude slower than collision-limited rates.[4,5] Similarly, the $Mn(CO)_x^+$ ions undergo CO exchange at only 1/3 to 1/10 of the collision-limited rate. The relatively low efficiencies of the ion-molecule reactions argue that the incoming CO somehow remains unique in the major fraction of collisions. One situation where this might occur, illustrated in Figure 4, is when a crossing between two attractive surfaces (A and B in the Figure) is involved. As CO approaches $Mn(CO)_x^+$ on surface B, the $Mn(CO)_{x+1}^+$ ground surface A is encountered. If the crossing occurs, the $Mn(CO)_{x+1}^+$ well is sampled and the uniqueness of the incoming CO is lost; exchange occurs when unlabeled CO is lost from the collision complex. If the crossing does not occur, the incoming CO remains unique and the collision does not result in exchange.

Alternatively, the low efficiencies may be explained more simply in terms of the requirements for geometric relaxation.[5] It is expected that some rearrangement of the bound ligands is generally required to accommodate the incoming, labeled ligand, and if a great deal of such relaxation is necessary, it is likely that the exchange process will be inefficient.

Figure 4. Schematic potential energy surfaces depicting crossings between attractive surfaces A and B and between attractive surface A and repulsive surface C. An exit channel barrier results in the latter case.

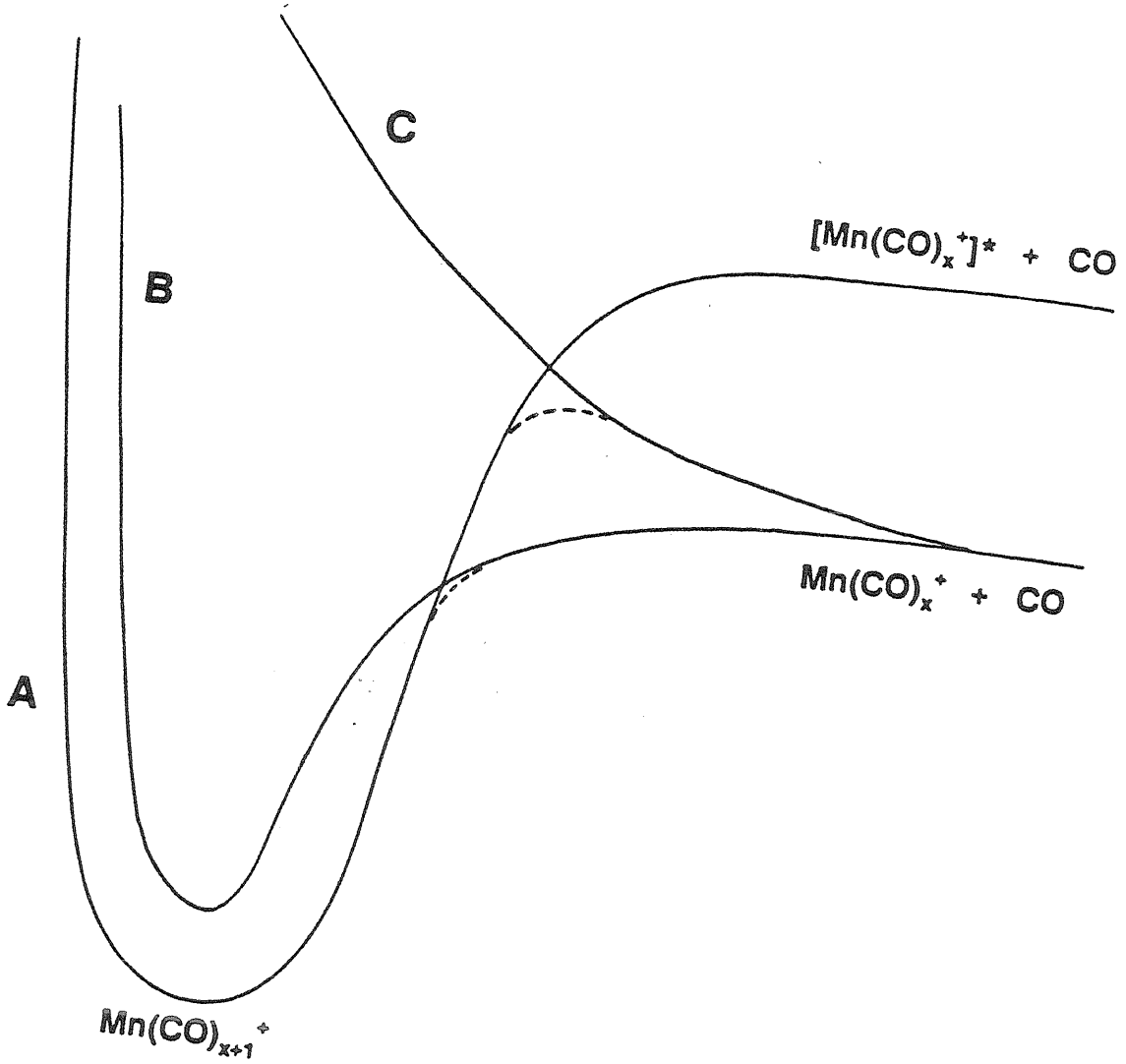
C
B
A
[Mn(CO)x+]* + CO
Mn(CO)x+ + CO
Mn(CO)x+1+

Kinetic Energy Release Studies. The CO exchange rate studies alone do not answer the question of the importance of spin conservation in the $Mn(CO)_x^+$ system. For further information we turn to the results of the kinetic energy release experiments.

These experiments are used to probe the nature of the potential surface in the exit channel. If CO loss is spin-forbidden it is possible a barrier exists in the exit channel. One possibility is illustrated in Figure 4, where the avoided crossing between the repulsive surface C and the ground state surface A results in an exit channel barrier. Such a barrier should be detectable since it would almost certainly give rise to a non-statistical kinetic energy release characterized by a broad distribution of energies shifted away from zero. In the absence of a barrier, a narrow distribution peaking near zero would be expected since the reaction coordinate in such a case is in statistical equilibrium with the other modes of the transition state.[15]

The trend in the widths of the kinetic energy release distributions, with x = 6 giving the broadest and x = 2 giving the narrowest (see Figure 3), at first seems counterintuitive: one might expect that the average energy released into translation should be largest for the smaller members of the series since these have the fewest degrees of freedom into which energy must be statistically partitioned. When the lifetime requirements for observation are considered, this apparent problem is resolved. Since metastable detection requires that dissociation take place in the second field-

free region, the observed metastables must decompose approximately 5-20 μsec after exiting the source. To have decomposition rates appropriate for observation, the larger members of the series must have considerably more excess energy than the smaller members, for which the appropriate energy is just above threshold. This is illustrated in Figure 5, where unimolecular decomposition rates calculated using RRKM theory are plotted as a function of internal energy. Even though the larger molecules have more modes among which energy must be partitioned, the larger excess energy they contain more than compensates, with the result being the noted trend. It is interesting to note that the kinetic energy release distributions for the photodissociation reactions,[21] with the lifetime requirements removed, have widths which follow the intuitive order: the larger molecule, with more modes among which to distribute the fixed amount of internal energy contributed by the 514-nm photon, produces the narrower distribution.

By using the method discussed below, it was possible to reproduce the kinetic energy release distributions for x = 2-6 using phase space theory.[29,30,31] Details of the phase space calculations can be found in Appendices A and B. The metastable decompositions (x = 2-6) could be described as statistical reactions on "Type I" surfaces; i.e., for x = 2-6 there is no barrier to the reverse of reaction 4[15] since none of the energy distributions show the shift away from zero and the broadening characteristic of non-statistical energy releases.[15] Consequently, there is no barrier to the

Figure 5. Unimolecular decomposition rate constants k_u as a function of ion internal energy above threshold, $E^{\ddagger}$, calculated using RRKM theory employing Whitten-Rabinovitch state counting. Bond energies listed in Table 3, with log *A* = 15, were used in the calculations.

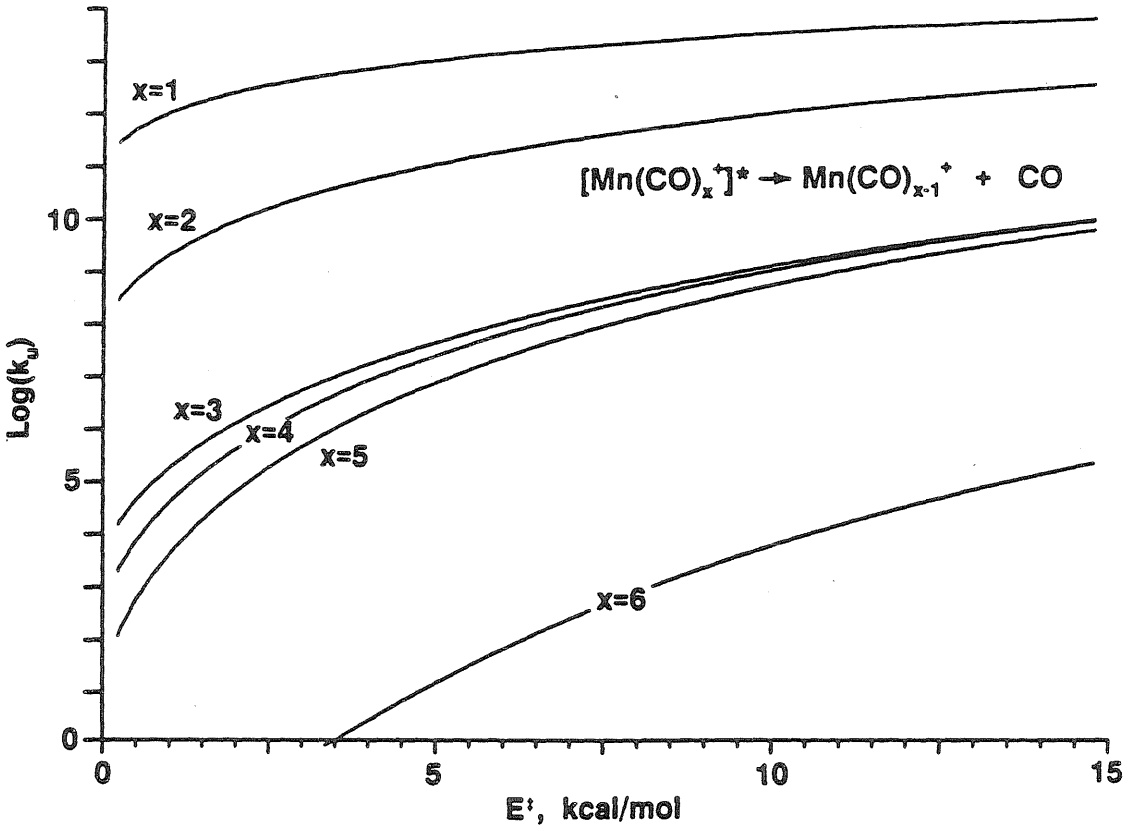
x=1
x=2
x=3
x=4
x=5
x=6
[Mn(CO)x+]* → Mn(CO)x-1+ + CO
Log(k)
E‡, kcal/mol
0
5
10
15

addition of CO to $Mn(CO)_x^+$, x = 1-5, while the question of the presence of a barrier in the addition of CO to bare Mn^+ remains open.

These results are consistent in at least one case with theoretical calculations on isoelectronic species. For $Cr(CO)_5$ there is no barrier to CO addition.[32] Although the effects of surface crossings were not directly observed, the lack of barriers has implications about the type of surface crossings which might occur along the reaction coordinate as CO interacts with $Mn(CO)_x^+$. If crossings occur, they must be between *attractive* surfaces, since crossing with a repulsive surface would lead to a barrier in the resulting diabatic surface. This is illustrated in Figure 4, where the avoided crossing of attractive surfaces A and B results in a diabatic surface without an exit channel barrier, while the crossing of surface A and the repulsive surface C necessarily leads to a barrier.

Several recent theoretical calculations indicate that the bonding in first-row transition metal monocarbonyl ions is qualitatively different from that of the corresponding neutrals. One study, employing GVB methods at the CI level[33], suggests that the bonding in the ions is primarily electrostatic rather than the usual σ-donor π-acceptor picture envisioned for neutral metal carbonyls. If such were the case, the spin state of the metal center would not be expected to be important to the formation of an electrostatic bond. However, this idea only pushes the problem to a larger member of the series, since it is inconceivable that the bonding in $Mn(CO)_6^+$ is predominantly electrostatic; the low lability of the ligands as measured in the

exchange experiment is inconsistent with bonding dominated by electrostatics and is in agreement with expectation for a closed-shell, 18-electron ion. Even if the electrostatic model is correct for small metal carbonyl ions, at some point as ligands are added a more conventional bonding mode must come into play.

Another possibility is that spin transitions do occur as CO's are added, but that, in contrast to the neutral systems, spin conservation is relatively unimportant to the reaction dynamics. If crossings take place between attractive surfaces which are strongly coupled, no barrier would result in the exit channel and exchange rates would not be affected strongly. Or, if crossings take place at long range between narrowly separated surfaces, the result is the same. The experimental observations can also be explained if spin is not a good quantum number in the $Mn(CO)_x^+$ system. It seems reasonable that d^6 species, with the possibility of a large number of spin states further complicated by spin-orbit interactions, might exhibit a great deal of spin state mixing. Further experimental and theoretical work is needed to resolve the question. High-level calculations to determine the ground states and structures of the $Mn(CO)_x^+$ ions would be especially illuminating.

Extraction of Bond Energies From Kinetic Energy Release Data. According to the phase space description, the statistical kinetic energy release distribution is a strong function of the amount of energy above

threshold in the energized molecule[15], $E^{\ddagger}$, which in the dissociation of $Mn(CO)_x^+$ metastables is just the difference between ΔH and E^*, the internal energy of the metastable. Other parameters (see Appendix A) are required for phase space calculation of kinetic energy release distributions, but these are either well-known or easily estimated, and generally do not have a strong effect on the calculated distribution. When E^* is known and the kinetic energy release is statistical, ΔH for the decomposition can be derived by fitting the experimental data with the theoretical energy release predicted by phase space theory.[15,34] The technique has until now been limited by the requirement that E^* be well-defined. In this section it will be shown that quantitative results can also be extracted when the ions have a broad range of internal excitation, since the experiment places severe constraints on the values of E^* which contribute to the measured distribution.

The $Mn(CO)_x^+$ system is an example of the situation just mentioned. The ions were all produced by electron impact followed by fragmentation, with the result that the internal energies of the metastables were unknown. This difficulty was circumvented by taking note that the lifetime requirements for the observation of metastables are stringent: the metastables must decompose during the time they are in the second field-free region, a window of approximately 5-20 μsec after extraction from the source. The lifetime requirement in turn places limitations on E^*. If E^* is too large, most metastable decomposition occurs before the ions reach the second field-free region and the resulting signal is weak. If E^* is too small, most

metastables will decompose after transiting the second field-free region and again the signal is weak. These limitations can be quantified using statistical kinetic theory to determine decomposition rates as a function of ion internal energy. The energies are then assigned weights $W(E^*)$ according to equation 6, using theoretically determined rate constants for unimolecular decomposition, $k_u(E^*)$.

$$W(E^*) = \exp[-k_u(E^*)(t_i + t_r)] - \exp[-k_u(E^*)(t_f + t_r)] \quad (6)$$

The transit times from the source to the entrance and exit of the second field-free region are given by t_i and t_f, respectively, while t_r is the residence time of the ion in the source between formation and extraction. In this work $t_r = 0$ was assumed, since over a reasonable range of residence times the results do not depend strongly on t_r.

RRKM theory[35] was employed to determine the unimolecular rate constants. This takes advantage of the observation that dissociation rates are best described using tight transition states, even though the release of energy into product separation is best described by an orbiting transition state.[36,37] The results have a strong dependence on the tightness of the RRKM transition state chosen, which in turn is quantitatively reflected by the size of the frequency factor (hereafter denoted *A*-factor). To our knowledge experimental *A*-factors for loss of CO from $Mn(CO)_x^+$ have not been determined, so several means were used to estimate the values. First,

comparison was made with a study[38] of the *A*-factors for CO loss from the neutrals $Fe(CO)_5$, $Cr(CO)_6$, $Mo(CO)_6$, and $W(CO)_6$. Log *A* was found to be in the range 15.5-16.0 for those species. This should serve as an upper limit for ionic $Mn(CO)_6^+$, where log *A* might be expected to be lower because the charge-induced dipole interaction causes the transition state to be tighter in the ion than in the neutral case. Second, equation 7 may be used to estimate *A*.[39]

$$A = (ekT/h)\exp(\Delta S^{\ddagger}/R) \qquad (7)$$

If it is assumed that the transition state is tight (i.e. similar to the reactant), then ΔS is small and can be ignored except for a statistical factor deriving from the reaction path degeneracy. At 350 K, using a path degeneracy of six, equation 7 gives log *A* = 14.1 for CO loss from $Mn(CO)_6^+$. This is also consistent with a careful choice of vibrational frequencies based on reasonable assumptions about the transition state (see Appendix A). We conclude that log *A* for $Mn(CO)_6^+$ decomposition is somewhere in the range 13-15.5, and fit the kinetic energy releases by varying ΔH at each of these extremes. The resulting bond energies, given in Table III, are bracketed accordingly. Details of the procedures used in obtaining the fits are given in Appendix B.

Examples of the fits obtained for the kinetic energy release distributions in reaction 4, x = 2-6, are given in Figure 6. The distributions

Table III. Metastable Kinetic Energy Releases and $Mn(CO)_x^+$ Bond Energies.

x	$\langle E_t \rangle$ [a]	s [b]	Log *A* [c]	E^*_{max} [d]	$D_o^o(Mn(CO)_{x-1}^+-CO)$ [e]
6	55	33	15.0	50.	37.
			13.0	40.	27.
5	24	27	15.0	21.2	19.
			13.0	15.3	13.
4	19	21	15.3	24.2	23.
			13.0	18.1	17.
3	16	15	15.4	37.7	37.
			13.0	26.0	25.
2	11	10	[f]	[f]	<25.
1	[g]	4	[f]	[f]	> 7.

[a]Measured average translational energy release in metastable decomposition, meV.

[b]Number of vibrational oscillators in $Mn(CO)_x^+$.

[c]Frequency factor assumed for calculation of metastable internal energy.

[d]Determined using equation (6) from text. Units: kcal/mol.

[e]See text. Units: kcal/mol.

[f]Fit not achieved. See text.

[g]Not determined. See text.

Figure 6. Comparison of theoretical kinetic energy release distributions to experimental distributions, obtained using the approach described in the text. Experiment, solid line. Theory at low log *A* limit, short dashed line. Theory at high log *A* limit, long-short dashed line. Theoretical fits correspond to parameters given in Table 3. Note change of scale for x = 6.

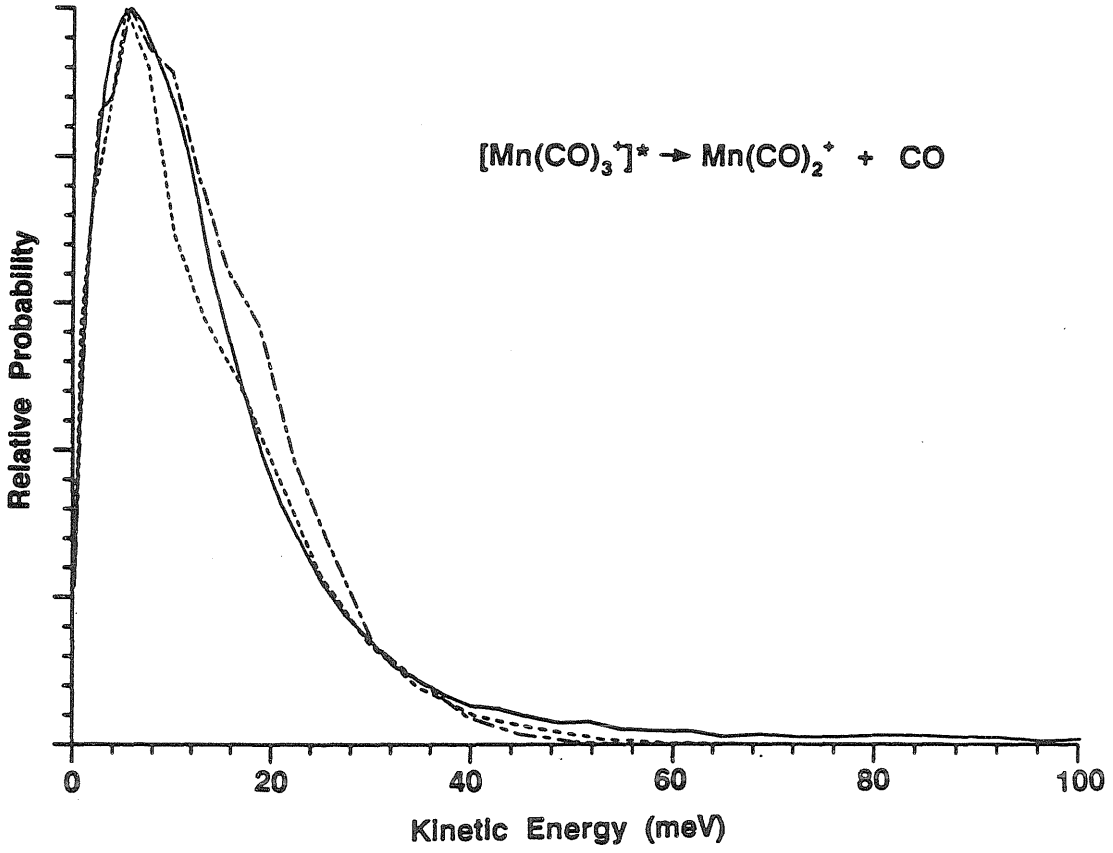
[Mn(CO)3+]* → Mn(CO)2+ + CO
Relative Probability
0
20
40
60
80
100
Kinetic Energy (meV)

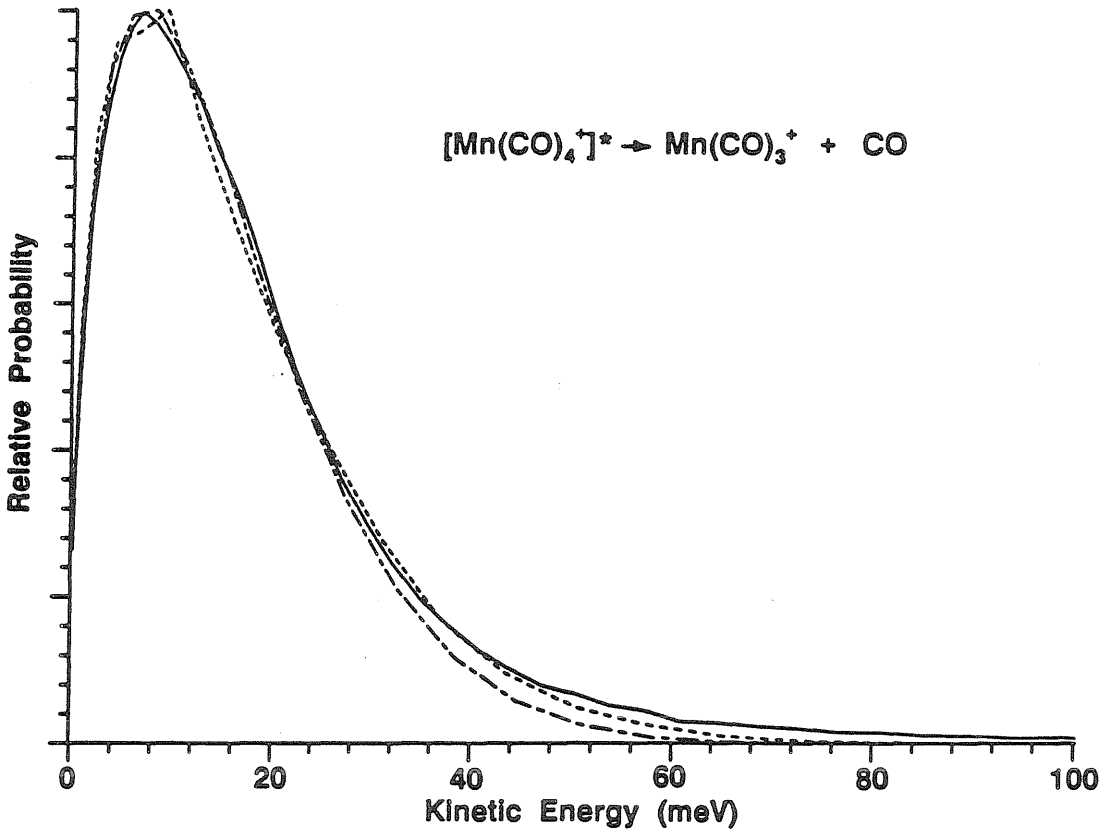
[Mn(CO)4+]* → Mn(CO)3+ + CO
Relative Probability
0
20
40
60
80
100
Kinetic Energy (meV)

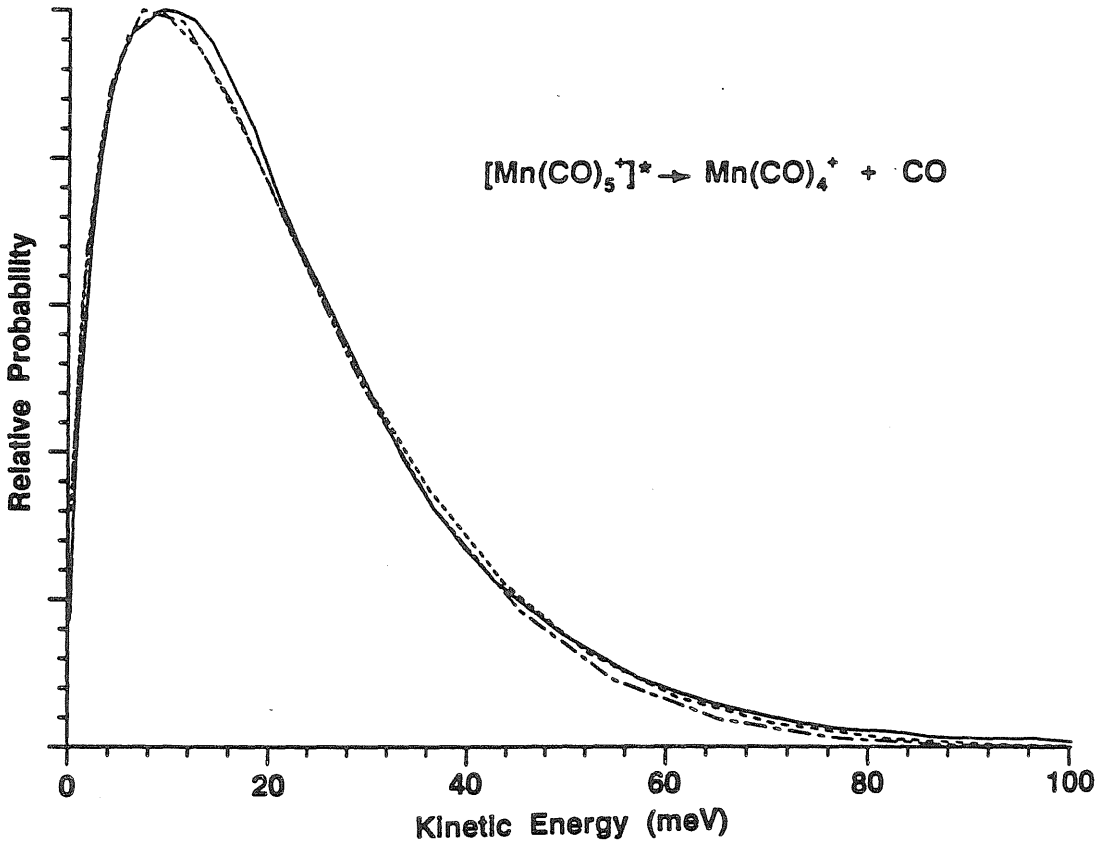
[Mn(CO)5+]* → Mn(CO)4+ + CO
Relative Probability
0
20
40
60
80
100
Kinetic Energy (meV)

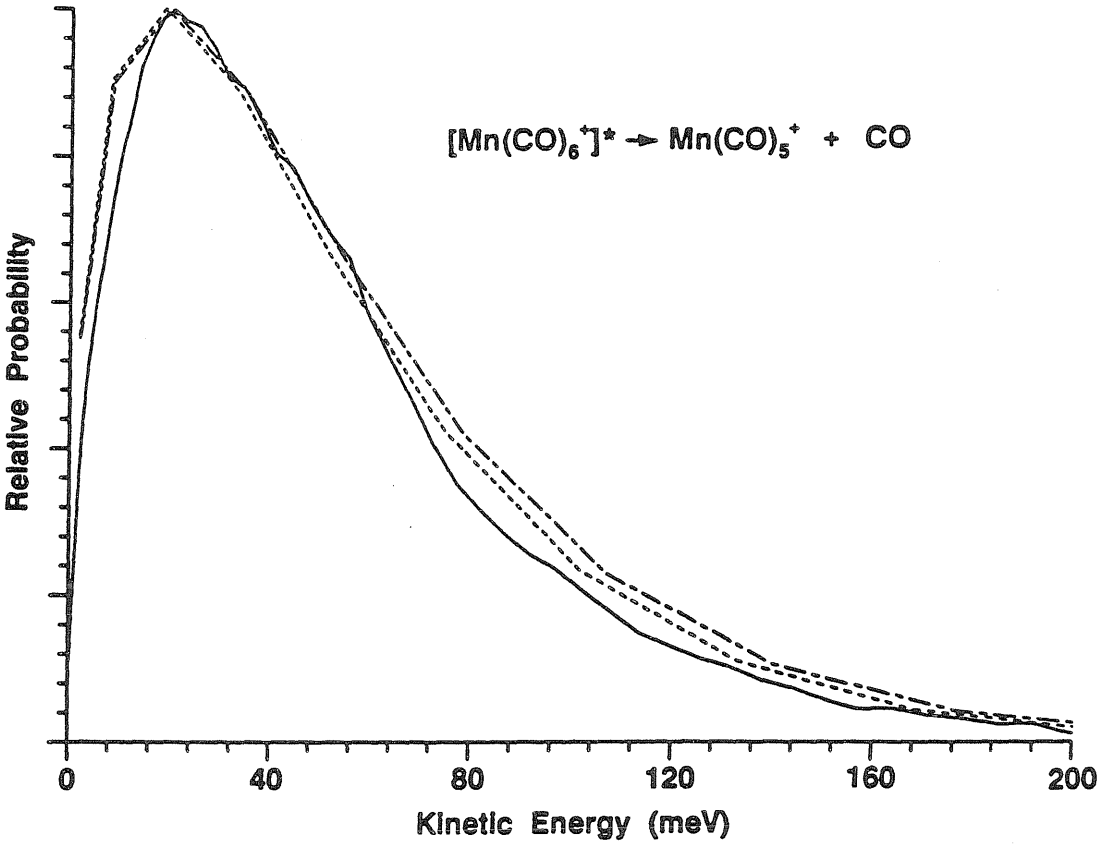
[Mn(CO)6+]* → Mn(CO)5+ + CO
Relative Probability
0
40
80
120
160
200
Kinetic Energy (meV)

for the larger values of x were easily reproduced by the theory, but for x < 4 the quality of the fit deteriorates markedly as x decreases. For x = 2, the experimental data could not be fit within the bounds of the *A*-factor discussed above. This may reflect the fact that the larger molecules, with greater internal energy and more modes into which it may be partitioned, are better described using statistical theory than are the smaller molecules, where quantum effects and other types of non-statistical behavior are likely to be more important. It may also indicate a shortcoming in the method used to generate the limits on the *A*-factors.[40]

Bond Energies. If values of E^* weighted as described above are used in the phase space calculations, and ΔH is varied until a good fit between the phase space prediction and the experimental kinetic energy release is obtained, the bond energies listed in Table III are derived. Only an upper limit is reported for $D(MnCO^+\text{-}CO)$ since, as noted above, a good fit to the $Mn(CO)_2^+$ dissociation data could not be obtained.

Although the individual bond energies have not been measured by other means, the values given here may be compared with averages reported elsewhere. A recent *ab initio* study obtained a mean intrinsic bond energy of 32 kcal/mol in $Mn(CO)_6^+$ to the lowest singlet state of Mn^+ arising from a d^6 configuration, in which the t_{2g} orbitals are fully populated.[41] If 1/6 of the promotion energy required to produce the lowest known singlet state of Mn^+ is subtracted from this value, the result is 14 kcal/mol.

This is considerably less than the 25 kcal/mol average of the measured values for $D(Mn(CO)_5^+-CO)$, $D(Mn(CO)_4^+-CO)$, $D(Mn(CO)_3^+-CO)$, and $D(Mn(CO)_2^+-CO)$ from Table III, but the theoretical results were also low by comparison to experiment for Cr, Mo, and W hexacarbonyls.

Further comparisons come from experimental results, and the agreement found is good. Since $\Delta H^\circ_f(Mn(CO)_5^+)$ is known[11], ΔH can be calculated for reaction 8.

$$Mn(CO)_5^+ \rightarrow Mn^+ + 5CO \qquad (8)$$

ΔH for this reaction, 99 kcal/mol, is the sum of all the Mn^+-CO bond energies in $Mn(CO)_5^+$, so the average Mn^+-CO bond energy is 19.8 kcal/mol. This agrees well with the average of $D(Mn(CO)_4^+-CO)$, $D(Mn(CO)_3^+-CO)$, and $D(Mn(CO)_2^+-CO)$ from Table III, 22 kcal/mol. More recently, the loss of two carbonyls from $Mn(CO)_5^+$ was studied by photodissociation threshold measurements, and the average of those two bond energies was determined to be <21.9 kcal/mol[42], again in good agreement with the average from Table III, 18 kcal/mol.

Finally, the photodissociation study of reaction 5 gives an upper limit to the sum of $D(MnCO^+-CO)$ and $D(Mn^+-CO)$. From energy conservation, the relation of equation 9 is derived.

$$D_o^\circ(MnCO^+-CO) + D_o^\circ(Mn^+-CO) =$$

$$h\nu + E_{int}(Mn(CO)_2^+) - E_{int}(CO) - E_{int}(Mn^+) - E_t \qquad (9)$$

$E_{int}(X)$ is the internal energy of X and E_t is the translational energy of the photofragments. The value of $E_{int}(CO)$ will be small due to the widely spaced vibrational levels in CO, and $E_{int}(Mn^+)$ is zero since the first excited state of Mn^+ is 1.17 eV above the ground state. A very small fraction of the $Mn(CO)_2^+$ ions will have enough energy to dissociate ($\sim 10^{-5}$), but the average internal energy in $Mn(CO)_2^+$ will be small (of the order of 2 ± 2 kcal/mol). Consequently (9) can be simplified to (10).

$$D_o^\circ(MnCO^+\text{-}CO) + D_o^\circ(Mn^+\text{-}CO) \approx h\nu - E_t(max) \qquad (10)$$

$E_t(max)$ is the maximum kinetic energy released in the photofragmentation. The value for $D_0^0(MnCO^+\text{-}CO) + D_0^0(Mn^+\text{-}CO)$ so obtained, 32 ± 3 kcal/mol, is in excellent agreement with the 32 kcal/mol difference between ΔH for reaction 8 and the sum of our determined bond energies. In summary, in every case the values obtained by fitting the data using phase space theory agree with experimental values measured by independent methods. This lends support to the values of the various bond energies we have determined (Table II).

Few theoretically determined bond energies are available for comparison with the values reported here for the $Mn(CO)_x^+$ series. The value for $D(Mn(CO)_5^+\text{-}CO)$ obtained in the present work is intermediate

between a value of 22 kcal/mol obtained using density functional theory,[41] and the 49.6 kcal/mol obtained by modified extended Huckel calculations[43]. The density functional results, however, were low relative to a number of experimental values reported for $D(Cr(CO)_5\text{-}CO)$, $D(Mo(CO)_5\text{-}CO)$ and $D(W(CO)_5\text{-}CO)$, while the extended Huckel value might be expected to be high; the same calculation yielded 59 kcal/mol as the threshold for CO loss from the isoelectronic $Cr(CO)_6$, while photoacoustic calorimetry measurements gave 37 ± 5 kcal/mol for the same bond.[44] The reason for the discrepancy is unknown. Hartree-Fock calculations for $D(Cr(CO)_5^+\text{-}CO)$ also resulted in a higher value, 49.8 kcal/mol.[32] For the coordinatively unsaturated fragments, less information is available. The modified extended Huckel calculations noted above give 46.4 kcal/mol for $D(Mn(CO)_4^+\text{-}CO)$, in poor agreement with the current result of 16 ± 3 kcal/mol. These calculations are expected to do poorly in cases where spin is not conserved,[43] as may be the case here.

The variation in bond energies among the members of the $Mn(CO)_x^+$ series is not unique. As noted in Table IV, large variations in bond energies among members of $M(CO)_x$ series have previously been reported for iron[8] and nickel[9]. Appearance potential measurements have yielded a similar result for $Cr(CO)_x^+$ and $Mn(CO)_xBz^+$ (Bz = $CH_2C_6H_5$) ions.[10,11] The similarity in the bond strengths for $Mn(CO)_x^+$ and $Cr(CO)_x^+$, x = 3-6, is striking.

Table IV. Bond Energies in Metal Carbonyls.

	Species M					
Bond	Mn^+ [a]	Cr [b]	Cr^+ [c]	$MnBz^+$ [d]	Fe [e]	Ni [f]
$M(CO)_5$-CO	32±5	37±5	33	--	--	--
$M(CO)_4$-CO	16±3	25±5	14	10	55±11	--
$M(CO)_3$-CO	20±3	--	21	21	5± 5	25± 2
$M(CO)_2$-CO	31±6	--	28	12	32± 7	13± 10
$M(CO)_1$-CO	<25	--	35	25	23± 7	54± 15
M-CO	> 7	--	31[g]	30	21± 7	29± 15

[a]This work.

[b]Reference 4c.

[c]Reference 10.

[d]Reference 11.

[e]Reference 8.

[f]Reference 9.

[g]A more recent experimental result gives 26±5 kcal/mol for this bond energy (Georgiadis, R.; Armentrout, P. B. *J. Mass Spectrom. Ion Proc.*, submitted for publication). In addition, theoretical calculations at the CI level suggest a somewhat lower value of 15 kcal/mol (see reference 33).

Several things are apparent from the trends in bond energies. First, the $Mn(CO)_6^+$ ion exhibits special stability, as is evident from the large value of $D(Mn(CO)_5^+\text{-}CO)$. This seems reasonable since $Mn(CO)_6^+$ is an octahedral species[45] with all six valence electrons singlet paired in the t_{2g} orbitals. Formation of the last Mn^+-CO bond results in a coordinatively saturated species. A similar situation exists for $D(Fe(CO)_4\text{-}CO)$, where the energy of this bond, at 55 kcal/mol, is the largest of the $Fe(CO)_x$ series.[8]

$D(Mn(CO)_5^+\text{-}CO)$ is weaker than the measured bond energies for group VI neutral hexacarbonyls in solution (Cr, 37 ± 5; Mo, 34 ± 5; and W, 38 ± 5 kcal/mol)[44], and in the gas phase (Cr, 37 ± 5 kcal/mol)[4c], since in the ion the π bonding interactions are weakened relative to those of the neutrals. The same observation can be made when comparing $D(M(CO)_4\text{-}CO)$ values for M = Mn^+ (16 ± 3 kcal/mol) and M = Cr (25 ± 5 kcal/mol).[4c] For ions, one might expect σ bonding to be more important in relation to π interactions than in corresponding neutrals, since the charge on the metal should stabilize σ donation and decrease the amount of π back-donation. High-level theory supports intuition. *Ab initio* calculations on $NiCO^+$ using a double zeta basis at the SCF and MCSCF levels[46] found that, in contrast to the corresponding neutral NiCO, the ion has little π bonding. Similar results were obtained in Hartree-Fock calculations on $CuCO^+$ using a large, polarized basis set at the SCF and MP4 levels.[47] It is expected that the relative importance of the π interactions might increase as ligands are added to the metal and the ability

to delocalize the charge increases, but even for $Mn(CO)_6^+$, theory predicts that back-bonding is less important than in the isoelectronic $Cr(CO)_6$, due to the charge on the metal center.[41]

For the smaller fragment ions, the relationship between their relative stabilities and their structures is difficult to characterize because of limited structural information.

For $MnCO^+$, the bonding is expected to be weak, since formation of the bond would require promotion of the 4s electron to a d orbital. The lowest known state arising from a d^6 configuration of the Mn^+ ion (^5D) lies 41 kcal/mol above the ground state[25]. It is interesting to note the evidence from Table IV that Cr^+, having a ground state deriving from a d^5 configuration which lacks the 4s electron, forms a strong bond to CO. The data indicate that $MnCO^+$ is bound by >7 kcal/mol, in contrast to MnCO, where analysis of matrix IR data indicate that the neutral is not bound.[48] The fact that absorption of 514-nm light results exclusively in loss of both CO's from $Mn(CO)_2^+$ argues that $D(Mn^+\text{-}CO)$ is weak. The matrix isolation data also support that conclusion. Of the measured CO stretching frequencies in first-row transition metal monocarbonyl neutrals, only those of NiCO and CuCO are higher than that for CrCO, indicating a weak Cr-CO bond. Since Mn^+-CO is isoelectronic with CrCO, a weak Mn^+-CO bond is suggested.

Summary

Many questions remain concerning the influence of spin conservation on the reactivity and bonding of metal carbonyls, but it is clear that spin is less important in the $Mn(CO)_x^+$ system than in the neutral $Fe(CO)_x$ system. While changes in spin multiplicity must occur as CO ligands are successively added to Mn^+, their effects are not manifested in terms of CO exchange rates or barriers in the exit channel for CO loss. The reasons for this behavior are unclear, but may lie in the differences in the bonding of neutral metal atoms and ionic metal centers to CO as suggested by *ab initio* calculations. In addition, it is likely that the d^6 $Mn(CO)_x^+$ system is electronically more complex than the d^8 $Fe(CO)_x$ system, with the result that spin is a poorer quantum number for the $Mn(CO)_x^+$ ions.

Useful thermochemical information can be extracted by modeling kinetic energy release distributions using statistical dynamic theories. This technique should be generally applicable to metastable ions which decompose with no barrier to the reverse association reaction. It is not necessary to take special care that the internal energy of the metastable be well-defined; energy selection is built into the experiment by the requirement that decomposition occur during a narrow time window. A further advantage is that, unlike many physical methods for measuring thermochemistry, this method works best with relatively large molecules, where the statistical description of energy transfer is most accurate due to

high state densities. In addition, the average kinetic energy release is larger (and therefore easier to measure), since larger ion internal energies are necessary to achieve optimum decomposition rates than for smaller molecules.

The application of these techniques to the $Mn(CO)_x^+$ system has resulted in measurements of a number of metal carbonyl bond energies for this system, which are in agreement with average bond energies measured using other methods. The bonding trends can be rationalized in terms of simple molecular orbital arguments, with the bonding in the ions being simpler than that in the corresponding neutrals due to the relative unimportance of π bonding in the ions. The reasons for the differences in the importance of spin in the neutral metal carbonyls and the $Mn(CO)_x^+$ system are unclear and warrant further investigation.

Acknowledgement. This work has been funded by the National Science Foundation through grant number CHE87-11567 (JLB) and CHE85-12711 (MTB) and graduate fellowship support (DVD). In addition, we wish to thank the Shell Foundation for graduate fellowship funding (DVD), and the donors of the Petroleum Research Fund, administered by the American Chemical Society, for additional support. The help of Tim Swager in synthesizing $Mn(CO)_5COCH_3$ is also appreciated, and we thank John Bercaw for providing ^{13}CO for use in the exchange experiments.

Appendix A: Parameters for Statistical Calculations

Fundamental vibrational frequencies for $Mn(CO)_6^+$ have been assigned based on infrared and Raman spectra of $Mn(CO)_x^+PF_6^-$,[49] and these frequencies were used to estimate those of the gas phase ions. In general, the frequencies were adjusted to produce the desired *A*-factor. It should be noted that the results have only a weak dependence on the frequencies chosen, as long as the *A*-factor remains constant.

Structures for the various $Mn(CO)_x^+$ ions were assumed as noted. $Mn(CO)_6^+$ was assumed to be an octahedral complex with Mn-C bond lengths of 1.87 Å and C-O bond lengths of 1.14 Å.

Two possibilities are considered for $Mn(CO)_5^+$: a C_{4v} structure resulting from removal of one CO ligand from octahedral $Mn(CO)_6^+$, and a rearranged trigonal bipyramidal structure. The C_{4v} geometry has been predicted by Burdett for singlet d^6 metal pentacarbonyl.[14] Further support for the C_{4v} geometry comes from x-ray crystallographic data[50] and gas-phase electron diffraction data[51] for $HMn(CO)_5$, as well as modified extended Huckel calculations[45] on $Mn(CO)_5^+$. Bond lengths were taken from theory.[45] The isoelectronic $Cr(CO)_5^+$ has also been determined to have C_{4v} geometry on the basis of its infrared spectrum.[52] $Fe(CO)_5^+$ on the other hand, is believed to be trigonal bipyramidal.[14]

For $Mn(CO)_4^+$, C_{2v}, D_{4h}, and T_d geometries were considered. It has been predicted that singlet d^6 metal tetracarbonyls should have the C_{2v}

geometry.[14] Infrared spectra[53] and CO addition rates[4,5] for the isoelectronic $Cr(CO)_4$ indicated that this molecule has a C_{2v} ground state, while modified extended Huckel calculations[54] on neutral $Mn(CO)_4$ also predict this structure. Calculated bond lengths were used.[45] Burdett argues, on the basis of theory, that quintet d^6 metal tetracarbonyls should have the T_d structure.[14]

Three geometric possibilities, C_{3v}, D_{3h}, and C_{2v}, are considered for $Mn(CO)_3^+$. Burdett has predicted that the C_{3v} d^6 metal tricarbonyl has a singlet ground state, while the C_{2v} geometry results in a triplet and the D_{3h} geometry is a quintet. Infrared spectral data[53] for the isoelectronic neutrals $Mo(CO)_3$ and $Cr(CO)_3$ are consistent with C_{3v} geometry for both species. Bond lengths were assumed: Mn-C, 1.84 Å; C-O, 1.15 Å.

Appendix B: Method of Calculation

Fits of theoretical kinetic energy release distributions to the measured experimental distributions were obtained as follows. Initially, a guess was made for the bond energy in question, and this value was used to estimate metastable internal energies assuming the low extreme for log *A* as discussed above. Decomposition rate constants were calculated using RRKM theory,[55] with the assumed bond energy and log *A*, for a range of ion internal energies. The internal energies were then assigned weights by using the calculated rate constants in equation 6, and phase space calculations[56] were performed using the weighted internal energies. The same bond energy was used in the phase space calculation as was

assumed for the RRKM calculation. Based on the comparison of the calculated kinetic energy distribution to the experimental distribution, the bond energy was revised and the process was repeated with a new RRKM calculation. This iteration was continued until the bond energy was bracketed for the low log *A* value, generally to ± 0.5 kcal/mol. At that point the high value for log *A* was assumed, a new guess was made for the bond energy, and iterations were performed until the fit converged on a bond energy at the high log *A* value. It is important to note that RRKM theory was used only to determine the metastable internal energies; otherwise, the phase space calculations and fitting procedures did not depend on the RRKM calculations.

References and Notes

1. Ouderkirk, A. J.; Wermer, P.; Schultz, N. L.; Weitz, E. *J. Am. Chem. Soc.* **1983**, *105*, 3354-3355.

2. Seder, T. A.; Ouderkirk, A. J.; Weitz, E. *J. Chem. Phys.* **1986**, *85*, 1977-1986.

3. Barton, T. J.; Grinter, R.; Thomson, A. J.; Davies, B.; Poliakoff, M. *J. Chem. Soc., Chem. Commun.* **1977**, 841-842.

4. a) Fletcher, T. R.; Rosenfeld, R. N. *J. Am. Chem. Soc.* **1985**, *107*, 2203-2212. b) Fletcher, T. R.; Rosenfeld, R. N. *J. Am. Chem. Soc.* **1986**, *108*, 1686-1688. c) Fletcher, T. R.; Rosenfeld, R. N. *J. Am. Chem. Soc.* **1988**, *110*, 2097-2101.

5. a) Seder, T. A.; Church, S. P.; Ouderkirk, A. J.; Weitz, E. *J. Am. Chem. Soc.* **1985**, *107*, 1432-1433. b) Seder, T. A.; Church, S. P.; Weitz, E. *J. Am. Chem. Soc.* **1986**, *108*, 4721-4728.

6. Rayner, D. M.; Nazran, A. S.; Drouin, M.; Hackett, P. A. *J. Phys. Chem.* **1986**, *90*, 2882-2888.

7. Graham, J. R.; Angelici, R. J. *Inorg. Chem.* **1967**, *6*, 2082-2085.

8. Engelking, P. C.; Lineberger, W. C. *J. Am. Chem. Soc.* **1979**, *101*, 5569-5573.

9. Stevens, A. E.; Feigerle, C. S.; Lineberger, W. C. *J. Am. Chem. Soc.* **1982**, *104*, 5026-5031.

10. Michels, G. D.; Flesch, G. D.; Svec, H. J. *Inorg. Chem.* **1980**, *19*, 479-485.

11. Simoes, J. A. M.; Schultz, J. C.; Beauchamp, J. L. *Organometallics* **1985**, *4*, 1238-1242.

12. Sugar, J.; Corliss, C. *J. Phys. Chem. Ref. Data* **1985**, *14*, 351-363.

13. Beach, N. A.; Gray, H. B. *J. Am. Chem. Soc.* **1968**, *90*, 5713-5721.

14. Burdett, J. K. *J. Chem. Soc. Faraday Trans. II* **1974**, *70*, 1599-1693.

15. Hanratty, M. A.; Beauchamp, J. L.; Illies, A. J.; van Koppen, P. A. M.; Bowers, M. T. *J. Am. Chem. Soc.* **1988**, *110*, 1-14.

16. Stevens, A. E.; Beauchamp, J. L. *Chem. Phys. Lett.* **1981**, *78*, 291-295.

17. Jarrold, M. F.; Illies, A. J.; Bowers, M. T. *Chem. Phys.* **1982**, *65*, 19.

18. a) Jarrold, M. F.; Illies, A. J.; Bowers, M. T. *J. Chem. Phys.* **1983**, *79*, 6086. b) Jarrold, M. F.; Illies, A. J.; Bowers, M. T. *J. Chem. Phys.* **1984**, *81*, 214-221. c) Jarrold, M. F.; Illies, A. J.; Bowers, M. T. *J. Chem. Phys.* **1985**, *82*, 1832.

19. For a discussion of the theory used in obtaining kinetic energy release distributions using metastable peak shapes, see Jarrold, M. F.; Illies, A. J.; Kirchner, N. J.; Wagner-Redeker, W.; Bowers, M. T.; Mandich, M. L.; Beauchamp, J. L. *J. Phys. Chem.* **1983**, *87*, 2213-2221.

20. Casey, C. P.; Scheck, D. M. *J. Am. Chem. Soc.* **1980**, *102*, 2728-2731.

21. van Koppen, P. A. M.; Bowers, M. T.; Dearden, D. V.; Beauchamp, J. L. To be published.

22. Hieber, W.; Wollmann, K. *Chem. Ber.* **1962**, *95*, 1552.

23. Noted in a review: Werner, H. *Angew. Chem. Int. Ed. Engl.* **1968**, *7*, 930-941.

24. a) Seder, T.; Ouderkirk, A.; Church, S.; Weitz, E. in "High Energy Processes in Organometallic Chemistry", Suslick, K. S., ed.; ACS: Washington, D. C., 1987. b) Weitz, E. *J. Phys. Chem.* **1987**, *91*, 3945-3953.

25. Sugar, J.; Corliss, C. *J. Phys. Chem. Ref. Data* **1985**, *14*, 351-363.

26. This estimate is based on values calculated for Mn^+ in Schilling, J. B., Ph. D. Thesis, California Institute of Technology, 1987. Assuming s-d exchange terms of 4 kcal/mol, and conservatively estimating d-d exchange terms of 10 kcal/mol, and by noting that formation of the singlet will cause the loss of at least 5 s-d and 4 d-d exchange terms, the total exchange energy lost in forming the singlet is 60 kcal/mol. This ignores the additional energetic cost of promoting the 4s electron to the 3d orbital.

27. The excited state population produced in surface ionization, electron impact, and drift cell ionization sources has recently been discussed: Sunderlin, L. S.; Armentrout, P. B. *J. Phys. Chem.* **1988**, *92*, 1209-1219.

28. For an example of metastable electronic predissociation in $CrCO^+$ and $Cr(CO)_2^+$ see Jarrold, M. F.; Misev, L.; Bowers, M. T. *J. Phys. Chem.* **1984**, *88*, 3928-3929.

29. For discussion of the application of phase space theory to the fitting of kinetic energy release distributions, see a) Chesnavich, W. J.; Bowers, M. T. *J. Am. Chem. Soc.* **1977**, *99*, 1705-1711; b) Jarrold, M. F.; Wagner-Redeker, W.; Illies, A. J.; Kirchner, N. J.; Bowers, M. T. *Int. J. Mass Spectrom. Ion Processes*, **1984**, *58*, 63-95; c) Reference 30.

30. Chesnavich, W. J.; Bass, L.; Su, T.; Bowers, M. T. *J. Chem. Phys.* **1981**, *74*, 2228-2246

31. Chesnavich, W. J.; Bowers, M. T. *Prog. React. Kinetics* **1982**, *11*, 137.

32. Sherwood, D. E., Jr.; Hall, M. B. *Inorg. Chem.* **1983**, *22*, 93-100.

33. Allison, J.; Mavridis, A.; Harrison, J. F. *Polyhedron*, in press.

34. van Koppen, P. A. M.; Jacobsen, D. B.; Illies, A. J.; Bowers, M. T.; Hanratty, M. A.; Beauchamp, J. L. *J. Am. Chem. Soc.* (submitted).

35. Robinson, J. P.; Holbrook, K. A. *Unimolecular Reactions*; Wiley (Interscience): New York, 1972. Forst, W. *Theory of Unimolecular Reactions*; Academic Press: New York, 1973.

36. This is another way of saying that metastable lifetimes are determined by the tight transition state, but that the reaction coordinate remains coupled to the internal modes as products separate to the orbiting transition state and dissociate. See Reference 30.

37. RRKM theory can also be used, with the RRKM transition state, to calculate product kinetic energy release. This was done for the x = 5 case. Since it ignores the constraints imposed by angular momentum, the RRKM calculation fails to predict the dropoff in the distribution as kinetic energy approaches zero, but does reasonably well in fitting the higher-energy portion of the experimental distribution, with bond energies within the range calculated using phase space theory.

38. Lewis, K. E.; Golden, D. M.; Smith, G. P. *J. Am. Chem.* Soc. **1984**, *106*, 3905-3912.

39. Benson, S. W. *Thermochemical Kinetics*, 2nd ed.; Wiley (Interscience): New York, 1976.

40. The concept of "preexponential" or "Arrhenius" *A*-factor is only strictly valid for systems in thermal equilibrium. Such systems generate canonical ensembles of energy states. In our electron impact generated $Mn(CO)_x^+$

ions we have a microcanonical ensemble of energy states that depends on the energy deposition function for the initial ionization step and the energy partitioning as sequential CO ligands are lost. Hence the method used here only semiquantitatively mimics the real situation. Since the *A*-factors are used only to set limits on the bond energies the procedure is probably satisfactory.

41. Ziegler, T; Tschinke, V.; Ursenbach, C. *J. Am. Chem. Soc.* **1987**, *109*, 4825-4837.

42. Tecklenburg, R. E. Jr.; Russell, D. H. *J. Am. Chem. Soc.* **1987**, *109*, 7654-7662.

43. McKinney, R. J.; Pensak, D. A. *Inorg. Chem.* **1979**, *18*, 3413-3417.

44. Bernstein, M.; Simon, J. D.; Peters, K. S. *Chem. Phys. Lett.* **1983**, *100*, 241-244.

45. Modified extended Huckel calculations were performed for $Mn(CO)^{+}_{6}$, $Mn(CO)^{+}_{5}$, and $Mn(CO)_{4}$: Pensak, D. A.; McKinney, R. J. *Inorg. Chem.* **1979**, *18*, 3407-3413.

46. Bauschlicher, C. W., Jr.; Bagus, P. S.; Nelin, C. J. Roos, B. O. *J. Chem. Phys.* **1986**, *85*, 354-364.

47. Morgantini, P.-Y.; Weber, J. *J. Mol. Struct. Theochem.*, to be published.

48. Bach, S. B. H.; Taylor, C. A.; Van Zee, R. J.; Vala, M. T.; Weltner, W. Jr. *J. Am. Chem. Soc.* **1986**, *108*, 7104-7105.

49. McLean, R. A. N. *Can. J. Chem.* **1974**, *52*, 213-215.

50. La Placa, S. J.; Hamilton, W. C.; Ibers, J. A. *Inorg. Chem.* **1964**, *3*, 1491-1495.

51. Robiette, A. G.; Sheldrick, G. M.; Simpson, R. N. F. *J. Mol. Struct.* **1969**, *4*, 221-231.

52. Huber, H.; Kundig, E. P.; Ozin, G. A.; Poe, A. J. *J. Am. Chem. Soc.* **1975**, *97*, 308-314.

53. Perutz, R. N.; Turner, J. J. *J. Am. Chem. Soc.* **1975**, *97*, 4800-4804

54. Elian, M.; Hoffmann, R. *Inorg. Chem.* **1975**, *14*, 1058-1076. Also see Reference 45.

55. RRKM calculations were performed using "A General RRKM Program", by W. L. Hase and D. L. Bunker. Grouped harmonic frequency direct counting was used to determine sums and densities of states in the activated complexes, while the Whitten-Rabinovitch approximation (see reference 35) was used for energized molecules.

56. A more recent version of the phase space programs used has been submitted to QCPE: Chesnavich, W. J.; Bass, L.; Grice, M. E.; Song, K.; Webb, D. A. *Quantum Chemistry Program Exchange*, "TSTPST: Statistical Theory Package for RRKM/QET/TST/PST Calculations".

CHAPTER 2

A NEW PROBE OF POTENTIAL ENERGY SURFACES FOR COMPLEX SYSTEMS: BARRIER-IMPOSED ANGULAR MOMENTUM CONSTRAINTS IN ION-MOLECULE INTERACTIONS. APPLICATION TO THE REACTIONS OF Fe^+ AND Co^+ WITH SMALL ALKANES.

A NEW PROBE OF POTENTIAL ENERGY SURFACES FOR COMPLEX SYSTEMS: BARRIER-IMPOSED ANGULAR MOMENTUM CONSTRAINTS IN ION-MOLECULE INTERACTIONS. APPLICATION TO THE REACTIONS OF Fe^+ AND Co^+ WITH SMALL ALKANES.

David V. Dearden, Margaret A. Tolbert, and J. L. Beauchamp*

Arthur Amos Noyes Laboratory of Chemical Physics

California Institute of Technology

Pasadena, CA 91125

Petra A. M. van Koppen, Jennifer Brodbelt-Lustig,

and Michael T. Bowers*

Department of Chemistry

University of California

Santa Barbara, CA 93106

Abstract.

In the demethanation reactions of Fe^+ with propane, n-butane, and isobutane, and of Co^+ with propane, the kinetic energy release distribution for the products is narrower than predicted by statistical theory. These translationally cold distributions occur when barriers in the potential energy surface with energy near the energy of the reactants restrict the total angular momentum available to products. The usual criterion for predicting an upper limit to ion-molecule reaction cross sections requires that the relative kinetic energy exceed the height of the centrifugal barrier in the entrance channel to allow for a close approach of the reaction partners. Consideration of centrifugal contributions to the effective potential energy surface at smaller separations than the orbiting separation reveals that if a barrier in the J=0 surface lies near, but below, the asymptotic energy of the reactants, systems with large values of J may be able to undergo orbiting collisions without being able to undergo further reaction. Instead, they dissociate back to reactants due to reflection from the effective barrier. Phase space calculations with restricted product angular momentum, as well as literature values for reaction cross sections at low relative energies, are consistent with this explanation, although discrimination effects in the experimental measurements of kinetic energy release lead to discrepancies with the cross section measurements for larger alkanes. Experiments conducted under conditions where the initially formed adduct can be collisionally stabilized indicate that adduct formation occurs at rates near the

Langevin collision rate, but that in cases where J is large, dissociation of the collision complex to reactants is rapid compared to bond insertion processes leading to alkane loss.

Introduction

Study of the reactions of bare gas phase transition metal ions with small hydrocarbons presents a unique opportunity to examine systems which are inherently complex (due to the large number of valence electrons) under conditions where detailed chemical understanding of the system is possible.[1] These studies are particularly valuable for gaining insight into elementary processes, such as C-H and C-C activation, which have proven difficult to study in detail in the presence of solvents. A number of studies employing ion cyclotron resonance[2] and ion beam[3] techniques have been carried out under low-pressure, single collision conditions, yielding information on reactivity patterns, product branching ratios, and reaction cross sections. Exothermic processes for first-row transition metal ions reacting with alkanes include dehydrogenation and elimination of smaller alkane species. At higher pressures, under multiple collision conditions, collisionally stabilized M^+-(hydrocarbon) adducts are observed.[4]

A schematic potential energy surface which has been proposed for reactions of transition metal ions with alkanes is illustrated in Figure 1. Initially, long-range ion-induced dipole interactions lead to the formation of an adduct species, which can subsequently dissociate back to reactants, or undergo insertion of the metal into C-H or C-C bonds and eventually lead to loss of a stable fragment such as a small alkane or H_2. While this type of potential energy surface has been useful as a general guideline, many fundamental issues are still open to question.

Figure 1. Schematic potential energy surface for dehydrogenation and demethanation of an alkane HR by a transition metal ion M^+.

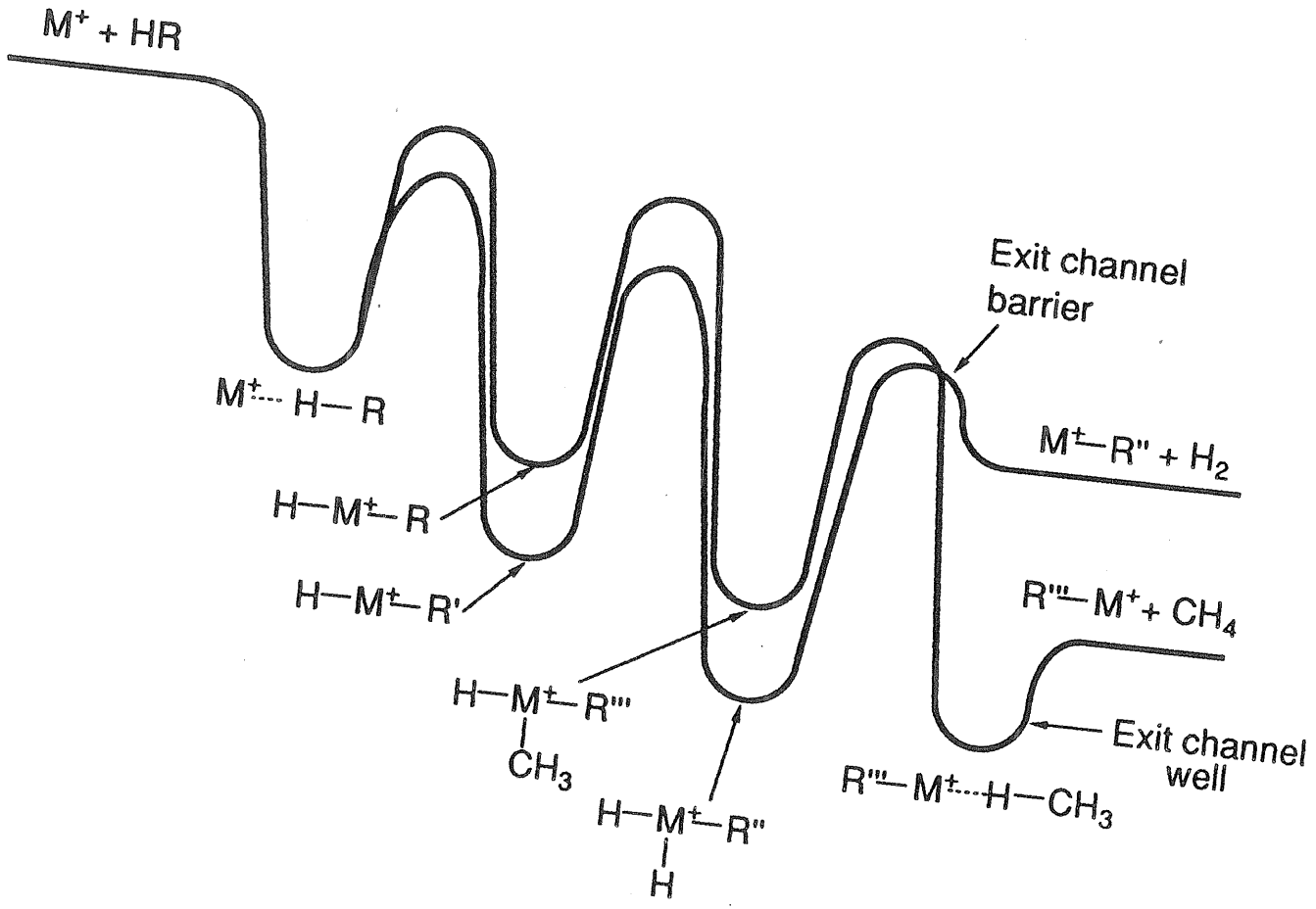
M+ + HR
M+··· H—R
H—M+—R
H—M+—R'
H—M+—R'''
CH3
H—M+—R''
H
Exit channel barrier
M+—R'' + H2
R'''—M+ + CH4
Exit channel well
R'''—M+···H—CH3

For instance, the structure of the initially formed adduct is unknown. Several possibilities have been suggested,[4] including the so-called cluster ion M^+-(alkane), the C-H insertion product, the C-C insertion product, and agostic structures which combine features of the cluster ion and the C-H inserted adduct. Assuming the surface suggested by Figure 1 is qualitatively correct, a further question arises as to whether C-H or C-C insertion is the first step following adduct formation. Finally, the simple surface of Figure 1 assumes that adduct decomposition to reactants, dehydrogenation, and alkane loss all are competitive processes originating from the adduct of the first well. It remains to be established whether this simple description is adequate.

Recently, measurement of kinetic energy release distributions for the decompositions of metastable ions has been added to the array of techniques used to probe the reactions of transition metal ions with hydrocarbons.[5,6] When a metastable ion decomposes, the amount of energy released into product translation is an easily measured, sensitive reflection of the topology of the potential energy surface in the region of the exit channel.[7,5] If there is no exit channel barrier (aside from the centrifugal barrier imposed by conservation of angular momentum), the kinetic energy release is expected to be statistical. In other words, energy is partitioned statistically to the internal modes of the separating products and to the external degrees of freedom including relative translation. The exit channel for methane loss in Figure 1 is an example where statistical

kinetic energy release is expected. Exit channel barriers are manifested by release of energy from the reaction coordinate into product translation, with the consequence that the resulting kinetic energy release distribution is broader than statistical theory would predict.[5] The dehydrogenation exit channel in Figure 1 is one where non-statistical kinetic energy release is anticipated, due to the presence of a barrier in the exit channel.

In cases where the kinetic energy release is statistical, it is often possible to extract thermochemical information by fitting the experimental energy release distribution using phase space theory.[8] The phase space calculation is quite sensitive to reaction exothermicity, which is used as the single free parameter in performing the fit. These techniques have proven particularly useful for measuring heats of formation for gas phase organometallic ions.[5,6]

Previous kinetic energy release studies of organometallic metastable ions have established the value of the technique in probing the existence of barriers in the exit channel.[5,6] A number of dehydrogenation reactions exhibit broad distributions of product kinetic energies, characteristic of an exit channel barrier. Many alkane losses, on the other hand, display kinetic energy release distributions which can be described using statistical theory, assuming no barrier in the exit channel. This implies the existence of the final well in the exit channel of Figure 1, corresponding to a Lewis acid-base adduct in which randomization of energy occurs as the products separate.

Recently, we have examined a number of reactions where the kinetic energy release is *narrower* than predicted by statistical theory. We will refer to these distributions which are "too narrow" as translationally cold distributions. These results are intriguing, since most non-statistical processes yield kinetic energy release distributions *broader* than the statistical prediction. In this work we show that, in the case of a translationally cold kinetic energy release, the distribution can be sensitive to features of the potential surface remote from the exit channel, and can reveal information about the dynamics of the adduct-forming collision. Implications for the model surface of Figure 1 will be discussed, particularly with regard to the initially formed adduct.

Experimental Section

Kinetic energy release measurements were carried out at UCSB using a double-focusing, reversed-geometry mass spectrometer (VG Industries, ZAB-2F[9]) with a home-built pressure- and temperature-variable electron impact source. The methods used in metastable and collision-induced dissociation studies have been described.[10] Briefly, Co^+, generated by 150-eV electron impact on $Co(CO)_3NO$ (Aldrich), or Fe^+, from electron impact on $Fe(CO)_5$, was allowed to react in the source with the hydrocarbon of interest to form a $M(hydrocarbon)^+$ adduct. Total source pressures were typically 1-5 x 10^{-3} Torr, monitored with a Baratron capacitance manometer. The ratio of volatile metal compound and hydrocarbon pressures was

approximately 1:1, and was varied to maximize adduct signal. The source temperature was maintained at approximately -10° to 0° C to minimize the decomposition of metal-containing compounds on insulating surfaces. Ions exiting the source were accelerated to 8 keV and mass selected. Fragment ions from metastable decomposition in the second field-free region (downstream from the magnet) were energy analyzed with an electrostatic sector, and were detected using pulse counting techniques. The background pressure in the second field-free region is typically less than 10^{-9} Torr. The resolution of the main ion beam was typically 2 eV fwhm. At this resolution, the contribution of the main beam energy spread to the width of the kinetic energy release distribution in the center-of-mass reference frame is negligible.[11]

Raw data were smoothed using a moving average algorithm, and the kinetic energy release distribution was obtained from the metastable peak shape using published methods.[7]

The ion beam apparatus used in collisional stabilization studies of Co^+ reacting with propane has been described previously.[12] Briefly, beams of Co^+ are produced by vaporization of $Co(CO)_3NO$ onto a hot rhenium filament with subsequent surface ionization at 2500 K. The metal ions are collimated, mass and energy selected, and focussed into a collision chamber containing the neutral reactant and a non-reactive collision gas (CH_4, CF_4, or C_2D_6) at ambient temperature. The kinetic energy of the ion beam was the minimum for which the instrument would operate, yielding nominal

center-of-mass relative energies of approximately 0.2 eV. This is comparable to the thermal spread in ion energies, so the actual center-of-mass energy may be lower. The collisional stabilization buffer and reactant gases were added to the collision chamber using a dual inlet system. The buffer gas pressures used in these experiments ranged from 1 to 20 mTorr as measured by using a capacitance manometer. Product ions scattered in the forward direction are mass analyzed using a quadrupole mass spectrometer. The flight time of the ions through the apparatus is approximately 10-30 μs, which may be shorter than the excited-state lifetimes of metal ions. Although a substantial fraction of the ions in the beam (~15%)[13] are probably formed in thermally populated excited electronic states, no correction is made, and the observed reactions may have contributions from excited electronic states.

Results

Kinetic energy release distributions. The reactions studied are listed in Table I, along with reaction exothermicities and experimental average kinetic energy releases for each distribution, $\langle E_t \rangle_{exp}$. The reported values of $\langle E_t \rangle_{exp}$ are reproducible to better than 5%. The thermochemistry of these systems is reasonably well characterized (Appendix A), making it possible to use phase space theory to calculate statistical kinetic energy release distributions for each reaction, as well as average energy releases,

Table I. Average Kinetic Energy Releases from Experiment and Phase Space Theory.

	Reaction	$-\Delta H$	$\langle E_t \rangle_{exp}$ [a]	$\langle E_t \rangle_{calc}$ [b]	x [c]	$\langle E_t \rangle_{div}$ [d]
		(all energies eV)				
1	Co^+ + propane → $Co(ethene)^+$ + CH_4	1.04	0.099	0.150	5.	0.104
2	Co^+ + isobutane → $Co(propene)^+$ + CH_4	1.14	0.130	0.130	1.	0.130
3	Co^+ + neopentane → $Co(isobutene)^+$ + CH_4	1.175	0.105	0.124	3.	0.100
4	Fe^+ + propane → $Fe(ethene)^+$ + CH_4	0.598	0.080	0.124	6.	0.078
5	Fe^+ + butane → $Fe(propene)^+$ + CH_4	0.776	0.111	0.117	1.5	0.110
6	Fe^+ + butane → $Fe(ethene)^+$ + C_2H_6	0.447	0.077	0.087	2.	0.069
7	Fe^+ + isobutane → $Fe(propene)^+$ + CH_4	0.698	0.089	0.113	3.	0.084
8	Fe^+ + neopentane → $Fe(isobutene)^+$ + CH_4	0.798	0.079	0.109	3.	0.083

[a] Experimental average kinetic energy release.

[b] Calculated average kinetic energy release using phase space theory with $0 \leq J \leq J_{max}$ allowed.

[c] See text.

[d] Calculated average kinetic energy release using phase space theory with $0 \leq J \leq J_{max}/x$ allowed.

$\langle E_t \rangle_{calc}$. Details of the calculations are presented in Appendix B and discussed below. All of the reactions of Table I, with the exception of 2 (which is statistical), have average energy releases less than predicted by theory. The discrepancy between the experimental and statistical results is even more striking when the experimental and calculated distributions are plotted together, as in Figures 2-8.

Metastable intensities. Metastable intensities for the reactions of Fe^+ and Co^+ with propane, propane-d_2, and propane-d_8 are listed in Table II. These experiments are sensitive to metastables decomposing on a time scale of 5-15 μs, and hence show the relative populations of the various channels with unimolecular decomposition rates of 6.7×10^4 - 2.0×10^5 s^{-1}. In the metastable experiments involving propane, we detect the low-energy portion of the distribution of internal energies. This is confirmed by rate calculations employing phase space theory and assuming an orbiting transition state for dissociation of the ion-molecule association complex adduct. The calculations give an average adduct lifetime of about 4 μs at a collision energy of 0.5 kcal/mol (see Appendix B for details). If the rate-limiting step involves a C-D bond, the effect of deuteration is to shift the observed metastables to a higher range of internal energies to obtain the same rate constants. The ion beam is depleted at higher energies since most high-energy adducts decompose before reaching the second field-free

Figure 2. Experimental kinetic energy release distribution for demethanation of propane by Co^+ (solid line), and distributions calculated using phase space theory with no restrictions on angular momentum (solid circles) and with angular momentum restricted to values less than or equal to $J_{max}/5$ (open circles). Calculations assumed $D_0^0(Co^+$-ethene) = 42 kcal/mol.

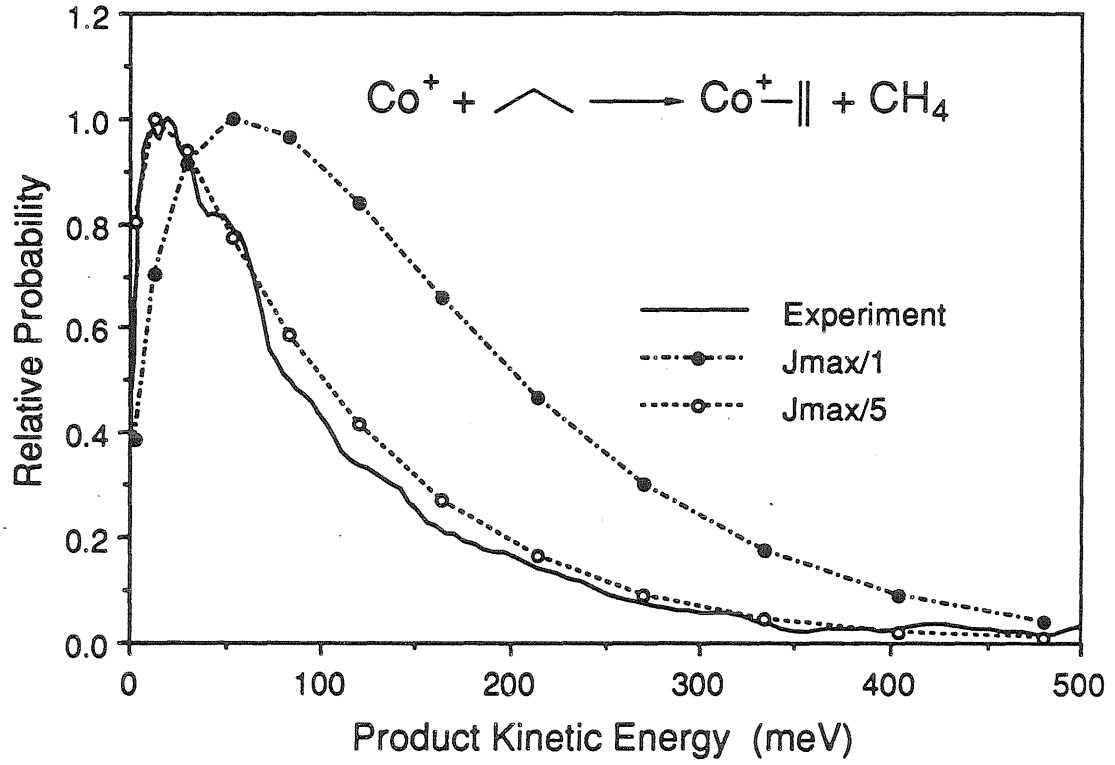
1.2
1.0
0.8
0.6
0.4
0.2
0.0
Relative Probability
0
100
200
300
400
500
Product Kinetic Energy (meV)
Co+ + ⟶ Co+—‖ + CH4
Experiment
Jmax/1
Jmax/5

Figure 3. Experimental kinetic energy release distribution for demethanation of propane by Fe^+ (solid line), and distributions calculated using phase space theory with no restrictions on angular momentum (solid circles) and with angular momentum restricted to values less than or equal to $J_{max}/6$ (open circles). Calculations assumed $D_0^0(Fe^+$-ethene) = 32 kcal/mol.

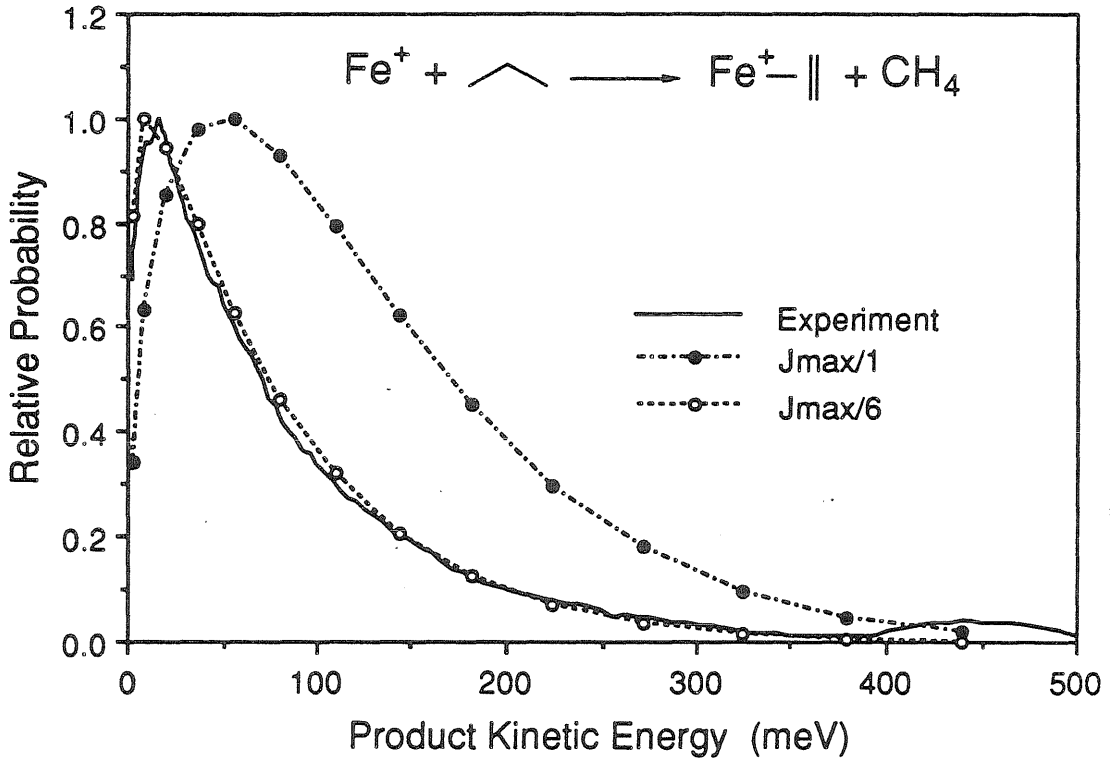
Fe+ + ⌒ ⟶ Fe+—‖ + CH4
Relative Probability
1.2
1.0
0.8
0.6
0.4
0.2
0.0
0
100
200
300
400
500
Product Kinetic Energy (meV)
Experiment
Jmax/1
Jmax/6

Figure 4. Experimental kinetic energy release distribution for demethanation of n-butane by Fe^+ (solid line), and distributions calculated using phase space theory with no restrictions on angular momentum (solid circles) and with angular momentum restricted to values less than or equal to $J_{max}/1.5$ (open circles). Calculations assumed $D_0^0(Fe^+$-propene) = 34 kcal/mol.

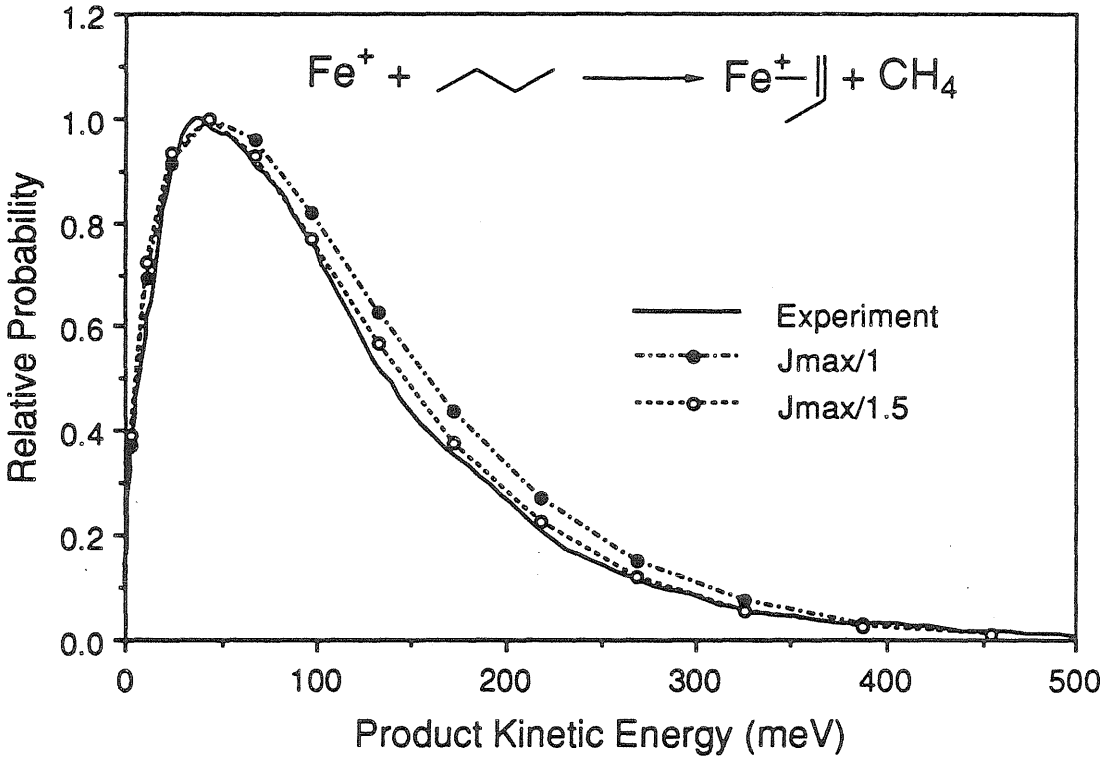
Fe+ +
Fe+ + CH4
Experiment
Jmax/1
Jmax/1.5
Relative Probability
Product Kinetic Energy (meV)
0.0
0.2
0.4
0.6
0.8
1.0
1.2
0
100
200
300
400
500

Figure 5. Experimental kinetic energy release distribution for loss of ethane from metastable Fe^+(n-butane) (solid line), and distributions calculated using phase space theory with no restrictions on angular momentum (solid circles) and with angular momentum restricted to values less than or equal to $J_{max}/2$ (open circles). Calculations assumed $D_0^0(Fe^+$-ethene) = 32 kcal/mol.

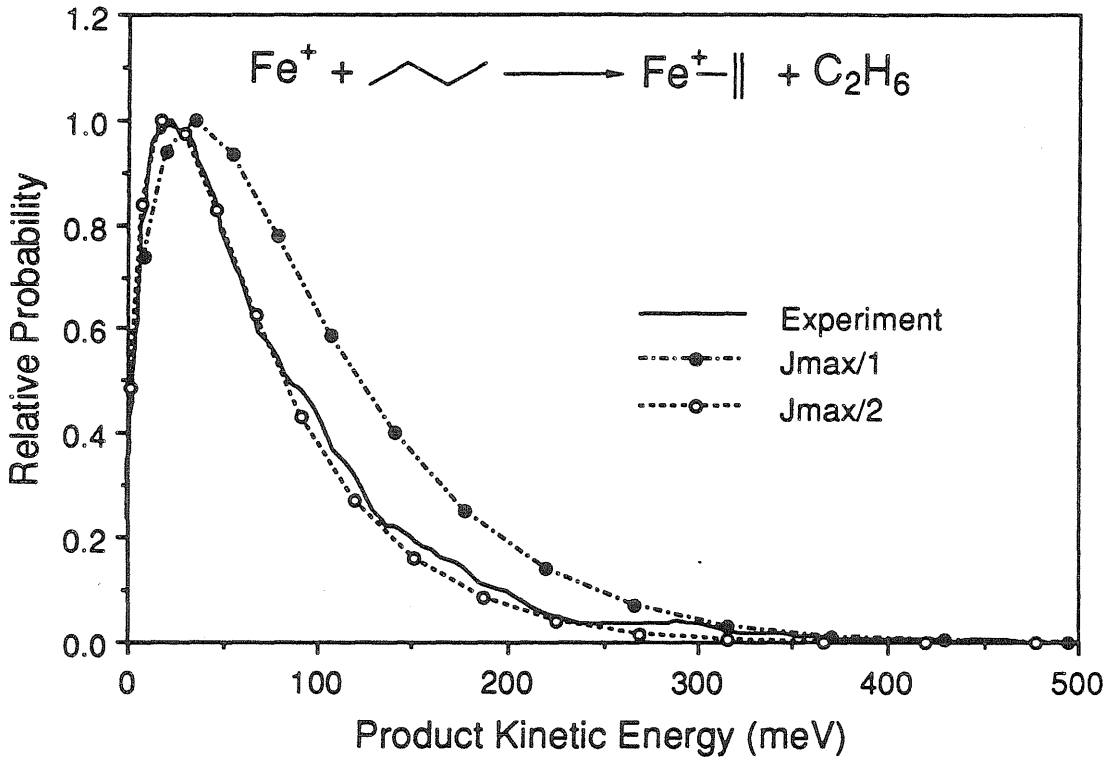
Fe+ + → Fe+–‖ + C2H6
Relative Probability
1.2
1.0
0.8
0.6
0.4
0.2
0.0
0
100
200
300
400
500
Product Kinetic Energy (meV)
Experiment
Jmax/1
Jmax/2

Figure 6. Experimental kinetic energy release distribution for demethanation of isobutane by Fe^+ (solid line), and distributions calculated using phase space theory with no restrictions on angular momentum (solid circles) and with angular momentum restricted to values less than or equal to $J_{max}/3$ (open circles). Calculations assumed $D_0^0(Fe^+$-propene) = 34 kcal/mol.

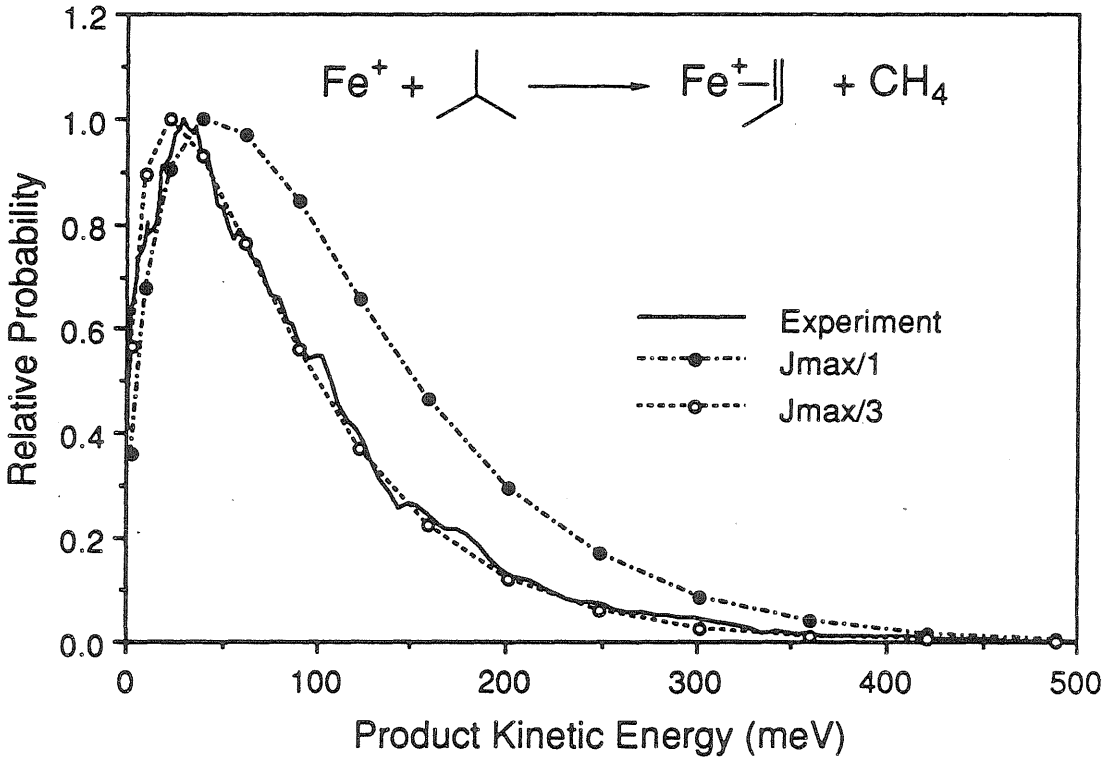
Fe+ +
Fe+
+ CH4
Experiment
Jmax/1
Jmax/3
Relative Probability
Product Kinetic Energy (meV)
0.0
0.2
0.4
0.6
0.8
1.0
1.2
0
100
200
300
400
500

Figure 7. Experimental kinetic energy release distribution for demethanation of neopentane by Fe^+ (solid line), and distributions calculated using phase space theory with no restrictions on angular momentum (solid circles) and with angular momentum restricted to values less than or equal to $J_{max}/3$ (open circles). Calculations assumed $D_0^0(Fe^+$-isobutene) = 36 kcal/mol.

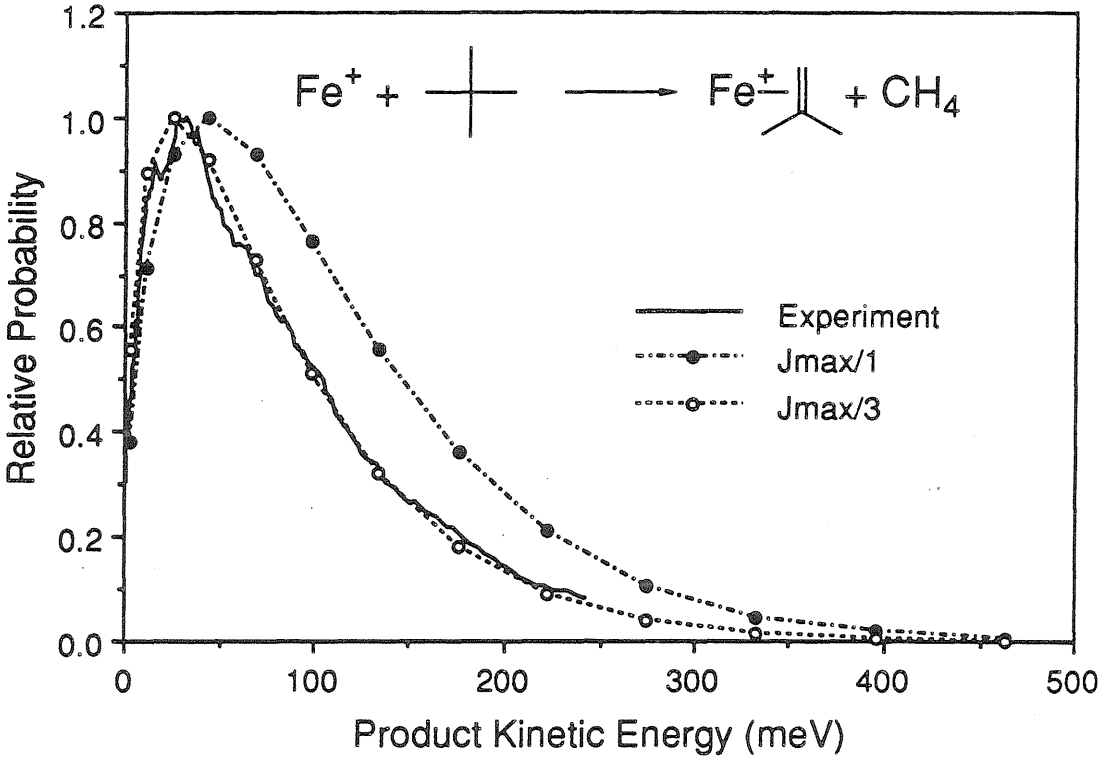
1.2
1.0
0.8
0.6
0.4
0.2
0.0
Relative Probability
0
100
200
300
400
500
Product Kinetic Energy (meV)
Fe+ +
Fe+
+ CH4
Experiment
Jmax/1
Jmax/3

Figure 8. Experimental kinetic energy release distribution for demethanation of neopentane by Co^+ (solid line), and distributions calculated using phase space theory with no restrictions on angular momentum (solid circles) and with angular momentum restricted to values less than or equal to $J_{max}/3$ (open circles). Calculations assumed $D_0^0(Co^+$-isobutene) = 46 kcal/mol.

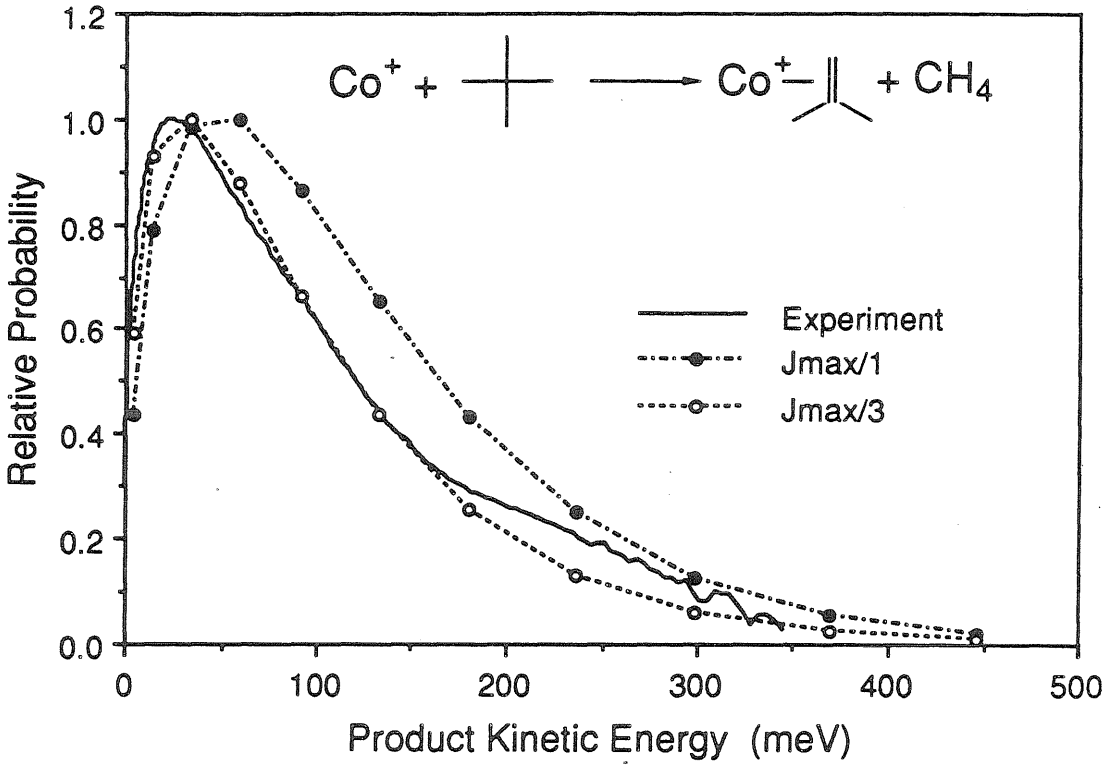
Co+ +
Co+
+ CH4
Experiment
Jmax/1
Jmax/3
Relative Probability
1.2
1.0
0.8
0.6
0.4
0.2
0.0
0
100
200
300
400
500
Product Kinetic Energy (meV)

Table II. Metastable Product Branching Ratios for Deuterium-Substituted Propanes

Neutral Product	Metastable Ion	
	$Co(propane)^+$	$Fe(propane)^+$
H_2	77.	40.
CH_4	2.	25.
C_3H_8	21.	35.
	$Co(propane\text{-}2,2\text{-}d_2)^+$	$Fe(propane\text{-}2,2\text{-}d_2)^+$
H_2	<1.	0.
HD	53.	6.
CH_4	4.	22.
CH_3D	0.	0.
$C_3H_6D_2$	43.	70.
	$Co(propane\text{-}d_8)^+$	$Fe(propane\text{-}d_8)^+$
D_2	41.	0.
CD_4	<1.	<1.
C_3D_8	59.	100.

region, so the net outcome of deuterating a bond involved in the rate-limiting step is to decrease the metastable intensity for the resulting product channel.

Inspection of Table II shows the effects of deuteration on metastable intensities. Trends are similar for Fe^+ and Co^+, but will be discussed with reference to the Fe^+ results, since they are more pronounced for the Fe^+ case. A major change in metastable intensities occurs on substitution of D for H in the 2 position. Very little H_2 loss is observed, indicating that 1,3 dehydrogenation is negligible. This also shows that scrambling is not important in the dehydrogenation process, indicating that the β-H transfer involved is not reversible. Further, the sum of the H_2 and HD channels is a substantially smaller fraction of the products than was H_2 loss from un-deuterated propane. The methane loss channel is essentially unaffected, while adduct decomposition to reactants accounts for most of the decrease in dehydrogenation, as expected. For perdeuterated propane, both demethanation and dehydrogenation are greatly reduced, to the extent that these channels are not observed in the reaction with Fe^+.

Collisional stabilization studies. The lifetimes of metal ion-hydrocarbon adducts can be estimated by examining the rates at which they can be collisionally stabilized.[14] Figure 9 displays the results of experiments where products of the reaction of Co^+ with propane were measured as a function of the pressure of an inert collision gas.

Figure 9. Product distributions for the reactions of Co^+ with propane as a function of the pressure of inert collision gases (a) CF_4, (b) CH_4, and (c) C_2D_6. The plotted product yields are normalized such that Σ(products) = 1.

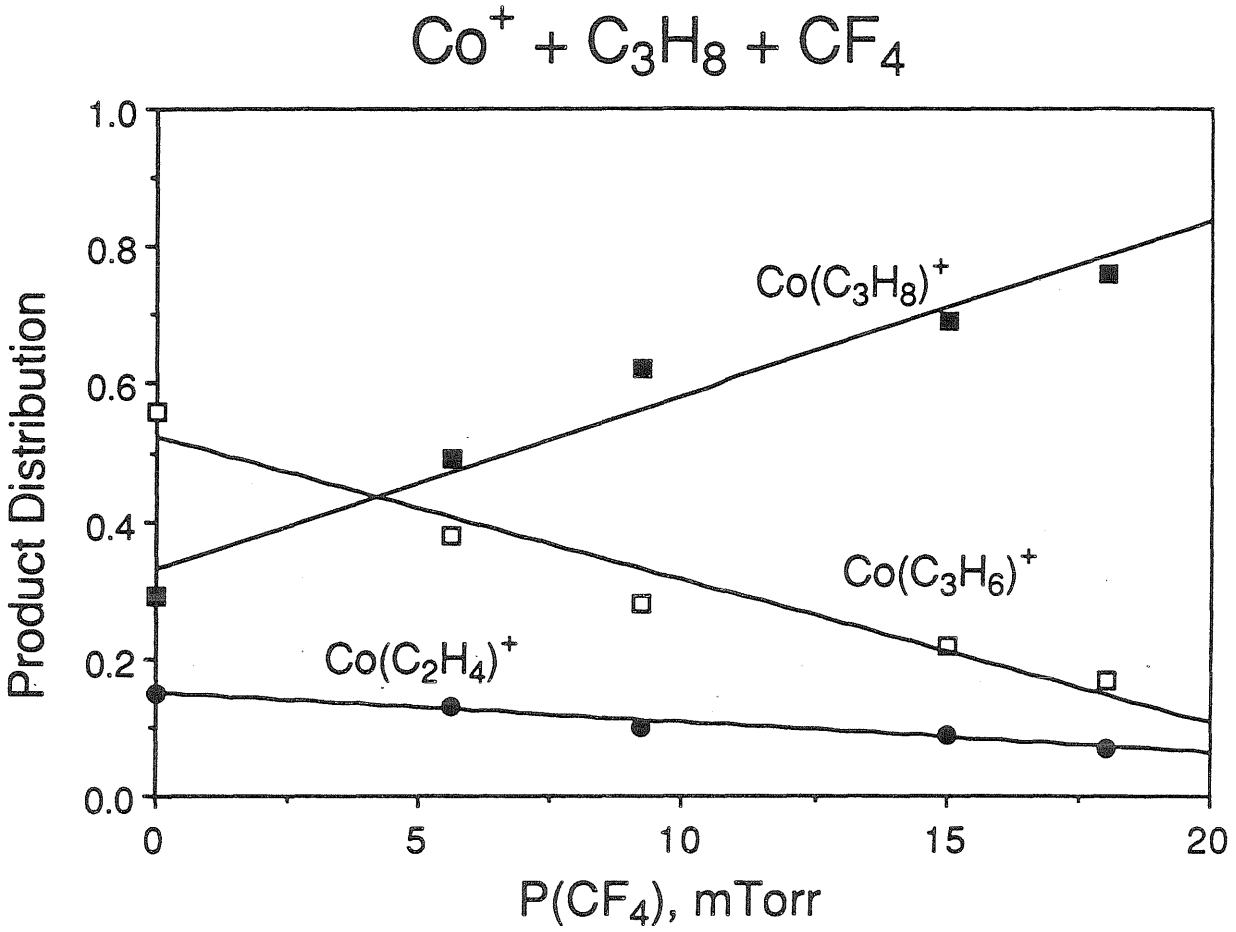
Co+ + C3H8 + CF4
Product Distribution
1.0
0.8
0.6
0.4
0.2
0.0
0
5
10
15
20
P(CF4), mTorr
Co(C3H8)+
Co(C3H6)+
Co(C2H4)+

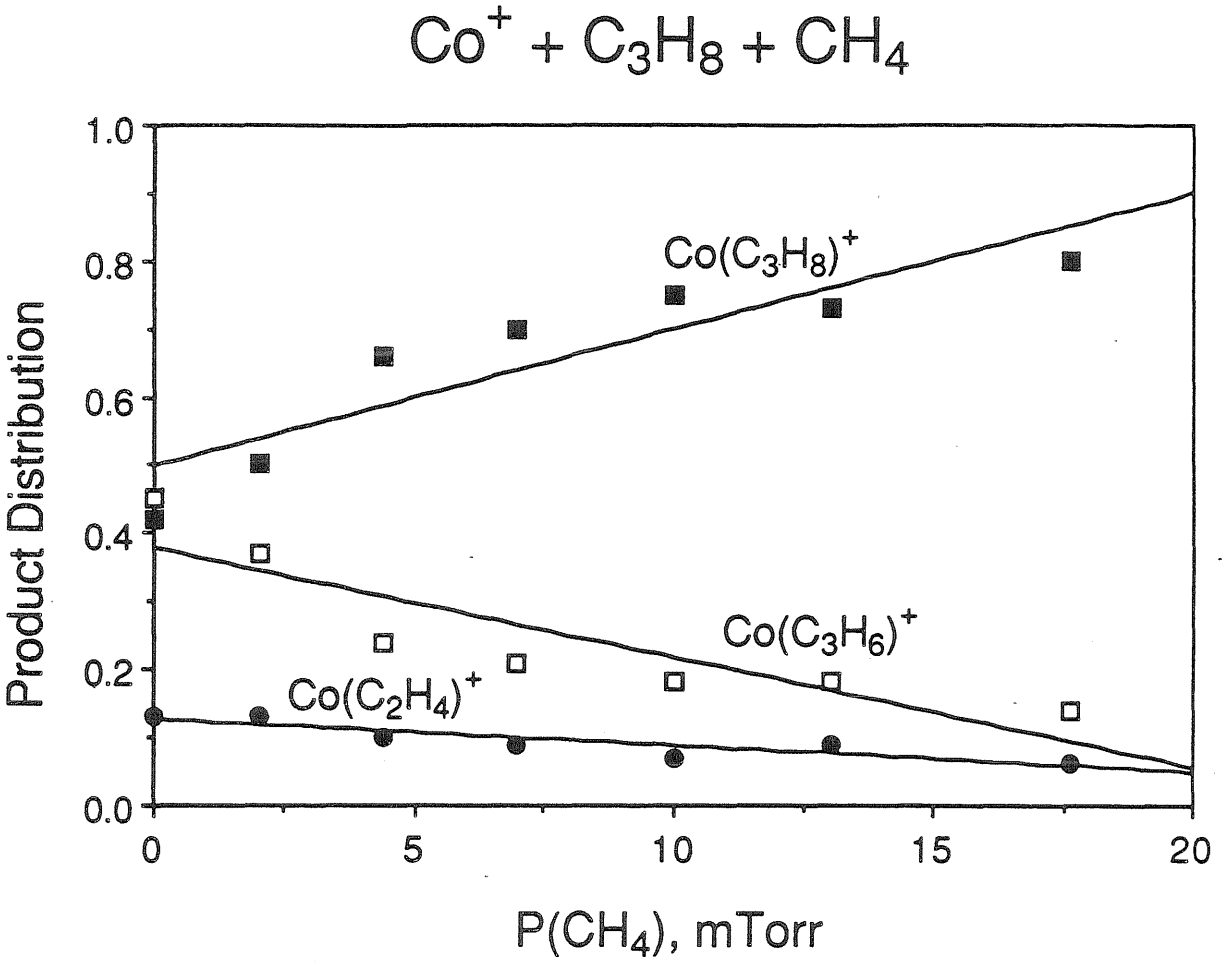
$Co^+ + C_3H_8 + CH_4$
Product Distribution
1.0
0.8
0.6
0.4
0.2
0.0
0
5
10
15
20
$P(CH_4)$, mTorr
$Co(C_3H_8)^+$
$Co(C_3H_6)^+$
$Co(C_2H_4)^+$

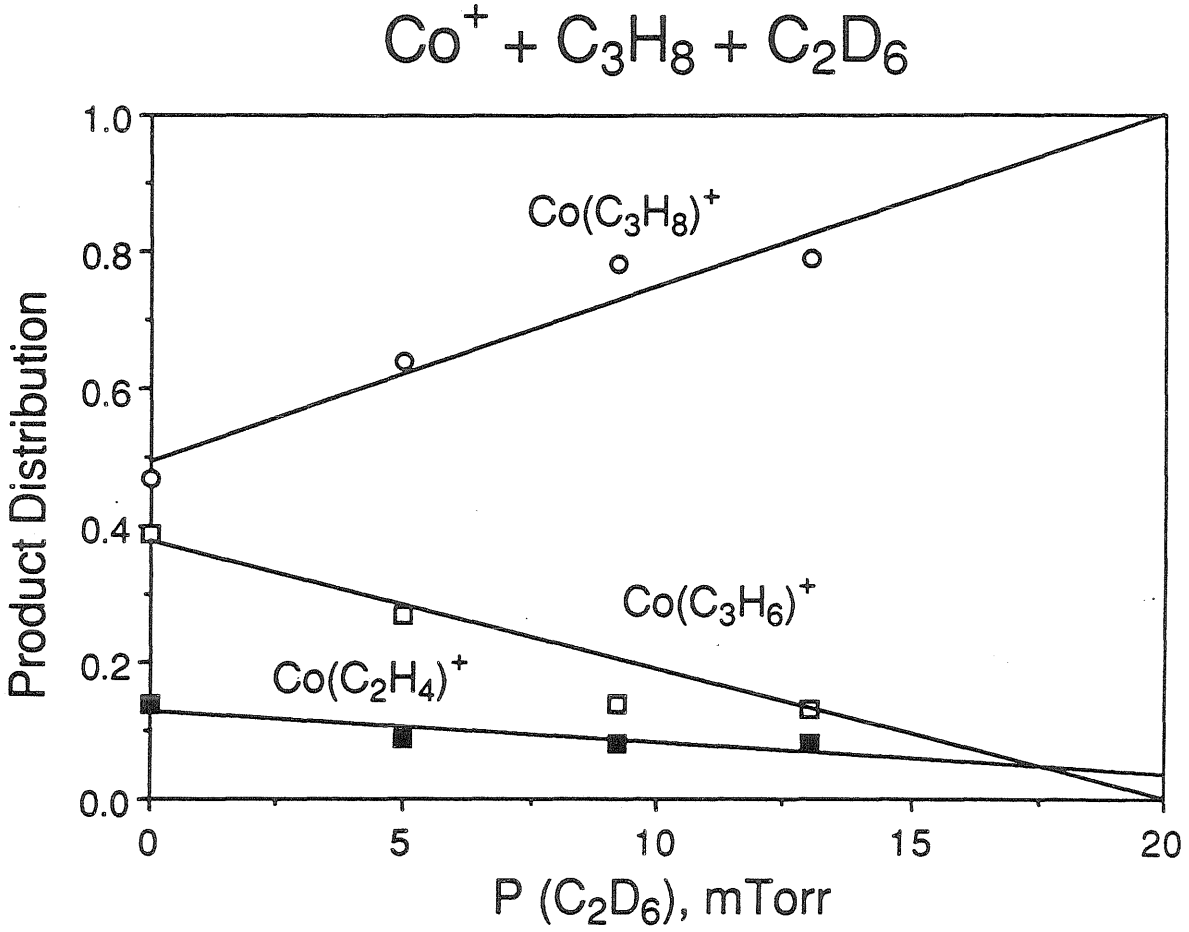
$Co^+ + C_3H_8 + C_2D_6$
Product Distribution
1.0
0.8
0.6
0.4
0.2
0.0
0
5
10
15
20
P (C_2D_6), mTorr
$Co(C_3H_8)^+$
$Co(C_3H_6)^+$
$Co(C_2H_4)^+$

The collision gases employed were CF_4, CH_4, and C_2D_6. Some variations in branching ratios for elimination of H_2 and CH_4 from the collision complex are evident with the different collision gases. At a CF_4 pressure of 1 mTorr, the average time between collisions of the adduct with CF_4 is 27 μs.[15] This is comparable to the 10-30 μs required for ions to transit the instrument, so even at the lowest pressures used, adducts with lifetimes longer than about 30 μs have a significant chance of undergoing collisions such that they can be stabilized and observed. However, most adducts will have lifetimes substantially less than 30 μs, since adduct signal is small on the 10 μs time scale of an ion beam experiment[16] and the calculated adduct lifetime is only 4 μs at 0.5 kcal/mol collision energy. Hence, the collisional stabilization experiment is biased toward adducts with low internal energies and long lifetimes.

Discussion

The J restriction model for kinetic energy release. What accounts for translationally cold energy release? One possibility can be quickly dismissed. If the M(alkane)$^+$ adduct were to undergo collisions in the source, the resulting loss of energy might produce a narrow kinetic energy release. Two factors argue strongly against this. First, similar systems studied at comparable pressures yield statistical kinetic energy release distributions,[5,6] indicating that deactivating collisions are not important.

Second, assuming that each collision is strongly deactivating, the experiment is biased against such collisionally stabilized species, since the metastable signal intensity from such species is much less than that from unstabilized species containing the full energy generated in adduct formation.

Another possibility arises from the method used to produce the metastable ions. Electron impact on either $Co(CO)_3NO$ or $Fe(CO)_5$ results in a number of fragment ions in addition to the atomic metal ion. Rather than forming the $[M^+(alkane)]^*$ metastable by direct association of the atomic metal ion with the alkane (reaction 9), it is possible that the alkane displaces a ligand X from a metal-containing fragment ion (reaction 10, for example), with the departing ligand carrying away energy and leading to a cooler metastable than would be produced in the direct association.

$$M^+ + \text{alkane} \rightarrow [M^+(\text{alkane})]^* \qquad (9)$$

$$MX^+ + \text{alkane} \rightarrow [M^+(\text{alkane})]^* + X \qquad (10)$$

This possibility can be discounted (if reactants are in their ground states) for the case of $MX^+ = CoCO^+$, alkane = propane, since the overall reaction producing $Co(ethene)^+$ and CH_4 is 8 kcal/mol endothermic. The overall thermodynamics for this reaction with X = NO should be even less favorable. Thermochemical information is not available to rule out the possible influence of displacement reactions in every case, but for the

results reported here displacement is not believed to be important.

A third possibility involves discrimination in the instrument used to study kinetic energy release. The metastable ions studied in this work are formed by bimolecular ion-molecule reactions. The instrument is selective for ions moving in the direction of the exit slit of the source chamber. In cases where the orbital angular momentum L_i generated in the collision is much larger than the rotational angular momentum of the reactants, the total angular momentum J in the collision complex will be dominated by L_i, and will in general lie in a plane perpendicular to the ion beam in the source. This condition is satisfied in the present studies, where the most probable reactant rotational angular momenta for thermal propane and neopentane are 6.8 $h/2\pi$ and 10.3 $h/2\pi$, versus values of 156 $h/2\pi$ and 200 $h/2\pi$ for L_{max} in collisions of Co^+ with propane and neopentane, respectively. The beam direction is rotated 60° as it passes through the magnetic sector, while the plane containing J remains in its initial orientation. The instrument is sensitive for the products of metastable decompositions scattered in the forward or backward direction of the ion beam. Other product velocity directions tend to scatter products out of the entrance of the electrostatic sector so that they are not detected. If angular momentum is conserved chiefly through product orbital angular momentum L_f, the relative velocity of the products will lie chiefly in a plane with a normal inclined 30° from the beam direction. Hence, the instrument discriminates against collisions where angular momentum is conserved mainly through L_f,

in favor of those where the final angular momentum lies more in the rotation of product molecules. Therefore, when J is dominated by L_i, the instrument geometry causes the experiment to be selective for products which are translationally somewhat colder, and rotationally somewhat hotter, than those expected if instrument geometry were not a factor.

The angular distribution of products in crossed beam reactions of alkali metals with alkali salts,[17] and of alkali salts with alkali salts,[18] has been determined previously. The product distribution is strongly peaked in the forward and reverse directions. The dynamics of these alkali salt reactions are similar to those of the present case in that L_i dominates J, with cross sections much larger than the physical size of the molecules. Measurements of product angular distributions more directly relevant to the current experiments have been made for the gas phase dehydration reaction of Li^+ with *tert*-butyl alcohol.[19] These studies also found that the product distribution is strongly peaked at 0° and 180°. The analysis of product angular distributions developed for the alkali salt reactions can be used to estimate the effect of instrumental discrimination on the present results. If it is assumed that we observe only products scattered at 0° and 180° with respect to the beam direction, the corresponding angle between the relative velocity of the reactants and that of the products is 30°. However, at this observation angle there is very little discrimination due to differences in product rotational temperatures,[20] especially at the relatively low product rotational temperatures which should accompany large kinetic energy

releases. It is unlikely that instrumental discrimination of this type has a large effect on the observed kinetic energy releases.

A second type of instrumental discrimination is possible. This type occurs because the only metastables observed are those which decompose within a narrow time window of approximately 5-15 μs after exiting the ion source. If most of the metastable population is decomposing slowly with respect to this time window, the experiment will be biased in favor of observing metastables which decompose more rapidly than average. Faster than average decomposition may occur if the internal energy of the metastable is greater than average, but high metastable energies are inconsistent with the experimental results since this would also lead to a broadening of the kinetic energy release distribution rather than the observed narrowing. Faster than average decomposition can also occur for complexes formed with small impact parameter. For metastables with a given internal energy, those which were formed at small impact parameter will decompose more rapidly than those formed at large impact parameter, since in the latter case a larger fraction of the available energy is fixed in the overall rotation of the complex and is unavailable for promoting decomposition. This concept is dealt with in more detail below. This type of discrimination should become increasingly important for larger alkanes, since decomposition rates decrease with alkane size due to the increase in quantum state density with size. This explanation cannot account for the distributions observed in the demethanations of propane and the isomeric

butanes, since, as is detailed below, the distributions for the propane reactions are translationally colder than those for the butanes. It may be important for larger alkanes.

A more likely explanation also derives from the influence of angular momentum conservation on reaction dynamics.[21] A two body collision can be described classically in center-of-mass coordinates as the interaction of a particle of reduced mass μ with an attractive potential V(r), where r is the mutual separation of the particles. For a collision between an ion and a nonpolar molecule, V(r) is well described at long range using the theory of Langevin, Gioumousis, and Stevenson (hereafter denoted LGS theory).[22] For nonzero impact parameters b, the effective potential V_{eff} governing the collision is given by equation 11, where E_{rel} is the relative kinetic energy of the system in the center-of-mass frame, q is the ion charge, and α is the neutral polarizability.

$$V_{eff} = -(q^2\alpha)/(2r^4) + E_{rel}(b/r)^2 \qquad (11)$$

The repulsive centrifugal term is inversely dependent on r^2. The result of adding the two terms is the creation of a centrifugal barrier in V_{eff} for sufficiently small values of E_{rel} and b. The maximum impact parameter, b_o, for which the system can surmount the centrifugal barrier, and the corresponding ion-neutral separation, r_o, are easily calculated.[22]

Both LGS theory and the phase space calculations used to model kinetic energy release assume that for a given value of E_{rel}, all collisions with $b < b_o$ are reactive. In the phase space calculation, the problem is cast in terms of the total angular momentum J of the collision complex, which is in turn determined by the vector sum of the rotational angular momentum of the reactants and the orbital angular momentum generated by the collision. If the total angular momentum of the system is too large, the collision complex cannot form and the collision is nonreactive. The maximum value of J for a given E_{rel}, J_{max}, for which a capture collision can occur, is determined using LGS capture theory in a straightforward manner.[22]

Consider the schematic potential surface of Figure 10, leading to alkane elimination. If reactants collide with energy and impact parameter such that the centrifugal barrier can be surmounted, they sample the first well of Figure 10 and form an adduct stabilized by the attractive ion-molecule interaction. Subsequent steps involve insertion of M^+ into the C-H and C-C bonds of the alkane, and reductive elimination of a smaller alkane. Bond insertion, and the accompanying barrier, occur at a M^+-alkane separation $r = r_i$. A crucial point is that $r_i < r_o$. For example, in reaction 1, assuming E_{rel} = 1 kcal/mol (a typical thermal energy), r_o calculated using LGS theory[23] is 5.7 Å, while we estimate values of 2-3 Å for r_i.

Figure 10. Schematic potential energy surfaces for demethanation of an alkane HR by a transition metal ion M^+. The lower surface represents a collision with J = 0, while the partial upper surface includes (exaggerated) centrifugal contributions which are present for J > 0. A trajectory with relative energy such as that shown for the dotted arrows can proceed to products on the J = 0 surface, but is reflected back to reactants by the insertion barrier for sufficiently large values of J.

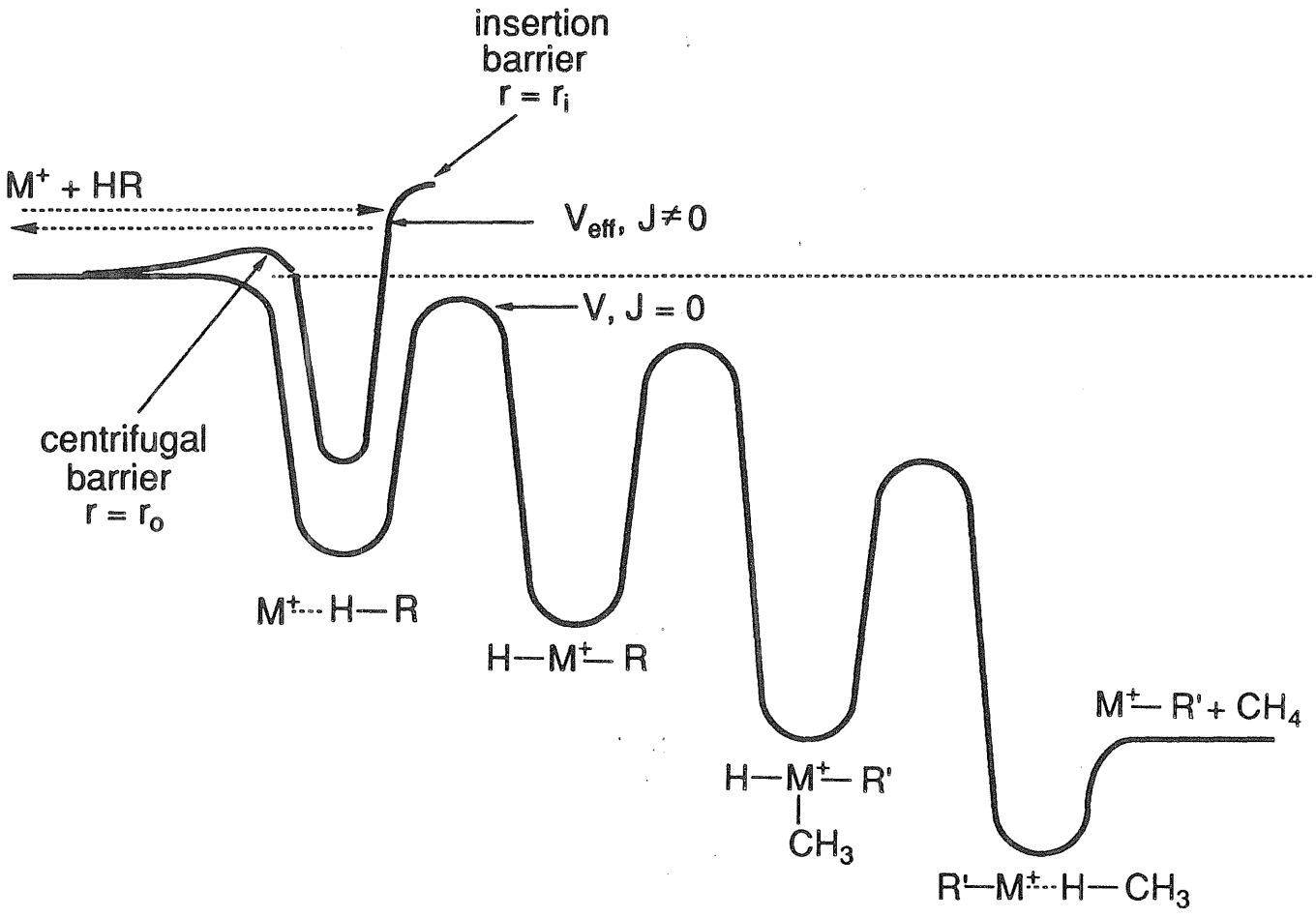
insertion
barrier
r = r_i
$M^+ + HR$
V_{eff}, J≠0
V, J = 0
centrifugal
barrier
r = r_o
$M^{\pm}$···H—R
H—$M^{\pm}$—R
H—$M^{\pm}$—R'
CH_3
$M^{\pm}$—R' + CH_4
R'—$M^{\pm}$···H—CH_3

Consequently, the centrifugal contribution to V_{eff} is greater at the insertion barrier than at the centrifugal barrier, since this contribution is inversely proportional to r^2. If the barrier to insertion is large enough, it is possible that the system can cross the centrifugal barrier and still be unable to approach closely enough to undergo insertion. Trajectories such as that of the dotted arrow in Figure 10, which can result in adduct formation, are reflected at the effective insertion barrier.

To summarize, at a given energy, on a potential surface such as that of Figure 10, with a barrier approaching the asymptotic energy of the reactants, angular momentum has a profound effect on the outcome of capture collisions. For capture collisions involving large angular momentum, the non-fixed energy available for reaction is decreased since conservation of angular momentum requires that most of the energy be fixed in rotation. A consequence is that the lifetime of the collision complex is *increased* in such a collision, since the number of dissociating states accessible (including those which dissociate back to reactants) is decreased at low non-fixed energy. States which lead to insertion chemistry may be completely inaccessible, even though a long-lived complex can form. Hence, in collisional stabilization experiments, large angular momentum collisions resulting in long-lived adducts are those which are most likely to be collisionally stabilized, while collisions with low angular momentum produce shorter-lived complexes which may exit to products before collisional stabilization can occur.

Potential energy surface barriers below the reactant asymptotic energy have been invoked before to explain the large range of reaction efficiencies observed for gas phase nucleophilic displacement reactions involving attack of anionic nucleophiles on substituted methanes.[24] The branching ratio between dissociation of a long-lived complex back to reactants and rearrangement leading to products was modeled using a potential energy surface with double wells, representing reactant- and product-like anion-molecule complexes, separated by a barrier corresponding to an S_N2 transition state. The analysis compared the transition states leading back to reactants and forward to products. Reaction rates less than the LGS collision rate were explained by noting that the sum of vibrational and rotational quantum states for the transition state leading back to reactants is greater than the corresponding sum for the transition state leading to products. This "entropic" model does not consider the effects of angular momentum, and has been applied to potential energy surfaces which are approximately symmetric about the central barrier. This contrasts with the J restriction model, which explicitly considers angular momentum and which assumes that angular momentum restriction can occur at a barrier anywhere on the potential energy surface between reactants and products (although most likely the barrier is an early one).

A similar treatment which treats phase space bottlenecks in terms of entropic restrictions has been applied to the reaction of Li^+ with *tert*-butyl alcohol,[19] reaction 12.

$$Li^+ + (CH_3)_3COH \rightarrow Li(C_4H_8)^+ + H_2O \qquad (12)$$
$$\rightarrow Li(H_2O)^+ + C_4H_8$$

In that study, ions from both product channels were observed, as well as Li^+ resulting from decomposition of the collision complex back to reactants. Phase space theory was used to model the translational energy release, with the restriction that the transition state was placed at a fixed product separation of 5 Å rather than allowing the position of the transition state to vary with product translational energy. The theoretical calculation gave a reasonable fit to experiment at low product kinetic energies, but underestimated the high kinetic energy portion of the distribution.

The J restriction model predicts that the existence of a barrier on the potential energy surface with an energy near the energy of the reactants should be experimentally observable in at least two ways. First, the discrimination against large angular momentum should be manifested as a reduction in the high kinetic energy release portion of the product kinetic energy distribution, since large values of J contribute to the higher kinetic energy portion of the distribution. To demonstrate this effect, phase space calculations of kinetic energy release were carried out as a function of impact parameter in the following manner. The total range of allowable J, from 0 to J_{max}, was divided into four regions of equal cross sectional area by considering i) $0 \leq J \leq J_{max}/2$, ii) $J_{max}/2 \leq J \leq J_{max}/2^{1/2}$, iii) $J_{max}/2^{1/2}$

$\leq J \leq 3^{1/2}J_{max}/2$, iv) $3^{1/2}J_{max}/2 \leq J \leq J_{max}$. It should be pointed out that for a given energy, assuming that the orbital angular momentum generated by an ion-molecule collision dominates the total angular momentum of the collision complex, each allowable value of J up to the orbiting value corresponds to a unique value of b. Kinetic energy release distributions were calculated for each of the four regions, with the results given in Figure 11 modeling the demethanation of isobutane by Fe^+. The figure shows that collisions with large impact parameter account for broader kinetic energy release distributions than those with small impact parameter. The narrowing of the distribution with impact parameter is a direct consequence of the restriction of the phase space available to the system, imposed by restricting the impact parameter (and total angular momentum) to small values. This effect is not predicted by the entropic model.[24]

Second, the total reaction cross section for bond insertion processes should be less than that predicted by LGS capture theory. Capture collisions with large angular momentum will not lead to bond insertion, but rather will result in dissociation back to reactants. Both the J restriction model and the entropic model predict this effect.

Fitting experimental distributions using the J restriction model. According to the analysis given above, it should be possible to model translationally cold kinetic energy release using statistical theory, as long as care is taken to exclude contributions from capture collisions involving large

Figure 11. The effect of impact parameter b on the shape of the kinetic energy release distribution, calculated using phase space theory for the demethanation of isobutane by Fe^+. The distribution was calculated separately for each region as follows, where b_o is the orbiting impact parameter: i) $0 \leq b \leq b_o/2$, ii) $b_o/2 \leq b \leq b_o/2^{1/2}$, iii) $b_o/2^{1/2} \leq b \leq 3^{1/2}b_o/2$, iv) $3^{1/2}b_o/2 \leq b \leq b_o$. Each region accounts for 1/4 of the orbiting cross section. Restricting the impact parameter results in a narrower distribution of product kinetic energies.

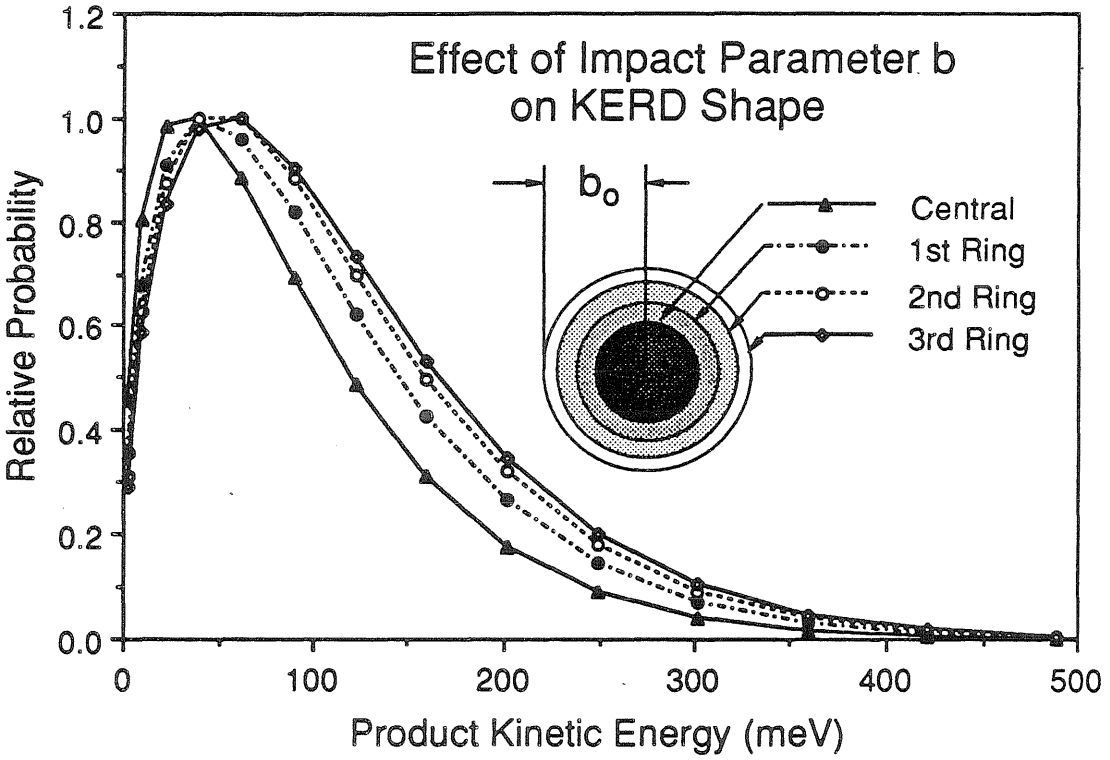
Effect of Impact Parameter b
on KERD Shape
b_o
Central
1st Ring
2nd Ring
3rd Ring
Relative Probability
1.2
1.0
0.8
0.6
0.4
0.2
0.0
0
100
200
300
400
500
Product Kinetic Energy (meV)

angular momentum, which do not result in product formation. Since the general features of the potential energy surface exit channel are the same as in previously studied cases of statistical alkane elimination[5,6] (i. e., the last feature of the exit channel before product separation is a well, where statistical partitioning of energy between product internal modes and relative translation occurs, rather than a barrier, which would force energy into the reaction coordinate and hence into product translation), a modified phase space calculation which excludes large angular momentum capture collisions from the products should be able to reproduce the experimental results.

To test the model, calculations were performed as follows. In the algorithm normally employed for our phase space calculations, LGS collision theory is used to calculate a maximum value for the total angular momentum of the orbiting transition state, J_{max}, for each value of reactant relative energy. All values of angular momentum less than or equal to J_{max} are included in the integrals used to calculate the kinetic energy release distribution.[8] For the translationally cold distributions reported here, the same calculations were carried out with one modification: instead of integrating from 0 to J_{max}, high angular momentum capture collisions were prevented from contributing to product kinetic energy release by changing the upper limit of the integral to a value J_{max}/x, with $x > 1$. In all other respects, the phase space calculation was performed in the usual manner. Kinetic energy release distributions calculated in this way are included in Figures 2-8. Consistent with the J restriction model, in all cases it was

possible to achieve good fits to the experimental data. The value of x needed to produce a good fit, given for each reaction in Table I, serves as a simple means of quantifying the effect.

The values of x listed in Table I exhibit several interesting trends. For both Fe^+ and Co^+, the effect is seen to decrease in going from propane to isobutane. This is a reflection of the increasing polarizability of the alkane with size. Greater polarizability corresponds to deepening of the first well of Figure 10, the ion-molecule association complex, such that the energy of subsequent barriers along the surface is decreased relative to the reactant asymptotic energy. As a result, for a given collision energy, as the size of the alkane increases, the range of impact parameters which can access the product channels is increased, and the product kinetic energy release distribution is broadened toward the statistical limit where all impact parameters up to the orbiting value contribute. This limit is reached in the reaction of Co^+ with isobutane, where $x = 1$. For larger alkanes, the trend reverses. Possible reasons for this reversal are discussed below.

Comparison of the results for Fe^+ and Co^+ with a given alkane is also informative. In the two cases for which data are available, a larger value of x is required to fit the data for Fe^+ than for Co^+. The ion-induced dipole interaction between each of these two transition metal ions and an alkane should be approximately the same, so the difference must be due to differences in how easily the metal ion can insert into the bonds of the alkane. It has been argued previously[4] that C-H insertion is less

facile for Fe^+ than for Co^+, due to differences in the electronic configurations of the ground states of these ions. The ground state of Fe^+ derives from a $3d^6 4s^1$ electronic configuration, while that of Co^+ derives from $3d^8$.[25] Based on electrostatic, molecular orbital, and spin arguments, occupancy of the 4s orbital is expected to be destabilizing with respect to C-H insertion, even though the resulting bonds are expected to be stronger for Fe^+ than for Co^+.[26] The kinetic energy release results, as well as the results of deuterium labeling, support the conclusion that the barrier to C-H insertion is larger for Fe^+ than for Co^+.

Variations in reaction mechanism due to the geometry of the alkane are also reflected in the extent to which the kinetic energy release distribution is narrowed by angular momentum effects. For demethanation of n-butane by Fe^+, $x = 1.5$ was sufficient to fit the data, while for demethanation of isobutane, $x = 3$ was required. The polarizabilities of these two alkanes are essentially equal, so the depth of the adduct well cannot account for the difference. A plausible explanation comes from a closer look at the proposed mechanisms. Methane loss from n-butane involves insertion into a *secondary* C-H bond, whereas for isobutane only insertion into a *primary* C-H bond can result in demethanation. Since the secondary bond is several kcal/mol weaker than the primary,[27] the barrier to insertion is lower in n-butane than in isobutane, allowing a fuller range of impact parameters to result in products for the n-butane case. As a result, the demethanation of n-butane is almost fully statistical, although

methane loss from isobutane exhibits a larger J restriction effect. A similar explanation can account for the differences between losses of methane and ethane in the reaction of Fe^+ with n-butane. Once again, the J restriction effect is larger in the case of ethane loss (x = 2), which involves insertion into a secondary C-H bond, than in the case of methane loss (x = 1.5), which results from primary C-H insertion. Small differences in the height of the barrier to insertion can have profound effects on the kinetic energy release distribution.

Experimental Consequences: Reaction Cross Sections. In cases where cross section information at low relative energy is available, the results can be compared with the predictions based on conservation of angular momentum made above. Cross sections at low collision energy are listed in Table III in terms of fractions of σ_{LGS}. It should be noted that in these experiments adducts which dissociate back to reactants on a time scale of less than tens of μsec are not detected. The implication is that the difference between the total experimentally measured cross section and the LGS collision cross section is due to adducts which form and quickly decompose.

Qualitatively, the correlation between cross sections and the magnitude of the J restriction effect is good for alkanes smaller than neopentane. In cases where x is large, the cross section is reduced to values substantially

Table III. Total Reaction Cross Sections Relative to the Langevin Collision Cross Section

Reaction	σ^a/σ_{LGS}	$(1/x^2)^b$
Co^+ + propane → all products	0.07[c]	
Co^+ + propane → $Co(ethene)^+$ + CH_4	0.02[c]	0.04
Co^+ + propane → $Co(propene)^+$ + H_2	0.05[c]	
Co^+ + isobutane → all products	1.00[c]	
Co^+ + isobutane → $Co(propene)^+$ + CH_4	0.67[c]	1.00
Co^+ + isobutane → $Co(C_4H_8)^+$ + H_2	0.33[c]	
Co^+ + neopentane → $Co(C_4H_8)^+$ + CH_4[d]	0.80[e]	0.11
$Fe^+(^6D)$ + propane → all products	0.13[f]	
$Fe^+(^6D)$ + propane → $Fe(ethene)^+$ + CH_4	0.10[?, f]	0.03
$Fe^+(^6D)$ + propane → $Fe(propene)^+$ + H_2	0.03[?, f]	

[a] σ is the cross section measured in an ion beam experiment at minimum relative energy (typically about 0.05-0.2 eV in the center of mass frame).

[b] Values of x, defined in the text, are taken from Table I. The value $1/x^2$ should serve as an upper limit to σ/σ_{LGS}.

[c] Georgiadis, R.; Fisher, E. R.; Armentrout, P. B. *J. Am. Chem. Soc.*, submitted for publication.

[d] This is the only product observed from these reactants.

[e] Armentrout, P. B., personal communication. These values have an error of ±0.2.

[f] Schultz, R. H.; Elkind, J. L.; Armentrout, P. B. *J. Am. Chem. Soc.* 1988, *110*, 411-423.

Table III continued

Reaction	σ^a/σ_{LGS}	$(1/x^2)^b$
$Fe^+(^6D, {}^4F)^g$ + isobutane → all products	0.50[e]	
$Fe^+(^6D, {}^4F)^g$ + isobutane → $Fe(propene)^+$ + CH_4	0.33[e]	0.11
$Fe^+(^6D, {}^4F)^g$ + isobutane → $Fe(C_4H_8)^+$ + H_2	0.17[e]	
$Fe^+(^6D, {}^4F)^g$ + neopentane → $Fe(C_4H_8)^+$ + CH_4[d]	0.80[e]	0.11

[g]Cross section measured using a surface ionization source at approximately 2300 K, including contributions from both ^6D (approximately 80%) and ^4F (approximately 20%) states. See Elkind, J. L.; Armentrout, P. B.; *J. Am. Chem. Soc.* 1986, *108*, 2765-2767; *J. Phys. Chem.* 1986, *90*, 5736-5745.

less than the LGS collision rate. For example, the cross sections for demethanation of propane by Fe^+ and Co^+ are 10% and 2% of σ_{LGS}, respectively, while the values of x required to fit the methane loss kinetic energy release in these two cases are 6 and 5, respectively. Changes in the branching ratios for losses of CH_4 and H_2 at higher relative Co^+-propane energies have also been explained by postulating a barrier in the potential surface near the reactant asymptotic energy,[28] and the current results support that assertion.

As was noted, the magnitude of the J restriction effect decreases in going from propane to the isomeric butanes. One implication is that when barriers to bond insertion are substantially less than the reactant asymptotic energy, as with the larger, more polarizable alkanes, the cross sections for bond insertion processes should approach the LGS collision cross section. Comparison of the cross sections for demethanation of propane and isobutane by Fe^+ and Co^+, and the corresponding values of x for the methane loss channels in each case, shows that both trends occur as predicted. As alkane size increases, the kinetic energy release distribution approaches that predicted when each orbiting collision leads to reaction, and cross sections approach σ_{LGS}. The LGS limit is reached in the reaction of Co^+ with isobutane, where the total cross section is the same as the LGS collision cross section, and the kinetic energy release for the methane loss channel is fully statistical with no restrictions on J.

Quantitatively, the relation between cross sections and the J restriction effect is less clear. Restriction of J to a maximum of J_{max}/x corresponds to a reduction in cross section σ_{LGS} to σ_{LGS}/x^2, since at fixed energy each J corresponds to one value of b. In the absence of instrumental J discrimination, the σ_{LGS}/x^2 value should represent an upper limit, since it does not take into account competing reaction channels. For reaction 1, a value of 5 for x implies that an upper limit to σ should be 4% of σ_{LGS}, in agreement with the literature cross section reported in Table III, which is 2% of σ_{LGS}. The experimental data and phase space fits are also in agreement for reaction 2, with a measured cross section 67% of σ_{LGS} compared with a predicted upper limit of 100%. In other cases the quantitative agreement is poor. For example, fits to the kinetic energy release distribution for demethanation of propane, isobutane, and neopentane by Fe^+, and of neopentane by Co^+, underestimate the experimental cross sections in each case. The reasons for this lack of agreement are not known. Cross section measurements at low relative energy are difficult due to the thermal energy distribution of ions in the beam. Uncertainty in the small rotational constants for large product molecules may also affect the phase space calculations. Further, if steric factors favor certain directions for the final relative velocity of the products, or if the critical configuration determining the partitioning of angular momentum between product rotation and orbital motion is oblate, rather than prolate,[17] instrumental discrimination may become important. Discrimination in favor of small J due to

observation in a narrow time window may also be important. Both of these latter problems are expected to increase in significance with alkane size.

Finally, the possibility that D(M^+-alkene) decreases in the series ethene, propene, isobutene should be considered. To investigate, it was attempted to use phase space theory to fit the methane loss KERD for reaction 3, by reducing the reaction exothermicity rather than by restricting J. The results of those calculations are shown in Figure 12. The best fit achieved implied D(Co^+-isobutene) = 26 kcal/mol, far weaker than expected. Further, it was not possible to reproduce the experimental KERD at all kinetic energies by this method, since the shape of the calculated KERD was inappropriate. This contrasts with the fit obtained using J restriction, where the proper shape resulted. This constitutes strong evidence that angular momentum restriction, not inaccurate thermochemistry, accounts for the observed translationally cold distributions. While weak M^+-alkene bond energies cannot be completely ruled out, we consider that explanation unlikely.

Mechanistic considerations. Assuming that the most likely steps leading to intermediates from which reductive elimination of H_2 or small alkanes can occur are C-H and C-C insertions, followed by β-H or β-alkyl transfers, the mechanisms of Scheme I can be constructed. Previous work

Figure 12. Comparison of the fit obtained using a strong (46 kcal/mol) Co^+-isobutene bond and restricting J to values less than or equal to $J_{max}/3$ (solid circles) with that obtained assuming a weaker (26 kcal/mol) Co^+-isobutene bond and no restrictions on J, both for demethanation of neopentane by Co^+. The best fit to the experimental data (solid line) is given by assuming the stronger bond and restricting J.

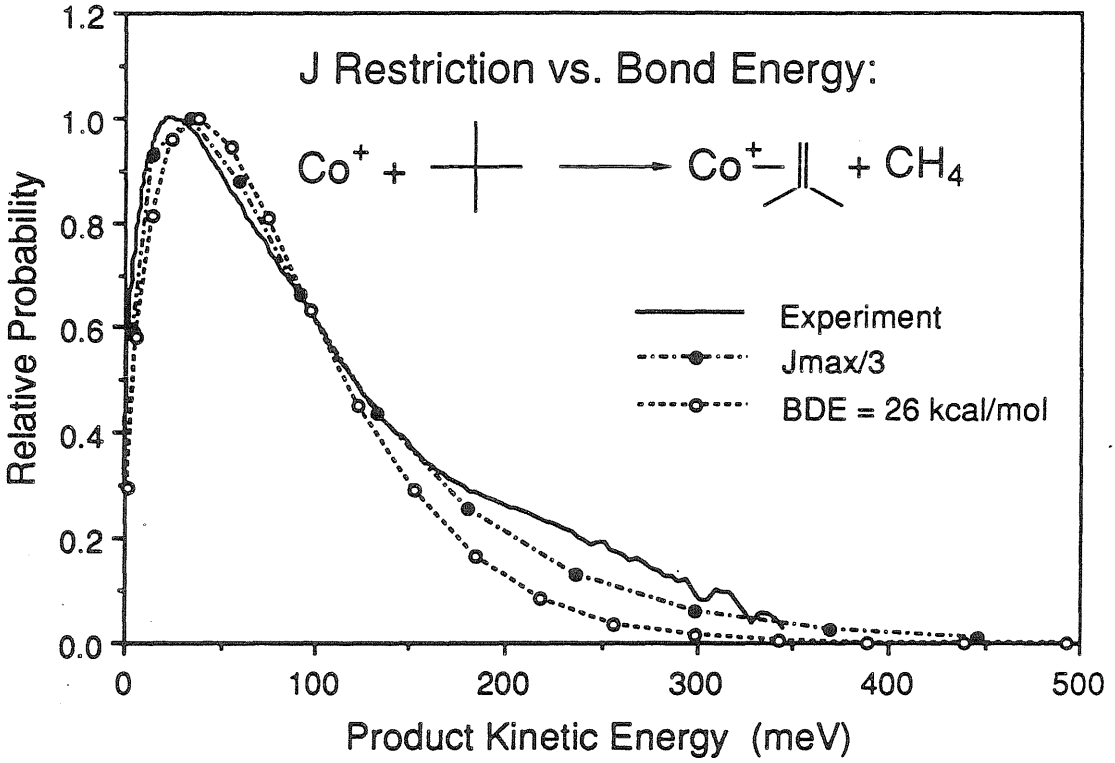
J Restriction vs. Bond Energy:
Co+ +
Co+
+ CH4
Experiment
Jmax/3
BDE = 26 kcal/mol
Relative Probability
1.2
1.0
0.8
0.6
0.4
0.2
0.0
0
100
200
300
400
500
Product Kinetic Energy (meV)

Scheme I. Mechanistic pathways for reactions of Co^+ with propane, isobutane, and neopentane.

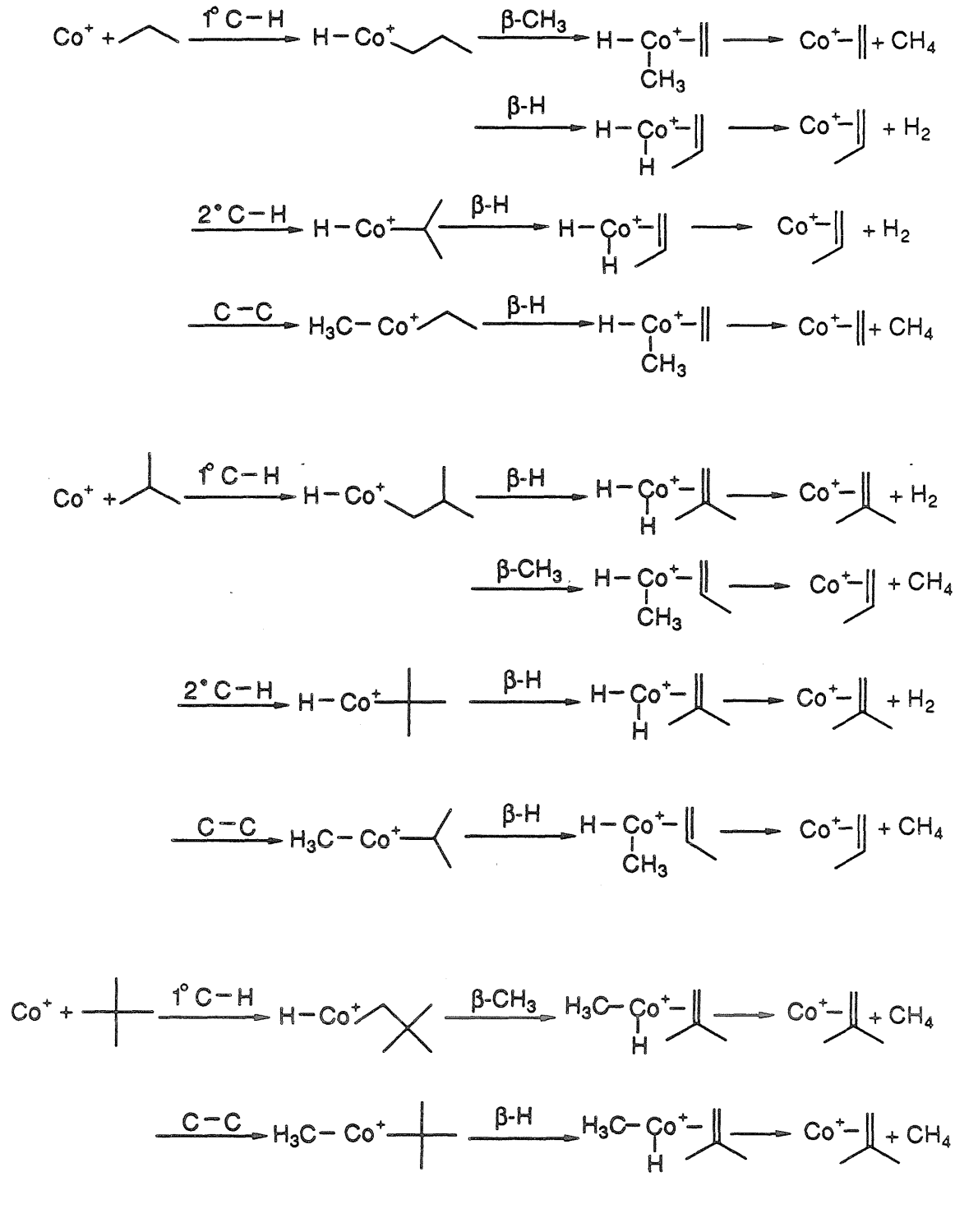
Co+ + 1° C–H → H–Co+ β-CH3 → H–Co+–CH3 → Co+– + CH4
β-H → H–Co+–H → Co+– + H2
2° C–H → H–Co+ β-H → H–Co+–H → Co+– + H2
C–C → H3C–Co+ β-H → H–Co+–CH3 → Co+– + CH4
Co+ + 1° C–H → H–Co+ β-H → H–Co+–H → Co+– + H2
β-CH3 → H–Co+–CH3 → Co+– + CH4
2° C–H → H–Co+ β-H → H–Co+–H → Co+– + H2
C–C → H3C–Co+ β-H → H–Co+–CH3 → Co+– + CH4
Co+ + 1° C–H → H–Co+ β-CH3 → H3C–Co+–H → Co+– + CH4
C–C → H3C–Co+ β-H → H3C–Co+–H → Co+– + CH4

in the gas phase[3c] and in solution[29] indicates that these mechanistic assumptions are reasonable. The simplest case is that of neopentane, which contains only primary C-H bonds. Demethanation, which is the only observed reaction channel, can result from initial insertion into a C-C bond, followed by β-H transfer, or from C-H insertion followed by β-CH_3 transfer. In propane and isobutane, both primary and secondary C-H bonds are present and the mechanistic pathways are similar. Both demethanation and dehydrogenation are possible if insertion into the primary C-H is the first step, but initial insertion into the secondary C-H results only in dehydrogenation. Likewise, demethanation is the only product channel resulting from insertion into the C-C bond. For n-butane, the situation is complicated by the presence of both primary and secondary C-C bonds, and numerous reaction pathways. Consequently, the n-butane case will not be discussed further.

Metastable branching ratios for deuterium-labeled propanes reacting with Fe^+ and Co^+ shed some light on the mechanistic possibilities. The large decrease in dehydrogenation for propane-2,2-d_2 indicates that either metal insertion into the secondary C-H, or M^+-H bond cleavage in the reductive elimination step, is rate-limiting for dehydrogenation. The fact that CH_4 loss is not affected by deuteration of the 2 position is also consistent with the proposed mechanism, which invokes initial insertion into the unlabeled primary C-H for methane production. The complete elimination of the methane loss channel in propane-d_8 indicates that C-H insertion is

also the rate-limiting step in methane production, and argues against the C-C insertion channel as a major source of methane. It is unlikely that the reductive elimination step is rate-limiting, since whatever barrier exists for this step should lie well below the reactant asymptotic energy. Based on first and second bond dissociation energies measured for $M(CH_3)_2^+$ species,[26] the C-C insertion step is estimated to be substantially exothermic; 11 kcal/mol for Fe^+, and 25 kcal/mol for Co^+.[30] If C-C insertion is the first step leading to demethanation, subsequent steps are expected to be fast because the C-C insertion step releases a large amount of non-fixed energy. The C-C insertion route to demethanation cannot easily account for the observed isotope effects, and is therefore considered unlikely.

Thermochemical estimates for the C-H insertion indicate that the process is likely to be exothermic, but are not as clear-cut as in the case of C-C insertion. If the strengths of the first and second M^+-H bonds are comparable, insertion into the secondary C-H should be exothermic for Fe^+ and Co^+ (by 13 and 3 kcal/mol, respectively), while primary C-H insertion is approximately 10 kcal/mol exothermic for Fe^+ and thermoneutral for Co^+.

More support for the proposed mechanisms comes from cross sections measured for the reactions of Co^+ with deuterated propanes.[31] Reaction cross sections for both the dehydrogenation and demethanation channels decrease with increasing deuteration, but the branching ratio between the two channels remains the same. Cross sections for propane-*2,2-d*$_2$ decrease slightly relative to propane, by a factor of about 1.5, while

those for propane-d_8 show a clear decrease to less than 1/3 those of propane. The reduction in cross section for dehydrogenation and demethanation is accompanied by a corresponding increase in that for formation of collisionally stabilized Co(propane)$^+$ adduct. This is consistent with insertion into the primary C-H bond being the initial, rate-limiting step for both product channels. The fact that identical branching ratios are obtained for propane-2,2-d_2 is curious, since it indicates that the isotope effect for β-H transfer is small and that β-deuteration has little effect on the yield of dehydrogenation relative to demethanation. Evidence for the relatively small significance of an isotope effect in β-H transfer reactions involving first-row transition metal ions is available from the literature. Branching ratios for H_2 and HD in the dehydrogenation of propane-2-d_1 by Ni^+ indicate that k_H/k_D for β-H transfer is about 1.3 or smaller.[3c]

To summarize, the propane data support the mechanism of Scheme I, where rate-limiting, initial insertion into a primary C-H bond leads to methane loss. It is unlikely that initial C-C insertion is responsible for demethanation. Insertion into either a primary or a secondary C-H bond in the first step, followed by β-H transfer, leads to dehydrogenation. For the latter process, it is unclear whether C-H insertion or the following β-H transfer is the rate-limiting step. Either is consistent with the data.

Reconciliation of single- and multiple-collision results: implications for the potential energy surface. Analysis of the kinetic energy release

results in light of the J restriction model gives insight into details of the potential energy surface and helps in interpreting results obtained by other methods. In this section the results of experiments conducted under high-pressure conditions will be compared with low-pressure, single-collision results. Emphasis will be placed on the Co^+-propane reaction, since it is the most extensively studied.

Inspection of Figure 9 reveals that, in the reactions of Co^+ with propane, adduct formation appears to be competitive with the dehydrogenation process. Growth of signal from collisionally stabilized adduct is accompanied by a corresponding decrease in the dehydrogenation channel, for all three collision gases. This implies a common intermediate in these two channels. Based on the mechanism of Figure 1, the Co^+-propane ion-molecule association complex is a reasonable choice for this intermediate. The demethanation channel appears to be quenched less efficiently than dehydrogenation for all three collision gases, indicating that demethanation proceeds through a different intermediate. However, it may be that the two types of intermediate are distinguished not by differences in their chemical structure, but by total angular momentum, J. As was noted above, only collisions with low J result in methane loss, since high J collisions cannot overcome the barrier to primary bond insertion leading to demethanation. It follows that collisions accessing the dehydrogenation channel, which may involve initial insertion into the secondary C-H bond, have a higher average J than those in the demethanation channel. However, larger J corresponds

to smaller non-fixed energy, and therefore to slower adduct decomposition. The adducts with large J are therefore longer lived, and more likely to undergo collisional stabilization, than the relatively short-lived, low J collisions. Phase space calculations were carried out to estimate the effect of J on adduct decomposition rate. The rate of Co^+-propane adduct decomposition back to reactants was calculated in three ways: i), allowing all values $0 \leq J \leq J_{max}$; ii), restricting the calculation to low J, such that $0 \leq J \leq J_{max}/3$; iii), restricting the calculation to high J, such that $J_{max}/3 \leq J \leq J_{max}$. For E_{rel} = 0.5 kcal/mol, the average decomposition rate for the high J case iii is less than 1/10 that obtained when J is restricted to low values (case ii).

If it is assumed that every collision results in stabilization, and further that dissociation of the adduct back to reactants and insertion of the metal into the C-H bond are competitive processes as in Scheme II, equation 13 can be used to determine an upper limit to the insertion rate.[14]

$$S/I = (k_s[C_3H_8] + k_s'[A])/(k_i + k_d) \qquad (13)$$

The ratio of stabilized adducts, S, to the dehydrogenation and demethanation products of C-H insertion, I, is given by this equation. Assuming $[C_3H_8] << [A]$, the slope of a plot of S/I as a function of [A] is $k_s'/(k_i + k_d)$. An upper limit for k_s' is easily calculated using LGS theory.[15] Assuming that every collision with an A molecule results in formation of a stabilized adduct, the calculation of an upper limit to $k_i + k_d$ is straightforward.

Scheme II. Kinetics for reactions of Co^+ with propane.

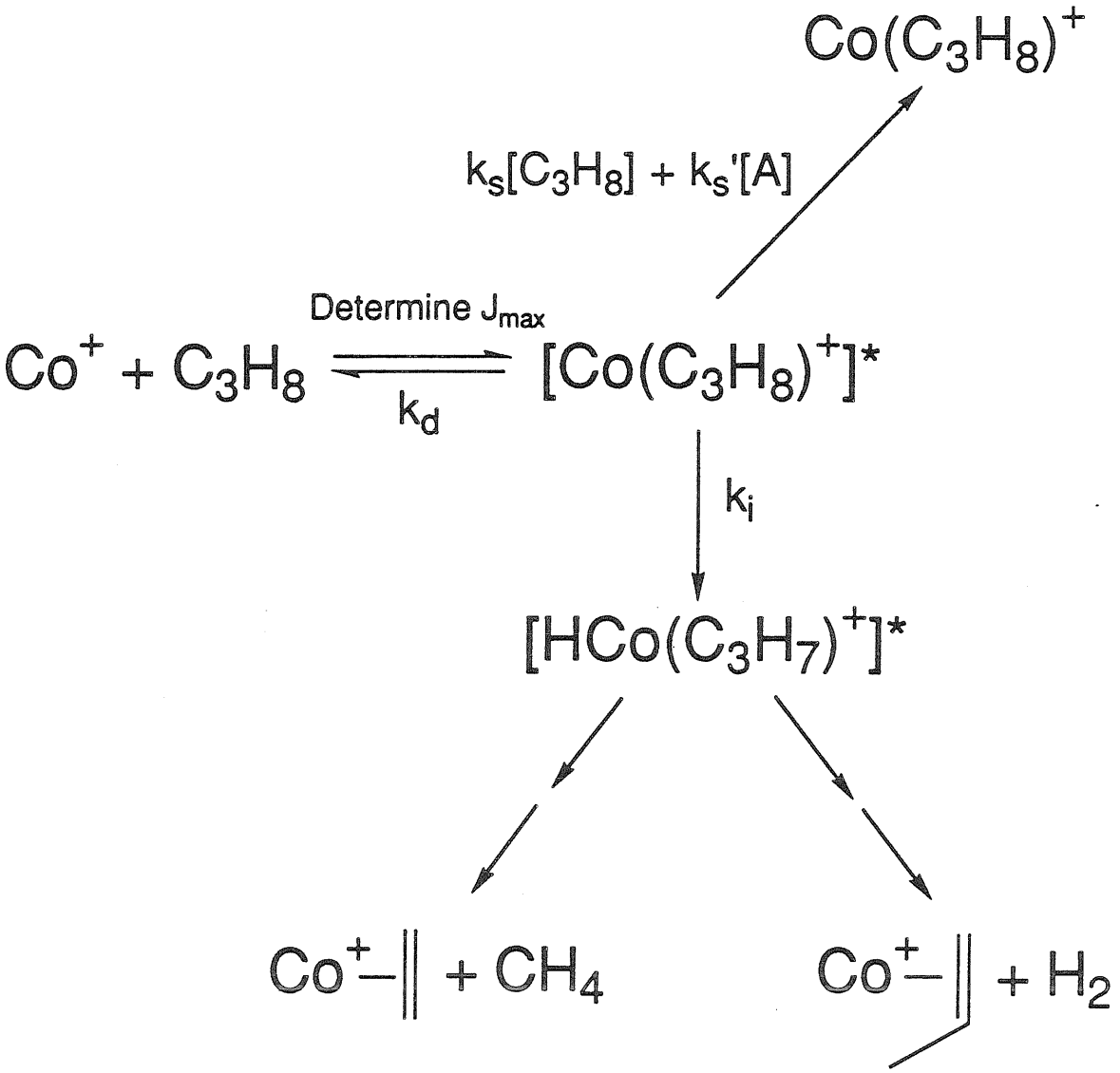
Co(C3H8)+
ksC3H8 + ks'A
Determine Jmax
Co+ + C3H8
kd
[Co(C3H8)+]*
ki
[HCo(C3H7)+]*
Co+ + CH4
Co+ + H2

Plots of S/I for CF_4, CH_4, and C_2D_6 collision gases are given in Figure 13, and the calculated upper limits for $k_i + k_d$ are listed in Table IV. These rates are within an order of magnitude of rates calculated assuming an orbiting transition state for decomposition of the adduct to reactants, and a tight transition state (log(A) = 13) for insertion into the C-H bond. The corresponding lifetimes are consistent with observation of these processes on a 10 μs time scale.

It is interesting to compare cross section measurements for the reaction of Co^+ with propane, taken under single collision conditions,[28] with those determined in the presence of 0.75 Torr He.[4] At low pressure, the total cross section for this reaction is about 7% of σ_{LGS}, while the high-pressure cross section is 83% of σ_{LGS}, with most of the difference being due to the additional channel observed at high pressure, formation of stabilized adduct. The results imply that nearly all Co^+-propane collisions result in formation of a hot adduct species, which in the absence of stabilizing collisions usually dissociates back to reactants. Dissociation to reactants is largely quenched at 0.75 Torr of He. The fact that the dehydrogenation and demethanation channels are only partially quenched indicates that the adduct lifetime with respect to these processes is comparable to the average time between collisions, which is about 80 ns at this pressure.[15] Two problems arise from this analysis. First, the high-pressure data[4] indicate that the bond insertion processes occur at rates less than or equal to 1.6×10^6 s^{-1}, while the upper limit derived above from pressure dependence data was about one order of magnitude lower.

Figure 13. Ratio of adduct signal to the sum of the signal from dehydrogenation and demethanation of propane by Co^+, as a function of the pressure of collision gas A (A = CF_4, CH_4, and C_2D_6).

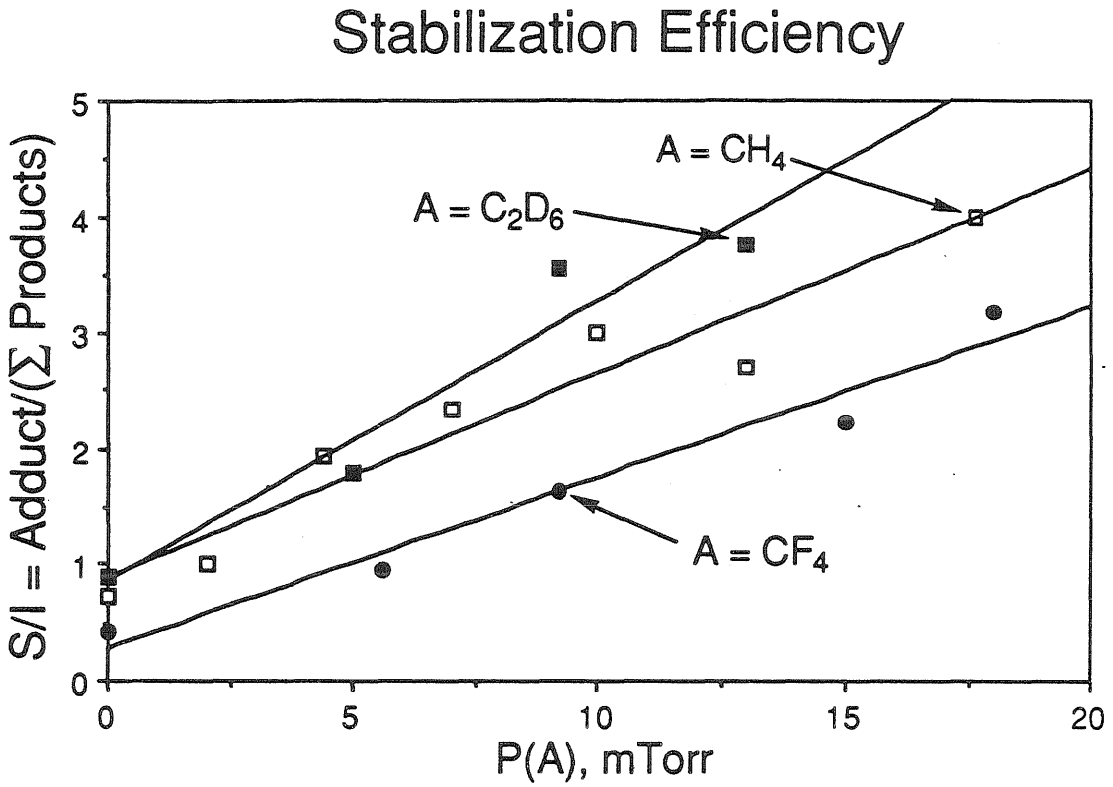
Stabilization Efficiency
S/I = Adduct/(∑ Products)
P(A), mTorr
A = CH4
A = C2D6
A = CF4
0
1
2
3
4
5
0
5
10
15
20

Table IV. Rate Constants for Stabilization and Decomposition of Co(propane)$^+$ Adduct

stabilization gas	k_s',[h] cm^3 $molecule^{-1}$ s^{-1}	$(k_i + k_d)$,[i] s^{-1}
CH_4	1.01×10^{-9}	1.9×10^5
CF_4	5.74×10^{-10}	1.3×10^5
C_2D_6	9.59×10^{-10}	1.3×10^5

[h]Gioumousis, G.; Stevenson, D. P. *J. Chem. Phys.* 1958, *29*, 294.

[i]Upper limit, details in text.

The discrepancy is easily resolved by noting that He is a poor collisional quenching gas,[32] so the higher limit obtained using He probably reflects the inefficiency of He as a quencher. Second, if the bond insertion processes are more rapid than decomposition to reactants, and nearly every orbiting collision leads to formation of an adduct, why are the cross sections for bond insertion not close to σ_{LGS}? The answer now is clear. Many collisions which result in adduct formation cannot yield insertion products because of barrier-imposed angular momentum constraints. Bond insertion, although rapid at low J, cannot occur in the majority of the collisions, and the slower adduct decomposition dominates.

Conclusions

Kinetic energy release measurements, metastable intensities for both isotopically labeled and unlabeled species, cross section measurements, and product branching ratios under single- and multiple-collision conditions are all consistent with the schematic potential energy surface of Figure 1. A likely first step in the reactions of Fe^+ and Co^+ with alkanes is formation of an ion-molecule association complex, which can subsequently undergo decomposition back to reactants or bond insertion processes which lead to elimination of H_2 or smaller alkanes. The observed isotope effects for deuterated propanes support insertion into the primary C-H bond as being the prevalent route for the latter processes. For Fe^+- and Co^+-propane, and probably for at least some of the larger alkanes as well, the transition

state leading to C-H insertion and eventual elimination of CH_4 lies at an energy near the reactant asymptotic energy.

The existence of this barrier and its proximity to the energy of the separated reactants has important consequences for the shape of the kinetic energy release distribution, causing the distribution to be narrower than predicted by statistical theory. While both J restriction and an entropic description of this type of potential energy surface rightly assert that the total reaction cross sections for product formation should be less than σ_{LGS}, the J restriction model has the advantage of a transition state with well-defined parameters, the orbiting transition state. The use of phase space theory with the J restriction model also correctly reproduces the experimental kinetic energy release distributions.

One characteristic which sets ion-molecule reactions apart from reactions between neutrals is that ion-molecule cross sections are quite large compared to the hard sphere "size" of the species involved. As a result, conservation of angular momentum in the reaction is largely dominated by the initial orbital angular momentum generated in the collision. Large orbital angular momenta are typical of the products in these reactions, and can have dominant effects on the kinetic energy release distribution. The shape of the distribution in turn yields information about the reaction probability as a function of the initial orbital angular momentum. Factors such as potential surface features near, but below, the reactant asymptotic energy can have a profound influence on whether a collision at a given energy

and impact parameter will lead to product formation. Such features, which are very difficult to observe by other methods, can easily be detected by their effects on the shape of the kinetic energy release distribution.

Acknowledgement. We thank the National Science Foundation for supporting this research through grant numbers CHE87-11567 (JLB) and CHE88-17201 (MTB). We are also grateful to the Shell Foundation for graduate fellowship funding (DVD), and to the donors of the Petroleum Research Fund, administered by the American Chemical Society, for additional support. In addition, we thank Peter Armentrout for providing us with a number of results prior to publication, and Denley Jacobson for some of the initial data collection.

Appendix A. Thermochemical Quantities

The phase space calculations depend strongly on reaction exothermicity, and hence on the bond energies chosen for the organometallic products. The bond energies used in the calculations are listed in Table AI, and justified here. The value of $D_0^0(Co^+\text{-propene})$, 44±5 kcal/mol, has been established through fitting the kinetic energy release distributions for reactions A1 and A2 using phase space theory, with $\Delta H^o_f(Co^+\text{-propene})$ as the only adjustable parameter. Both reactions yielded the same value.

$$Co^+ + \text{isobutane} \rightarrow \qquad \text{(A1)}$$

$$[Co^+(\text{isobutane})]^* \rightarrow Co(\text{propene})^+ + CH_4$$

$$Co^+ + \text{cyclopentane} \rightarrow \qquad \text{(A2)}$$

$$[Co^+(\text{cyclopentane})]^* \rightarrow Co(\text{propene})^+ + C_2H_4$$

This value can be compared with measurements which give $D_{298}^0(CpNi^+\text{-propene}) < 45$ kcal/mol.[33] For M = Co^+ or Ni^+, ligand exchange experiments under equilibrium conditions indicate that $M^+\text{-}(C_nH_{2n})_2$ bond strengths for small alkenes increase with increasing n, the increase being approximately 2-4 kcal for each CH_2 group added.[34]

Table AI. Bond Energies for Fe^+ and Co^+ to Alkenes

Bond	D_0^0 (kcal/mol)[a]
Fe^+-ethene	32.0±5
Co^+-ethene	42.0±5
Fe^+-propene	34.0±5
Co^+-propene	44.0±5
Fe^+-isobutene	36.0±5
Co^+-isobutene	46.0±5

[a]Bond energies based on discussion in Appendix A.

Accordingly, we estimate $D_0^0(Co^+\text{-ethene})$ to be 2 kcal/mol less than $D_0^0(Co^+\text{-propene})$, consistent with ion beam results which place a lower limit on $D_0^0(Co^+\text{-ethene})$ of 36 kcal/mol.[3a,b] The value of 34±5 kcal/mol for $D_0^0(Fe^+\text{-propene})$ is estimated from ion cyclotron resonance results where reaction A3 was observed and assumed to be exothermic while reaction A4 was not, and was assumed to be endothermic, yielding a value of 37±2 kcal/mol for $D_{298}^0(Fe^+\text{-propene})$.[35]

$$Fe^+ + \text{cyclopentane} \rightarrow Fe(\text{propene})^+ + C_2H_4 \qquad \text{(A3)}$$

$$Fe^+ + \text{cyclohexane} \rightarrow Fe(\text{propene})^+ + C_3H_6 \qquad \text{(A4)}$$

A value for $D_0^0(Fe^+\text{-ethene})$ can be estimated from the observation that dehydrogenation of ethane by Fe^+ is exothermic, implying $D_0^0(Fe^+\text{-ethene}) > 30$ kcal/mol[16, 27], and from photodissociation threshold measurements which indicate $D_0^0(Fe^+\text{-ethene}) < 39$ kcal/mol.[36] Consistent with these observations and the estimate above for $D_0^0(Fe^+\text{-propene})$, we estimate $D_0^0(Fe^+\text{-ethene}) = 32\pm5$ kcal/mol. Values for heats of formation used in this work are compiled in Table AII.

Table AII. Thermochemical Quantities Used in this Work[a]

Species	$\Delta H^{\circ}_{f,0\ K}$ (kcal/mol)
Co^{+}	282.5
Fe^{+}	280.4
CH_4	-16.0
C_2H_6	-16.4
C_3H_8	-19.6
n-C_4H_{10}	-23.5
iso-C_4H_{10}	-25.3
neo-C_5H_{12}	-32.4
methylcyclopentane	-15.3
C_2H_4	14.5
C_3H_6	8.3

[a]Values taken from the following: (1) Hanratty, M. A.; Beauchamp, J. L.; Illies, A. J.; van Koppen, P. A. M.; Bowers, M. T. *J. Am. Chem. Soc.* **1988**, *110*, 1-14. (2) van Koppen, P. A. M.; Jacobson, D. B.; Illies, A. J.; Bowers, M. T.; Hanratty, M. A.; Beauchamp, J. L. *J. Am. Chem. Soc.* **1989**, *111*, 1991-2001. (3) Lias, S. G.; Bartmess, J. E.; Liebman, J. F.; Holmes, J. L.; Levin, R. D.; Mallard, W. G. *J. Phys. Chem. Ref. Data, Supplement 1* **1988**, *17*. Where values at 0 K were not reported, values at 298 K were converted to 0 K following the conventions described in Stull, D. R.; Prophet, H. *JANAF Thermochemical Tables (NSRDS-NBS 37)*; 2nd Ed.; U. S. Department of Commerce, National Bureau of Standards; 1971.

Table AII continued

Species	$\Delta H^{\circ}_{f,0\ K}$ (kcal/mol)
isobutene	1.2
3-methylcyclopentene	10.2
$Co(ethene)^{+}$	255.
$Co(propene)^{+}$	247.
$Co(isobutene)^{+}$	239.
$Fe(ethene)^{+}$	263.
$Fe(propene)^{+}$	255.
$Fe(isobutene)^{+}$	2.

Appendix B. Rate Calculations

Rates were calculated using a statistical theory package available in the literature.[37] At each collision energy, J_{max} for the collision complex is determined using LGS collision theory.[15,22] This value functions as an upper limit for the integration over J, used to calculate sums of states for the activated complexes. Standard techniques from the phase space[38] and RRKM[39] descriptions, respectively, were used to treat the decomposition of the collision complex to reform reactants and to generate products of bond insertion processes. The initial insertion of the metal into an alkane C-H bond was assumed to be rate-limiting in the latter case. Equation B1 was employed to calculate unimolecular rate constants k_u for decomposition of the collision complex to reactants and for rearrangement to a bond-inserted structure, where E is the internal energy of the collision complex, $E^{\ddagger}$ is the non-fixed internal energy at the transition state, $W(E^{\ddagger})$ is the sum of states of the activated complex up to an energy $E^{\ddagger}$, h is Planck's constant, and $\rho^*(E)$ is the density of states of the collision complex at energy E.

$$k_u(E) = W(E^{\ddagger})/(h\rho^*(E) \qquad \text{(B1)}$$

The depth of the well for the $[M^+\text{-}C_3H_8)]$ collision complex is arbitrarily assumed to be 15 kcal/mol, and the well is assumed to be energetically symmetric, i.e., the barriers to C-H insertion and to dissociation to reactants

are assumed to be equal. Vibrational frequencies in the collision complex are taken to be those of the free alkane, plus three 10 cm^{-1} vibrations to represent hindered rotations in the complex which become translational degrees of freedom upon dissociation. Vibrational frequencies are taken from the literature[40] where possible, or estimated from those of similar species. For the tight transition state leading to bond insertion, the preexponential factor was arbitrarily assumed to be 10^{13}. The calculation is insensitive to the specific values of the vibrational frequencies chosen as long as the preexponential does not change. Rotational constants are taken from the literature[41] when available. Rotational constants for the collision complex are estimated by assuming two point masses for the metal ion and alkane, separated by the orbiting radius, r_o. Polarizabilities are taken from the literature or estimated using the ahc method.[42] Sums and densities of states were evaluated using the Beyer-Swinehart direct count algorithm.[43]

References and Notes

1. For a recent review, see Armentrout, P. B.; Beauchamp, J. L. *Acct. Chem. Res.*, manuscript in preparation.

2. For example, see: a) Allison, J.; Freas, R. B.; Ridge, D. P. *J. Am. Chem. Soc.* **1979**, *101*, 1332. b) Larson, B. S.; Ridge, D. P. *J. Am. Chem. Soc.* **1984**, *106*, 1912. c) Jones, R. W.; Staley, R. H. *J. Am. Chem. Soc.* **1982**, *104*, 1235-1238. d) Uppal, J. S.; Staley, R. H. *J. Am. Chem. Soc.* **1982**, *104*, 1238. e) Byrd, G. D.; Burnier, R. C.; Freiser, B. S. *J. Am. Chem. Soc.* **1982**, *104*, 3565. f) Jacobson, D. B.; Freiser, B. S. *J. Am. Chem. Soc.* **1983**, *105*, 5197.

3. For example, see: a) Armentrout, P. B.; Beauchamp, J. L. *J. Am. Chem. Soc.* **1981**, *103*, 784. b) Halle, L. F.; Armentrout, P. B.; Beauchamp, J. L. *Organometallics* **1982**, *1*, 963. c) Houriet, R.; Halle, L. F.; Beauchamp, J. L. *Organometallics* **1983**, *2*, 1818-1829. d) Tolbert, M. A.; Beauchamp, J. L. *J. Am. Chem. Soc.* **1984**, *106*, 8117. e) Elkind, J. L.; Armentrout, P. B. *J. Phys. Chem.* **1985**, *89*, 5626. f) Aristov, N.; Armentrout, P. B.; *J. Am. Chem. Soc.* **1986**, *108*, 1806. g) Elkind, J. L.; Armentrout, P. B. *J. Am. Chem. Soc.* **1986**, *108*, 2765. h) Sunderlin, L.; Aristov, N.; Armentrout, P. B. *J. Am. Chem. Soc.* **1987**, *109*, 78.

4. Tonkyn, R.; Ronan, M.; Weisshaar, J. C. *J. Phys. Chem.* **1988**, *92*, 92-102.

5. (a) Hanratty, M. A.; Beauchamp, J. L.; Illies, A. J.; Bowers, M. T. *J. Am. Chem. Soc.* **1985**, *107*, 1788. (b) Hanratty, M. A.; Beauchamp, J. L.; Illies, A. J.; van Koppen, P. A. M.; Bowers, M. T. *J. Am. Chem. Soc.* **1988**, *110*, 1-14.

6. van Koppen, P. A. M.; Jacobson, D. B.; Illies, A. J.; Bowers, M. T.; Hanratty, M. A.; Beauchamp, J. L. *J. Am. Chem. Soc.*, in press.

7. Jarrold, M. F.; Illies, A. J.; Kirchner, N. J.; Wagner-Redeker, W.; Bowers, M. T.; Mandich, M. L.; Beauchamp, J. L. *J. Phys. Chem.* **1983**, *87*, 2213-2221.

8. (a) Chesnavich, W. J.; Bowers, M. T. *J. Am. Chem. Soc.* **1977**, *99*, 1705-1711. (b) Chesnavich, W. J.; Bass, L.; Su, T.; Bowers, M. T. *J. Chem. Phys.* **1981**, *74*, 2228-2246. (c) Jarrold, M. F.; Wagner-Redeker, W.;

Illies, A. J.; Kirchner, N. J.; Bowers, M. T. *Int. J. Mass Spectrom. Ion Processes*, **1984**, *58*, 63-95.

9. Morgan, R. P.; Beynon, J. H.; Bateman, R. H.; Green, B. N. *Int. J. Mass Spectrom. Ion Phys.* **1978**, *28*, 171-191.

10. Jarrold, M. F.; Illies, A. J.; Bowers, M. T. *Chem. Phys.* **1982**, *65*, 19.

11. The energy resolution in the center-of-mass frame ΔT is related to that of the main beam in the laboratory frame ΔE by the equation $\Delta T = \Delta E[(M_1^2T)/(M_2M_3V_1)]^{1/2}$, where M_1 is the mass of the parent metastable ion, M_2 and M_3 are the masses of the ionic and neutral fragments, V_1 is the lab kinetic energy of the parent metastable ion, and T is the center of mass kinetic energy. This formula is taken from Hanratty, M. A. Ph.D. Thesis, California Institute of Technology, 1985. For an example, consider the demethanation of propane by Fe^+. With a main beam resolution of 2 eV and a center-of-mass kinetic energy of 200 meV, the spread in center-of-mass kinetic energy due to the spread in the main beam is 27 meV. The contribution from ΔE is much less significant for fragmentations involving heavier neutrals.

12. a) Armentrout, P. B.; Beauchamp, J. L. *Chem. Phys.* **1980**, *50*, 21. b) Armentrout, P. B.; Beauchamp, J. L. *J. Chem. Phys.* **1981**, *74*, 2819.

13. The thermal population of excited states should be similar to that published for Fe^+ produced by surface ionization. See: Elkind, J. L.; Armentrout, P. B. *J. Phys. Chem.* **1986**, *90*, 5736-5745.

14. The treatment closely follows that of: Tolbert, M. A.; Beauchamp, J. L. *J. Am. Chem. Soc.* **1986**, *108*, 7509-7517.

15. Calculations used the formula $k_s = k_c = 2\pi q(\alpha/\mu)^{1/2}$, where k_s is the collisional stabilization rate, assumed to be equal to k_c, the collision rate; q is the ion charge, α is the neutral polarizability, and μ is the reduced mass. See Gioumousis, G.; Stevenson, D. P. *J. Chem. Phys.* **1958**, *29*, 294.

16. Schultz, R. H.; Elkind, J. L.; Armentrout, P. B. *J. Am. Chem. Soc.* **1988**, *110*, 411-423.

17. Miller, W. B.; Safron, S. A.; Herschbach, D. R. *Disc. Farad. Soc.* **1967**, *44*, 108-122.

18. Miller, W. B.; Safron, S. A.; Herschbach, D. R. *J. Chem. Phys.* **1972**, *56*, 3581-3592.

19. Creasy, W. R.; Farrar, J. M. *J. Chem. Phys.* **1986**, *85*, 162-178.

20. See reference 17, especially Figure 10. The critical configuration, assumed to be an ion-molecule complex of M^+(alkene) with CH_4, can likely be approximated by a prolate symmetric top. Assuming the orbiting separation between CH_4 and M^+(alkene), and a rotational temperature of 500 K for the complex, it is estimated that X = 13 for Co^+-propane, and X = 7.5 for Co^+-neopentane, in the nomenclature of reference 17. At a 30° observation angle, the effect on the two distributions is roughly identical.

21. For detailed discussion of the influence of angular momentum on molecular collisions, see Levine, R. D.; Bernstein, R. B. *Molecular Reaction Dynamics and Chemical Reactivity*; Oxford University Press: New York, 1987; Chapter 2.

22. For discussion of LGS theory and more sophisticated treatments dealing with polar molecules, see Su, T.; Bowers, M. T. In *Gas Phase Ion Chemistry*; Bowers, M. T., Ed.; Academic Press: New York, 1979; Vol. 1, Chapter 3, and references cited therein.

23. Calculations used the formula $r_o = (2q^2\alpha/E_{rel})^{1/4}/(2)^{1/2}$, where q is the ion charge and α is the polarizability of the neutral. The polarizability of propane is 6.29 $Å^3$, from Miller, K. J.; Savchik, J. A. *J. Am. Chem. Soc.* **1979**, *101*, 7206-7213.

24. (a) Olmstead, W. N.; Brauman, J. I. *J. Am. Chem. Soc.* **1977**, *99*, 4219-4228. (b) Pellerite, M. J.; Brauman, J. I. *J. Am. Chem. Soc.* **1980**, *102*, 5993-5999.

25. Moore, C. E. *Natl. Bur. Stand. Circ. (U. S.)* **1949**, Vol. I, No. 467, **1958**, Vol. II.

26. Armentrout, P. B.; Georgiadis, R. *Polyhedron* **1988**, *7*, 1573-1581.

27. McMillen, D. F.; Golden, D. M. *Ann. Rev. Phys. Chem.* **1982**, *33*, 493.

28. Georgiadis, R.; Fisher, E. R.; Armentrout, P. B. *J. Am. Chem. Soc.*, submitted for publication.

29. Watson, P. L.; Roe, D. C. *J. Am. Chem. Soc.* **1982**, *104*, 6471.

30. The exothermicity is $D(CH_3CH_2\text{-}CH_3)$ - $D(M^+\text{-}CH_3)$ - $D(H_3CM^+\text{-}CH_2CH_3)$. Assuming $D(CH_3CH_2\text{-}CH_3)$ = 85 kcal/mol, and further assuming that $D(H_3CM^+\text{-}CH_2CH_3) \approx D(H_3CM^+\text{-}CH_3)$, values from reference 26 can be used to estimate the cited exothermicities for C-C insertion.

31. Armentrout, P. B., personal communication.

32. Ferguson, E. E. *J. Phys. Chem.* **1986**, *90*, 731-738.

33. Corderman, R. R.; Beauchamp, J. L. *J. Am. Chem. Soc.* **1976**, *98*, 3998-4000.

34. a) Jones, R. W.; Staley, R. H. *J. Phys. Chem.* **1982**, *86*, 1387. b) Kappes, M. M.; Staley, R. H. *J. Am. Chem. Soc.* **1982**, *104*, 1819.

35. Jacobson, D. B.; Freiser, B. S. *J. Am. Chem. Soc.* **1983**, *105*, 7492-7500.

36. Freiser, B. S. *Talanta* **1985**, *32*, 697-708.

37. Chesnavich, W. J.; Bass, L.; Grice, M. E.; Song, K.; Webb, D. A. "TSTPST: Statistical Theory Package for RRKM/QET/TST/PST Calculations," *QCPE*, submitted for publication.

38. a) Pechukas, P.; Light, J. C. *J. Chem. Phys.* **1965**, *47*, 3281. b) Marcus, R. A. *J. Chem. Phys.* **1975**, *62*, 1872. c) Klots, C. E. in *Kinetics of Ion-Molecule Reactions*; P. Ausloos, ed.; Plenum Press: New York, 1979. d) Bowers, M. T.; Chesnavich, W. J. *Prog. React. Kinet.* **1982**, *11*, 137. e) Pechukas, P. *Ann. Rev. Phys. Chem.* **1981**, *32*, 159. f) Truhlar, D. G.; Hase, W. L.; Hynes, J. T. *J. Phys. Chem.* **1983**, *87*, 2664. g) Truhlar, D. G.; Garrett, B. C. *Ann. Rev. Phys. Chem.* **1984**, *35*, 159.

39. a) Marcus, R. A.; Rice, O. K. *J. Phys. Colloid Chem.* **1951**, *55*, 894. b) Marcus, R. A. *J. Chem. Phys.* **1952**, *20*, 359. c) Robinson, J. P.; Holbrook, K. A. *Unimolecular Reactions*; Wiley-Interscience: New York, 1972. c) Forst, W. *Theory of Unimolecular Reactions*; Academic Press: New York, 1973.

40. a) Shimanouchi, T. *Table of Molecular Vibrational Frequencies, NSRDS-NBS 39*, Consolidated, Vol. I; National Bureau of Standards: Washington, D. C., 1972. b) Sverdlov, L. M.; Kovner, M. A.; Krainov, E. P. *Vibrational Spectra of Polyatomic Molecules*; Wiley: New York, 1970.

41. *H. H. Landolt-Bornstein, Numerical Data and Functional Relationships in Science and Technology*, New Series, Group II, Volume 7; K. H. Hellwege and A. M. Hellwege, eds.; Springer-Verlag: Berlin, 1976. *ibid.*, Volume 6, 1974.

42. Miller, K. J.; Savchik, J. A. *J. Am. Chem. Soc.* **1979**, *101*, 7206-7213.

43. Stein, S. E.; Rabinovitch, B. S. *J. Chem. Phys.* **1973**, *58*, 2438-2445.

CHAPTER 3

KINETIC ENERGY RELEASE STUDIES OF THE MECHANISM OF FORMATION, THERMOCHEMICAL STABILITY, AND REARRANGEMENTS OF HYDRIDOCYCLOPROPYL, METALLACYCLOBUTANE, AND PROPENE COMPLEXES OF ATOMIC COBALT IONS IN THE GAS PHASE

KINETIC ENERGY RELEASE STUDIES OF THE MECHANISM OF FORMATION, THERMOCHEMICAL STABILITY, AND REARRANGEMENTS OF HYDRIDOCYCLOPROPYL, METALLACYCLOBUTANE, AND PROPENE COMPLEXES OF ATOMIC COBALT IONS IN THE GAS PHASE

David V. Dearden and J. L. Beauchamp

Arthur Amos Noyes Laboratory of Chemical Physics
California Institute of Technology
Pasadena, CA 91125

Petra A. M. van Koppen and Michael T. Bowers

Department of Chemistry
University of California
Santa Barbara, CA 93106

Abstract.

The gas phase reactions of Co^+ with the isomers cyclobutanone, cyclopropanecarboxaldehyde, and crotonaldehyde result in the formation of structurally distinct $Co(C_4H_6O)^+$ species. These species were studied by measuring the kinetic energy release distributions (KERDs) for losses of CO and C_3H_6 from metastable parent Co(cyclobutanone)$^+$, Co(cyclopropane-carboxaldehyde)$^+$, and Co(crotonaldehyde)$^+$ ions. The CO loss processes exhibit statistical partitioning of energy between product internal modes and relative translation, and can be modeled using phase space theory. Co(cyclobutanone)$^+$ rearranges to a metallacyclic structure which eliminates either CO or cyclopropane. Co(cyclopropanecarboxaldehyde)$^+$ also eliminates either CO or cyclopropane, but does so from a (H)(cyclopropyl)Co^+(CO) species. The heat of formation (0 K) of the resulting (H)Co^+(cyclopropyl) ion is determined to be 274 ± 5 kcal/mol, similar to the value of 274 ± 5 kcal/mol determined for cobaltacyclobutane ion, and distinct from the known value of 247 ± 5 kcal/mol for Co(propene)$^+$. Co(crotonaldehyde)$^+$ rearranges to (CO)Co^+(propene), with loss of mass 42 corresponding to loss of propene in this case rather than cyclopropane. Rearrangements of (CO)cobaltacyclobutane and (H)(cyclopropyl)Co^+(CO) ions to the lowest energy structure, (CO)Co(propene)$^+$, do not occur on the time scale of the KERD experiment. All the observed C_3H_6 losses have KERDs much broader than predicted by statistical theory.

Introduction

Gas phase studies of transition metal ions and their reactions with organic species have proven to be a valuable complement to more traditional experiments carried out in solution.[1] Elementary processes can be investigated in the absence of solvents and other ligating species, enabling examination of the intrinsic reactivity and thermochemistry of the species involved. Gas-phase analogues for many structures and processes observed in solution have been found, such as oxidative addition across C-H and C-C bonds, and reductive elimination of alkanes and alkenes.

A number of studies have invoked gas phase metallacycles, to explain dehydrogenation in the absence of β-H transfer,[2] as reactive intermediates resulting from C-C insertion into cyclic alkanes or from dehydrocyclization,[3,4,5,6] and as products arising from decarbonylation of cyclic ketones.[7,8,9,10,11] A thorough understanding of the chemistry of metallacycles is important, due to its influence on such commercially important and scientifically interesting processes as olefin metathesis,[12] the cracking and isomerization of hydrocarbons,[13] and epoxidation.[14] Gas phase work in this area is complementary to condensed phase research, in helping to unravel the rich, complex chemistry involved.

Cobaltacyclobutane ion has previously been studied in detail, using Fourier transform ion cyclotron resonance (FTICR)[9] and by measurement of the kinetic energy release distribution (KERD)[11] for decomposition of

$Co(C_4H_6O)^+$. Both investigations produced the metallacycle by decarbonylation of cyclobutanone, reaction 1.

(1)

However, from the FTICR results, millisecondsafter formation the stable structure appears to be Co(propene)$^+$, rather than cobaltacyclobutane ion. Acetonitrile, ethene, and 2-methylpropene are all observed to displace C_3H_6 exclusively from $Co(C_3H_6)^+$ produced in reaction 1. Identical displacement reactions are observed when reaction 2 is used to generate $Co(C_3H_6)^+$, most likely with a Co(propene)$^+$ structure.

(2)

These results can be contrasted with those for $Fe(C_3H_6)^+$, which, when generated by a reaction analogous to reaction 1, incorporates CH_3CN with losses of C_2H_4 (60%) or C_3H_6 (40%). $Fe(C_3H_6)^+$ made by the analog of reaction 2, on the other hand, loses only C_3H_6 in displacement reactions with acetonitrile, ethene, or 2-methylpropene. Collision-induced dissociation (CID), with Ar as the collision gas, was also used to demonstrate that $Co(C_3H_6)^+$ and $Fe(C_3H_6)^+$ produced by decarbonylating cyclobutanone have different structures. CID of $Fe(C_3H_6)^+$ results in losses of both C_2H_4 and C_3H_6, while that of $Co(C_3H_6)^+$ results in exclusive loss of C_3H_6 at all

collision energies studied. When the $M(C_3H_6)^+$ species are generated by dehydrogenation of propane, the only CID product for both Fe^+ and Co^+ is bare metal ion resulting from C_3H_6 loss. These results were interpreted as indicating that both Fe^+ and Co^+ initially form metallacycles, but that the cobaltacyclobutane ion rapidly rearranges to Co(propene)$^+$, while ferracyclobutane ion does not.[9]

The results of the KERD experiment[11] are in apparent conflict with the FTICR findings. For statistical dissociation processes such as loss of CO from Co(cyclobutanone)$^+$, reaction 3, the KERD can be modeled using phase space theory.[15] Current theory is inadequate to model non-statistical processes such as the other observed metastable reaction of Co^+ with cyclobutanone, reaction 4.

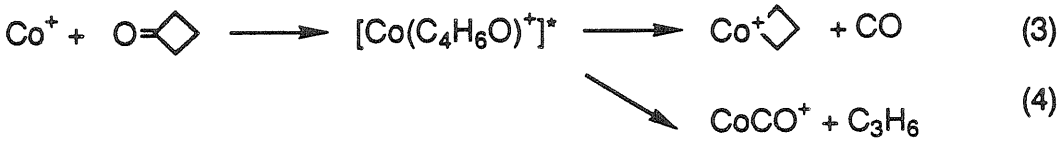

The only free parameter to which the model calculation is particularly sensitive is ΔH for the reaction, so in cases where all reactant and product heats of formation are well known except for one, that of the remaining species can be determined by varying ΔH to fit the experimental KERD. In this way $\Delta H^0_{f,0K}$ = 274 ± 5 kcal/mol for the $Co(C_3H_6)^+$ product of reaction 3 was measured. Previous KERD studies[15] using reactions 5 and 6, where on mechanistic grounds a Co(propene)$^+$ structure is expected,

determined that $\Delta H^0_{f,0K}(Co(propene)^+)$ = 247 ± 5 kcal/mol.

(5)

(6)

The difference in heats of formation was explained by postulating that the structure of $Co(C_3H_6)^+$ from reaction 3 is that of the metallacyclobutane ion. This conclusion was rationalized with the FTICR results by arguing that the presence of the CO ligand inhibits isomerization to the metal alkene structure. It should also be noted that the time scales for the two types of experiments are different. KERD observations are made on a micro-second time scale, while the FTICR measurements occur on a scale of milliseconds to seconds. An alternative explanation for the differences in the two studies is that rearrangement of the metallacycle to the metal alkene is slow on the microsecond scale but fast on a scale of tens of milliseconds.

The purpose of the current work is to take a closer look at cobal-tacyclobutane ion and other isomeric structures by using alternate methods to produce $Co(C_3H_6)^+$. Additional motivation for these studies comes from recent solution work where $Cp^*Rh(PMe_3)$ (PMe_3 = trimethylphosphine) was observed to insert at -60° C into the C-H bond of cyclopropane to form a hydridocyclopropyl species, which upon warming to -20 °C rearranges, by migration of the $Cp^*Rh(PMe_3)$ unit into the α-C-C bond of the ring, to

a rhodacyclobutane structure.[16] It is also proposed that in solution this rearrangement proceeds through an η^2 C-H alkane σ-complex.[16,17] The general mechanism proposed for the reactions of Co^+ with aldehydes and ketones[10] involves initial insertion into the C-C bond α to the carbonyl, suggesting that reaction 7 should result in formation of a hydridocyclopropyl-cobalt ion structure.

(7)

One question which arises is whether reactions 3 and 7 lead to distinct $Co(C_3H_6)^+$ structures. A related question is whether a rearrangement analogous to that observed in solution occurs for hydridocyclopropylcobalt ion in the gas phase. The reductive elimination of C_3H_6 is also of interest, since both cyclopropane and propene are possible products. There is some evidence for elimination of cyclopropane from metallacyclobutanes in solution.[18] Finally, a KERD study should shed light on the importance of the η^2 C-H alkane σ-complex mechanism in the metastable loss of C_3H_6 from $Co(C_4H_6O)^+$. If $Co(C_4H_6O)^+$ were to lose C_3H_6 through a σ-complex mechanism, it is expected that the resulting KERD should be statistical since the dissociation could occur through simple bond cleavage. KERD analysis has proven particularly useful for distinguishing statistical processes from those which are non-statistical.[15,11]

Experimental Section

Kinetic energy release measurements were carried out at UCSB using a double-focusing, reversed-geometry mass spectrometer (VG Industries, ZAB-2F)[19] with a home-built pressure- and temperature-variable electron impact source. The methods used in metastable and collision-induced dissociation studies have been described.[20] Briefly, Co^+, generated by 100-300 eV electron impact on $Co(CO)_3NO$ (Aldrich), was allowed to react in the source with the hydrocarbon of interest. Electron energies were varied to maximize the ion beam intensity. Typical total source pressures of 2-5 mTorr were employed, and were monitored with an MKS Instruments Baratron capacitance manometer. The ratio of $Co(CO)_3NO$ and hydrocarbon pressures was approximately 1:1, and was varied to maximize adduct signal. Ions exiting the source were accelerated to 8 keV and mass selected. Fragment ions from metastable decomposition in the field-free region (known as the second field-free region) downstream from the magnet (background pressure < 10^{-9} Torr) were energy analyzed with an electrostatic sector, and were detected using pulse counting techniques. The resolution of the main ion beam was 4 eV fwhm. At this resolution, the contribution of the energy spread of the main beam to the width of the center-of-mass product translational energy distribution is negligible.[21]

Collision-induced dissociation (CID) was performed by admitting He into a collision cell in the second field-free region until the ion beam was

attenuated 50%. CID fragments were analyzed by scanning the electric sector.

Cyclobutanone and crotonaldehyde (Aldrich) were used as supplied. Cyclopropanecarboxaldehyde was synthesized from cyclopropyl carbinol (Aldrich) using published methods.[22] The product was verified using NMR.

The methods for obtaining kinetic energy release distributions from metastable peak shapes have been described.[23] Raw data were smoothed using a moving average algorithm, after which numerical differentiation and conversion to the center-of-mass reference frame were carried out. Phase space theory was used to model the distributions. In these calculations, the only free parameter having a large influence on the fit to the experimental data was ΔH for the reaction. The use of phase space theory to determine reaction enthalpies has been discussed.[15,24,25]

Results

Table I reports metastable product intensities for complexes generated from Co^+ with cyclobutanone and cyclopropanecarboxaldehyde. These experiments are sensitive to metastables decomposing on a time scale of 5-15 μs, and hence show the relative populations of the various channels with unimolecular decomposition rates of 6.7×10^4 - 2.0×10^5 s^{-1}. Loss of CO is the major decomposition channel for both metastables. Regeneration of the bare Co^+ ion is a minor channel in both cases. Loss

Table I. Metastable Product Distributions for Co^+ Complexes with Cyclobutanone and Cyclopropanecarboxaldehyde

Reaction	Percent Metastable Intensity
$Co(cyclobutanone)^+$	
$\rightarrow Co(C_3H_6)^+ + CO$	80.
$\rightarrow CoCO^+ + C_3H_6$	18.
$\rightarrow Co^+ + C_4H_6O$	2.
$Co(cyclopropanecarboxaldehyde)^+$	
$\rightarrow Co(C_3H_6)^+ + CO$	92.
$\rightarrow CoCO^+ + C_3H_6$	3.
$\rightarrow Co^+ + C_4H_6O$	5.

of C_3H_6 constitutes 18% of the metastable intensity from Co(cyclobutanone)$^+$, but only 3% of that from Co(cyclopropanecarboxaldehyde)$^+$.

Kinetic energy release distributions for reaction 8, with C_4H_6O = a) cyclobutanone,[11] b) cyclopropanecarboxaldehyde, and c) crotonaldehyde, are plotted in Figure 1, along with KERDs predicted using phase space theory.

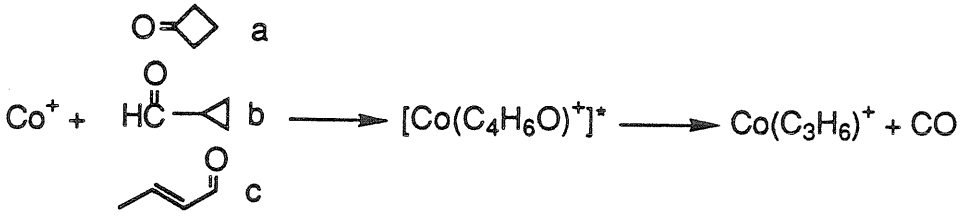

(8)

The distributions are narrow and peak at low kinetic energy release, which is characteristic of statistical metastable decompositions.[15] The phase space fits to all three KERDs are good, supporting the statistical nature of these CO losses. The apparent discrepancy between the experimental KERD and the phase space theory fit for loss of CO from Co(crotonaldehyde)$^+$ at high product kinetic energies is likely due to instrumental exaggeration of high kinetic energy release.[26] The average kinetic energy released in each of these processes, $\langle E_t \rangle$, is listed in Table II, along with the exothermicities for each reaction. The $\langle E_t \rangle$ values are seen to scale roughly with ΔH, as expected for statistical processes where the vibrational and rotational modes of the species involved are similar. The possibility that the neutral lost is C_2H_4, rather than CO, cannot strictly be ruled out, but we consider it highly unlikely in view of published FTICR[9] results. In those studies, the

Figure 1. Experimental kinetic energy release distributions (solid lines), in the center-of-mass frame, for decarbonylation of (a) cyclobutanone, (b) cyclopropanecarboxaldehyde, and (c) crotonaldehyde by Co^+. Distributions calculated using phase space theory (filled circles) assume ΔH^0_f(Cobalta-cyclobutane$^+$) = 274 kcal/mol in (a), ΔH^0_f[(H)(cyclopropyl)-Co^+] = 274 kcal/mol in (b), and ΔH^0_f[Co^+(propene)] = 247 kcal/mol in (c).

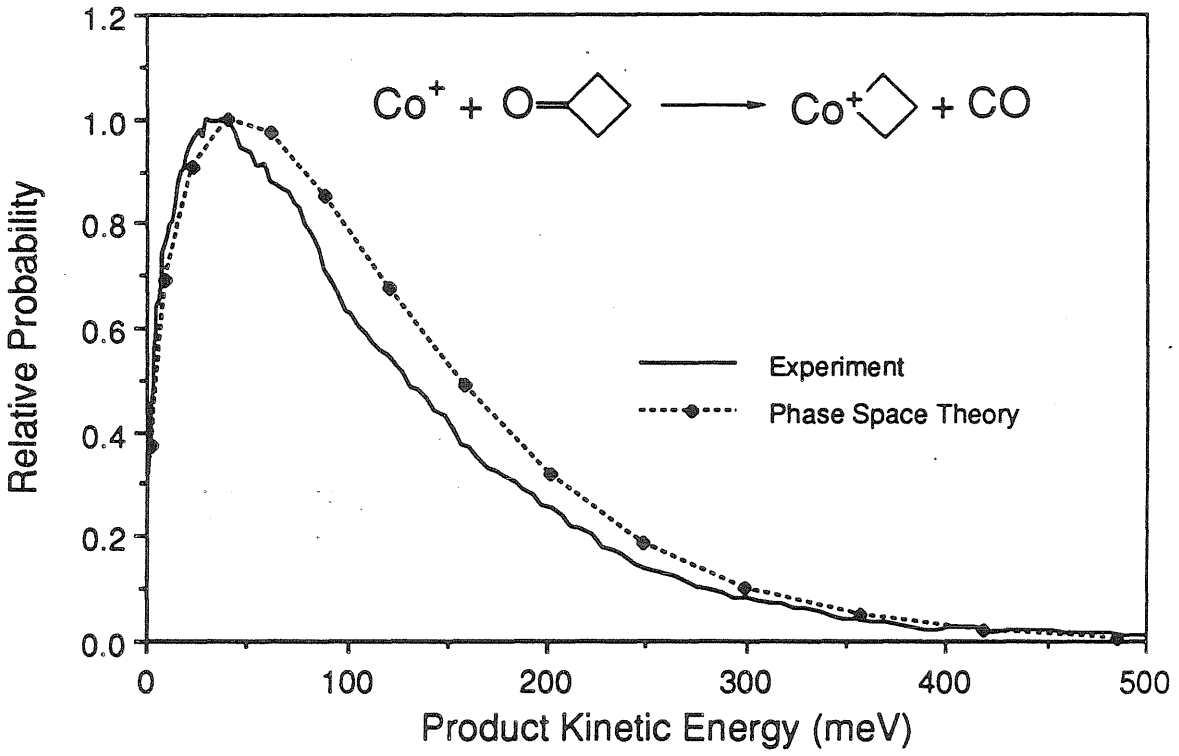
1.2
1.0
0.8
0.6
0.4
0.2
0.0
Relative Probability
0
100
200
300
400
500
Product Kinetic Energy (meV)
Co+ + O
Co+
+ CO
Experiment
Phase Space Theory

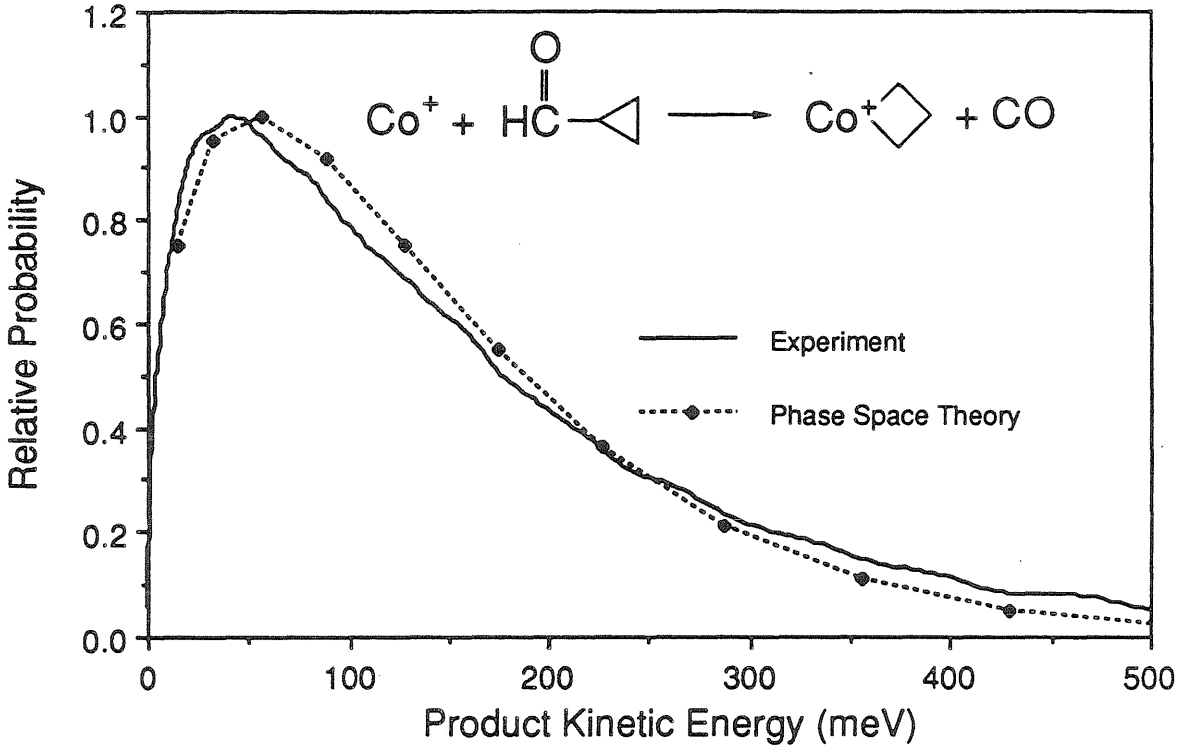
1.2
1.0
0.8
0.6
0.4
0.2
0.0
Relative Probability
0
100
200
300
400
500
Product Kinetic Energy (meV)
O
Co+ + HC
Co+
+ CO
Experiment
Phase Space Theory

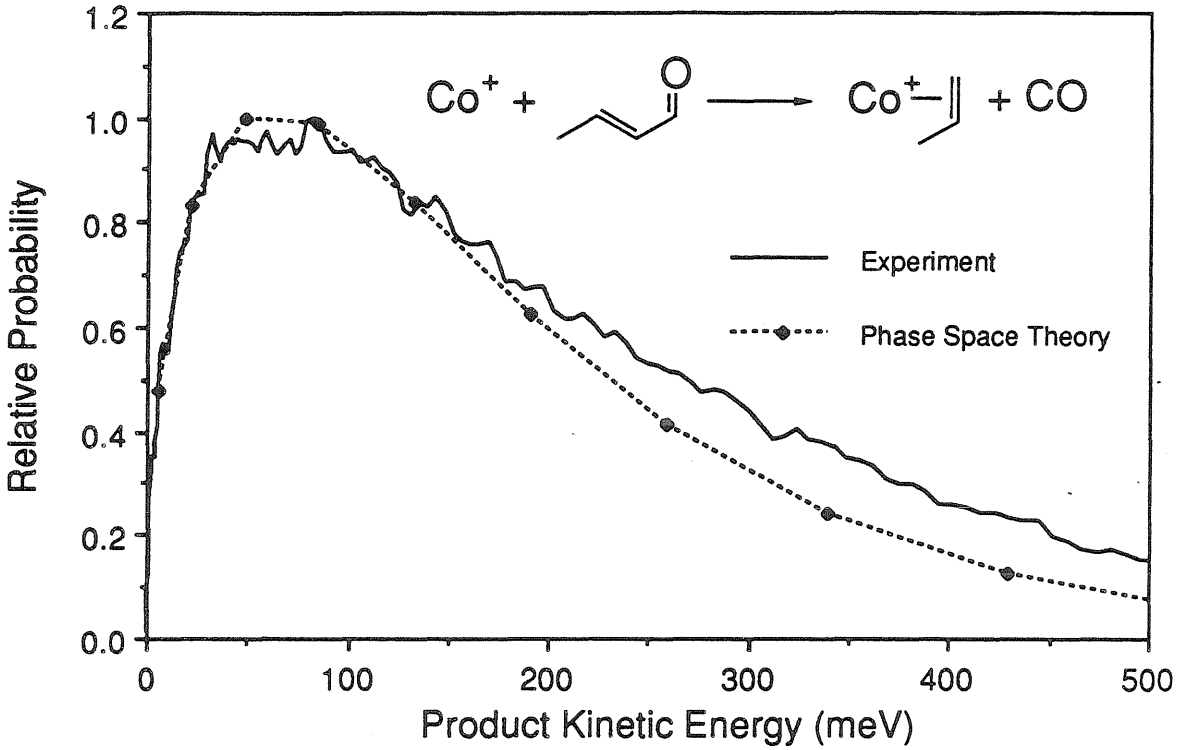
1.2
1.0
0.8
0.6
0.4
0.2
0.0
Relative Probability
0
100
200
300
400
500
Product Kinetic Energy (meV)
Co+ +
+ CO
Experiment
Phase Space Theory

Table II. Experimental and Calculated Average Kinetic Energy Releases

Reaction	$-\Delta H^a$	$\langle E_t \rangle_{exp}{}^a$	$\langle E_t \rangle_{calc}{}^a$	
Co^+ + cyclobutanone → cobaltacyclobutane + CO	0.69	0.11	8.	
Co^+ + cyclopropanecarboxaldehyde → hydridocyclopropylcobalt$^+$ + CO	1.12[b]	0.15	0.14	
Co^+ + crotonaldehyde → Co(propene)$^+$ + CO	1.82	0.22	0.18	
Co^+ + cyclobutanone → $CoCO^+$ + cyclopropane	0.95	0.32	0.11	
Co^+ + cyclopropanecarboxaldehyde → $CoCO^+$ + cyclopropane	1.38	0.23	0.13	
Co^+ + crotonaldehyde → $CoCO^+$ + propene	1.28	0.21	6.	

[a]Units: eV.

[b]Assuming ΔH_f°(hydridocyclopropylcobalt$^+$) = ΔH_f°(cobaltacyclobutane)

excellent mass resolution capability of the FTICR technique was used to distinguish peaks resulting from losses of C_2H_4 and CO, with the result that only CO loss was observed. Further, since reaction 8 occurs in the ion source as well as in the second field-free region, it is possible to clarify the structure of the ionic product using CID, Table III. Fragment ions at m/z 98, 97, and 74, which cannot result from CID of $Co(C_2H_2O)^+$, are present in the CID spectrum.

Kinetic energy release distributions for reaction 9, loss of C_3H_6 from metastable $Co(C_4H_6O)^+$, are given in Figure 2.

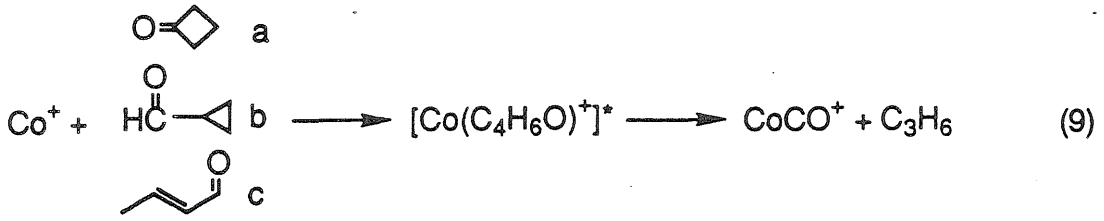

(9)

All three distributions are broad and could not be fit using phase space theory, which is consistent with non-statistical release of kinetic energy. Average energy releases and exothermicities are included in Table II. No correlation between $\langle E_t \rangle$ and ΔH is apparent. The metastable peaks from Co(cyclopropanecarboxaldehyde)$^+$ and Co(crotonaldehyde)$^+$ were very weak (less than 200 counts s^{-1}, maximum). It is possible that these peaks are not due to true metastables, but to CID resulting from collisions with residual background gases. As was noted previously,[11] it was not possible in these experiments to distinguish losses of C_3H_6 from losses of ketene, C_2H_2O, since the metastable peaks from these processes overlap. However,

Table III. Collision-Induced Dissociation Spectra of $Co(C_3H_6)^+$ Ions Formed from Reaction of Co^+ with Propene, Cyclopropane, Cyclobutanone and Cyclopropanecarboxaldehyde.

		Fragment Intensities[a]			
Reactant Neutrals:		Propene	cyclo-propane	cyclo-butanone	cyclopropane-carboxaldehyde
Fragment	m/z				
$CoC_3H_5^+$	100.	1.2	tr[b]	tr[b]	1.5
$CoC_3H_4^+$	99.	1.2	1.4	1.4	1.1
$CoC_3H_3^+$	98.	3.1	2.9	2.2	2.3
$CoC_3H_2^+$	97.	2.1	2.2	1.4	tr[b]
$CoC_2H_2^+$	85.	3.6	3.4	2.9	2.7
CoC_2H^+	84.	2.2	1.6	1.6	1.0
$CoCH_3^+$	74.	3.8	3.6	2.3	2.5
$CoCH_2^+$	73.	2.8	8.4	9.8	4.6
$CoCH^+$	72.	1.4	1.7	2.1	1.2
CoC^+	71.	1.1	1.5	1.7	1.0
CoH^+	60.	tr[b]	tr[b]	tr[b]	5.6
Co^+	59.	73.7	70.0	70.2	72.6
$C_3H_3^+$	39.	1.3	1.0	tr[b]	tr[b]

[a]All values normalized to ΣI_i, excluding Co^+ as a fragment ion.

[b]Less than 1%.

Figure 2. Experimental kinetic energy release distributions (solid lines), in the center-of-mass frame, for loss of m/z 42 from (a) Co(cyclobutanone)$^+$, (b) Co(cyclopropanecarboxaldehyde)$^+$, and (c) Co(crotonaldehyde)$^+$. Distributions calculated using phase space theory (filled circles) assumed the products drawn.

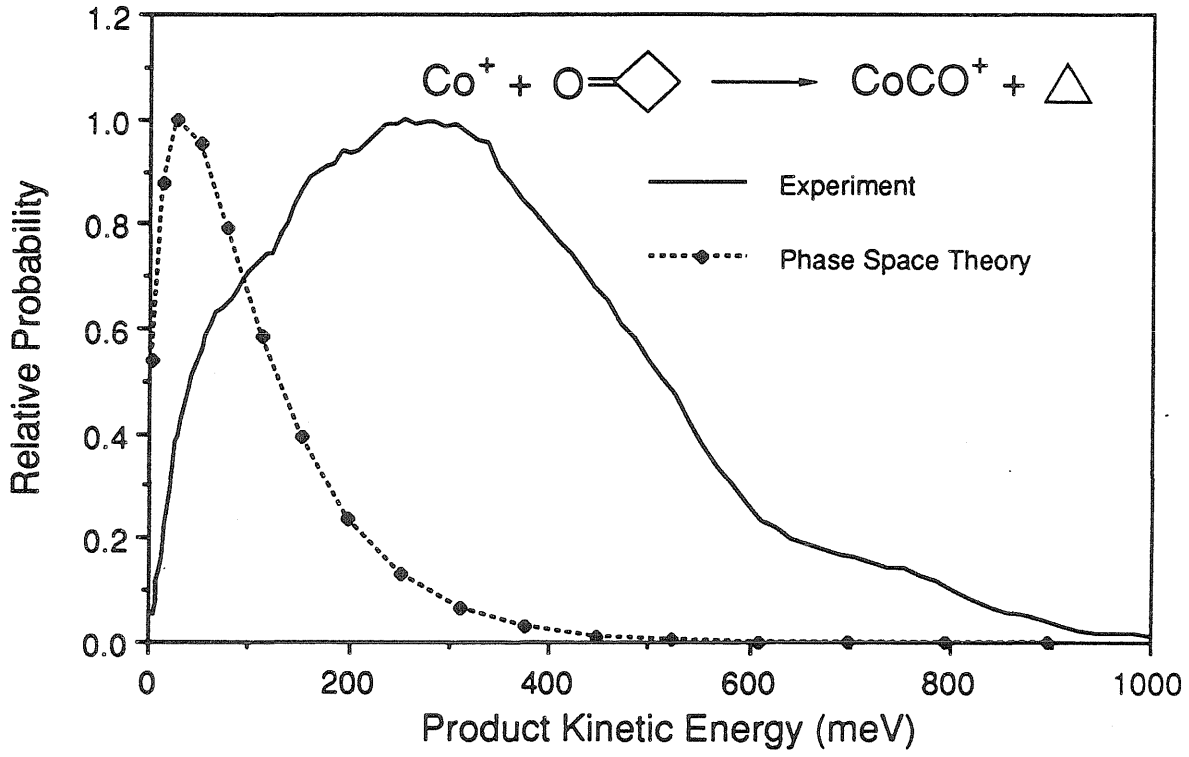
Co+ + O=◇ ⟶ CoCO+ + △
Experiment
Phase Space Theory
Relative Probability
Product Kinetic Energy (meV)
0.0
0.2
0.4
0.6
0.8
1.0
1.2
0
200
400
600
800
1000

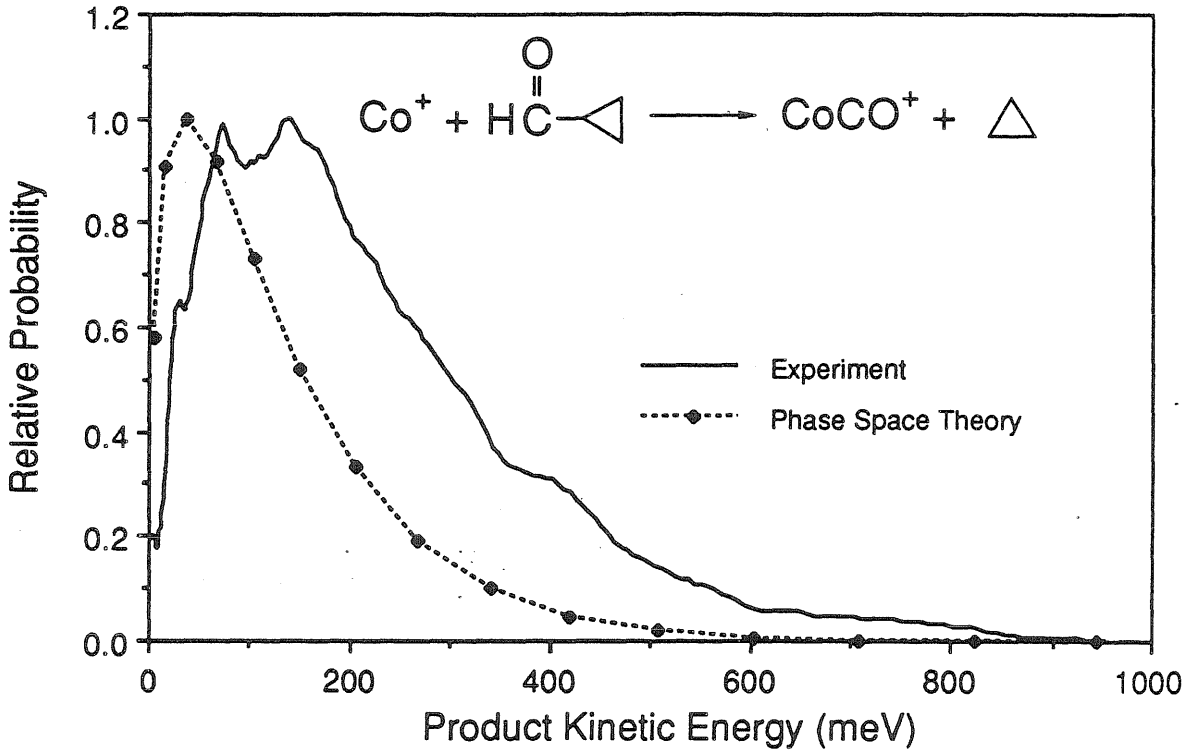
1.2
1.0
0.8
0.6
0.4
0.2
0.0
Relative Probability
0
200
400
600
800
1000
Product Kinetic Energy (meV)
Co+ + HC
CoCO+ +
Experiment
Phase Space Theory

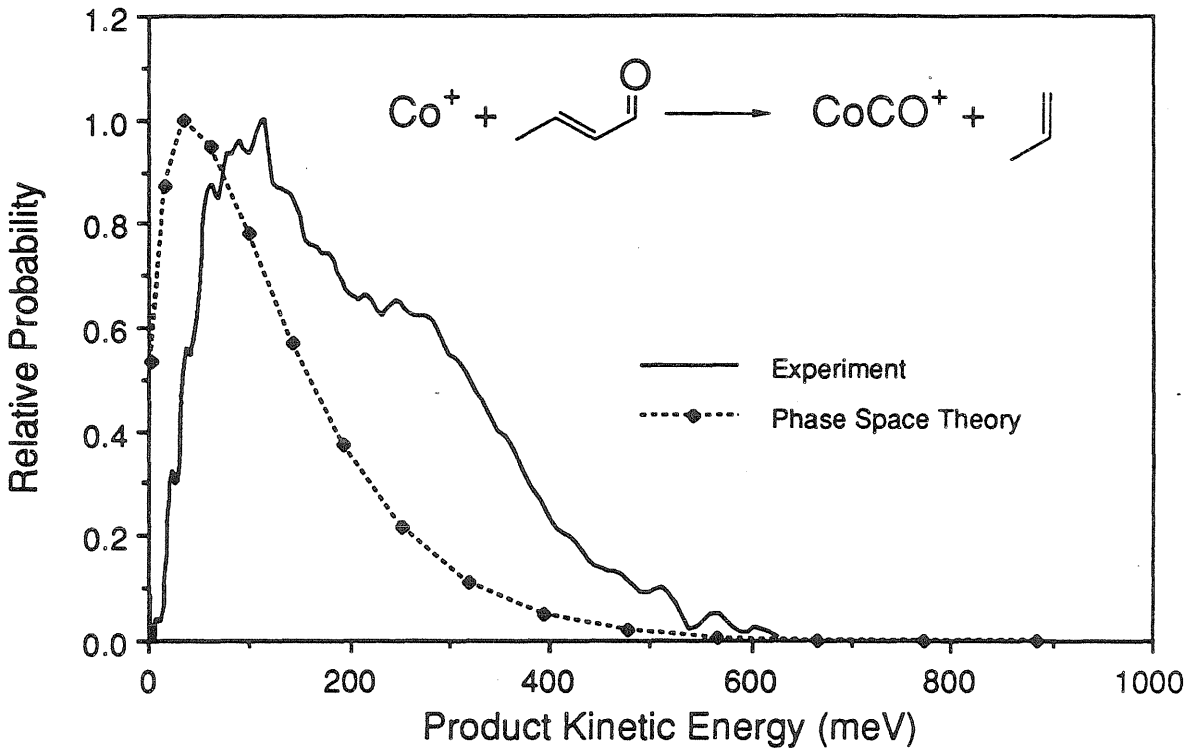
1.2
1.0
0.8
0.6
0.4
0.2
0.0
Relative Probability
0
200
400
600
800
1000
Product Kinetic Energy (meV)
Co+ +
CoCO+ +
Experiment
Phase Space Theory

no ketene loss was observed in the FTICR experiment involving cyclobutanone.[9] Because the energetics and expected dynamics for losses of C_3H_6 and C_2H_2O are different, if both were occurring a bimodal KERD should be evident. The KERDs do not appear to be bimodal, except possibly in the case of crotonaldehyde, where the corresponding metastable peak was very weak.

Discussion

$Co(C_3H_6)^+$ isomers and their interconversion. At least five plausible structures can be suggested for $Co(C_3H_6)^+$: a π-allyl hydrido complex **1**, a carbene ethene complex **2**, cobaltacyclobutane **3**, a cobalt propene complex **4**, and a hydrido cyclopropyl complex **5**.

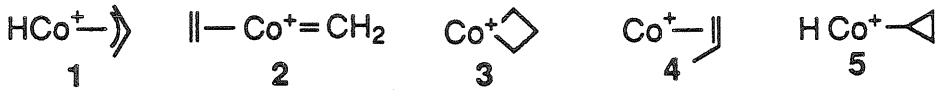

1 2 3 4 5

Production of structure **2** from cyclobutanone has been shown to be unlikely by CID and ligand displacement studies employing FTICR techniques.[9] By the same analysis, structure **1** probably does not result from reaction of Co^+ with cyclobutanone, since loss of C_3H_5 was not observed in either displacement or CID processes.[9] We consider **1** and **2** unlikely, although they cannot be strictly ruled out. Heats of formation for structures **3** and **4** have been determined to be 274 ± 5 kcal/mol[11] and 247 ± 5 kcal/mol,[15] respectively. On mechanistic grounds, it is expected that

reaction 8b should result initially in formation of **5**.

In an attempt to gain structural information on the various ionic products, CID studies were performed. Adducts with stoichiometry Co-$(C_4H_6O)^+$ were made by reaction of Co^+ with cyclobutanone and cyclopropanecarboxaldehyde, for comparison with those formed by reaction of $CoCO^+$ with propene and cyclopropane. The results are listed in Table III. The CID spectrum of Co(cyclobutanone)$^+$ resembles that of (CO)Co(cyclopropane)$^+$, especially at the most intense fragment peaks, at masses 101, 87, and 73. Similar structures are expected in these two cases, based on earlier work which found that Co^+ and $CoCp^+$ (Cp = cyclopentadienyl) can insert into a C-C bond in cyclopropane to form metallacyclobutanes.[3,6] The similarity is even stronger in Table IV, which reports CID spectra for $Co(C_3H_6)^+$ species. The spectrum for $Co(C_3H_6)^+$ produced by decarbonylating cyclobutanone resembles that of Co(cyclopropane)$^+$ much more closely than that of Co(propene)$^+$. The conclusion, that reaction of Co^+ with cyclobutanone results in formation of a cobaltacyclobutane ion, **3**, is in agreement with the earlier KERD study.[11]

CID experiments cast less light on the structure of Co(cyclopropanecarboxaldehyde)$^+$. The $Co(C_4H_6)^+$ CID pattern marginally resembles (CO)Co(propene)$^+$ more strongly than (CO)Co(cyclopropane)$^+$, especially at masses 87 and 73. However, the CID spectrum of $Co(C_3H_6)^+$ produced by decarbonylating cyclopropanecarboxaldehyde shows similarities to both Co(propene)$^+$ and Co(cyclopropane)$^+$. Some support for structure **5** comes

Table IV. Collision-Induced Dissociation Spectra of $Co(C_4H_6O)^+$ Ions Formed from Reaction of Co^+ with Cyclobutanone and Cyclopropanecarboxaldehyde, and from Reaction of $CoCO^+$ with Propene and Cyclopropane.

		Fragment Intensities[a]			
Reactant Neutrals:		Propene	cyclo-propane	cyclo-butanone	cyclopropane-carboxaldehyde
Fragment	m/z				
$CoC_3H_6^+$	101.	65.0	51.7	37.8	55.0
$CoC_3H_5^+$	100.	4.8	4.2	5.4	-
$CoC_3H_4^+$	99.	2.2	2.0	2.0	2.6
$CoC_3H_3^+$	98.	3.7	4.4	2.8	1.4
$CoCO^+$	87.	11.2	20.2	33.8	9.2
$CoC_2H_2^+$	85.	4.4	3.1	1.0	2.0
CoC_2H^+	84.	1.1	1.2	-	tr[b]
$CoCH_3^+$	74.	3.3	2.9	5.5	5.5
$CoCH_2^+$	73.	2.4	9.3	10.1	2.5
$CoCH^+/CoC^+$[c]	71.5	1.9	2.1	3.2	-
CoH^+	60.	tr[b]	tr[b]	-	-
$C_3H_6^+/C_3H_5^+$[c]	41.5	tr[b]	tr[b]	1.4	1.0
$C_3H_3^+$	39.	tr[b]	tr[b]	tr[b]	tr[b]

[a]All values normalized to ΣI_i, excluding Co^+ as a fragment ion.

[b]Less than 1%.

[c]Peaks not resolved in CID spectrum. Reported intensities are for the sum of of the unresolved peaks.

from the CID peak at mass 60, loss of C_3H_5, which was absent for all other methods of preparing $Co(C_3H_6)^+$. However, this peak is difficult to distinguish from the large neighboring C_3H_6 loss peak, and is therefore not definitive. The H-loss peak at m/z 100 is also consistent with **5**. It is possible that the ion beam consists of several different structures, especially if **5** is formed initially and undergoes rapid isomerization. Assuming that H bound to the metal center is labile and that oxidative addition of D_2 to the metal is facile, **5** should exchange H for D in the presence of excess D_2. FTICR experiments in the presence of excess D_2, conducted to examine H/D exchange in this species, failed to observe any exchange.[27]

From fitting the KERD for reaction 8b using phase space theory, the heat of formation of the $Co(C_3H_6)^+$ product is 274 ± 5 kcal/mol, identical to the heat of formation for structure **3** obtained in the decarbonylation of cyclobutanone.[11] Therefore, either structures **3** and **5** have very similar heats of formation, or isomerization to a metallacyclic structure (reaction 10) is rapid on the 5-15 μs time scale of the KERD experiment.

(10)

Assuming simple bond additivity, it is possible to estimate the heat of formation for structure **5**. Formation of **5** from Co^+ and cyclopropane involves breaking the C-H bond of cyclopropane and formation of Co^+-H and Co^+-C bonds. We estimate that **5** lies 3-11 kcal/mol lower than Co^+

+ cyclopropane,[28] giving a heat of formation of 292 ± 10 kcal/mol by this crude method. If this analysis is correct, it is improbable that similarity in the heats of formation for **3** and **5** can explain the results, even though this interpretation cannot be ruled out. In light of the results for loss of mass 42 from $Co(C_4H_6O)^+$ (*vide infra*), similar heats of formation may still be the most likely explanation.

The KERD for loss of CO from Co(crotonaldehyde)$^+$, reaction 8c, can be fit reasonably well using 247 kcal/mol for the heat of formation of $Co(C_3H_6)^+$. Use of the cobaltacyclobutane ion structure and thermochemistry gives a much poorer fit. The implication of the KERD results is that structure **4** is generated from crotonaldehyde. Considerable rearrangement of the crotonaldehyde structure is necessary to afford this product, illustrating once again the facility with which transition metal ions effect hydrocarbon isomerizations.

To summarize, CO losses from all of the $Co(C_4H_6O)^+$ species studied exhibit statistical KERDs. Modeling the KERDs using phase space theory yields heats of formation for the $Co(C_3H_6)^+$ products. Co(cyclobutanone)$^+$ and Co(cyclopropanecarboxaldehyde)$^+$ yield $Co(C_3H_6)^+$ with $\Delta H^0_{f,0K}$ = 274 ± 5 kcal/mol, indicating either that Co(cyclopropanecarboxaldehyde)$^+$ isomerizes to the same structure as Co(cyclobutanone)$^+$ prior to CO loss, or that the heats of formation of distinct structures **3** and **5** from the two precursors are coincidentally similar. Information to distinguish between these two possibilities is available from the reductive elimination C_3H_6 loss

studies presented below. Co(crotonaldehyde)$^+$ loses CO to yield a product with Co(propene)$^+$ structure 4.

Reductive elimination processes. Metastable loss of mass 42 from all of the Co(C_4H_6O)$^+$ species studied is non-statistical. In particular, the KERD for elimination of m/z 42 from Co(cyclobutanone)$^+$ is considerably broader, and is displaced to higher energies, than statistical theory predicts. The KERD extends to approximately the full exothermicity of the reaction, in a manner similar to that observed earlier for non-statistical dehydrogenation processes.[15] An earlier study[11] attributed this KERD to non-statistical reductive elimination of cyclopropane. This conclusion seems plausible in light of the evidence above that cobaltacyclobutane ion is formed from cyclobutanone, particularly in view of condensed phase results which indicate that transition metal ions can catalyze cyclopropanation through a metallacyclobutane intermediate.[18] Ketene loss is unlikely to account for this KERD, since it is very similar to the high-energy component of the bimodal KERD[11] resulting from loss of C_3H_6 from Co(1-pentene)$^+$, where no oxygen is present.

Intuitively, a barrier to the reverse process, insertion of Co$^+$ into a cyclopropane C-C bond, appears reasonable, since the process most likely involves concerted C-C cleavage and Co$^+$-C bond formation. If the barrier is large enough, it may dominate the KERD for cyclopropane elimination even if there is a well (resulting from formation of an association complex

of Co^+ with cyclopropane) in the potential energy surface as products separate. Rapid passage of the system through this region of the potential energy surface could prevent statistical randomization. Similarly, if the barrier occurs at longer range than the association complex, complete energy randomization is not expected as the products separate. In either event, the expected result is non-statistical energy release.

In a simplistic approach to the energetics of the elimination process, it might be anticipated that the most exothermic reaction should give the broadest KERD. The other factors governing energy dispersal (such as reduced masses, polarizabilities, rotational constants, number of internal modes, and vibrational frequencies) are either similar or equal for all the decomposing species. Certainly this would be the case if the final decomposing $Co(C_4H_6O)^+$ structures were all identical, for then the potential energy surface leading to products would be the same in every instance. That they are not is clearly evident from the KERD results for loss of mass 42. For any structure assumed for m/z 42, the order of exothermicities for the various reactants is Co(crotonaldehyde)$^+$ ≈ Co(cyclobutanone)$^+$ < Co(cyclopropanecarboxaldehyde)$^+$. However, the observed trend in $\langle E_t \rangle$ is Co(crotonaldehyde)$^+$ ≈ Co(cyclopropanecarboxaldehyde)$^+$ < Co(cyclobutanone)$^+$.

If, as is indicated above, Co(cyclobutanone)$^+$ forms a metallacyclobutane which eliminates cyclopropane, the final decomposing structure leading to loss of mass 42 from Co(cyclopropanecarboxaldehyde)$^+$ cannot

be the same metallacyclobutane. If it were, the larger amount of energy available to the Co(cyclopropanecarboxaldehyde)$^+$ system (0.43 eV, or 9.9 kcal/mol) would necessitate a broader KERD than that found for loss of cyclopropane from Co(cyclobutanone)$^+$. However, the broader KERD comes from Co(cyclobutanone)$^+$, showing conclusively that the final decomposing structures are different. It might be argued that the losses of CO and C_3H_6 from Co(cyclopropanecarboxaldehyde)$^+$ are not competing processes; i. e., that CO loss occurs from the metallacycle and that C_3H_6 loss occurs from a hydrido cyclopropyl species. This is not plausible in view of the low metastable intensity for C_3H_6 loss. Any process yielding rapid isomerization to the metallacycle should also lead to C_3H_6/CO loss branching ratios at least as great as those found for Co(cyclobutanone)$^+$, 18:80, rather than the observed 3:95 ratio.

The CO loss data presented above indicate that Co(crotonaldehyde)$^+$ rearranges to (CO)Co$^+$(propene) prior to loss of CO. Loss of mass 42 from the same intermediate should therefore correspond to elimination of propene. If both Co(cyclopropanecarboxaldehyde)$^+$ and Co(crotonaldehyde)$^+$ eliminate propene, the former should have the larger $\langle E_t \rangle$, since that process is 0.47 eV (10.8 kcal/mol) more exothermic. But, the $\langle E_t \rangle$ values for these two processes are approximately equal, again implying that the products are different.

Since all of the metastable losses of mass 42 involve non-statistical releases of kinetic energy, it is unlikely that an η^2 C-H alkane σ-complex

governs the final energy partitioning. Dissociation of a σ-complex should involve simple cleavage of a weak bond, analogous to that observed in the reductive elimination of small alkanes from transition metal-alkane ion complexes via a Lewis acid-base structure. All alkane losses observed so far are either statistical[15] or narrower than predicted by statistical theory.[29] Although cyclopropane is the expected neutral product in the loss of mass 42 from both Co(cyclobutanone)$^+$ and Co(cyclopropanecarboxaldehyde)$^+$, the KERDs are clearly non-statistical, providing examples of alkane losses with kinetic energy release greater than predicted by phase space theory.

Conclusions

Despite their identical stoichiometry, the $Co(C_4H_6O)^+$ ions formed from Co(cyclobutanone)$^+$, Co(cyclopropanecarboxaldehyde)$^+$, and Co(crotonaldehyde)$^+$ exhibit distinct chemistry. All of the data can be explained if Co(cyclobutanone)$^+$, Co(cyclopropanecarboxaldehyde)$^+$, and Co(crotonaldehyde)$^+$ retain distinct structures on the time scale of the KERD experiments. Co(cyclobutanone)$^+$ rearranges to a metallacyclic structure which eliminates either CO or cyclopropane. Co(cyclopropanecarboxaldehyde)$^+$ also eliminates either CO or cyclopropane, but does so from a (H)(cyclopropyl)Co$^+$(CO) species. Co(crotonaldehyde)$^+$ rearranges to (CO)Co$^+$(propene), with loss of mass 42 corresponding to loss of propene in this case rather than cyclopropane. Rearrangements of (CO)cobaltacyclobutane and (H)(cyclopropyl)Co$^+$(CO) ions to the lowest energy structure, (CO)Co(pro-

pene)$^+$, do not occur on the time scale of the KERD experiment, in contrast to observations made at longer times in both the gas phase[9] and in solution.[16] All the observed C_3H_6 losses are non-statistical. This argues against the importance of complexes with weak interactions between the metal center and a C-H σ bond (σ-complexes) in governing the partitioning of energy among the products. All of the transition states involved must be fairly "late," to account for the large kinetic energy releases observed.

Acknowledgement. We thank the National Science Foundation for supporting this research through grant numbers CHE87-11567 (JLB) and CHE88-17201 (MTB). We are also grateful to the Shell Foundation for graduate fellowship funding (DVD), and to the donors of the Petroleum Research Fund, administered by the American Chemical Society, for additional support. In addition, we thank Denley Jacobson for some of the initial data collection.

References and Notes

1. For a recent review of work in gas phase transition metal ion chemistry, see: Armentrout, P. B.; Beauchamp, J. L. *Acct. Chem. Res.*, manuscript in preparation.

2. Armentrout, P. B.; Beauchamp, J. L. *J. Am. Chem. Soc.* **1981**, *103*, 784-791.

3. Armentrout, P. B.; Halle, L. F.; Beauchamp, J. L. *J. Am. Chem. Soc.* **1981**, *103*, 6628-6632.

4. Jacobson, D. B.; Freiser, B. S. *J. Am. Chem. Soc.* **1983**, *105*, 7492-7500.

5. Houriet, R.; Halle, L. F.; Beauchamp, J. L. *Organometallics* **1983**, *2*, 1818-1829.

6. Jacobson, D. B.; Freiser, B. S. *J. Am. Chem. Soc.* **1985**, *107*, 7399-7407.

7. Halle, L. F.; Houriet, R.; Kappes, M.; Staley, R. H.; Beauchamp, J. L. *J. Am. Chem. Soc.* **1982**, *104*, 6293-6297.

8. Jacobson, D. B.; Freiser, B. S. *J. Am. Chem. Soc.* **1983**, *105*, 5197-5206.

9. Jacobson, D. B.; Freiser, B. S. *Organometallics* **1984**, *3*, 513-519.

10. Halle, L. F.; Crowe, W. E.; Armentrout, P. B.; Beauchamp, J. L. *Organometallics* **1984**, *3*, 1694-1706.

11. van Koppen, P. A. M.; Jacobson, D. B.; Illies, A. J.; Bowers, M. T.; Hanratty, M. A.; Beauchamp, J. L. *J. Am. Chem. Soc.* **1989**, *111*, 1991-2001.

12. (a) Grubbs, R. H. *Prog. Inorg. Chem.* **1979**, *24*, 1. (b) Calderon, N.; Lawrence, J. P.; Ofstead, E. A. *Adv. Organomet. Chem.* **1979**, *17*, 449. (c) Katz, T. J. *Ibid.* **1977**, *16*, 283. (d) Casey, C. P.; Scheck, D. M.; Shusterman, A. J. "Fundamental Research in Homogeneous Catalysis"; Tsutsui, M.; Ed.; Plenum Press: New York, 1979; Vol. 3, p. 141. (e) Herrison, J. L.; Chauvin, Y. *Makromol. Chem.* **1970**, *141*, 161. (f) Grubbs,

R. H.; Hoppin, C. J. *J. Am. Chem. Soc.* **1979**, *101*, 1499. (g) Mocella, M. T.; Rovner, R.; Muetterties, E. L. *J. Am. Chem. Soc.* **1976**, *98*, 4689. (h) Grubbs, R. H.; Miyashita, A. "Fundamental Research in Homogeneous Catalysis"; Tsutsui, M.; Ed.; Plenum Press: New York, 1979; Vol. 3, p. 151. (i) Grubbs, R. H. *Inorg. Chem.* **1979**, *18*, 2623.

13. (a) Dartigues, J. M.; Chambellan, A.; Gault, F. G. *J. Am. Chem. Soc.* **1976**, *98*, 856. (b) Foger, K.; Anderson, J. R. *J. Catal.* **1978**, *54*, 318. (c) Irvin, K. J.; Rooney, J. J.; Stewart, C. D.; Green, M. L. H.; Mahtab, R. J. *J. Chem. Soc., Chem. Commun.* **1978**, 604.

14. Sharpless, K. B.; Teranishi, A. Y.; Backvall, J. E. *J. Am. Chem. Soc.* **1977**, *99*, 3120.

15. a) Hanratty, M. A.; Beauchamp, J. L.; Illies, A. J.; Bowers, M. T. *J. Am. Chem. Soc.* **1985**, *107*, 1788. b) Hanratty, M. A.; Beauchamp, J. L.; Illies, A. J.; van Koppen, P. A. M.; Bowers, M. T. *J. Am. Chem. Soc.* **1988**, *110*, 1-14.

16. Periana, R. A.; Bergman, R. G. *J. Am. Chem. Soc.* **1986**, *108*, 7346-7355.

17. Periana, R. A.; Bergman, R. G. *J. Am. Chem. Soc.* **1986**, *108*, 7332-7346.

18. Hanks, T. W.; Jennings, P. W. *J. Am. Chem. Soc.* **1987**, *109*, 5023-5025.

19. Morgan, R. P.; Beynon, J. H.; Bateman, R. H.; Green, B. N. *Int. J. Mass Spectrom. Ion. Phys.* **1978**, *28*, 171-191.

20. Jarrold, M. F.; Illies, A. J.; Bowers, M. T. *Chem. Phys.* **1982**, *65*, 19.

21. The energy resolution in the center-of-mass frame ΔT is related to that of the main beam in the laboratory frame ΔE by the equation $\Delta T = \Delta E[(M_1^2T)/(M_2M_3V_1)]^{1/2}$, where M_1 is the mass of the parent metastable ion, M_2 and M_3 are the masses of the ionic and neutral fragments, V_1 is the lab kinetic energy of the parent metastable ion, and T is the center of mass kinetic energy. This formula is taken from Hanratty, M. A. Ph.D. Thesis, California Institute of Technology, 1985. For an extreme example, consider the dehydrogenation of cyclopentene by Fe^+. With a main beam resolution of 2 eV and a center-of-mass kinetic energy of 200 meV, the spread in center-of-mass kinetic energy due to the spread in the main beam is 79 meV. The contribution from ΔE is much less significant for fragmentations involving heavier neutrals.

22. Young, B. L.; Trahanovsky, W. S. *J. Org. Chem.* **1967**, *32*, 2349-2350.

23. a) Jarrold, M. F.; Illies, A. J.; Bowers, M. T. *J. Chem. Phys.* **1983**, *79*, 6086. b) Jarrold, M. F.; Illies, A. J.; Kirchner, N. J.; Wagner-Redeker, W.; Bowers, M. T.; Mandich, M. L.; Beauchamp, J. L. *J. Phys. Chem.* **1983**, *87*, 2213-2221.

24. Dearden, D. V.; Hayashibara, K.; Beauchamp, J. L.; Kirchner, N. J.; van Koppen, P. A. M.; Bowers, M. T. *J. Am. Chem. Soc.* **1989**, *111*, 2401-2409.

25. A more recent version of some of the phase space routines employed has been submitted to QCPE: Chesnavich, W. J.; Bass, L.; Grice, M. E.; Song, K.; Webb, D. A. "TSTPST: Statistical Theory Package for RRKM/QET/TST/PST Calculations", *QCPE*.

26. van Koppen, P. A. M.; Bowers, M. T., personal communication.

27. Dearden, D. V.; Beauchamp, J. L., unpublished results.

28. Assuming D(*cyclo*-C_3H_5-H) = 95 kcal/mol, and using values of 46.6±1.4 kcal/mol for D(Co^+-H), and 55±4 kcal/mol for D(Co^+-C), estimated using values compiled in: Armentrout, P. B.; Georgiadis, R. *Polyhedron* **1988**, *7*, 1573-1581.

29. Dearden, D. V.; Beauchamp, J. L.; van Koppen, P. A. M.; Brodbelt-Lustig, J.; Bowers, M. T. Manuscript in preparation. See Chapter 2 of this thesis.

CHAPTER 4

STATISTICAL KINETIC ENERGY RELEASE IN DEHYDROGENATION PROCESSES: REACTIONS OF TRANSITION METAL IONS WITH CYCLOALKANES IN THE GAS PHASE.

STATISTICAL KINETIC ENERGY RELEASE IN DEHYDROGENATION PROCESSES: REACTIONS OF TRANSITION METAL IONS WITH CYCLOALKANES IN THE GAS PHASE.

David V. Dearden and J. L. Beauchamp

Arthur Amos Noyes Laboratory of Chemical Physics

California Institute of Technology

Pasadena, CA 91125

Petra A. M. van Koppen, Denley B. Jacobson, and Michael T. Bowers

Department of Chemistry

University of California

Santa Barbara, CA 93106

Abstract.

The product kinetic energy release distributions measured for the final hydrogen loss in the double dehydrogenations of cyclopentane and cyclohexane by Fe^+ and Co^+ are remarkably similar to those obtained for single dehydrogenations of cyclopentene and cyclohexene by the same metal ions. This similarity is explained by participation of electronically excited metal ions in the double dehydrogenation processes, which accounts for the necessary additional metastable energy. Previous work observed that dehydrogenation of linear alkanes by Co^+ and Ni^+ in the gas phase is characterized by release of more energy into product translation than is accounted for by statistical theory. This rule is not general, since dehydrogenation of cyclopentene and cyclohexene by Fe^+ is well-described by a statistical analysis with the best fit of phase space theory to experiment yielding $D^0_0(Fe^+\text{-}C_5H_6)$ = 55±5 kcal/mol and $D^0_0(Fe^+\text{-}C_6H_8)$ = 70±5 kcal/mol. Validity of the statistical theory requires that there be no barrier for the reverse association reaction, in agreement with earlier studies showing that H/D exchange occurs for $Fe(C_5H_6)^+$ in the presence of excess D_2 at about 5% of the Langevin collision rate. Dehydrogenations of cyclopentene and cyclohexene by Co^+ yield broader kinetic energy release distributions, indicating either that the processes are non-statistical even though the distributions can be fit with phase space theory, that electronically excited Co^+ is involved, or that the resulting Co^+-ligand bonds are surprisingly strong. If the last possibility is correct, it may indicate a hydridocyclopentadienyl structure for $Co(C_5H_6)^+$.

Introduction

The dehydrogenation of hydrocarbons by transition metal ions has been extensively investigated. From studies of isotopically labeled butanes, it has been established that at least two distinct dehydrogenation mechanisms are operative. The reactions of Co^+ and Ni^+ with 2-methylpropane-*2-d*$_1$ result in exclusive loss of HD, indicating that 1,2 dehydrogenation is the dominant route.[1] However, ion beam studies[1,2] of the dehydrogenation of butane-*1,1,1,4,4,4-d*$_6$ by Ni^+, as well as ligand exchange[2] and low-energy collision-induced dissociation experiments,[3] indicate that 1,4 dehydrogenation is the main process in this system. The reaction of Co^+ with butane-*1,1,1,4,4,4-d*$_6$ gives a mixture of dehydrogenation products, with losses of H_2, HD, and D_2 occurring with ratios 16:28:56.[1] To determine whether this mixture of products is due to competing 1,2- and 1,4-dehydrogenation, or to H-scrambling in the 1,4 process, the releases of kinetic energy in the 1,2-dehydrogenations of 2-methylpropane and 2-methylpropane-*2-d*$_1$ by Co^+, and in the 1,4-dehydrogenation of butane-*1,1,1,4,4,4-d*$_6$ by Ni^+, were examined for comparison with the kinetic energy release found in the dehydrogenation of butane-*1,1,1,4,4,4-d*$_6$ by Co^+.[4] Greater kinetic energy release was expected for the 1,4 process, since this is about 9 kcal/mol more exothermic than 1,2-dehydrogenation. The study concluded that 1,2- and 1,4-dehydrogenation give quite distinct kinetic energy release distributions (KERDs), with 1,4-dehydrogenation producing the broadest

release of energy. Losses of H_2, HD, and D_2 in the reaction of Co^+ with butane-*1,1,1,4,4,4-d*$_6$ all gave broad KERDs with shapes characteristic of the 1,4-process, establishing that the elimination of H_2 and HD is likely due to scrambling rather than 1,2-elimination. None of the KERDs studied could be modeled using statistical theories, and that result appeared to be general for dehydrogenation reactions.

In earlier work, KERDs substantially broader than predicted by statistical theory have been taken to be evidence of a barrier in the potential energy surface exit channel leading to product formation.[4,5] This necessitates a barrier to the reverse process, in this case oxidative addition of H_2 to the metal center. The products of the reactions cited above do not provide any evidence for a facile reverse reaction. However, in several systems there is evidence that oxidative addition of D_2 can occur with little or no barrier. For example, ion cyclotron resonance studies indicate that $M(C_5H_6)^+$ (M = Fe, Co), generated either by dehydrogenation of cyclopentene or by double dehydrogenation of cyclopentane, undergoes six H/D exchanges in the presence of excess D_2.[6] Likewise, $Co(C_5H_6)^+$ produced by reaction of Co^+ with either cycloheptatriene or norbornadiene, is observed to exchange all six hydrogens for deuterium.[7] These exchange reactions are fairly rapid, with the first exchange occurring at about 5% of the Langevin collision rate,[8] and the remaining exchanges proceeding with rates about one order of magnitude slower.[6]

The proposed mechanism for these exchange processes (Scheme I)[6,7] involves rapid equilibrium between the M^+-cyclopentadiene and $(H)M^+$-cyclopentadienyl structures, with D substitution occurring initially only in the *endo* position. This accounts for the first, rapid exchange. A rate-limiting 1,5-sigmatropic shift (exofacial migration) allows substitution at the remaining positions. The initial exchange could not occur if a barrier larger than thermal collision energies, 1-2 kcal/mol, were present for addition of D_2. Little chemical activation is expected from the ion-induced dipole interaction with D_2, since the polarizability of D_2 is low. The relatively low level of chemical activation afforded by interaction with D_2 is emphasized by comparing the ability of D_2 to induce H/D exchange with that of C_2D_4.[9] The latter is a strong deuterating agent in the gas phase, due to the chemical activation furnished through formation of a M^+-ethene bond, estimated to be at least 30 kcal/mol.[9] For example, propene complexes of Fe^+, Co^+, and Ni^+ are all observed to undergo 5 H/D exchanges in the presence of excess C_2D_4, while they are unreactive in the presence of D_2.[9]

If no barrier exists for oxidative addition of D_2, the reverse process, dehydrogenation, should exhibit a statistical KERD. The present work constitutes a reexamination of the proposition that dehydrogenation is characterized by non-statistical release of kinetic energy. Emphasis is placed on dehydrogenations, believed to be reversible, which form $Fe(C_5H_6)^+$ and $Co(C_5H_6)^+$. If dehydrogenation is statistical, modeling the process using statistical theory yields an additional benefit. Since the model calculations

Scheme I. Mechanism proposed for H/D exchange in $M(C_5H_6)^+$ species in the presence of excess D_2, where M = Fe, Co.

Scheme I

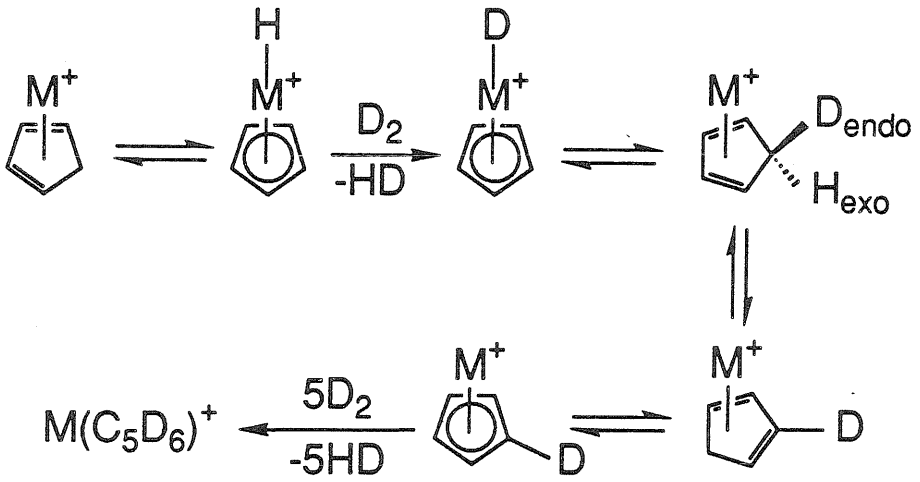

are sensitive to only one unknown parameter, the reaction exothermicity, variation of that parameter to achieve a good fit to the experimental results can be used to estimate the exothermicity. In this way, thermochemical information which is very difficult to determine by any other method can be obtained.

Experimental Section

Kinetic energy release measurements were carried out at UCSB using a double-focusing, reversed-geometry mass spectrometer (VG Industries, ZAB-2F[10]) with a home-built pressure- and temperature-variable electron impact source. The methods used in metastable and collision-induced dissociation studies have been described.[11] Briefly, Co^+, generated by 150 eV electron impact on $Co(CO)_3NO$ (Aldrich), or Fe^+, from electron impact on $Fe(CO)_5$, was allowed to react in the source with the hydrocarbon of interest to form a $M(hydrocarbon)^+$ adduct. Total source pressures were typically 1-5 x 10^{-3} Torr, monitored with a Baratron capacitance manometer. The ratio of volatile metal compound and hydrocarbon pressures was approximately 1:1, and was varied to maximize adduct signal. The source temperature was maintained at approximately -10° to 0° C to minimize the decomposition of metal-containing compounds on insulating surfaces. Ions exiting the source were accelerated to 8 keV and mass selected with a magnetic sector. Fragment ions from metastable decomposition in the second field-free region (downstream from the magnet) were energy

analyzed with an electrostatic sector, and were detected using pulse counting techniques. The background pressure in the second field-free region is typically less than 10^{-9} Torr. The resolution of the main ion beam was typically 2 eV fwhm. At this resolution, the contribution of the main beam energy spread to the width of the kinetic energy release distribution in the center-of-mass reference frame is not important.[12]

The methods for obtaining kinetic energy release distributions from metastable peak shapes have been described.[13] Raw data were smoothed using a moving average algorithm, after which numerical differentiation and conversion to the center-of-mass reference frame were carried out. Phase space theory was used to model the distributions. In these calculations, the only free parameter having a large influence on the fit to the experimental data was ΔH for the reaction. The use of phase space theory to determine reaction enthalpies has been discussed.[4,14,15]

Results and Discussion

KERDs for dehydrogenations of cyclopentane, cyclopentene, cyclohexane, cyclohexene, and cyclohexadiene are depicted in Figures 1-12. Experimental average kinetic energy releases for each process are compiled in Table I. Where appropriate, averages predicted using phase space theory are also included in Table I.

Figure 1. Experimental kinetic energy release distribution, in the center-of-mass frame, for single dehydrogenation of cyclopentane by Fe^+ (solid line), and distribution calculated using phase space theory with ΔH = -3 eV for the reaction (filled circles).

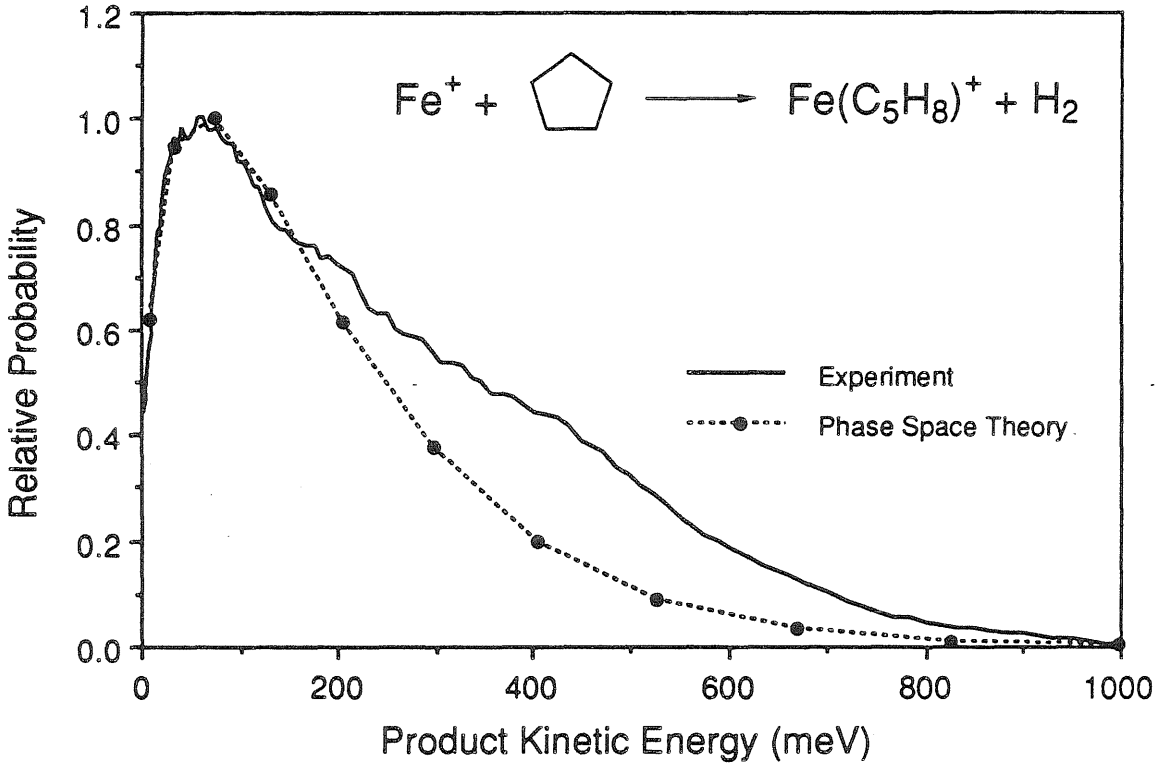
1.2
1.0
0.8
0.6
0.4
0.2
0.0
Relative Probability
0
200
400
600
800
1000
Product Kinetic Energy (meV)
Fe+ +
Fe(C5H8)+ + H2
Experiment
Phase Space Theory

Figure 2. Experimental kinetic energy release distribution, in the center-of-mass frame, for single dehydrogenation of cyclopentane by Co^+ (solid line), and distribution calculated using phase space theory with ΔH = -4 eV for the reaction (filled circles).

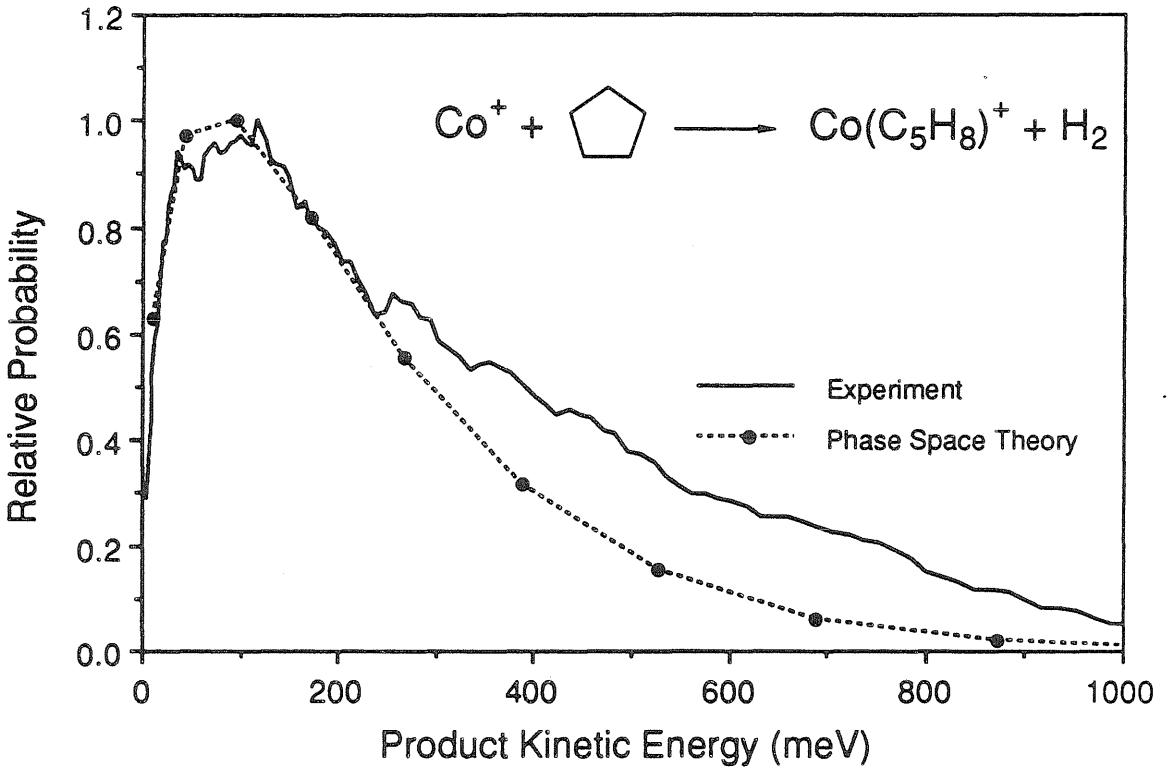
1.2
1.0
0.8
0.6
0.4
0.2
0.0
Relative Probability
0
200
400
600
800
1000
Product Kinetic Energy (meV)
Co+ +
Co(C5H8)+ + H2
Experiment
Phase Space Theory

Figure 3. Experimental kinetic energy release distribution, in the center-of-mass frame, for double dehydrogenation of cyclopentane by Fe^+ (solid line). Loss of the first H_2 molecule occurs in the ion source, and the measured distribution is for loss of the second H_2.

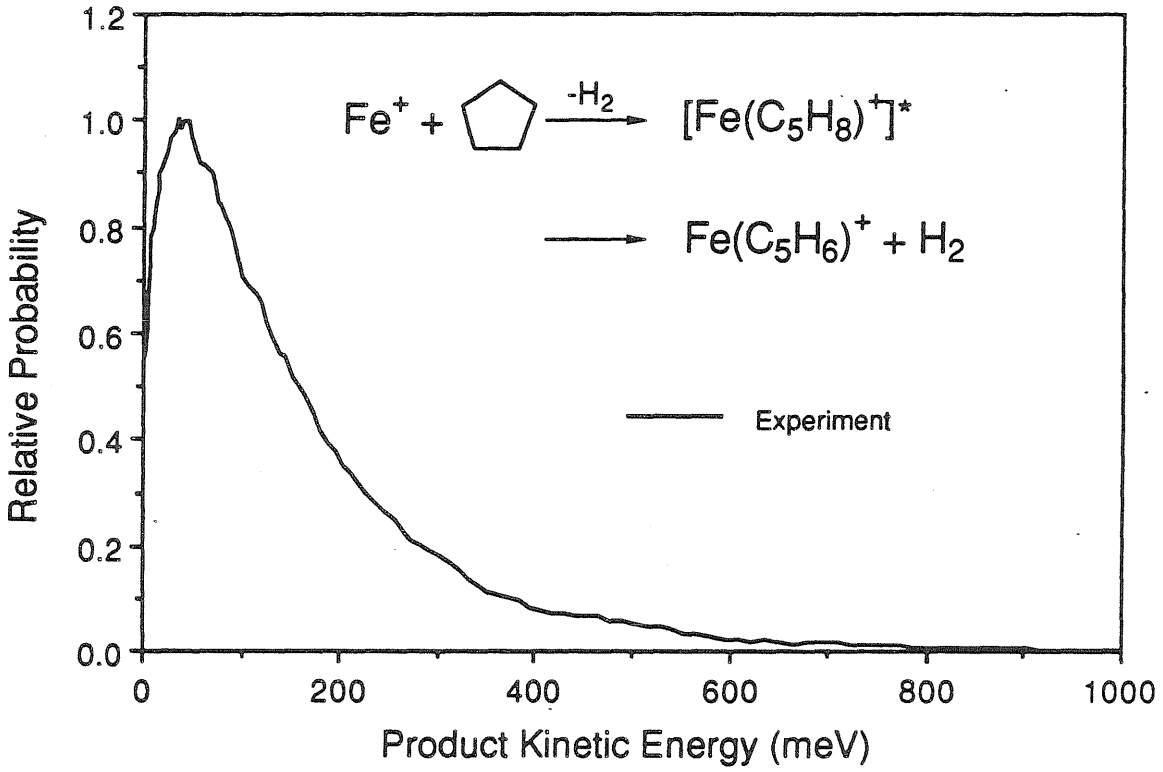
1.2
1.0
0.8
0.6
0.4
0.2
0.0
Relative Probability
0
200
400
600
800
1000
Product Kinetic Energy (meV)
Fe+ +
-H2
[Fe(C5H8)+]*
Fe(C5H6)+ + H2
Experiment

Figure 4. Experimental kinetic energy release distribution, in the center-of-mass frame, for dehydrogenation of cyclopentene by Fe^+ (solid line), and distribution calculated using phase space theory with $D_0^0(Fe^+\text{-}C_5H_6)$ = 55 kcal/mol (filled circles).

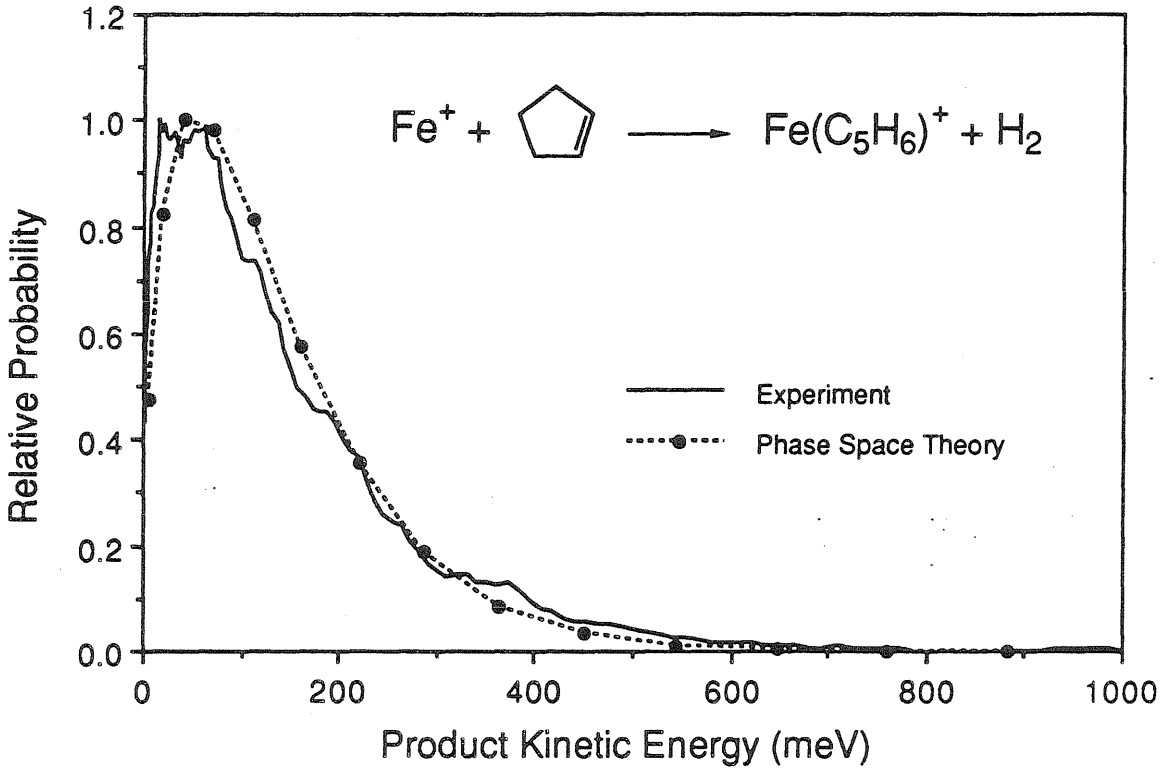
1.2
1.0
0.8
0.6
0.4
0.2
0.0
Relative Probability
0
200
400
600
800
1000
Product Kinetic Energy (meV)
Fe+ +
Fe(C5H6)+ + H2
Experiment
Phase Space Theory

Figure 5. Experimental kinetic energy release distribution, in the center-of-mass frame, for double dehydrogenation of cyclopentane by Co^+ (solid line). Loss of the first H_2 molecule occurs in the ion source, and the measured distribution is for loss of the second H_2.

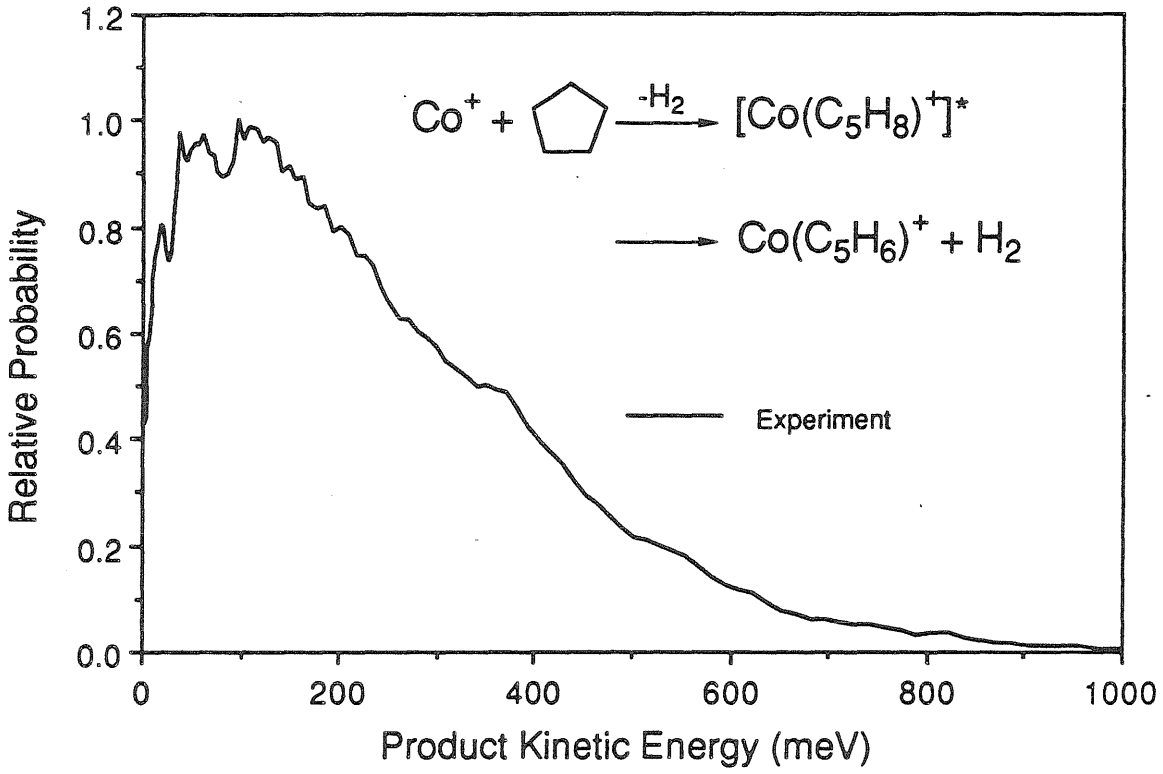
1.2
1.0
0.8
0.6
0.4
0.2
0.0
Relative Probability
0
200
400
600
800
1000
Product Kinetic Energy (meV)
Co+ + -H2 → [Co(C5H8)+]*
→ Co(C5H6)+ + H2
Experiment

Figure 6. Experimental kinetic energy release distribution, in the center-of-mass frame, for dehydrogenation of cyclopentene by Co^+ (solid line), and distribution calculated using phase space theory with $D_0^0(Co^+\text{-}C_5H_6)$ = 113 kcal/mol (filled circles).

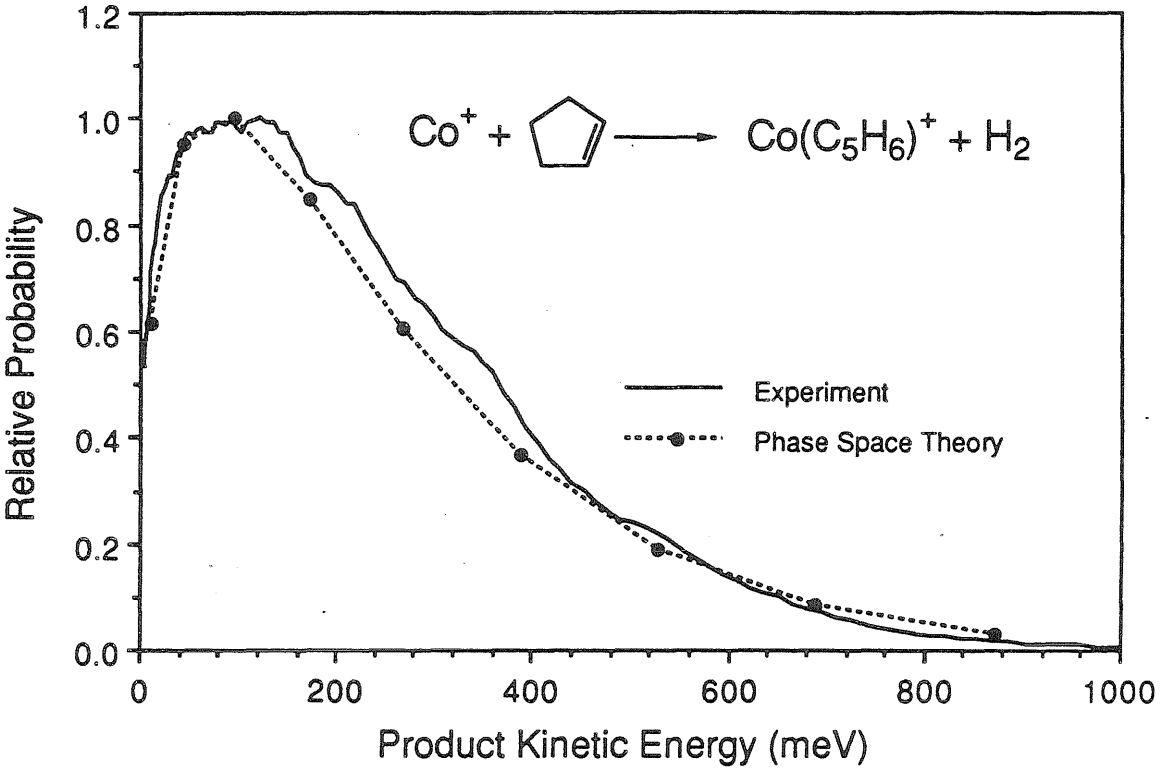
1.2
1.0
0.8
0.6
0.4
0.2
0.0
Relative Probability
0
200
400
600
800
1000
Product Kinetic Energy (meV)
Co+ +
Co(C5H6)+ + H2
Experiment
Phase Space Theory

Figure 7. Experimental kinetic energy release distribution, in the center-of-mass frame, for double dehydrogenation of cyclohexane by Fe^+ (solid line). Loss of the first H_2 molecule occurs in the ion source, and the measured distribution is for loss of the second H_2.

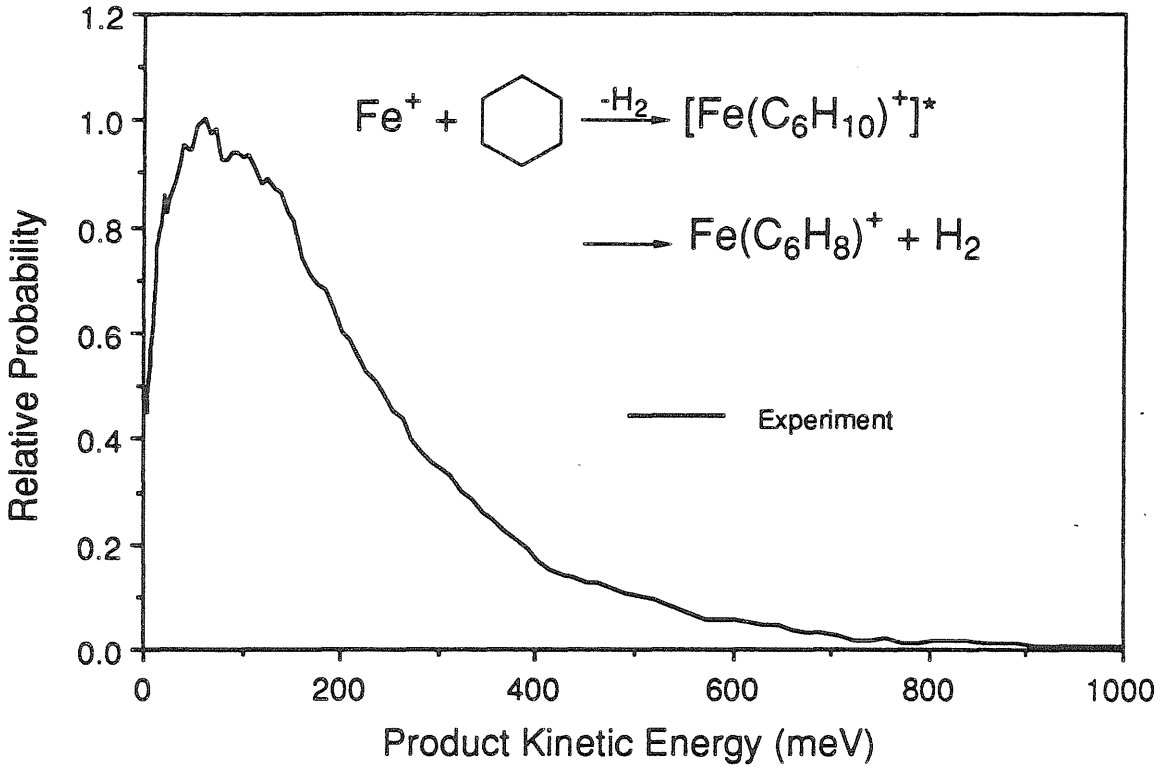
1.2
1.0
0.8
0.6
0.4
0.2
0.0
Relative Probability
0
200
400
600
800
1000
Product Kinetic Energy (meV)
Fe+ +
-H2
[Fe(C6H10)+]*
Fe(C6H8)+ + H2
Experiment

Figure 8. Experimental kinetic energy release distribution, in the center-of-mass frame, for single dehydrogenation of cyclohexene by Fe^+ (solid line), and distribution calculated using phase space theory with $D_0^0(Fe^+\text{-}C_6H_8)$ = 70 kcal/mol (filled circles).

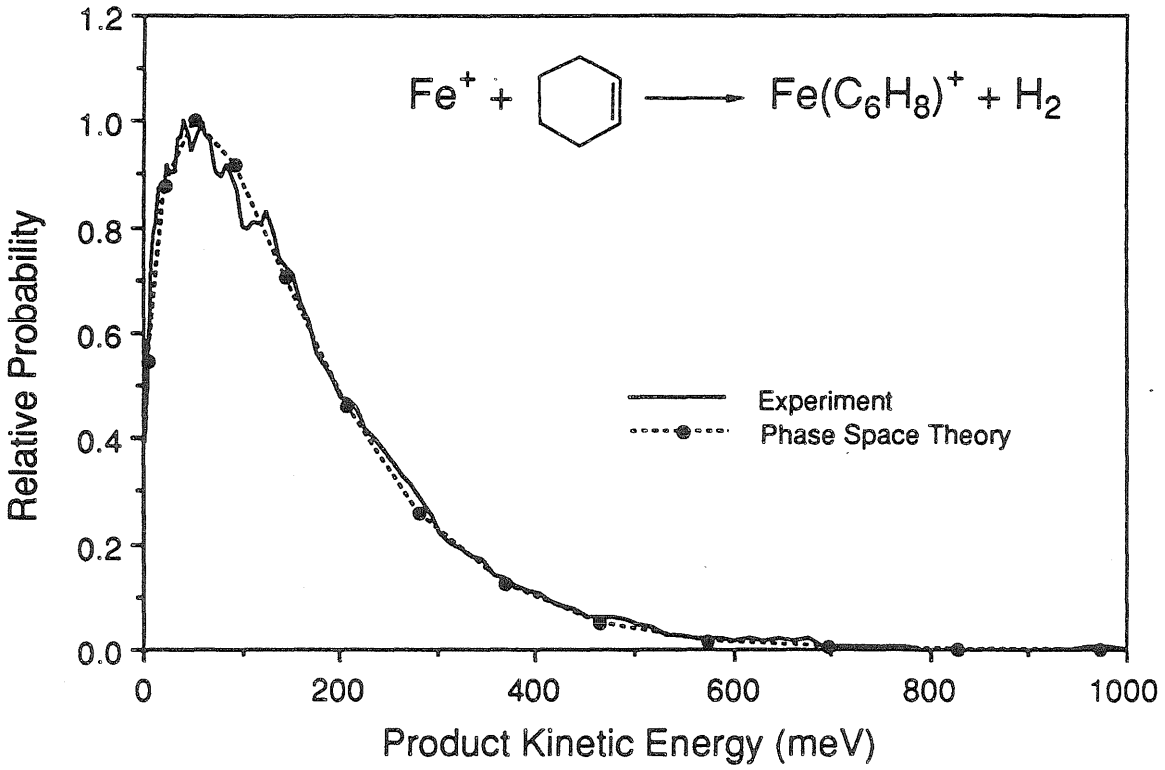
1.2
1.0
0.8
0.6
0.4
0.2
0.0
Relative Probability
0
200
400
600
800
1000
Product Kinetic Energy (meV)
Fe+ +
Fe(C6H8)+ + H2
Experiment
Phase Space Theory

Figure 9. Experimental kinetic energy release distribution, in the center-of-mass frame, for double dehydrogenation of cyclohexane by Co^+ (solid line). Loss of the first H_2 molecule occurs in the ion source, and the measured distribution is for loss of the second H_2.

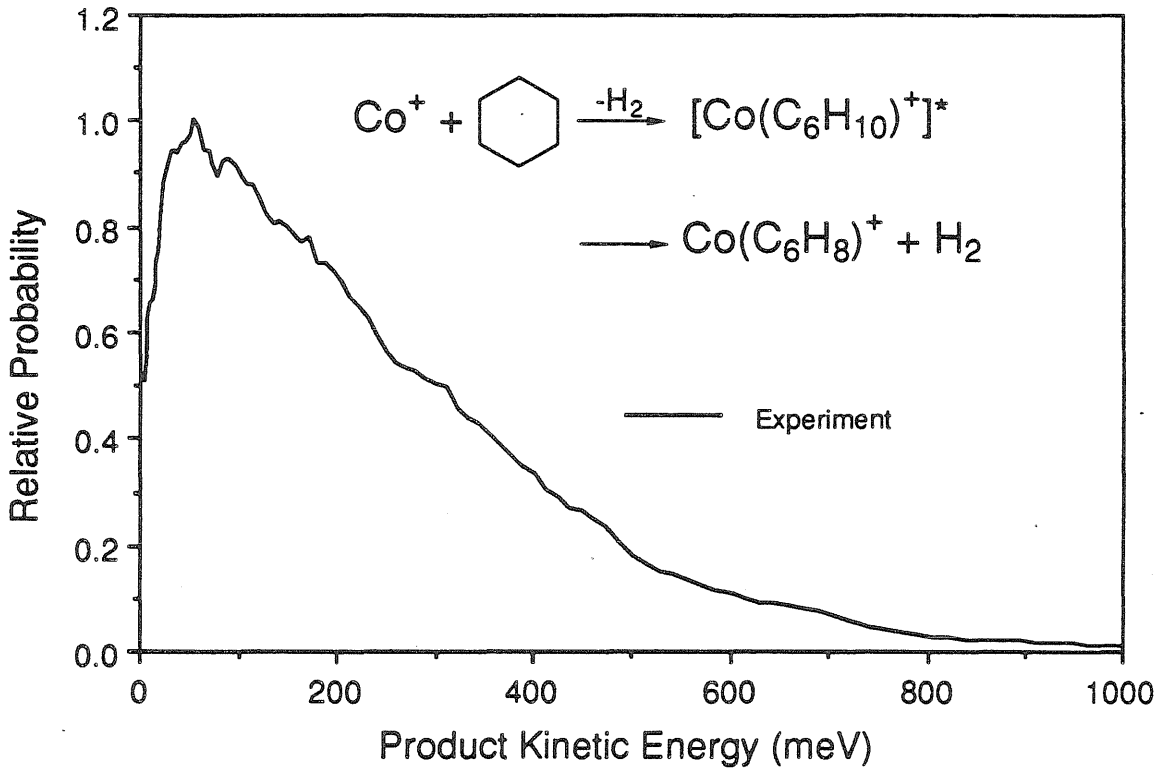
1.2
1.0
0.8
0.6
0.4
0.2
0.0
Relative Probability
0
200
400
600
800
1000
Product Kinetic Energy (meV)
Co+ +
-H2
[Co(C6H10)+]*
Co(C6H8)+ + H2
Experiment

Figure 10. Experimental kinetic energy release distribution, in the center-of-mass frame, for single dehydrogenation of cyclohexene by Co^+ (solid line), and distribution calculated using phase space theory with $D_0^0(Co^+\text{-}C_6H_8)$ = 88 kcal/mol (filled circles).

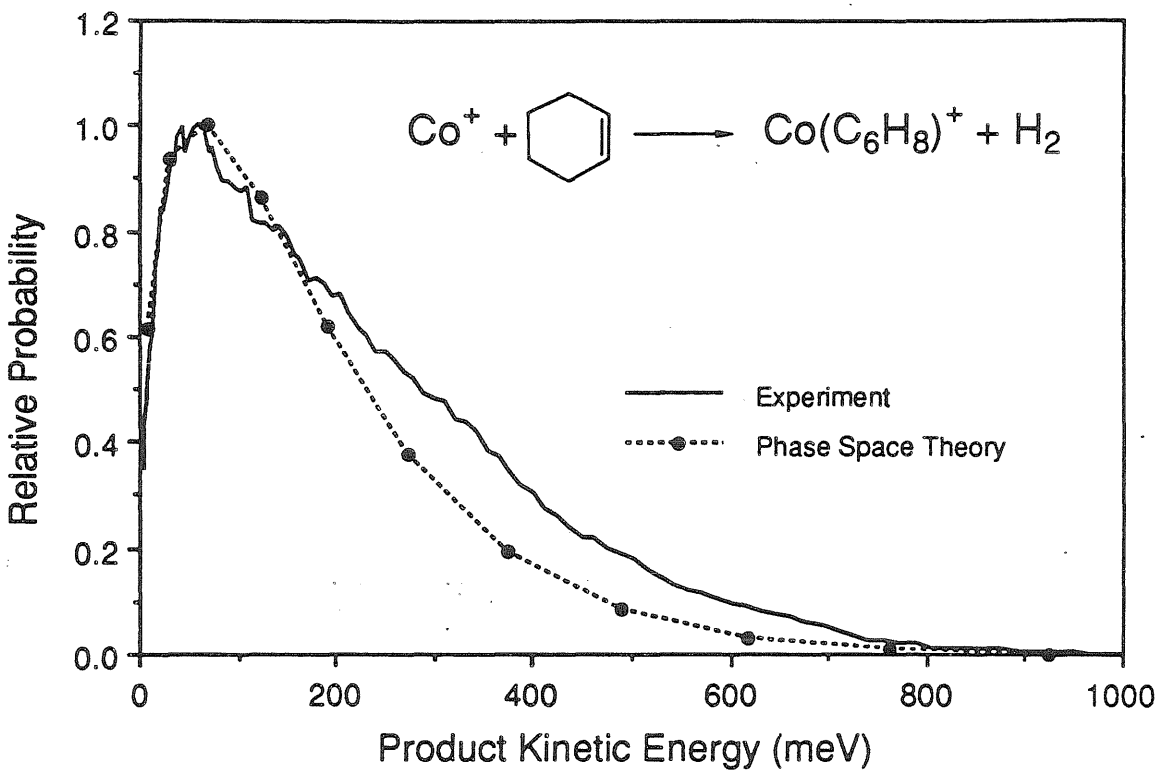
1.2
1.0
0.8
0.6
0.4
0.2
0.0
Relative Probability
0
200
400
600
800
1000
Product Kinetic Energy (meV)
Co+ +
Co(C6H8)+ + H2
Experiment
Phase Space Theory

Figure 11. Experimental kinetic energy release distribution, in the center-of-mass frame, for double dehydrogenation of cyclohexene by Fe^+ (solid line). Loss of the first H_2 molecule occurs in the ion source, and the measured distribution is for loss of the second H_2. Note the change in scale.

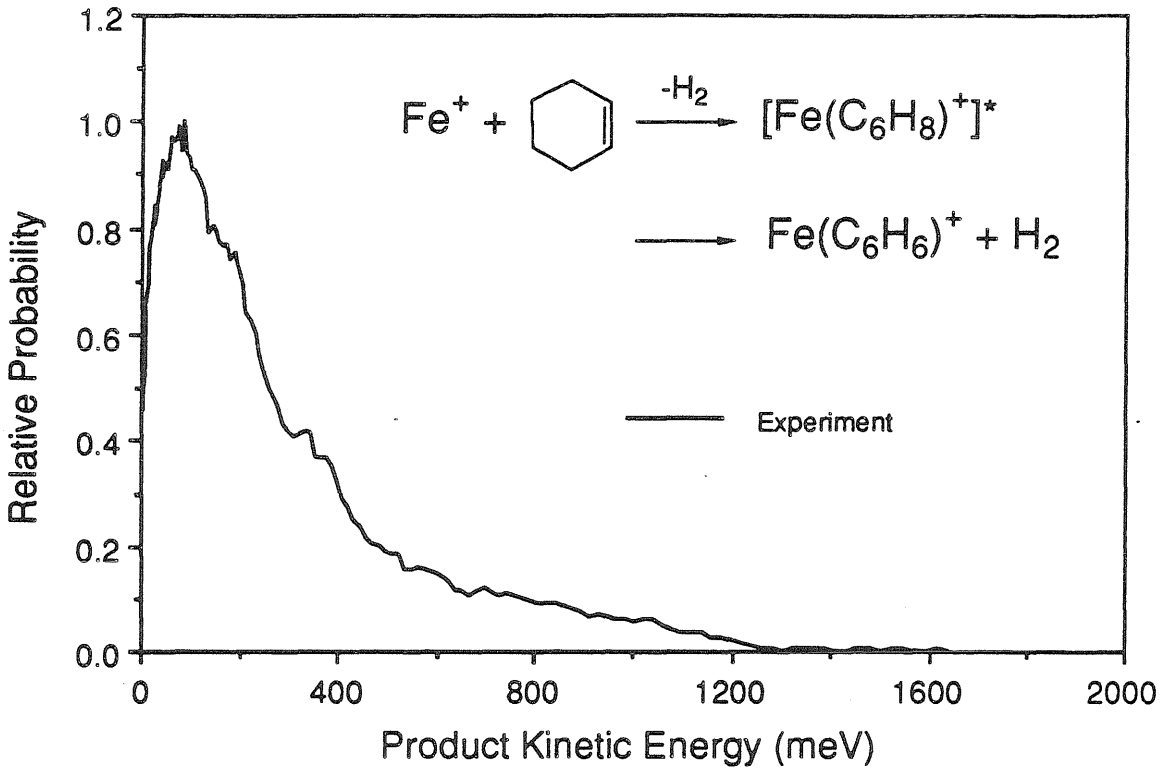
1.2
1.0
0.8
0.6
0.4
0.2
0.0
Relative Probability
0
400
800
1200
1600
2000
Product Kinetic Energy (meV)
Fe+ +
-H2
[Fe(C6H8)+]*
Fe(C6H6)+ + H2
Experiment

Figure 12. Experimental kinetic energy release distribution, in the center-of-mass frame, for dehydrogenation of 1,3-cyclohexadiene by Co^+ (solid line). Loss of the first H_2 molecule occurs in the ion source, and the measured distribution is for loss of the second H_2. Note the change in scale.

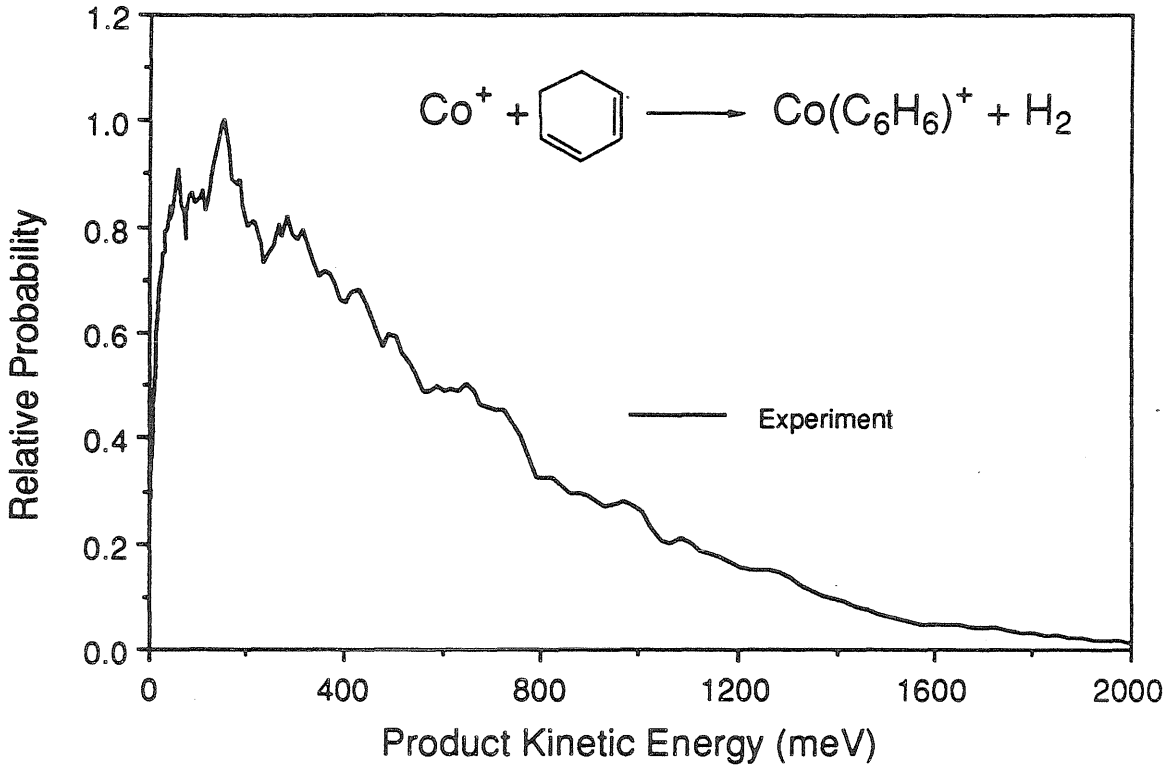
1.2
1.0
0.8
0.6
0.4
0.2
0.0
Relative Probability
0
400
800
1200
1600
2000
Product Kinetic Energy (meV)
Co+ +
Co(C6H6)+ + H2
Experiment

Table I. Average Kinetic Energy Releases $\langle E_t \rangle$ From Experiment and Phase Space Theory Calculations

Reaction	$\langle E_t \rangle_{exp}$ [a]	$\langle E_t \rangle_{calc}$ [a]
$Fe^+ + \text{cyclopentane} \rightarrow Fe(C_5H_8)^+ + H_2$	0.268	0.196
$Fe^+ + \text{cyclopentane} \rightarrow Fe(C_5H_6)^+ + 2H_2$	0.154	[b]
$Fe^+ + \text{cyclopentene} \rightarrow Fe(C_5H_6)^+ + H_2$	0.146	0.136
$Fe^+ + \text{cyclohexane} \rightarrow Fe(C_6H_8)^+ + 2H_2$	0.190	[b]
$Fe^+ + \text{cyclohexene} \rightarrow Fe(C_6H_8)^+ + H_2$	0.158	0.152
$Fe^+ + \text{cyclohexene} \rightarrow Fe(C_6H_6)^+ + 2H_2$	0.295	[b]
$Co^+ + \text{cyclopentane} \rightarrow Co(C_5H_8)^+ + H_2$	0.322	0.233
$Co^+ + \text{cyclopentane} \rightarrow Co(C_5H_6)^+ + 2H_2$	0.244	[b]
$Co^+ + \text{cyclopentene} \rightarrow Co(C_5H_6)^+ + H_2$	0.244	0.252
$Co^+ + \text{cyclohexane} \rightarrow Co(C_6H_8)^+ + 2H_2$	0.238	[b]
$Co^+ + \text{cyclohexene} \rightarrow Co(C_6H_8)^+ + H_2$	0.226	0.180
$Co^+ + \text{cyclohexadiene} \rightarrow Co(C_6H_6)^+ + H_2$	0.525	[b]

[a]Units: eV.

[b]Not calculated because of ambiguity in reactant internal energy.

$M(C_5H_8)^+$, M = Fe, Co. Single dehydrogenation of cyclopentane, reaction 1, was used to produce $M(C_5H_8)^+$.

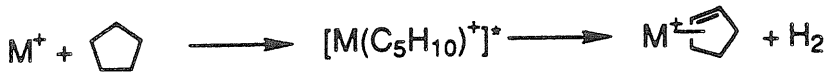

(1)

For both Fe^+ and Co^+, the KERDs for the dehydrogenation process are quite broad.[16] Phase space theory was unable to produce fits to the entire distributions. Fits of the low product kinetic energy portion of the distributions, shown with the experimental results in Figures 1 and 2, underestimate the high-energy portion in both cases. Reaction exothermicities of 69 kcal/mol and 92 kcal/mol were required to produce the fits shown for Fe^+ and Co^+, respectively. These values imply unreasonably large M^+-C_5H_8 bond energies in both cases. Both the inability to fit the experimental distributions with statistical theory, and the large exothermicities required to fit even the low-energy portions, strongly suggest that this dehydrogenation process is non-statistical, similar to those noted previously.

$M(C_5H_6)^+$, M = Fe, Co. $M(C_5H_6)^+$ species are formed by two successive dehydrogenations of cyclopentane, reaction 2, or by single dehydrogenation of cyclopentene, reaction 3.

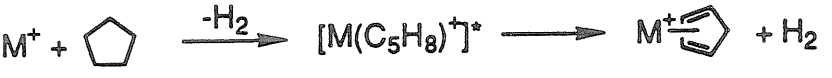

(2)

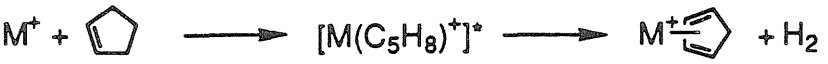

(3)

For reaction 2, the first H_2 loss occurs in the ion source, and the mass-selected ion is metastable $[M(C_5H_8)^+]^*$, which loses a second H_2 molecule in the second field-free region of the mass spectrometer. The KERD is measured for the loss of this second H_2. This process cannot be modeled using phase space theory in a straightforward manner, since an important input parameter, the level of internal excitation of $[M(C_5H_8)^+]^*$, is unknown.[17] In reaction 3, the mass-selected metastable is M^+(cyclopentene) adduct, and the phase space treatment is straightforward since in this case the energetics are fully determined by the heats of formation of the reactants.

A mechanism for reaction 3 is suggested in Scheme II. Initially, a M^+-cyclopentene adduct is formed by coordination of the metal to the double bond. Transfer of a β-H results in a hydridoallylic species, which rearranges by a second H-transfer to produce H_2M^+(cyclopentadiene). β-H transfer is a well-established mechanistic step for reactions of transition metal ions with alkanes in the gas phase[1] and in solution.[18] The H_2M^+(cyclopentadiene) species may reductively eliminate H_2, or reductive elimination may be preceded by another H-transfer to afford H_3M^+(cyclopentadienyl).

For both Fe^+ and Co^+, the similarity in both the overall shapes of the KERDs and in the average kinetic energy releases for reactions 2 and 3 is striking. The first dehydrogenation step of reaction 2 is known to be

Scheme II. Proposed mechanism for dehydrogenation of cyclopentene by a transition metal ion M^+.

Scheme II

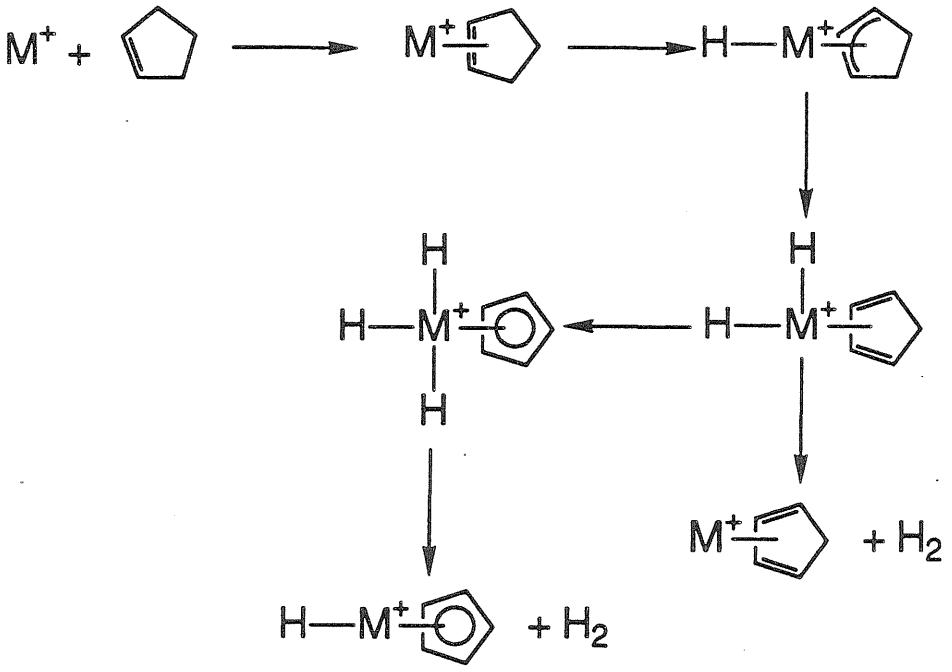

exothermic for both Fe^+ and Co^+ since it proceeds rapidly in the gas phase.[19,20] The exothermicity of this reaction is $D^0_0(M^+\text{-}C_5H_8)$, less the energy required to convert cyclopentane to cyclopentene + H_2, 25.1 kcal/mol (0 K). Based on available data for M^+-alkene bonds,[21] for either Fe^+ or Co^+ reaction 2 is probably at least 10-15 kcal/mol exothermic. Therefore, it is expected that the first loss of H_2 in reaction 2 should leave the $M(C_5H_8)^+$ product with substantial internal excitation due to the exothermicity of the first step less the energy lost to H_2 rotation and vibration and to relative translation. What remains is sufficient to promote the second H_2 loss.

Reaction 3 is chemically activated by the energy of association of M^+ with cyclopentene, so the level of internal excitation of the $[M(C_5H_8)^+]^*$ produced should reflect the strength of the $M^+\text{-}C_5H_8$ bond, with none of the loss processes of reaction 2. Consequently, reaction 3 should produce $[M(C_5H_8)^+]^*$ metastables which are at least 23-25 kcal/mol more excited than those of reaction 2. The KERDs from reactions 2 and 3 reflect the same potential surface features, since the metastable decomposition sampled is the same in each reaction. As far as the KERD is concerned, the only difference between reactions 2 and 3 is the difference in metastable internal energies due to forming the metastables by different processes.

How can the similarity in the KERDs be reconciled with the expected differences in metastable energies for the two processes? One possibility arises because metastable lifetimes are a very strong function of energy.

Perhaps in reaction 2 only metastable species with a high level of excitation can undergo the second dehydrogenation quickly enough to be observed on the 10^{-5} s scale of our experiment. We would therefore be selectively sensitive to those $[M(C_5H_8)^+]^*$ species from reaction 2 which have internal energies in the same range as are generated in the course of reaction 3. This requires that the decomposing metastables of reaction 2 have about 25 kcal/mol more internal energy than that available from forming the M^+-alkene bond. These energetic considerations are illustrated in the schematic potential energy surface of Figure 13.

One possible source of excitation is electronically excited M^+. The reaction of Fe^+ with methanol to generate $FeOH^+$ and methyl radical, which is believed to be 0.70±0.20 eV endothermic for ground state species,[22] has been observed for Fe^+ produced by electron impact on $Fe(CO)_5$.[23] The observation was explained by postulating that approximately 3% of the Fe^+ was formed in a long-lived excited state at least 0.5 eV above the ground state, which upon interaction with methanol can quickly cross to the ground state potential energy surface.[22] $Fe^+(^4D)$, derived from a $4s3d^6$ electronic configuration and lying 0.980 eV above the $Fe^+(^6D)$ ground state (which is also derived from $4s3d^6$),[24] may be responsible for the KERD for reaction 2 involving Fe^+. As is noted in Figure 13, the level of excitation, 22.6 kcal/mol, is in approximately the right range to produce $[Fe(C_5H_8)^+]^*$ with internal energies similar to those expected in reaction 3. Similar metastable

Figure 13. Schematic potential energy surface for the dehydrogenation reactions of Fe^+ with cyclopentane and cyclopentene, showing semiquantitative energetics for the various processes. Dehydrogenation of cyclopentane by $Fe^+(^4D)$ yields a Fe^+-cyclopentene species with approximately the same internal energy as that formed when $Fe^+(^6D)$ associates directly with cyclopentene.

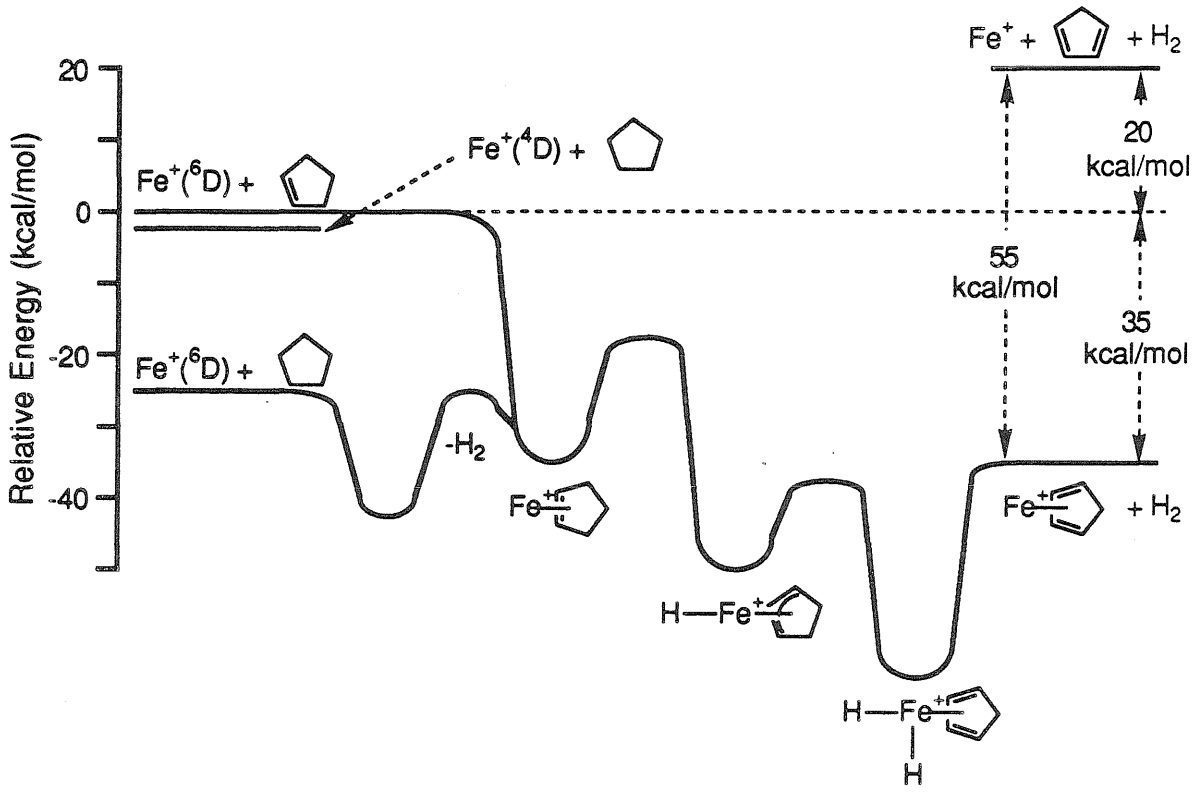
Relative Energy (kcal/mol)
20
0
-20
-40
Fe+(6D) +
Fe+(4D) +
Fe+(6D) +
-H2
Fe+ +
+ H2
20
kcal/mol
55
kcal/mol
35
kcal/mol
Fe+
+ H2
H—Fe+
H—Fe+
H

energies for reactions 2 and 3 could then account for the similarities in the KERDs.

Evidence that the double dehydrogenation of cyclopentane by Fe^+ is an excited state reaction comes from ion beam experiments. These studies, which use surface ionization as a source of Fe^+, are especially illuminating, since this ionization technique produces Fe^+ with the electronic states thermally populated. Under the experimental conditions used, approximately 80% of the beam should be in the ^6D ground state.[25] The results[26] indicate that the double dehydrogenation process is slightly endothermic, with a threshold less than 0.5 eV.

The double dehydrogenation of cyclopentane by Co^+ is also due to electronically excited Co^+. An ion beam study of this system[27] found that single dehydrogenation of cyclopentane by Co^+ in its electronic ground state is exothermic, while the double dehydrogenation process is endothermic. The loss of the second H_2 with substantial release of kinetic energy can only be due to a reaction involving excited Co^+. Co^+, like Fe^+, has a low-lying electronically excited state (^3F, derived from $4s3d^7$) in the appropriate energy range (28 kcal/mol above the ground state).[28]

Based on the ability of D_2 to effect H/D exchange with $Fe(C_5H_6)^+$ and $Co(C_5H_6)^+$, the reductive elimination step of reaction 3 is expected to be reversible, and dehydrogenation should proceed without a barrier in the exit channel of the potential energy surface. In a dissociation on such a potential energy surface, energy is partitioned statistically between the

internal modes of the products and their relative translation.[4,5] Phase space theory has successfully been applied to model this statistical energy partitioning.[29] The D_2 exchange results suggest that phase space modeling of reaction 3 should be possible. The only adjustable parameter used in obtaining a fit of the KERD calculated using phase space theory to the experimental KERD is ΔH for the reaction, so performing the fit also yields an estimate for ΔH. In cases such as reaction 3, where ΔH^0_f for all the reactants and products save one are known, the remaining value, $\Delta H^0_f(M(C_5H_6)^+)$, can be estimated, enabling a determination of $D(M^+\text{-}C_5H_6)$.

The results of the phase space calculations are plotted with the experimental KERDs in Figures 4 and 6. The theoretical and experimental KERDs agree quite well for dehydrogenation of cyclopentene by Fe^+, and reasonably well for dehydrogenation by Co^+. This provides further support for the lack of a barrier in the potential energy surface exit channel for reductive elimination of H_2. The best fit in the case of Fe^+ gives $D(Fe^+\text{-}C_5H_6)$ = 55±5 kcal/mol, in excellent agreement with a value of 55±5 kcal/mol obtained for this bond using photodissociation threshold techniques.[30] This value is also consistent with the observation of a small threshold for production of $Fe(C_5H_6)^+$ from the reaction of ground state Fe^+ with cyclopentane,[26] reaction 2, although the bond energy indicates that the threshold probably results from a barrier on the potential energy surface rather than from the overall thermodynamics of the reaction.

The KERD for dehydrogenation of cyclopentene by Co^+ is considerably broader, and in order to fit it a value of 113±10 kcal/mol for $D(Co^+\text{-}C_5H_6)$ was required. This value seems unreasonably large in comparison to the corresponding value for Fe^+, although larger bond energies might be expected for Co^+ than for Fe^+. The current estimates can be compared with average values for $\overline{D}(M^+\text{-}C_5H_5)$ estimated using the thermochemical cycle of Scheme III. Using this method, average values of $\overline{D}(Fe^+\text{-}C_5H_5)$ = 100 kcal/mol, and $\overline{D}(Co^+\text{-}C_5H_5)$ = 113 kcal/mol are calculated.[31] These average values can be compared with $D(M^+\text{-}C_5H_6)$ with the help of Scheme IV, if one additional parameter, $D(MC_5H_5^+\text{-}H)$, is available.[32] Using $D(FeC_5H_5^+\text{-}H)$ = 46±5 kcal/mol from a photodissociation threshold measurement[30] in combination with 55±5 kcal/mol for $D(Fe^+\text{-}C_5H_6)$, a value of $D(Fe^+\text{-}C_5H_5)$ = 80±10 kcal/mol is derived, in reasonably good agreement with the average value noted above.[33] The necessary parameters for the corresponding Co^+ bonds are not available. The value of 113±10 kcal/mol for $D(Co^+\text{-}C_5H_6)$ is in good agreement with an estimate of 115 kcal/mol for $D(CpNi^+\text{-}C_5H_6)$,[34] but the latter ion is a closed-shell species and the comparison of the two bond energies is questionable.

Assuming that the bond energies are correct, it is surprising that $D(Co^+\text{-}C_5H_6)$ is twice as large as $D(Fe^+\text{-}C_5H_6)$. The difference might be explained if the structures of the two species are different. For example, it is possible that $Fe(C_5H_6)^+$ exists as the metal ion bound to cyclopentadiene, and that $Co(C_5H_6)^+$ has a hydridocyclopentadienyl structure.

Scheme III. Thermochemical cycle used in determining average M^+-C_5H_5 bond energies.

Scheme III

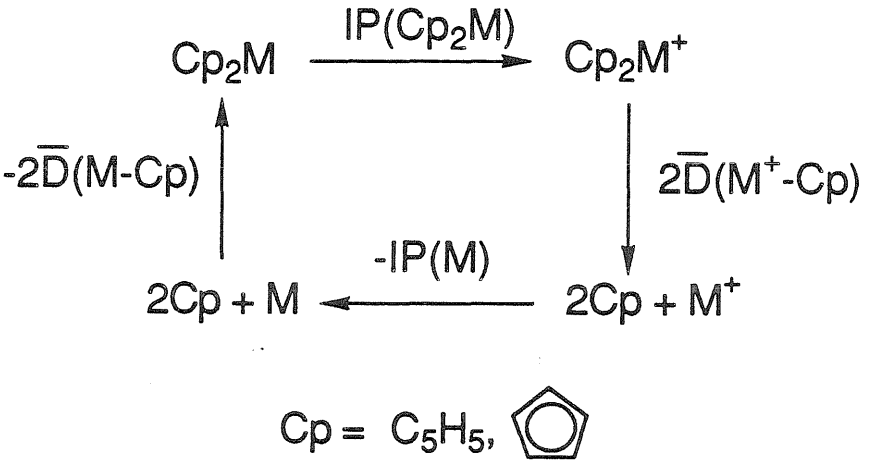

Cp = C_5H_5,

Scheme IV. Thermochemical cycle used to estimate $D(M^+-C_5H_5)$ from quantities derived in this work.

Scheme IV

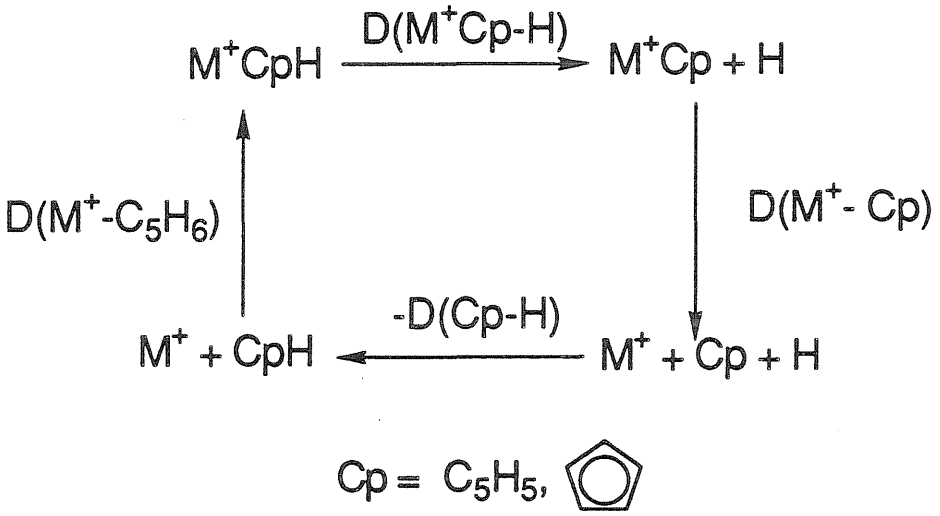

Cp = C_5H_5,

The latter structure is expected to be thermodynamically favored by approximately 40 kcal/mol,[35] in rough agreement with the difference in the bond energies of Fe^+ and Co^+ to C_5H_6.

Earlier work[6,7] postulated that both $Fe(C_5H_6)^+$ and $Co(C_5H_6)^+$ reversibly rearrange from M^+-cyclopentadiene to the hydridocyclopentadienyl species, based on the observation of H/D exchange. However, such a rearrangement is not necessary to explain the exchange results, and seems very unlikely if the hydridocyclopentadienyl structure is so heavily favored on thermodynamic grounds. An alternative mechanism for the H/D exchange process is suggested in Scheme V, involving a reversible hydrogen shift from the metal to the diene to give a π-allylic structure. This mechanism invokes oxidative addition of hydrogen to give the same structure as in the dehydrogenation mechanism. The KERD results indicate that there is no barrier to this process. The remaining steps are the same as in Scheme I. Scheme V is consistent with the observed H/D exchange kinetics, the initial exchange being rapid, and the rate of the remaining exchanges being limited by the rate of the sigmatropic shift. Further, Scheme V explains the results without resorting to the high metal oxidation state of the H_3M^+-cyclopentadienyl structure implicit in Scheme I.

$M(C_6H_8)^+$ and $M(C_6H_6)^+$, M = Fe, Co. $M(C_6H_8)^+$ is generated in double dehydrogenation of cyclohexane, reaction 4, or single H_2 loss from cyclohexene, reaction 5.

Scheme V. Proposed mechanism for H/D exchange in $M(C_5H_6)^+$ species. Reversible interconversion of M^+-diene and M^+-π-allylic structures accounts for the initial exchange.

Scheme V

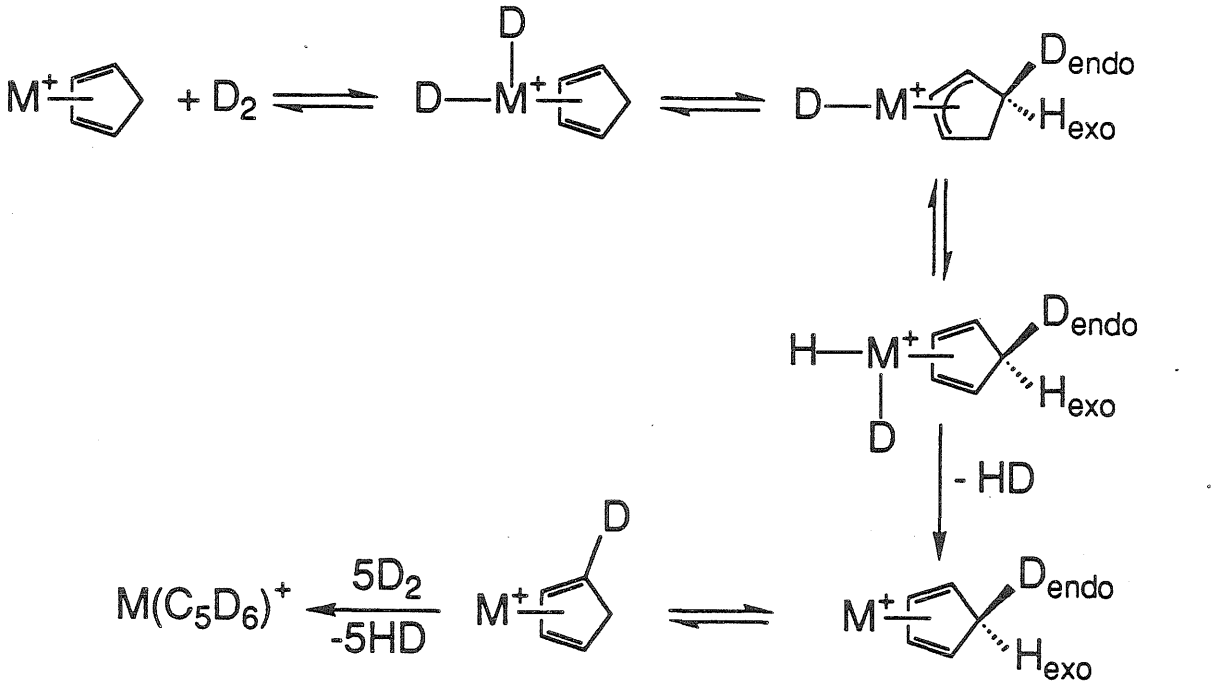
M+
+ D2
D
D—M+
D—M+
Dendo
Hexo
H—M+
D
Dendo
Hexo
- HD
M(C5D6)+
5D2
-5HD
D
M+
M+
Dendo
Hexo

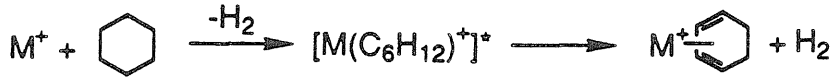

(4)

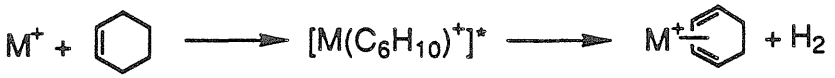

(5)

The same considerations apply to reaction 4 as to reaction 2. The KERD is measured for loss of the second H_2 molecule, and the process is not modeled since the metastable internal energy is not well defined. A mechanism analogous to that presented in Scheme II, based on successive β-H transfers followed by reductive elimination, is assumed to account for reaction 5. Rearrangement to $H_4M^+(C_6H_6)$ is not expected prior to reductive elimination of H_2, since the KERDs for H_2 losses to form $M(C_6H_6)^+$ for both Fe^+ (reaction 6, Figure 11) and Co^+ (reaction 7, Figure 12) are considerably broader than those which result in $M(C_6H_8)^+$ formation, indicating that formation of the $M(C_6H_6)^+$ structure involves a substantial exit channel barrier, unusually large exothermicity, or both.

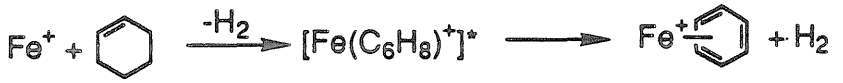

(6)

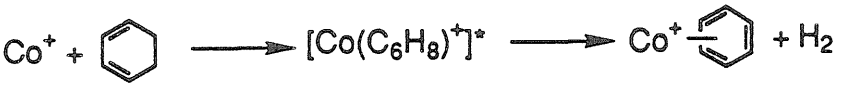

(7)

Formation of $Fe(C_6H_8)^+$ via reactions 4 and 5 produces KERDs which are distinct, that from reaction 4 being slightly broader. If the metastable decomposition occurs on the same surface for both reactions, this again suggests excited state participation in reaction 4 to account for excess energy in the $[Fe(C_6H_{10})^+]^*$ metastable. Co^+ gives KERDs for reactions 4 and 5 which are nearly identical. Electronically excited Co^+ is probably important in reaction 4, with the excitation energy making up for that lost in the first dehydrogenation step. It is also possible that energetic differences between $[Co(C_6H_{10})^+]^*$ formed in the first step of reaction 4 and that produced by the ion-molecule association of reaction 5 are masked by subsequent features of the potential energy surface, such as a barrier to the final H_2 elimination.

The results of phase space modeling of reaction 5 for Fe^+ and Co^+ are included in Figures 8 and 10, respectively. We are unaware of H/D exchange data for $Fe(C_6H_8)^+$ and $Co(C_6H_8)^+$, but the good fit achieved in the Fe^+ case indicates that this is a further example of statistical dehydrogenation. The value of $D(Fe^+\text{-}C_6H_8)$ derived from the fit is 70±5 kcal/mol. The phase space fit for reaction 5 in the case of Co^+ is much poorer, and the derived $D(Co^+\text{-}C_6H_8)$ is again high, 88±10 kcal/mol. Due to the poor quality of the phase space fit to the experimental KERDs and the high bond energy values derived, the bond energies for Co^+ should be viewed with caution. The reasons for the broad KERDs for Co^+ dehydrogenations are unclear, but it should be pointed out that among the systems studied

thus far, broad, non-statistical KERDs for dehydrogenation processes are more common than statistical KERDs. Excited state reactions may be responsible, since electron impact is expected to produce an appreciable population of $Co^+(^5F)$, 0.415 eV above the ground state.[28] The dynamics of dehydrogenation processes require further investigation.

A final comment involves the relative strengths of $D(Fe^+\text{-}C_5H_6)$ and $D(Fe^+\text{-}C_6H_8)$. Assuming (as seems likely) that both ligands are conjugated dienes, it is interesting that C_6H_8 binds Fe^+ 15 kcal/mol more strongly than C_5H_6. Condensed phase η^4-butadiene complexes of Fe are well-known, strongly bound species,[36] which can perhaps be used as models to ascertain the "ideal" geometry for a diene ligand bound to metal. The C-C-C angle of the butadiene ligand in η^4-butadiene iron(0) tricarbonyl has been determined to be 118° using X-ray diffraction,[37] somewhat compressed from the 122.4° found using electron diffraction for free butadiene in the gas phase.[38] Similarly compressed butadiene bond angles are found for several η^4-butadiene complexes of neutral Mn,[39] where the C-C-C angles in the diene unit are in the range 118.8°-119.6°. The structure of solid phase cyclopentadiene has been determined with X-ray techniques.[40] The ring is planar and quite distorted from ideal pentagonal geometry; the C-C-C bond angles of the diene unit are 112° and 107°. The corresponding bond angles in gaseous 1,3-cyclohexadiene are each 120.1°, measured using electron diffraction.[41] The similarity of the bond angles in free 1,3-cyclohexadiene and 1,3-butadiene bound to metal, combined with the higher

bond energy found for C_6H_8, suggests that the geometry of 1,3-cyclohexadiene is better suited for formation of a strong bond to Fe^+ than is the distorted geometry of cyclopentadiene.

Conclusion

Dehydrogenation does not necessarily occur with non-statistical release of kinetic energy. Energy releases observed for dehydrogenation reactions range from quite broad distributions which are clearly non-statistical, such as those seen for n-butane, to narrower, statistical distributions such as those presented here for dehydrogenation of cyclopentene and cyclohexene by Fe^+. The reasons for the wide diversity in dehydrogenation KERDs are still not understood. Undoubtedly the potential energy surfaces involved are very complex, while the methods used for interpreting KERDs are still in their infancy. The technique of fitting experimental KERDs using phase space theory holds promise as a new means for making thermochemical measurements in difficult systems, but should be used with care since the achievement of a fit does not guarantee that the KERD is statistical.

Acknowledgement. We thank the National Science Foundation for supporting this research through grant numbers CHE87-11567 (JLB) and CHE88-17201 (MTB). We are also grateful to the Shell Foundation for graduate fellowship funding (DVD), and to the donors of the Petroleum Research Fund, administered by the American Chemical Society, for

additional support. We are also indebted to Peter Armentrout for providing us with results prior to publication.

References and Notes

1. Houriet, R.; Halle, L. F.; Beauchamp, J. L. *Organometallics* **1983**, *2*, 1818-1829.

2. Halle, L. R.; Houriet, R.; Kappes, M. M.; Staley, R. H.; Beauchamp, J. L. *J. Am. Chem. Soc.* **1982**, *104*, 6293-6297.

3. (a) Jacobson, D. B.; Freiser, B. S. *J. Am. Chem. Soc.* **1983**, *105*, 5197-5206. (b) Jacobson, D. B.; Freiser, B. S. *J. Am. Chem. Soc.* **1983**, *105*, 736.

4. Hanratty, M. A.; Beauchamp, J. L.; Illies, A. J.; van Koppen, P.; Bowers, M. T. *J. Am. Chem. Soc.* **1988**, *110*, 1-14.

5. van Koppen, P. A. M.; Jacobson, D. B.; Illies, A.; Bowers, M. T.; Hanratty, M. A.; Beauchamp, J. L. *J. Am. Chem. Soc.* **1989**, *111*, 1991-2001.

6. Jacobson, D. B.; Freiser, B. S. *J. Am. Chem. Soc.* **1983**, *105*, 7492-7500.

7. Jacobson, D. B.; Byrd, G. D.; Freiser, B. S. *Inorg. Chem.* **1984**, *23*, 553-557.

8. (a) Gioumousis, G.; Stevenson, D. P. *J. Chem. Phys.* **1958**, *29*, 294. (b) Su, T.; Bowers, M. T. In *Gas Phase Ion Chemistry*; Bowers, M. T., Ed.; Academic Press: New York, 1979; Vol. 1, Chapter 3.

9. Jacobson, D. B.; Freiser, B. S. *J. Am. Chem. Soc.* **1985**, *107*, 72-80.

10. Morgan, R. P.; Beynon, J. H.; Bateman, R. H.; Green, B. N. *Int. J. Mass Spectrom. Ion Phys.* **1978**, *28*, 171-191.

11. Jarrold, M. F.; Illies, A. J.; Bowers, M. T. *Chem. Phys.* **1982**, *65*, 19.

12. The energy resolution in the center-of-mass frame ΔT is related to that of the main beam in the laboratory frame ΔE by the equation $\Delta T = \Delta E[(M_1{}^2T)/(M_2M_3V_1)]^{1/2}$, where M_1 is the mass of the parent metastable ion, M_2 and M_3 are the masses of the ionic and neutral fragments, V_1 is the lab kinetic energy of the parent metastable ion, and T is the center of mass kinetic energy. This formula is taken from Hanratty, M. A. Ph.D.

Thesis, California Institute of Technology, 1985. For an extreme example, consider the dehydrogenation of cyclopentene by Fe^+. With a main beam resolution of 2 eV and a center-of-mass kinetic energy of 200 meV, the spread in center-of-mass kinetic energy due to the spread in the main beam is 79 meV. The contribution from ΔE is much less significant for fragmentations involving heavier neutrals.

13. a) Jarrold, M. F.; Illies, A. J.; Bowers, M. T. *J. Chem. Phys.* **1983**, *79*, 6086. b) Jarrold, M. F.; Illies, A. J.; Kirchner, N. J.; Wagner-Redeker, W.; Bowers, M. T.; Mandich, M. L.; Beauchamp, J. L. *J. Phys. Chem.* **1983**, *87*, 2213-2221.

14. Dearden, D. V.; Hayashibara, K.; Beauchamp, J. L.; Kirchner, N. J.; van Koppen, P. A. M.; Bowers, M. T. *J. Am. Chem. Soc.* **1989**, *111*, 2401-2409.

15. A more recent version of some of the phase space routines employed has been submitted to QCPE: Chesnavich, W. J.; Bass, L.; Grice, M. E.; Song, K.; Webb, D. A. "TSTPST: Statistical Theory Package for RRKM/QET/TST/PST Calculations", *QCPE*.

16. The KERD for the dehydrogenation of cyclopentane by Co^+ has been published previously (Reference 4).

17. In situations where the kinetics of the decomposition process as a function of internal energy are known (or can be adequately estimated), it is still possible to carry out the phase space calculation of kinetic energy release by using the known lifetime of the metastable and the kinetics of its decomposition to back-calculate the internal energy of the metastable (See reference 14). However, the dehydrogenation processes of the current work were deemed too complex to be easily treated by this approach.

18. Watson, P. L.; Roe, D. C. *J. Am. Chem. Soc.* **1982**, *104*, 6471.

19. Byrd, G. D.; Burnier, R. C.; Freiser, B. S. *J. Am. Chem. Soc.* **1982**, *104*, 3565.

20. Armentrout, P. B.; Beauchamp, J. L. *J. Am. Chem. Soc.* **1981**, *103*, 6628.

21. $D_{298}^0(Fe^+\text{-propene})$ has been estimated at 37±2 kcal/mol (reference 6), and $D_0^0(Co^+\text{-propene})$ has been determined to be 44±5 kcal/mol (reference 4).

22. Reents, W. D., Jr.; Strobel, F.; Freas, R. B. III; Wronka, J.; Ridge, D. P. *J. Am. Chem. Soc.* **1985**, *89*, 5666-5670.

23. (a) Allison, J.; Ridge, D. P. *J. Am. Chem. Soc.* **1976**, *98*, 7445-7446. (b) Allison, J.; Ridge, D. P. *J. Am. Chem. Soc.* **1979**, *101*, 4998-5009.

24. Corliss, C.; Sugar, J. *J. Phys. Chem. Ref. Data* **1982**, *11*, 135-241.

25. Elkind, J. L.; Armentrout, P. B. *J. Phys. Chem.* **1986**, *90*, 5736-5745.

26. Schultz, R. H.; Armentrout, P. B., unpublished results.

27. Armentrout, P. B.; Beauchamp, J. L. *J. Am. Chem. Soc.* **1981**, *103*, 6628-6632.

28. Moore, C. E. *Natl. Bur. Stand. Circ. (U. S.)* **1949**, Vol. I, No. 467, **1958**, Vol. II.

29. (a) Chesnavich, W. J.; Bowers, M. T. *J. Am. Chem. Soc.* **1977**, *99*, 1705-1711. (b) Chesnavich, W. J.; Bass, L.; Su, T.; Bowers, M. T. *J. Chem. Phys.* **1981**, *74*, 2228-2246. (c) Jarrold, M. F.; Wagner-Redeker, W.; Illies, A. J.; Kirchner, N. J.; Bowers, M. T. *Int. J. Mass Spectrom. Ion Processes*, **1984**, *58*, 63-95.

30. Huang, Y.; Freiser, B. S., personal communication.

31. Supporting thermochemistry is as follows: $IP_a(Cp_2Fe)$ = 6.5 eV, $IP_a(Cp_2Co)$ = 4.8 eV, where IP_a is the adiabatic ionization potential and Cp = C_5H_5, from Cauletti, C.; Green, J. C.; Kelly, M. R.; Powell, P.; Van Tilborg, J.; Robbins, J.; Smart, J. *J. Electron Spectrosc. Rel. Phenom.* **1980**, *19*, 327-353. D(Fe-Cp) = 84 kcal/mol, D(Co-Cp) = 77 kcal/mol, from Pilcher, G.; Skinner, H. A. In *The Chemistry of the Metal Carbon Bond*; Hartley, F. R.; Patai, S., Eds.; John Wiley & Sons: London, 1982; Ch. 2. IP(Fe) = 7.870 eV, IP(Co) = 7.864 eV, from Lias, S. G.; Bartmess, J. E.; Liebman, J. F.; Holmes, J. L.; Levin, R. D.; Mallard, W. G. *J. Phys. Chem. Ref. Data, Supplement No. 1* **1988**, *17*.

32. Also needed is $D(C_5H_5\text{-}H)$ = 71.1±1.5 kcal/mol, from: McMillan, D. F.; Golden, D. M. *Ann. Rev. Phys. Chem.* **1982**, *33*, 493-532.

33. Appearance potential measurements can also be used to obtain $D(Fe^+\text{-}C_5H_5)$. Using an appearance potential of 13.162 eV for $FeC_5H_5^+$ from ferrocene (Bar, R.; Heinis, Th.; Nager, Ch.; Jungen, M. *Chem. Phys. Lett.* **1982**, *91*, 440-442.), $D(Fe^+\text{-}C_5H_5)$ = 46 kcal/mol is derived.

34. Corderman, R. R. Ph.D. Thesis, California Institute of Technology, 1977.

35. Formation of the hydridocyclopentadienyl species from M^+-cyclopentadiene involves breaking M^+-cyclopentadiene and $H\text{-}C_5H_5$ bonds and formation of M^+-H and $M^+\text{-}C_5H_5$ bonds. The bond breaking processes cost about 55 kcal/mol (this work) and 70 kcal/mol (Reference 32) respectively,

while the bond formation processes liberate about 50 kcal/mol for the M^+-H bond (Georgiadis, R.; Armentrout, P. B. *Polyhedron* **1988**, *7*, 1573-1581.) and about 115 kcal/mol for the M^+-C_5H_5 bond (estimated in this work).

36. Collman, J. P.; Hegedus, L. S.; Norton, J. R.; Finke, R. G. *Principles and Applications of Organotransition Metal Chemistry*; University Science Books: Mill Valley, CA, 1987.

37. Mills, O. S.; Robinson, G. *Acta Cryst.* **1963**, *16*, 758-761.

38. Almenningen, A.; Bastiansen, O.; Traeteberg, M. *Acta Chem. Scand.* **1958**, *12*, 1221-1225.

39. Harlow, R. L.; Krusic, P. J.; McKinney, R. J.; Wreford, S. S. *Organometallics* **1982**, *1*, 1506-1513.

40. Liebling, G.; Marsh, R. E. *Acta Cryst.* **1965**, *19*, 202-205.

41. Oberhammer, H.; Bauer, S. H. *J. Am. Chem. Soc.* **1969**, *91*, 10-16.

CHAPTER 5

CHARGE-REVERSED, RESONANCE ENHANCED MULTIPHOTON IONIZATION (CRREMPI) SPECTROSCOPY: CONCEPT AND INITIAL EXPERIMENTS INVOLVING PERFLUOROBENZENE AND ALLYL

CHARGE-REVERSED, RESONANCE ENHANCED MULTIPHOTON IONIZATION (CRREMPI) SPECTROSCOPY: CONCEPT AND INITIAL EXPERIMENTS INVOLVING PERFLUOROBENZENE AND ALLYL

David V. Dearden and J. L. Beauchamp

Arthur Amos Noyes Laboratory of Chemical Physics

California Institute of Technology

Pasadena, CA 91125

Abstract.

A new method for obtaining spectroscopic information on transient species is presented. It involves generation of trapped anions in an ion cyclotron resonance (ICR) spectrometer. Irradiation with a laser to photo-detach the anions produces the neutrals of interest, which absorb additional photons and undergo photoionization. The resulting cations are detected by ICR methods. Unsuccessful attempts to observe charge-reversed multiphoton ionization (CRMPI) of C_6F_6 are discussed. These studies were hampered by multiphoton ionization of background neutral C_6F_6, which completely obscured CRMPI signal. Allyl anion is suggested as a more promising subject for charge reversed, resonance enhanced multiphoton ionization (CRREMPI) studies, and preliminary experiments are briefly reported.

Introduction

The significance of transient species in many important chemical processes is widely recognized, and recent advances in experimental techniques have now made it possible to directly examine short-lived reactive intermediates. For example, femtosecond laser spectroscopy is capable of probing the generation and decay of transient species on the time scale of molecular vibrations.[1] While such methods are very powerful, they suffer from a number of limitations. The necessary equipment is expensive and difficult to operate. Further, to avoid problems in establishing the identity of the intermediates in question, most studies are limited to small molecules where the spectroscopy is well known.

One approach to transient studies is to carry them out under low-pressure, gas phase conditions where the time between molecular collisions is long. This affords an opportunity to probe the species of interest before they undergo reactive collisions. This strategy has been particularly useful in obtaining photoelectron spectra of organic free radicals, for example.[2] An obstacle to most studies of neutral intermediates is the difficulty of finding a source which produces the species of interest exclusively, with no ambiguity as to their identity. For example, in the photoelectron studies mentioned above, radicals are generally produced by flash vacuum pyrolysis of nitrites, and radical identities can be inferred from knowledge of nitrite thermal decomposition. However, in such a source there is always a large

background of organic alkyl precursor and other stable products of its thermal decomposition, such that only the radical bands at low ionization potential are observable. Bands at higher ionization potential are obscured by signal from more abundant, stable species. In addition, the radicals made in such a source retain sufficient internal energy that they undergo decomposition and isomerization on the same time scale as the photoelectron observation,[3] further complicating the identification of the radicals present.

In this chapter, a new approach to spectroscopic study of reactive intermediates is suggested, which incorporates a unique method of determining the mass of the intermediate under observation. It also affords the capability to synthesize species of interest under carefully controlled conditions. Initial experimental efforts in developing this approach are presented, along with suggestions for future work.

Concept

The use of ion cyclotron resonance (ICR) techniques to trap ions and monitor their masses is well established.[4] By reversing the voltage applied to the trapping plates from a negative value to a positive value, an ICR instrument can easily be switched from trapping and detection of anions to trapping and detection of cations. Further, ICR instruments are versatile tools for the synthesis of species of interest. Ions created by electron impact on neutral molecules or by other ionization techniques such as

photoionization can be modified by collision-induced dissociation or ion-molecule reaction with neutrals. This can be done cleanly, since unwanted masses can be ejected from the cell, leaving only the ionic species of interest. We take advantage of these unique features of ICR in suggesting the following approach.

Anions, produced and modified through any of the methods mentioned above, are irradiated with an intense pulse of laser light. Photodetachment[5] of the electron results, if the photon energy is greater than the electron affinity of the resulting neutral. This is usually the case for visible and shorter wavelengths, since most species have electron affinities less than 2-3 eV.[6] If the light pulse is sufficiently intense and of the proper wavelength, the neutral product of photodetachment may absorb additional photons and undergo resonance enhanced ionization to produce a cation. These cations can be trapped and observed by reversing the trapping potential of the ICR cell at the time of the laser shot. For anions initially moving at thermal velocities (10^4-10^5 cm s^{-1}), inversion of the trapping potential on a time scale of μs or less is rapid enough that they remain within the cell and are subject to the cation trapping conditions. Overall, the process is a charge-reversed, resonance enhanced multiphoton ionization (CRREMPI) event.

The CRREMPI approach offers significant advantages for spectroscopic measurements on the intermediate neutral species. Since the masses of the anion and resulting cation are well characterized, there is little ambiguity

in identifying the spectral signal carrier. Also, a wide range of species can be generated in the gas phase using known ion-molecule chemistry,[7] and photodetached to produce novel neutrals for spectroscopic study. Possible species of interest include metal hydrides, organometallic free radicals, long-lived excited states, and isomeric organic free radicals.

The likelihood of observing signal in a two-photon resonant ionization can be estimated as follows. The rate-limiting step is assumed to be formation of the resonant excited state in the ionization of the neutral. This is probably reasonable, since photodetachment is a one-photon process and should be fully saturated. In a multiphoton ionization process, the rate of production of a resonant excited state M* is given by equation 1.[8]

$$d[M^*]/dt = \delta I_0^2 M_0 \qquad (1)$$

In equation 1, δ is the two-photon absorptivity, estimated to be 10^{-48} cm^4 s for a strong two-photon transition,[8] I_0 is the incident laser intensity in photons cm^{-2} s^{-1}, and M_0 is the ground state number density. For a 30 mJ pulse at 500 nm focused to a 1 mm^2 spot, I_0 is 7.6×10^{26} photons cm^{-2} s^{-1}. M_0 is estimated to be about 10^6 cm^{-3} in a well-loaded ICR cell. Making the differential approximation and noting that the length of the laser pulse Δt is 10^{-8} s, we can calculate that ΔM^* for a single laser pulse is about 5700 cm^{-3}. It can further be assumed that under the same conditions, the transition from the resonant excited state to the ionization

continuum is saturated, so that all M* result in production of M^+. In other words, under the above assumptions about 0.6% of the anions initially present undergo CRREMPI to produce cations.

Initial attempts to observe CRREMPI involved generation of perfluorobenzene anions, $C_6F_6^-$, followed by irradiation with the output of an ArF excimer laser (193 nm, 6.4 eV/photon). This process should more aptly be termed "CRMPI," since the objective, photodetachment of $C_6F_6^-$ to produce the lowest-lying triplet state of neutral C_6F_6, followed by 1-photon ionization of the triplet state, is not a resonance enhanced process. It should be possible to access the lowest triplet state by 1-photon photodetachment of the anion, since the sum of the electron affinity of C_6F_6, 0.52±0.1 eV,[9] and the 3.86 eV excitation of the 1 $^3B_{1u}$ state above the ground state[10] is less than the photon energy. One additional 6.4-eV photon is sufficient to excite molecules in the 1 $^3B_{1u}$ state to levels above the ionization continuum, which lies 9.90 eV above the ground state.[11]

Further experiments, involving a resonant CRREMPI process, were aimed at detection of allyl radical. Allyl radical is a good subject for CRREMPI spectroscopy for several reasons. First, the 2+2 REMPI spectrum of allyl has been measured[12]. The strongest peak in the REMPI spectrum lies at 499.3 nm (2-photon energy 40056.8 cm^{-1}), and has been assigned to the 0_0^0 band of the 3s $^2A_1 \leftarrow X\ ^2A_2$ transition. Second, the electron affinity of allyl, 0.550±0.054 eV, is accurately known from threshold photodetachment measurements.[13] Therefore, a 1+2+2 CRREMPI process,

requiring one photon to detach the electron to produce ground state allyl radical, followed by 2+2 REMPI, is energetically feasible. In addition, the photoelectron spectrum of allyl anion (i.e., the kinetic energies of electrons photodetached from allyl anion using monochromatic light) has been measured.[14] Finally, several methods are available for producing $C_3H_5^-$ under ICR conditions, including proton abstraction from propene by OH^-,[13] and the methods of reactions (2) and (3):[15]

$$F^- + (CH_3)_3Si(C_3H_5) \rightarrow C_3H_5^- + (CH_3)_3SiF \qquad (2)$$

$$B^- + CH_3CHCH_2 \rightarrow C_3H_5^- + BH \qquad (3)$$

F^- can be made by dissociative electron attachment to NF_3. B^- refers to any strong anionic base. In reference 15, H^- and NH_2^- were the bases employed, produced by dissociative attachment of 5.1-eV electrons to ammonia.

Experimental Section

All experiments were conducted using a Fourier transform ion cyclotron resonance (FTICR) spectrometer equipped with a 1-in. cubic cell and a data acquisition system supplied by Ion Spec Corp. The FTICR instrument was modified to enable rapid switching of the trapping voltages. The modification[16] consists of an electronic switch which alternates between

the output of the circuit normally used to set the trapping voltage, and a voltage of opposite sign and approximately equal magnitude. The latter inverted voltage is generated by use of an operational amplifier with a gain of -1. The typical sequence of events in the C_6F_6 experiments is illustrated in Figure 1. An initial "quench" pulse is applied to the ICR cell to empty it of ions and begin an experimental cycle. This pulse is also used as a signal to cause the trapping voltages to be reset so as to guarantee that the experiment begins in the anion trapping mode. The quench pulse is followed by an electron beam pulse which generates anions as described below. In some instances, C_6F_6 was introduced into the cell using a pulsed valve, with the valve pulse occurring during the electron beam pulse (in the remaining cases, C_6F_6 introduction was via a continuous flow from a leak valve). A third pulse is sent to the auxiliary circuitry to arm the switch for inverting the trapping voltages. The rising edge of the laser fire pulse initiates inversion of the trapping voltages, and simultaneously triggers the firing of the laser (Lumonics, HyperEx 440, generating about 400 mJ/pulse at 193 nm).

Light emission from the excimer laser occurs 950 ns following the rising edge of the firing signal pulse, and lasts approximately 10-12 ns.[17] A variable delay of about 1000 ns is built into the inverting circuit so that inversion begins after actual light emission. The inversion of the trapping potential, as measured using a 20 MHz oscilloscope, has an integral-shaped waveform which is approximately 1 μsec long.

Figure 1. Typical sequence of events in CRMPI experiment. The horizontal axis is the time since the beginning of the electron beam pulse, in ms.

Pulse Sequence for CRMPI Experiment

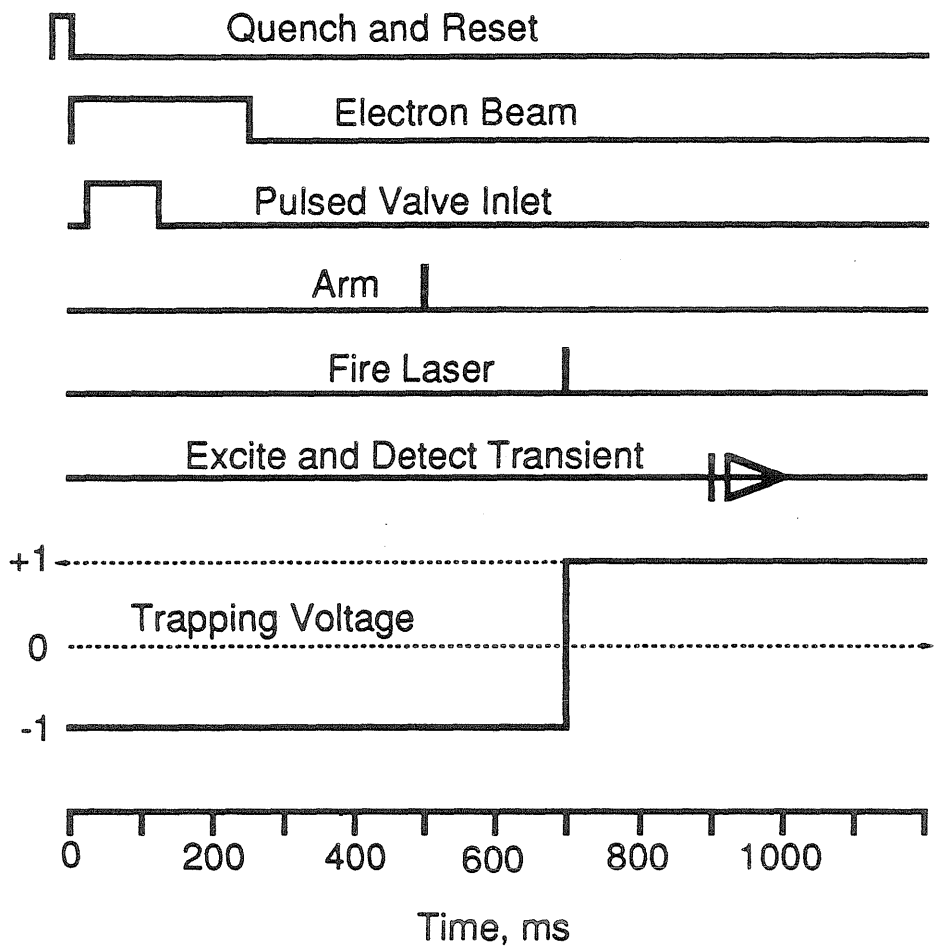

The inversion is balanced so that it is roughly symmetrical about ground. Anion trapping potentials of about -1 V were typically used, so the cation trapping potential after inversion was approximately +1 V. The MgF_2 window, used to admit the laser beam into the vacuum system, is masked to ensure that the beam passes cleanly through the cell without striking the metal plates which form the walls of the cell. Circular holes in the front and rear plates allow the beam to enter and exit the ICR cell. The beam impacts on the rear of the vacuum chamber after transiting the cell. A short delay (on the order of 10-100 ms) follows the laser pulse to allow the electronics to stabilize, after which conventional chirp excitation and detection are applied to observe the cation population of the cell.

Perfluorobenzene anions, m/z 186, were produced by electron attachment to neutral C_6F_6 (Aldrich). Two methods were used. The first employed an intense beam (currents of several μA) of low-energy (approximately 0.5-eV) electrons. The second, more successful method involved filament currents of about 0.1 μA and electrons accelerated to maximum energy, about 77 eV. Electron attachment cross sections are typically highest at low electron energies, implying that the second method generated abundant low-energy secondary electrons which were efficiently trapped in the cell and scavenged by neutral C_6F_6. Most of the attempts to detect cations produced by CRMPI concentrated on a narrow mass range within about 20 amu of the 186-amu mass of $C_6F_6^+$.

Allyl anions were produced by reacting allyltrimethylsilane (Aldrich) with F^- made by low-energy dissociative electron attachment to NF_3. All reactants were introduced into the cell continuously using variable leak valves. The total pressure in the cell was approximately 5-10 x 10^{-7} Torr. Under these conditions, reaction times of about 200 ms were sufficient to produce abundant allyl anions. The allyl anions were irradiated with the focused (using a 150-mm biconvex MgF_2 lens) output of an excimer-pumped dye laser (Lambda-Physik FL3002). Coumarin 500 is the dye employed.[18] Pulse energies of 5-14 mJ were reported to be sufficient to observe mass-resolved REMPI spectra using time-of-flight detection.[12] Energies of 10-20 mJ/pulse were used, as determined by a Gen-tec joulemeter (model ED-200).

Results and Discussion

One of the first objectives in the study of C_6F_6 was to observe the photodetachment process. For these experiments the trapping voltage was not switched; the instrument remained in the anion detection mode at all times. Further, since the excimer laser pulse generates large numbers of low-energy electrons, it was necessary in these experiments to continuously eject electrons by application of 5 MHz RF across the trapping plates. The results of two photodetachment experiments are shown in Figure 2. In the first, Figure 2a, the absolute signal intensity at m/z 186 is plotted as a function of time, with the laser firing pulses at 95 Hz beginning at a

Figure 2. (a) Absolute intensity of $C_6F_6^-$ signal as a function of time, while irradiated by pulses of 193-nm laser light at 95 Hz. The burst of laser pulses begins after the point at 2900 ms. (b) Absolute intensity of $C_6F_6^-$ signal as a function of time, with 95-Hz bursts of 193-nm laser light, beginning at t = 2835 ms, occurring during measurements for every other point. The first point including a laser burst is that at 2853 ms. Alternating points thereafter include increasingly long bursts.

$C_6F_6^-$ Photodetachment

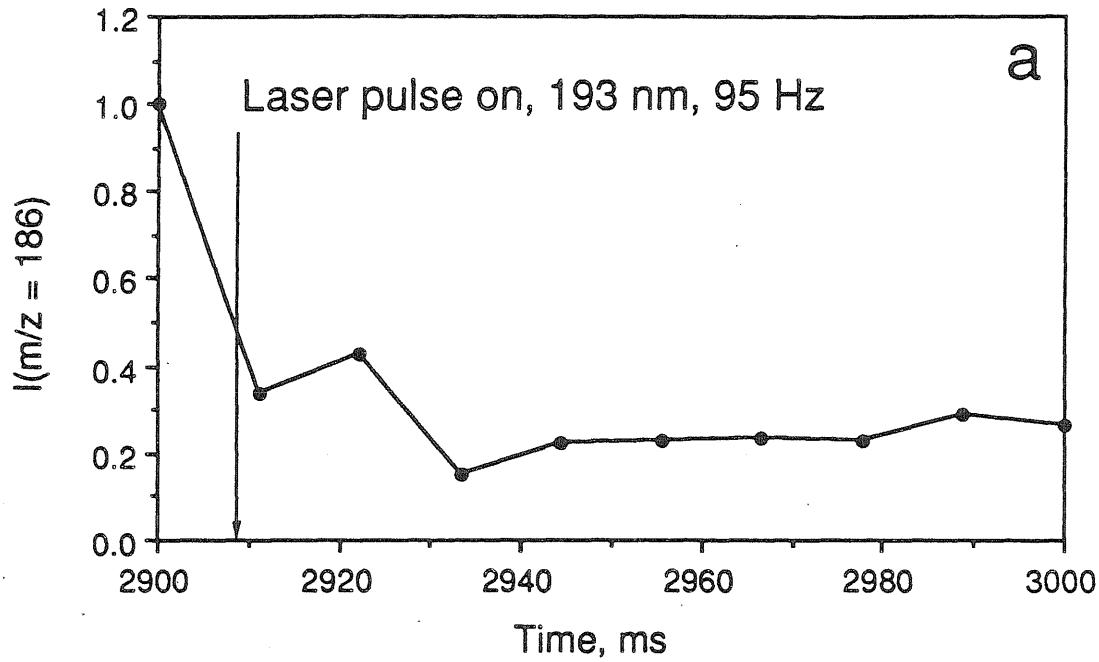

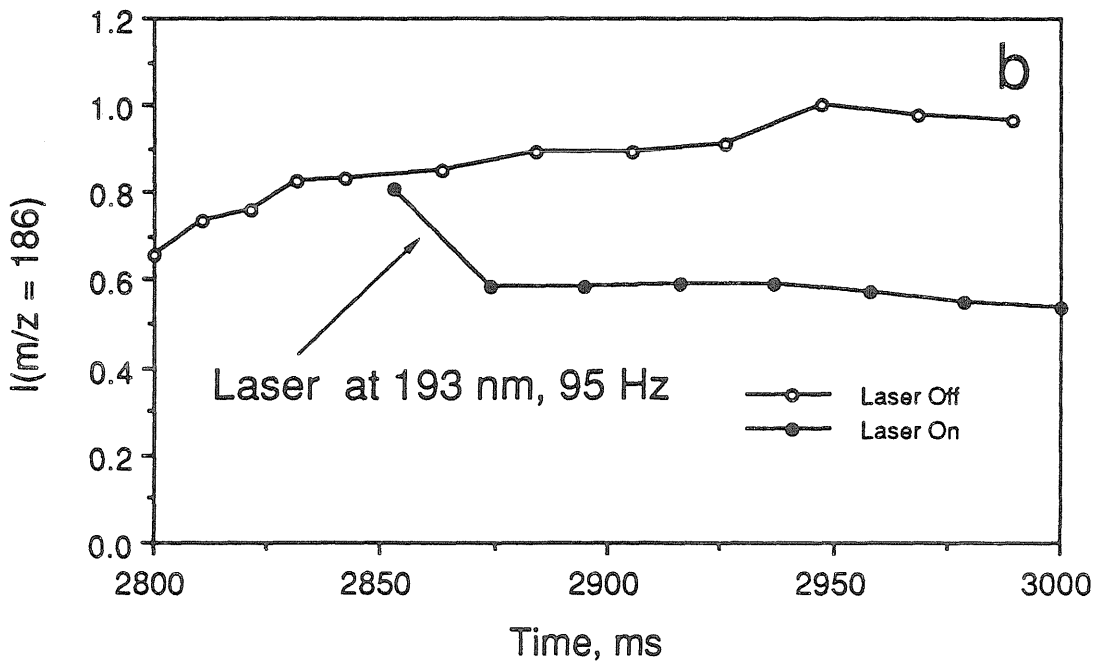

point 2900 ms after the start of the experimental cycle (no laser shots occurred at the 2900-ms point). The first laser pulse, at 2910 ms, is apparently sufficient to detach most of the anions in the irradiated volume. Additional pulses do not lead to further decreases in the m/z 186 signal. The same effect is seen in Figure 2b. In this experiment, increasingly long 95-Hz laser bursts beginning at 2835 ms are alternated with scans where the laser was not fired. The amount of decrease in signal is seen to reach a roughly constant, maximum value with the first scan containing more than one laser shot, at 2874 ms. These experiments clearly show that photodetachment of $C_6F_6^-$ at 193 nm is efficient.

Experiments which attempted to observe cations produced in charge-reversed multiphoton ionization were less successful. Initial attempts to observe CRMPI were met with observation of a very large cation signal at m/z 186, as expected for the CRMPI process. However, control experiments in which the anion-generating electron beam was turned off gave the same large signal, hinting that the results were due not to CRMPI but to non-resonant multiphoton ionization (MPI) of background neutral C_6F_6. Several approaches were attempted to eliminate the MPI and distinguish CRMPI from it. The first involved labeling the anions before the laser shot. This was accomplished by application of RF to the ICR cell to eject $^{12}C_6F_6^-$, thereby increasing the relative population of naturally abundant $^{13}C^{12}C_6F_6^-$. The enhanced abundance of $^{13}C^{12}C_6F_6^-$ is shown in the mass spectrum of Figure 3a, where the intensity of m/z 187 is about 60% that of m/z 186,

Figure 3. (a) Enhancement of signal from naturally abundant $^{13}C^{12}C_5F_6^-$ (m/z 187) achieved by resonant ejection of the $^{12}C_6F_6^-$ peak at m/z 186. The natural ratio of m/z 187:186 is 6.6%. (b) Spectrum obtained under CRMPI conditions using the anion population of Figure 3, which was isotopically labeled by 10-fold enrichment of the $^{13}C^{12}C_5F_6^-$ peak at m/z 187. No enrichment at m/z 187 is observed for these cations, indicating that they are due to MPI of background neutral C_6F_6 rather than CRMPI.

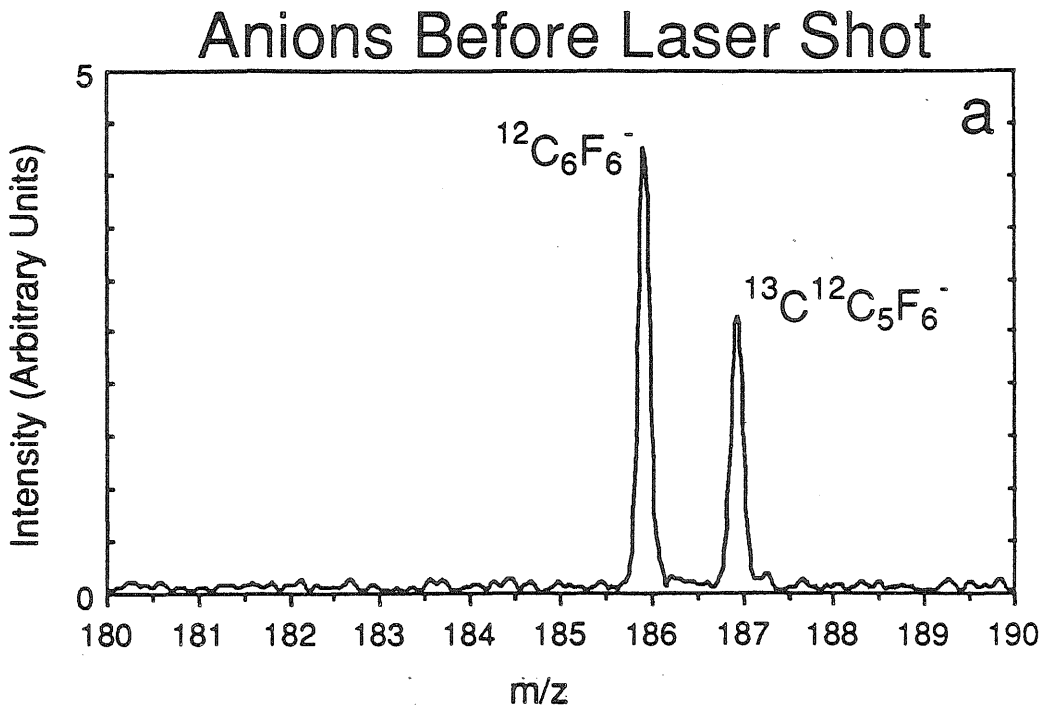
Anions Before Laser Shot
5
0
a
$^{12}C_6F_6^-$
$^{13}C^{12}C_5F_6^-$
Intensity (Arbitrary Units)
180 181 182 183 184 185 186 187 188 189 190
m/z

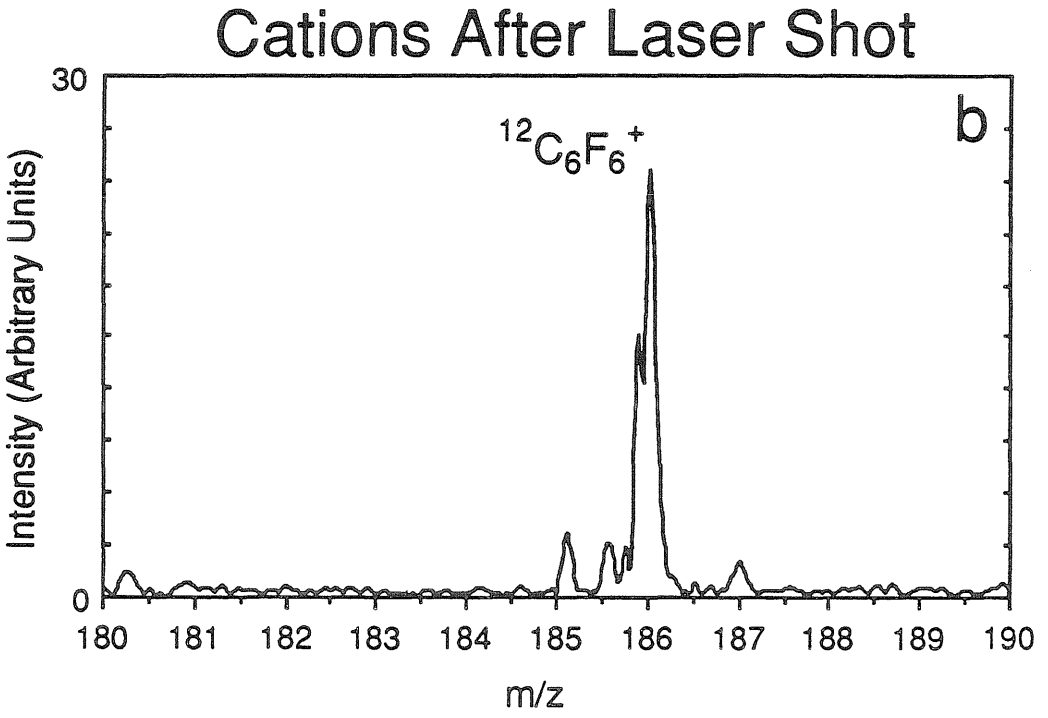
Cations After Laser Shot
30
0
b
$^{12}C_6F_6^+$
Intensity (Arbitrary Units)
180 181 182 183 184 185 186 187 188 189 190
m/z

rather than the naturally occurring 6.6%. Attempts to observe an enhanced 187:186 m/z ratio in the cations produced by the laser shot were always met with failure. Figure 3b is such a spectrum, obtained from the m/z-187-enhanced population of anions shown in Figure 3a.

A second method was to decrease the number density of neutrals during the laser shot by introducing C_6F_6 with a pulsed gas valve. Anions were created during the high-pressure period while the valve was open, after which a delay of 2-4 s was used to pump away the neutrals before firing the laser. While this approach did result in smaller MPI signal, control experiments showed that it was not eliminated. A final, novel method involved application of the ion excitation RF to the anions *before* the laser pulse. The objective was to carry out CRMPI on coherently excited anions, then attempt to detect coherently excited cations after the laser shot without applying any additional excitation. No signal was observed using this method, indicating either that CRMPI is not occurring in this system, or that the coherent excitation does not survive the laser shot and inversion of the trapping potential.

It is possible that $C_6F_6^+$ produced by CRMPI absorbs additional photons and dissociates. Some evidence for photofragmentation of perfluorobenzene cation by single and multiple losses of F was seen, but this possibility was not carefully investigated since most of the experimental work concentrated on the m/z 170-200 region. In particular, the isotopically labeled experiments did not address photofragmentation. Examination of a

wider mass range with isotopically labeled anions might prove fruitful.

The lack of success in observing CRMPI of $C_6F_6^-$ is discouraging, but in retrospect it is not surprising. The very energetic 6.4-eV photons employed easily produce large background signals which are very difficult to eliminate. Two-photon CRMPI, carried out on ions with number densities of 10^6 cm^{-3} or less, cannot compete with two-photon MPI of neutrals whose number densities are at least 3-4 orders of magnitude greater.

To circumvent these problems, resonant CRREMPI experiments with allyl anion were conducted. Use of less energetic visible photons should eliminate the background problems which have plagued the VUV CRMPI studies. At the wavelengths employed, the photon energies of about 2.5 eV/photon are not energetic enough to generate photoelectrons from the cell surfaces, and since the lowest adiabatic IP for the neutral precursors involved is 9.74 eV (for propene),[19] corresponding to at least four 500-nm photons, non-resonant MPI of the neutrals is not expected to compete with 1+2+2 resonant CRREMPI. In addition, since the allyl anions are created by an ion-molecule reaction rather than by electron attachment to a neutral precursor, there is no neutral allyl background. In the absence of photofragmentation of allyltrimethylsilane, the only route to production of m/z-41 cations is CRREMPI. As a result, focusing of the beam to facilitate the multiphoton CRREMPI process should not lead to large background signals.

A few preliminary experiments with allyl anions have been conducted. Maintaining constant anion trapping conditions, irradiation of the cell with one 12-mJ shot from a weakly focused 514.5-nm dye laser results in complete loss of allyl anions. Photodetachment under conditions germane to CRREMPI is therefore efficient. The choice of 514.5 nm for these experiments was made as follows. The published anion photodetachment spectrum[14] indicates that detachment using 488-nm light (from a CW Ar^+ laser operating at 75 W) results in excitation of the C-C-C bending vibration of allyl, the best Franck-Condon overlap being with the v = 3 state.[14] This occurs because the equilibrium C-C-C angle in allyl anion is 16° greater than in allyl radical.[14] If MPI of hot allyl radical results in ground state allyl cation, the vibrational excitation should result in a hot band shifted 1185 cm^{-1} from the 0_0^0 transition, corresponding to a wavelength of 514.5 cm^{-1}. The Franck-Condon overlap between the ground state of allyl radical and that of allyl cation appears qualitatively to be good, since in the MPI spectra the 0^0_0 band has the greatest intensity. No signal was observed at m/z 41 in CRREMPI experiments at 514.5 nm with 12-mJ laser pulses, although signals at masses 56, 75, 107, 109, and 610 were seen (Figure 4). The first of these peaks likely corresponds to Fe^+, and the peaks at m/z 107 and 109 may be from the two major isotopes of Ag^+. Both of these ions could be produced by laser vaporization of metals in the screen covering the opening to the ICR cell.

Figure 4. Mass spectrum of cations produced in the ICR cell in the allyl CRREMPI experiment. Peaks at m/z 56, 107, and 109 probably correspond to Fe^+ and the two isotopes of Ag^+. The peak at m/z 610 is unidentified.

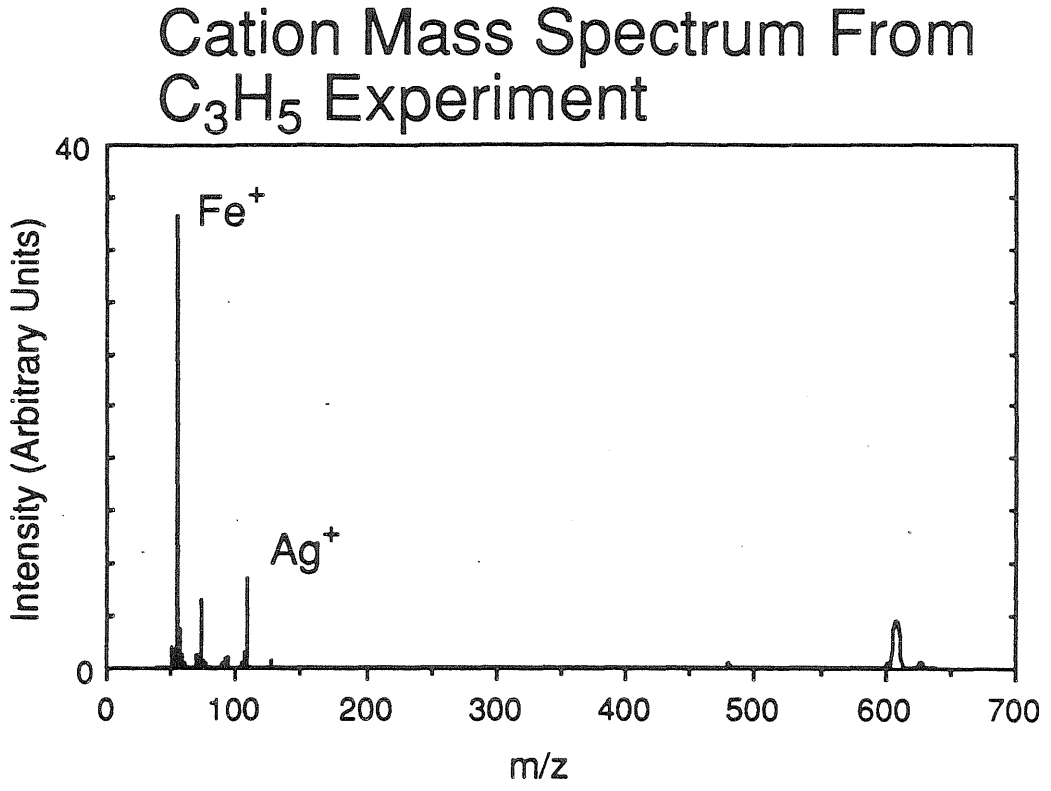
Cation Mass Spectrum From
C_3H_5 Experiment
40
0
Intensity (Arbitrary Units)
Fe^+
Ag^+
0
100
200
300
400
500
600
700
m/z

The peak at m/z 75 is likely a photoionized fragment of allyltrimethylsilane, corresponding to loss of 39 amu from the molecular ion. The identity of the high mass peak is unknown.

Prognosis

Failure to observe CRREMPI signal at m/z 41 should not be taken as conclusive or discouraging. One obvious further experiment is to vary the wavelength used, since the choice of 514.5 nm may not be optimal. No attempt was made in the above experiments to optimize the position of the focal point within the cell, and this is likely a crucial factor. Removal of the front screen and careful masking of the laser window should help to eliminate the background peaks. Since signal intensity is expected to vary with the square of the laser power, optimization of the dye laser to obtain the specified 30-mJ power level is highly desirable, since that would lead to a more than four-fold increase in the expected signal intensity. Also, use of pulsed valves to introduce samples into the cell could decrease potential interferences and increase the signal/noise ratio.

If no signal is observed from allyl, benzyl radical is another good test case for CRREMPI experiments. The MPI spectrum of benzyl radical has been observed,[20] as has the photodetachment spectrum of benzyl anion.[21] The exact nature of the resonance in the MPI spectrum is not known, but the maximum intensity occurs at 502.5 nm, near the maximum of the Coumarin 500 gain curve. The electron affinity of benzyl radical has been

determined from the photodetachment studies[21c] to be 0.86 eV, again easily less than the single photon energy. Benzyl anion can be produced by the reaction of F^- with benzyltrimethylsilane[21c] (which is commercially available) in a manner analogous to that discussed above for allyl anion.

Acknowledgement. We thank the National Science Foundation for supporting this research through grant number CHE87-11567 (JLB), especially for funds which enabled the purchase of the excimer and dye lasers. We are also grateful to the Shell Foundation for graduate fellowship funding (DVD), and to the donors of the Petroleum Research Fund, administered by the American Chemical Society, for additional support.

References and Notes

1. (a) Rosker, M. J.; Dantus, M.; Zewail, A. H. *Science* **1988**, *241*, 1200-1202. (b) Rosker, M. J.; Dantus, M.; Zewail, A. H. *J. Chem. Phys.* **1988**, *89*, 6113-6127. (c) Dantus, M.; Rosker, M. J.; Zewail, A. H. *J. Chem. Phys.* **1988**, *89*, 6128-6140. (d) Bernstein, R. B.; Zewail, A. H. *J. Chem. Phys.* **1989**, *90*, 829-842.

2. Kruppa, G. K.; Beauchamp, J. L. *Acct. Chem. Res.*, manuscript in preparation.

3. Dearden, D. V.; Beauchamp, J. L. *J. Phys. Chem.* **1985**, *89*, 5359-5365.

4. Lehman, T. A.; Bursey, M. M. *Ion Cyclotron Resonance Spectrometry*; Wiley-Interscience: New York, 1976.

5. For a review of anion photodetachment studies using ICR, see: Drzaic, P. S.; Marks, J.; Brauman, J. I. In *Gas Phase Ion Chemistry*; Bowers, M. T., Ed.; Academic: Orlando, FL, 1984; Ch. 21.

6. For a compilation of electron affinities, see: Christodoulides, A. A.; McCorkle, D. L.; Christophorou, L. G. "Electron Affinities of Atoms, Molecules, and Radicals" In *Electron Molecule Interactions and Their Applications*; Academic: New York, 1984; Vol. 2, Chapter 6.

7. For a survey of ion-molecule chemistry, see, for example, papers collected in: *Ion-Molecule Reactions, Part I: Kinetics and Dynamics*; Franklin, J. L., Ed.; Dowden, Hutchinson, & Ross: Stroudsburg, PA, 1979; and *Ibid., Part II: Elevated Pressures and Long Reaction Times*; Franklin, J. L., Ed.; Dowden, Hutchinson, & Ross: Stroudsburg, PA, 1979.

8. Friedrich, D. M. *J. Chem. Educ.* **1982**, *59*, 472-481.

9. Chowdhury, S.; Nicol, G.; Kebarle, P. *Chem. Phys. Lett.* **1986**, *127*, 130-132.

10. Frueholz, R. P.; Flicker, W. M.; Mosher, O. A.; Kuppermann, A. *J. Chem. Phys.* **1979**, *70*, 3057-3070.

11. (a) 9.91 eV from Rydberg analysis of UV spectrum: Philis, J.; Bolovinos, A.; Andritsopoulos, G.; Pantos, E.; Tsekeris, P. *J. Phys. B* **1981**, *14*, 3621-3635. (b) 9.90 eV from photoelectron spectroscopy: Streets, D.

G.; Caesar, G. P. *Mol. Phys.* **1973**, *26*, 1037-1052. Clark, I. D.; Frost, D. C. *J. Am. Chem. Soc.* **1967**, *89*, 244-247. Narayan, B.; Murrell, J. N. *Mol. Phys.* **1970**, *19*, 169-176.

12. (a) Hudgens, J. W.; Dulcey, C. S. *J. Phys. Chem.* **1985**, *89*, 1505-1509. (b) Sappey, A. D.; Weisshaar, J. C. *J. Phys. Chem.* **1987**, *91*, 3731-3736.

13. Zimmerman, A. H.; Brauman, J. I. *J. Am. Chem. Soc.* **1977**, *99*, 3565-3568.

14. Oakes, J. M.; Ellison, G. B. *J. Am. Chem. Soc.* **1984**, *106*, 7734-7741.

15. Wight, C. A.; Beauchamp, J. L. *J. Phys. Chem.* **1984**, *88*, 4426.

16. For details of the circuit, see: Dearden, D. V. Lab notebook, Vol. II, p. 248.

17. Specifications from Lumonics.

18. Coumarin 500, also known as Coumarin 307, has a tuning range of 479-553 nm with peak efficiency of 16.3% at 500 nm. It is available from Exciton Corp. for $35/gram. For each fill, 500 ml of 3.4 g/l solution in methanol must be prepared. The solution has a lifetime under XeCl pumping of 48 Wh. Efficiency and lifetime data are from the Lambda-Physik FL 3001/2 Dye Laser Manual.

19. Kimura, K.; Katsumata, S.; Achiba, Y.; Yamazaki, T.; Iwata, S. *Handbook of Hel Photoelectron Spectra of Fundamental Organic Molecules*; Japan Scientific Societies: Tokyo, 1981.

20. Hoffbauer, M. A.; Hudgens, J. W. *J. Phys. Chem.* **1985**, *89*, 5152-5154.

21. (a) Richardson, J. H.; Stephenson, L. M.; Brauman, J. I. *J. Chem. Phys.* **1975**, *63*, 74-76. (b) Meyer, F. K.; Jasinski, J. M.; Rosenfeld, R. N.; Brauman, J. I. *J. Am. Chem. Soc.* **1982**, *104*, 663-7 (IR multiphoton photodetachment). (c) Drzaic, P. S.; Brauman, J. I. *J. Phys. Chem.* **1984**, *88*, 5285-5290.

CHAPTER 6

IONIZATION ENERGETICS AND UNIMOLECULAR ISOMERIZATION AND DECOMPOSITION PATHWAYS OF GAS-PHASE PENTYL, HEXYL, AND HEPTYL RADICALS BY PHOTOELECTRON SPECTROSCOPY

Reprinted from The Journal of Physical Chemistry, 1985, 89, 5359.

Ionization Energetics and Unimolecular Isomerization and Decomposition Pathways of Gas-Phase Pentyl, Hexyl, and Heptyl Radicals by Photoelectron Spectroscopy

David V. Dearden and J. L. Beauchamp*

Arthur Amos Noyes Laboratory of Chemical Physics,† California Institute of Technology, Pasadena, California 91125 *(Received: May 20, 1985)*

1-Butyl, 1-pentyl, 2-pentyl, 1-hexyl, and 1-heptyl radicals were produced by flash vacuum pyrolysis of the appropriate nitrites and studied via photoelectron spectroscopy. Bands assigned to *sec*-alkyl radicals were observed in the photoelectron spectra of 1-pentyl and larger 1-alkyl radicals but not in the 1-butyl spectrum. Within experimental error, the *sec*-alkyl band in the 1-pentyl radical spectrum appeared at the same ionization potential as the first band in the spectrum of the directly produced 2-pentyl radical. Bands due to propylene, resulting from the β C–C cleavage of 2-alkyl radicals, were also seen in the spectra recorded for 1-pentyl and larger 1-alkyl radicals but not in the 1-butyl spectrum. The 2-alkyl radical band intensities decreased with increasing pyrolysis temperature. Ethylene and methyl radical bands were observed at high pyrolysis temperatures in all of the 1-alkyl spectra. The results are consistent with a mechanism involving isomerization via facile intramolecular H shift to produce *sec*-alkyl radicals, as well as decomposition of all radicals by β C–C cleavage. Radical adiabatic and vertical ionization potentials respectively were determined (eV): 1-pentyl, 8.13 ± 0.10, 8.50 ± 0.03; 1-hexyl, 8.10 ± 0.03, 8.49 ± 0.04; 1-heptyl, 8.10 ± 0.04, 8.50 ± 0.03; 2-pentyl, 7.22 ± 0.10, 7.51 ± 0.15; *sec*-hexyl, 7.17 ± 0.07, 7.38 ± 0.07; *sec*-heptyl, 7.17 ± 0.05, 7.41 ± 0.04. The values for the *sec*-hexyl and *sec*-heptyl ions likely correspond to several isomers which are not distinguished in the spectra.

Introduction

The reactions of large, unbranched alkyl radicals can be surprisingly complex. This is especially true for radicals with chain lengths of five carbons or more since these species are susceptible to isomerization by facile intramolecular hydrogen atom shifts.[1] Early studies of alkyl radical reactions were hampered by the lack of efficient analytical methods for hydrocarbons, but with the advent of gas chromatography it became possible to investigate the mechanisms of hydrocarbon radical reactions by observing reaction products. Coupled with isotopic labeling techniques, the product analysis studies made it possible to infer a number of mechanistic pathways for the thermal reactions of alkyl radicals in the gas phase. Radical systems are particularly amenable to analysis by the RRKM method,[2] and as a consequence a number of experiments have been carried out from which activation energies and preexponential factors have been deduced.[3-13] In general, these experiments involved the generation of radicals in a gas bulb via thermolysis or photolysis, after which the products were trapped, separated, and measured by gas chromatography. The chemistry of such systems is inherently complex. In addition to unimolecular bond cleavage and isomerization by intramolecular hydrogen abstraction, bimolecular hydrogen abstraction and radical recombination reactions also occur, leading to complicated kinetic analysis and uncertainties in the deduced activation parameters. For instance, abnormally low preexponential factors were reported[4,11] for reaction 1. Later it was realized that the

$$n\text{-}C_5H_{11} \rightarrow sec\text{-}C_5H_{11} \qquad (1)$$

n-pentyl radical decomposes to the methyl radical and propylene in addition to undergoing reaction 1, and inclusion of these channels in the data analysis resulted in an upward revision of the preexponential factors for isomerization.[14] Nevertheless, the revisions remain in dispute.[15,16] Studies dealing with the isomerization and decomposition reactions of alkyl radicals can be found in several reviews.[17]

Recent studies have demonstrated that photoelectron spectroscopy (PES) represents a viable experimental method for studying gas-phase free radicals.[18] In contrast to the methods involving product analysis, PES can be employed to observe transient species directly. This and other advantages of PES in studying free radical systems have been discussed.[18-20] Fortunately, bands due to ionization of unpaired electrons from radicals generally lie at lower ionization potentials than complicating bands from stable species. Since the geometries of the radical and the resulting cation are reflected in photoelectron band shapes, it is often possible to distinguish between isomeric structures. In addition, the use of low-pressure, fast-flow conditions minimizes the complexity of the reaction system by disfavoring processes which are not unimolecular. Systems studied by PES in this laboratory include allyl and benzyl radicals;[19] methyl, ethyl, isopropyl, and *tert*-butyl radicals;[21] cyclopentyl and cyclohexyl radicals;[22] products of gas–surface reactions over Bi_2O_3;[23] 1-propyl,

† Contribution No. 7181.

(1) Kossiakoff, A.; Rice, F. O. *J. Am. Chem. Soc.* **1943**, *65*, 590–595.
(2) Marcus, R. A.; Rice, O. K. *J. Phys. Colloid Chem.* **1951**, *55*, 894. Marcus, R. A. *J. Chem. Phys.* **1952**, *20*, 359.
(3) Pearson, M. J.; Rabinovitch, B. S. *J. Chem. Phys.* **1965**, *42*, 1624–1635.
(4) Endrenyi, L.; Le Roy, D. J. *J. Phys. Chem.* **1966**, *70*, 4081–4084.
(5) Larson, C. W.; Tardy, D. C.; Rabinovitch, B. S. *J. Chem. Phys.* **1968**, *49*, 299–312.
(6) Larson, C. W.; Rabinovitch, B. S. *J. Chem. Phys.* **1969**, *51*, 2293–2308.
(7) Watkins, K. W.; Ostreko, L. A. *J. Phys. Chem.* **1969**, *73*, 2080–2083.
(8) Frey, H. M.; Walsh, R. *Chem. Rev.* **1969**, *69*, 103–124.
(9) Hardwidge, E. A.; Larson, C. W.; Rabinovitch, B. S. *J. Am. Chem. Soc.* **1970**, *92*, 3278–3283.
(10) Watkins, K. W.; Lawson, D. R. *J. Phys. Chem.* **1971**, *75*, 1632–1640.
(11) Watkins, K. W. *J. Am. Chem. Soc.* **1971**, *93*, 6355–6359.
(12) Watkins, K. W. *J. Phys. Chem.* **1973**, *77*, 2938–2941.
(13) Gordon, A. S.; Tardy, D. C.; Ireton, R. *J. Phys. Chem.* **1976**, *80*, 1400–1404.
(14) Watkins, K. W. *Can. J. Chem.* **1972**, *50*, 3738–3740.
(15) Mintz, K. J.; Le Roy, D. J. *Can. J. Chem.* **1973**, *51*, 3534–3538.
(16) Le Roy, R. J. *Phys. Chem.* **1980**, *84*, 3508–3516.
(17) (a) Stepukhovich, A. D.; Babayan, V. I. *Russ. Chem. Rev.* **1972**, *41*, 750-758. (b) Pryor, W. A. "Free Radicals"; McGraw-Hill: New York, 1966; Chapter 17. (c) Kochi, J. K., Ed. "Free Radicals"; Wiley-Interscience: New York, 1973; Vol. 1. (d) Beckwith, A. L. J.; Ingold, K. U. In "Rearrangements in Ground and Excited States", de Mayo, P., Ed.; Academic Press: New York, 1980; Vol. 1, pp 162–310. (e) Nonhebel, D. C.; Walton, J. C. "Free Radical Chemistry"; Cambridge University Press: Cambridge, 1974; Chapter 13.
(18) (a) Schultz, J. C. Ph.D. Thesis, California Institute of Technology, Pasadena, CA, 1984. (b) Dyke, J. M.; Jonathan, N.; Morris, A. *Int. Rev. Phys. Chem.* **1982**, *2*, 3. (c) Bock, H.; Solouki, B. *Angew. Chem., Int. Ed. Engl.* **1981**, *20*, 427–444. (d) Dyke, J.; Jonathan, N.; Morris, A. *J. Electron Spectrosc.* **1979**, *15*, 45. (e) Berkowitz, J. In "Electron Spectroscopy: Theory, Techniques, and Applications", Brundle, C. R., Baker, A. D., Eds.; Academic Press: New York, 1977; Vol. 1, p 355. (f) Dyke, J. M.; Jonathan, N.; Morris, A. In "Electron Spectroscopy: Theory, Techniques and Applications", Brundle, C. R., Baker, A. D., Eds.; Academic Press: New York, 1977; Vol. 3 p 189.
(19) Houle, F. A.; Beauchamp, J. L. *J. Am. Chem. Soc.* **1978**, *100*, 3290–3294.
(20) Schultz, J. C.; Houle, F. A.; Beauchamp, J. L. *J. Am. Chem. Soc.* **1984**, *106*, 3917–3927.
(21) Houle, F. A.; Beauchamp, J. L. *J. Am. Chem. Soc.* **1979**, *101*, 4067–4074.
(22) Houle, F. A.; Beauchamp, J. L. *J. Phys. Chem.* **1981**, *85*, 3456–3461.
(23) Schultz, J. C.; Beauchamp, J. L. *J. Phys. Chem.* **1983**, *87*, 3587–3589.

0022-3654/85/2089-5359$01.50/0

1- and 2-butyl, isobutyl, and neopentyl radicals;[20] the various C_4H_7 radical isomers;[24] and 1- and 2-adamantyl radicals.[25] Related work on alkyl radicals has been performed elsewhere.[26]

The present work extends our PES studies of hydrocarbon radicals to include larger *n*-alkyl radicals and their isomerization and decomposition products. The objectives of this work were to identify the nascent products of the flash-vacuum pyrolysis of large *n*-alkyl nitrites by direct observation of their photoelectron spectra, to clarify the mechanistic pathways for their isomerization and decomposition, and to gain information on the ionization energetics of these species.

Experimental Section

Radicals were prepared by flash vacuum pyrolysis of *n*-alkyl nitrites produced as follows. Aqueous H_2SO_4 was added dropwise to a mixture of aqueous $NaNO_2$ (Baker) and the appropriate alcohol (1-pentanol, Baker; 2-methyl-1-pentanol, Alfa; 1-hexanol and 1-heptanol, Aldrich; 1-octanol, MCB) which was maintained at 0 °C throughout the addition. The resulting yellowish organic layer was then separated and dried over $MgSO_4$. The nitrites were checked for purity by NMR and found to contain negligible amounts of alcohol. The nitrites were used without further purification other than several freeze–pump–thaw cycles each time they were introduced on the instrument. The synthetic procedures have been described in detail.[27]

The nitrites were introduced into the spectrometer by means of an inlet equipped with a pyrolyzer. The pyrolyzer consisted of a quartz tube wrapped for the last 2.2 cm of its length with a resistive heating element and was situated on the inlet line inside the spectrometer approximately 1 cm upstream from the point where the photon beam intersects the inflowing sample. Pyrolysis temperatures were monitored by a thermocouple sandwiched between the heating coils and the quartz tube. The effective temperature of the product gases is probably 100–200 °C less than the measured temperature due to short (approximately 1 ms) contact times. Sample pressures in the pyrolyzer were approximately 10^{-3} torr. With this configuration, the transit time between the pyrolyzer and the photon beam is approximately 1 ms. The spectrometer and pyrolyzer have been described.[19] The spectrometer is of standard design, employing a 127° electrostatic sector for electron energy analysis. The light source was a rare gas resonance lamp. Most spectra were taken with He I radiation, but several were also obtained with Ne I in order to distinguish features due to He I β light. Spectra were recorded on a Tracor Northern NS-570A digital signal analyzer. Ar and CH_3I, as well as the NO and formaldehyde which are pyrolysis products of the nitrites, were used for calibration. Typical resolution was 35–45 meV, while the average count rate was approximately 20 counts/s for primary radicals and approximately 5 counts/s for secondary radicals. The reported vertical and adiabatic ionization potentials are the means of several determinations, with the indicated standard deviations. Decomposition products were identified from published spectra.[28]

Relative concentrations of species in the ionization region were estimated by comparison of band intensities (the first band in the case of the radical species). Such estimates should be valid when the bands are known to arise uniquely from the species under consideration, when the photoionization cross sections for the species and the specific ionic state being compared are similar, and when the transmission efficiency of the analyzer for electrons of different energies is accounted for.[18c] The first two conditions are assumed to be satisfied in the present work, while the third is unimportant for such rough estimates as those employed here since all the bands under consideration lie in a narrow energy range. More quantitative concentration determinations are difficult in the absence of an independent technique for calibrating the intensity/concentration correlation.

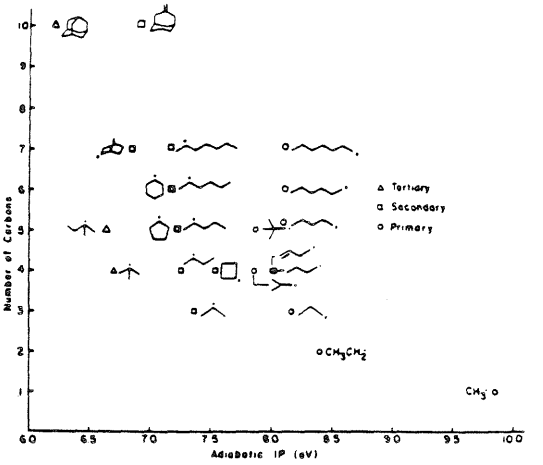

Figure 1. Adiabatic ionization potentials for a number of hydrocarbon radicals plotted against the number of carbon atoms in the radical. Data from ref 19–25.

Results

Nitrites. The photoelectron spectra of the nitrites used as radical precursors in this study are qualitatively similar to those of smaller *n*-alkyl nitrites which have been reported elsewhere.[20] Consequently, the spectra are not presented here. The first vertical ionization potentials (IP's) of 1-pentyl, 2-methyl-1-pentyl, 1-hexyl, 1-heptyl, and 1-octyl nitrite are each 10.5 eV.

Assignment of Radical Bands. As Figure 1 indicates, the adiabatic and vertical IP's of several primary and secondary *n*-alkyl radicals have been measured and found to lie within characteristic ranges.[19-26] Bands can therefore be assigned as due to primary or secondary radicals with some confidence. It is also evident from Figure 1 that problems arise in assigning bands to particular primary or secondary *n*-alkyl radicals with chain lengths of four carbon atoms or more. Except in special cases (e.g., when special factors such as constrained geometry lead to extra stabilization or destabilization), all primary alkyl radicals larger than *n*-propyl appear to have adiabatic IP's between 7.75 and 8.10 eV, while the corresponding secondary alkyl radicals have adiabatic IP's between about 7.00 and 7.25 eV. Therefore, although primary or secondary radical bands can be identified as such, with large radicals such as those studied in this work, it is not prudent to assign the bands to particular radicals. In fact, it is likely that the primary radical bands in some of the spectra which follow are due to mixtures of several radical species. Intuition suggests that through-bond and through-space stabilization is likely to increase with increasing cation size, and thus it is tempting to assign the observed adiabatic IP's to the largest radicals likely to be present. Such assignments should be viewed as tentative.

Pyrolysis of 1-Pentyl Nitrite. The He I spectrum of the low-IP region of 1-pentyl nitrite pyrolyzed at 385 °C is shown in Figure 2. No bands are evident in the 7.25–7.50-eV region where secondary radical bands are expected, although a very low-intensity signal begins at about 7.4 eV. This is the region where He I γ bands, resulting from the precursor onset, are expected, although secondary radicals cannot be ruled out. The low-intensity band which has an onset at 8.01 eV and a maximum at about 8.50 eV is assigned to the 1-butyl radical. Well-defined peaks due to NO (a vibrational progression beginning at 9.24 eV) and formaldehyde

(24) Schultz, J. C.; Houle, F. A.; Beauchamp, J. L. *J. Am. Chem. Soc.* **1984**, *106*, 7336–7347.
(25) Kruppa, G. H.; Beauchamp, J. L., manuscript in preparation.
(26) (a) Koenig, T.; Balle, T.; Snell, W. *J. Am. Chem. Soc.* **1975**, *97*, 662. (b) Koenig, T.; Snell, W.; Chang, J. C. *Tetrahedron Lett.* **1976**, *50*, 4569. (c) Koenig, T.; Chang, J. C. *J. Am. Chem. Soc.* **1978**, *100*, 2240. (d) Dyke, J.; Jonathan, N.; Lee, E.; Morris, A. *J. Chem. Soc., Faraday Trans. 2* **1976**, *72*, 1385. (e) Dyke, J.; Jonathan, N.; Lee, E.; Morris, A.; Winter, M. *Phys. Scr.* **1977**, *16*, 197.
(27) Levin, N.; Hartung, W. "Organic Syntheses"; Wiley: New York, 1955; Collect. Vol. III, p 192.
(28) Kimura, K.; Katsumata, S.; Achiba, Y.; Yamazaki, T.; Iwata, S. "Handbook of He I Photoelectron Spectra of Fundamental Organic Molecules"; Halsted Press: New York, 1981; and references cited therein.

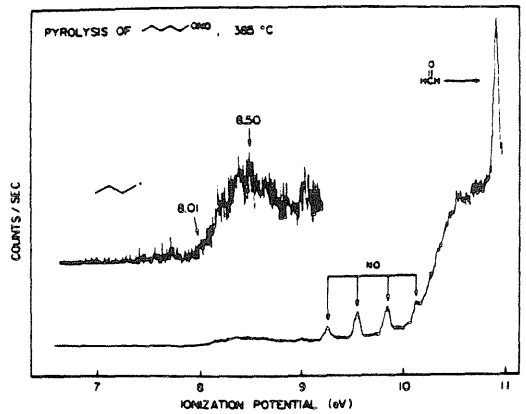

Figure 2. He I photoelectron spectrum of 1-pentyl nitrite pyrolyzed at 385 °C. Note the strong primary radical band and the absence of a corresponding secondary radical band.

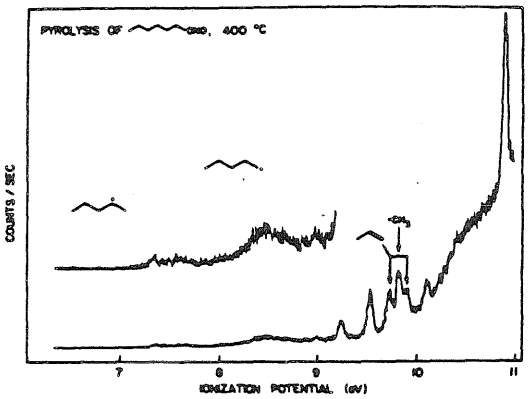

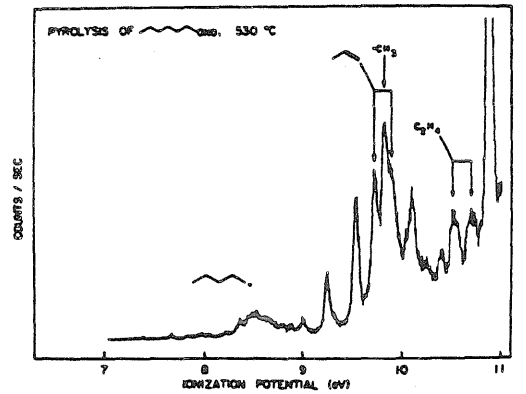

Figure 3. (a, top) He I photoelectron spectrum of 1-hexyl nitrite pyrolyzed at 400 °C. Both the 1-pentyl radical and its isomerization product, the 2-pentyl radical, are evident. (b, bottom) He I photoelectron spectrum of 1-hexyl nitrite pyrolyzed at 530 °C. The 2-pentyl radical band is no longer distinguished from background.

(the sharp peak at 10.88 eV), thermolysis products of the nitrite, are evident.

The Ne I spectrum of 1-pentyl nitrite pyrolyzed at 500 °C has been published[20] and is not reproduced here. Its appearance is very similar to that of the low-temperature pyrolysis spectrum, except that at the higher temperature bands at 10.50 and 10.71 eV, arising from ethylene, are clearly resolved. Some hint of propylene was also noted, but the evidence for the presence of propylene was inconclusive.

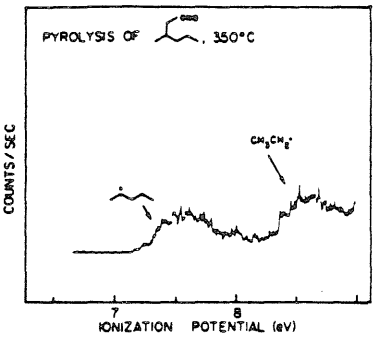

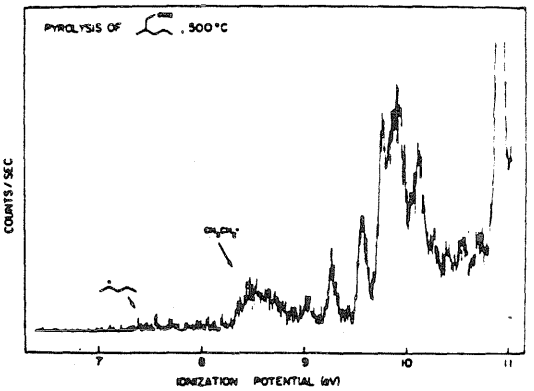

Figure 4. (a, top) He I photoelectron spectrum of 2-methyl-1-pentyl nitrite pyrolyzed at 350 °C. (b, bottom) He I photoelectron spectrum of 2-methyl-1-pentyl nitrite pyrolyzed at 500 °C. The 2-pentyl radical band is much smaller than at lower temperatures, due to extensive decomposition. Note the change of scale.

Pyrolysis of 1-Hexyl Nitrite. The He I spectrum of the low-IP region of 1-hexyl nitrite with a pyrolyzer temperature of 400 °C is shown in Figure 3a. The low-intensity band with an onset at about 7.25 eV is in the region where secondary radicals are to be expected (the 2-butyl radical has adiabatic and vertical IP's of 7.25 and 7.59 eV, respectively[20]) and is assigned to the 2-pentyl radical on that basis as well as on the basis of mechanistic arguments. This band decreases with increasing temperature. Another band begins at about 8.24 ± 0.04 eV and has a maximum at 8.50 ± 0.03 eV. This band grows with increasing temperature and is in the region where primary radical bands are expected; it is probably due to a mixture of *n*-pentyl and smaller primary radicals. The peaks at 9.74 and 9.90 eV are assigned to propylene. In addition, the peak in the NO progression at 9.84 eV is more intense with respect to the other NO peaks than it was in the pentyl nitrite pyrolysis spectrum. This is due to the presence of the methyl radical (IP = 9.84 eV[21]) which has a peak coincident with the NO peak.

Figure 3b shows the He I spectrum of 1-hexyl nitrite pyrolyzed at 530 °C. The secondary radical band has diminished to the extent that it is barely distinguishable from base line noise, while the primary radical band is enhanced relative to that of the 400 °C spectrum. The propylene and methyl bands are also enhanced. In addition, two peaks assigned to ethylene are resolved from the onset of the precursor spectrum and appear at 10.50 and 10.71 eV.

Pyrolysis of 2-Methyl-1-pentyl Nitrite. The 6.5–9.0-eV region of the He I photoelectron spectrum of 2-methyl-1-pentyl nitrite pyrolyzed at 350 °C is shown in Figure 4a. The first band, with an onset at 7.13 eV, is assigned to the 2-pentyl radical, the expected

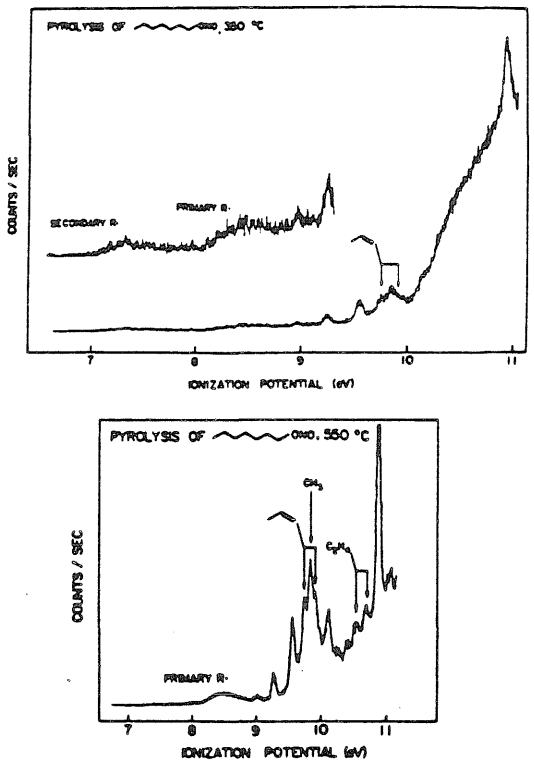

Figure 5. (a, top) He I photoelectron spectrum of 1-heptyl nitrite pyrolyzed at 350 °C. (b, bottom) He I photoelectron spectrum of 1-heptyl nitrite pyrolyzed at 550 °C. Note the change of scale.

pyrolysis product of 2-methyl-1-pentyl nitrite. The shoulder on the low IP side of the band, with a maximum at 7.24 eV, disappears at higher pyrolysis temperatures and may be an instrumental artifact. The band onset at higher temperatures occurs cleanly at 7.22 eV, and this is taken to be the adiabatic IP of the 2-pentyl radical. The structure and measured IP associated with the second band correspond to those determined for the ethyl radical.[21] Peaks on the low IP side of the band at 8.36 and 8.52 eV are consistent with an earlier pyrolysis spectrum of propyl nitrite where the adiabatic and vertical IP's of the ethyl radical were found to be 8.39 and 8.51 eV, respectively.[21] Although not shown in Figure 4a, peaks due to propylene, an expected decomposition product of the 2-pentyl radical, were also clearly evident at 9.74 and 9.90 eV.

The effects of higher pyrolysis temperature are demonstrated in Figure 4b, the He I photoelectron spectrum of 2-methyl-1-pentyl nitrite pyrolyzed at 500 °C. At this temperature, the secondary radical band is barely distinguishable from base line noise, while the intensity of the band assigned to ethyl radical has increased relative to that observed at lower temperatures. The intensities of the propylene peaks are also enhanced. Weak bands at 10.54 and 10.72 eV may be due to ethylene.

Pyrolysis of 1-Heptyl Nitrite. The low IP region of the He I photoelectron spectrum of 1-heptyl nitrite pyrolyzed at 350 °C is shown in Figure 5a. A low-intensity band assigned to secondary radicals has an onset at 7.09 eV and a maximum at 7.35 eV. As expected for low-intensity bands, the onset of this band appears to shift toward higher IP with increasing temperature as the band intensity decreases. For pyrolysis temperatures below 450 °C, the average of the five measurements of the onset of the secondary band was 7.17 ± 0.07 eV, while the band maximum was at 7.38 ± 0.07 eV. This band is attributed to the 2-hexyl radical, but may include contributions from the 3-hexyl radical as well. A band approximately twice as intense begins at about 8.05 eV with a maximum at about 8.50 eV; this is assigned to primary radicals, probably a mixture of *n*-hexyl with smaller decomposition products. Propylene peaks are observed but are not well-resolved.

The He I photoelectron spectrum of 1-heptyl nitrite pyrolyzed at 550 °C is shown in Figure 5b. At this temperature the secondary radical band is no longer distinguishable from noise. The primary radical band is more intense than at lower temperatures. Its onset is at 8.10 ± 0.03 eV, while its maximum occurs at 8.49 ± 0.04 eV. Bands assigned to propylene and ethylene are resolved at 9.73 and 9.90 eV (propylene) and at 10.55 and 10.70 eV (ethylene). These bands grow with increasing pyrolysis temperature. Methyl radicals are also evident in the enhanced intensity of the band at 9.84 eV. Possible deomposition products of 3-hexyl radical include 1-butene and 1-pentene, which have vertical IP's of 9.63 and 9.52 eV, respectively.[29] The 1-butene peak, if present, lies in a congested region, between the NO peak at 9.54 eV and the propylene peak at 9.73 eV. Comparison of Figures 3b and 5b shows that the signal is enhanced in this region of the 1-heptyl nitrite spectrum relative to that in the same region of the 1-hexyl nitrite spectrum where 1-butene is not a likely decomposition product. 1-Butene is therefore indicated, but the difference may be due only to poorer resolution in the 1-heptyl nitrite spectrum. No definite assignment can be made without more highly resolved spectra.

Comparison of the 1-hexyl nitrite and 1-heptyl nitrite spectra (Figures 3b and 5b) also indicates the possible presence of 1-pentene. The adiabatic IP of 1-pentene is 9.52 eV,[29] overlapping the NO peak at 9.54 eV. If 1-pentene is present, the intensity of the 9.54-eV peak should be enhanced. In Figure 3b, where 1-pentene is not expected, the peak at 9.54 eV is 2.11 times more intense than the peak at 9.25 eV. In the 1-heptyl nitrite pyrolysis spectrum, the same ratio is 2.66. The relative enhancement of the 9.54-eV peak is smaller at lower pyrolysis temperatures, but it still appears to be significant.

Pyrolysis of 1-Octyl Nitrite. The radical band region of the Ne I photoelectron spectrum of 1-octyl nitrite pyrolyzed at 350 °C is shown in Figure 6a. A band assigned to secondary radicals has an onset at 7.13 eV and a maximum at 7.39 eV. As the temperature increases, this band diminishes, but the band onset does not change with a discernable pattern. The average onset of this band at temperatures less than 400 °C is 7.17 ± 0.03 eV, and the average maximum is 7.41 ± 0.04 eV. On mechanistic grounds, 2-, 3-, and 4-heptyl radicals may all be contributing to this band. The relative intensity of this secondary band (approximately 50% of the primary radical band) is noteworthy. The onset of a band assigned to primary radicals is obscured by the secondary radical band but is estimated to lie at about 8.10 eV, with a maximum at 8.50 eV. Again, the primary band is probably due to a combination of *n*-heptyl and smaller primary radicals. The spectrum at higher IP is not shown in the figure, but it is qualitatively similar to that of 1-heptyl nitrite shown in Figure 5a: propylene is indicated but not clearly resolved, and no ethylene is detected at this temperature.

The He I photoelectron spectrum of 1-octyl nitrite pyrolyzed at 550 °C comprises Figure 6b. As with the smaller nitrites, at this temperature the secondary radical band has virtually disappeared. The onset of the band assigned to primary radicals is somewhat obscured by a band due to He I β ionization of NO and propylene but is estimated to be 8.04 eV. The band maximum lies at about 8.50 eV. Average values for the onset and maximum of the primary radical band are 8.10 ± 0.04 and 8.50 ± 0.03 eV, respectively. As in the high-temperature pyrolysis spectrum of 1-heptyl nitrite, bands assigned to propylene (9.74 and 9.89 eV) and ethylene (10.52 and 10.66 eV) are evident, as is methyl radical (9.84 eV).

Another similarity to the 1-heptyl high-temperature pyrolysis spectrum is the possibility that 1-butene and 1-pentene are indicated. Comparison of the region near the adiabatic IP of 1-

(29) Masclet, P.; Grosjean, D.; Mouvier, G. *J. Electron. Spectrosc.* 1973, *2*, 225.

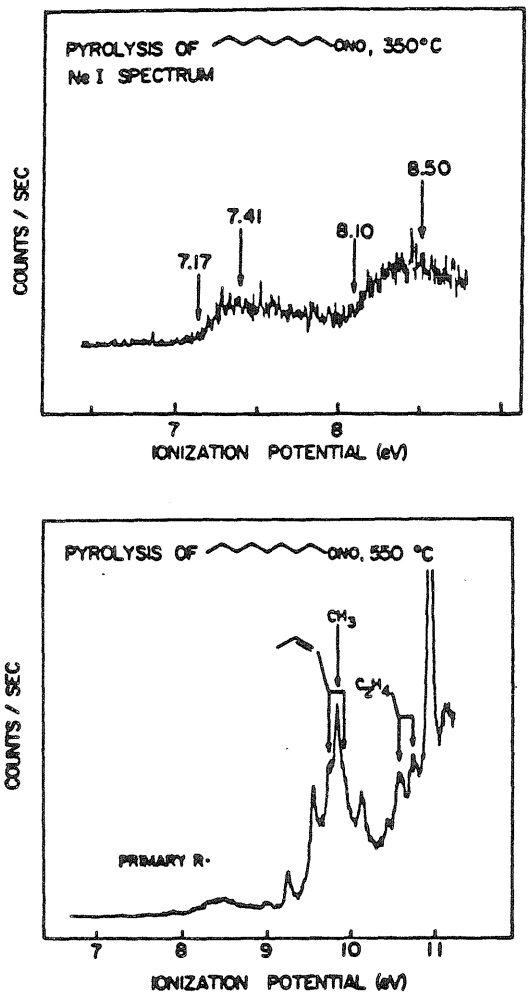

Figure 6. (a, top) Ne I photoelectron spectrum of 1-octyl nitrite pyrolyzed at 350 °C (low IP region). Note the intensity of the *sec*-alkyl radical band relative to the primary alkyl radical band. (b, bottom) He I photoelectron spectrum of 1-octyl nitrite pyrolyzed at 550 °C. Note the change of scale.

butene (at 9.63 eV) in Figures 3b and 6b shows there is considerably more signal in the 1-octyl nitrite spectrum than in the 1-hexyl nitrite spectrum; the latter spectrum returns almost to base line, while the former is approximately 100 counts/s above base line. Once again, it cannot be said definitively that 1-butene is present because the difference may be due to resolution differences in the two spectra. The prognosis for the presence of 1-pentene is also similar to that in the case of 1-heptyl nitrite pyrolysis. In Figure 5b the NO peak at 9.54 eV is 2.71 times as intense as the NO peak at 9.25 eV, while in Figure 3b the intensity of the peak at 9.54 eV is only 2.11 times that of the 9.25-eV peak.

Discussion

The observed isomerization and decomposition products of *n*-pentyl, 2-pentyl, *n*-hexyl, and *n*-heptyl radicals are accounted for by assuming unimolecular conditions and the reactions of Scheme I. A particular advantage of PES in these studies is the considerable simplification afforded by carrying out the experiments under unimolecular conditions. The reactions of Scheme I have been postulated in many earlier studies but were always accompanied by numerous bimolecular processes. In earlier work

SCHEME I

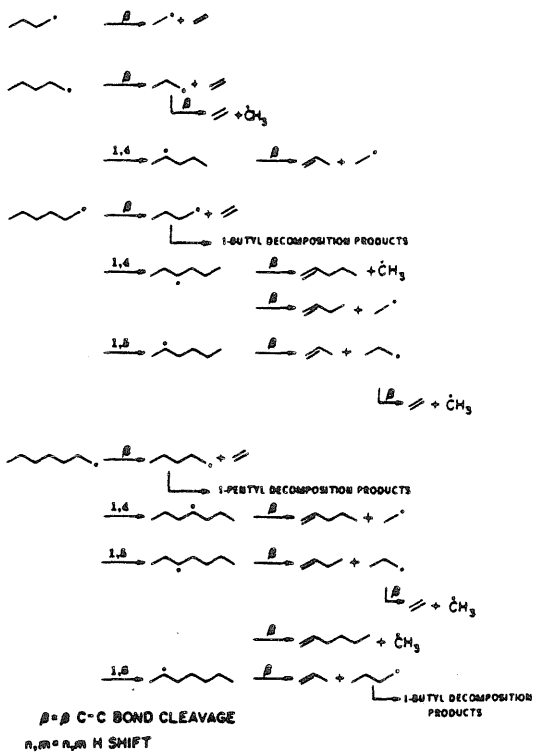

employing gas bulbs and gas chromatographic analysis, schemes involving 20 or more reactions were often necessary to explain the detected products. In the present experiments, simple collision rate calculations indicate that an average molecule undergoes less than one intermolecular collision while traversing the distance from the pyrolyzer to the photon beam. The relative unimportance of bimolecular reactions in this work is also demonstrated by the lack of significant secondary radical bands in the spectra of the 1-butyl and 1-propyl radicals obtained under similar conditions.[20] A more serious complication arises from the possibility of wall reactions; they are unavoidable with a system such as ours where collisions with the hot pyrolyzer wall are necessary to generate the nascent free radicals. Toluene, presumably the result of abstraction of H from organic deposits on the wall, has been observed in conjunction with benzyl radicals produced by pyrolysis of 2-phenylethyl nitrite.[19] Wall reactions have been investigated by the VLPP technique, where the number of wall collisions can be varied in a controlled fashion.[30] Unfortunately, the VLPP results are not directly applicable to the present study; while it is estimated that radicals in the pyrolyzer region of our apparatus undergo at most 15–20 wall collisions, VLPP studies typically involve 200–20 000 wall collisions.[30a] Wall reactions should therefore be much less important than in the VLPP work. Although it is likely that wall reactions play a role in the present experiments, it is not necessary to invoke them to account for the observed products. It will be assumed in the discussion that the unimolecular reactions of Scheme I play a dominant role. The effects of wall reactions deserve further investigation.

Radical Isomerization and Decomposition Reactions. 1,2- and 1,3-H Shifts. It has long been recognized that radical isomerizations occurring through cyclic transition states of five members or more are relatively facile,[1] but 1,2- and 1,3-H shift isomeri-

(30) (a) Golden, D. M.; Spokes, G. N.; Benson, S. W. *Angew. Chem., Int. Ed. Engl.* 1973, *12*, 534–546. (b) Golden, D. M.; Piszkiewicz, L. W.; Perona, M. J.; Beadle, P. C. *J. Am. Chem. Soc.* 1974, *96*, 1645–1653.

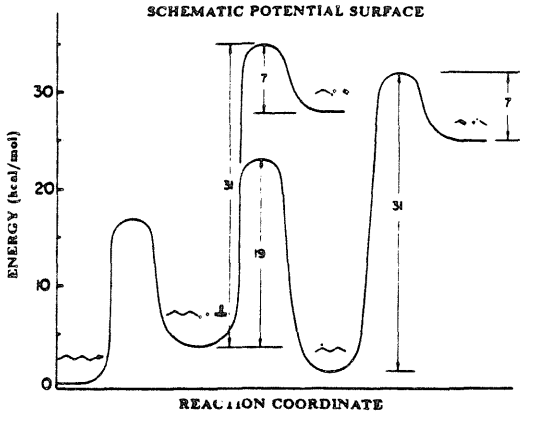

Figure 7. Schematic potential energy surface for reactions of the pentyl radical.[41]

zations of alkyl radicals are more elusive. Intuition suggests that the transition states for such isomerizations might be highly strained, and this is confirmed by GAUSSIAN 70 STO-3G RHF calculations which indicate that a linear C–H–C geometry is preferred in the H migration reactions of alkyl radicals.[31] To approach a linear C–H–C configuration, a highly strained, three- or four-membered cyclic transition state is required, and the strain energy contributes to a high activation barrier for these isomerizations. In a product analysis study of the thermal decomposition of ethane, 1,3-H shift isomerization of the 1-butyl radical to produce the 2-butyl radical, followed by decomposition to the methyl radical and propylene, was postulated as the main source of methane.[32] Later, Tardy explained an enhanced yield of 3-pentyl radical decomposition products relative to 1- and 2-pentyl decomposition products in terms of 1,2- and 1,3-H shift reactions with activation energies of 33 and 31 kcal/mol, respectively.[33] Product ratios observed in the decomposition of 1,1,1-trideuterioethane were also explained in terms of a 1,2-H shift.[13] Finally, in a previous photoelectron spectroscopic study a weak signal, possibly due to 2-butyl radicals, was observed in a spectrum of the 1-butyl radical,[20] but this may have resulted from bimolecular or wall processes.

No 1,2- and 1,3-H shift isomerizations were observed in the present work for several reasons. First, all the primary radicals studied (except 1-butyl) were large enough to isomerize to secondary radicals via transition states of five or more members. Since these processes are much more facile than 1,2- and 1,3-H shifts, secondary radicals produced through the larger transition states are expected to dominate the spectra. Another reason, discussed previously,[20,34] is evident from the energetics of the system (see Figure 7). Since the activation energy for isomerization is comparable to that required for β C–C bond cleavage, radicals with sufficient energy to isomerize also have sufficient energy to decompose, and since the Arrhenius A factors are typically larger for simple bond cleavage than for isomerization through a cyclic transition state, decomposition is expected to predominate over 1,2- or 1,3-H shift isomerization.

H Shifts through Larger Transition States and Decomposition. The literature on this subject is extensive and has been covered in several reviews.[17] H shift reactions of alkyl radicals through four- and five-membered transition states were used to explain product distributions in a number of early studies.[17] By examining product yields as a function of temperature, kinetic parameters for the rearrangements of reactions $1^{4,11}$ and $2^{7,12}$ were determined.

$$n\text{-}C_6H_{13} \rightarrow sec\text{-}C_6H_{13} \qquad (2)$$

The reported A factors for both reactions were low. For reaction 1, for instance, the experimental value was 1.4×10^{7},[4] while the value for log A expected on the basis of transition-state theory was about 10.5.[8] The discrepancy was large enough that some authors were led to suggest that the experimental values were in error.[8,9] A suggestion that the decomposition of *sec*-pentyl radicals to propylene and ethyl radicals is significant in these experiments allowed revision of the experimental A factors to values consistent with the theoretical values,[14] but this suggestion was not universally accepted.[15] Reexamination of reaction 2 also led to a larger A factor which was in accord with the theoretical values.[12] However, theoretical attempts to reproduce the "low" A factors continued.[16]

In the present work, secondary radicals, the immediate products of the isomerization of primary radicals by H transfer through transition states of five or more members, are observed directly by PES. The observed secondary radical bands cannot be accounted for by bimolecular H abstractions from precursor or other molecules since they were not observed for *n*-pentyl and smaller nitrites but are detected for *n*-hexyl nitrite and are comparable in intensity to the primary radical bands seen in the low-temperature pyrolyses of *n*-heptyl and *n*-octyl nitrites. These results are also consistent with those of collisional activation mass spectroscopic work performed under similar pressure conditions.[35] In those studies, primary C_1–C_8 alkyl radicals produced in the fragmentation of the radical cations of amines and ketones were trapped with 7,7,8,8-tetracyanoquinodimethan along with the secondary radicals which result from isomerization. Isomerized products were observed only for C_5 and larger alkyl radicals.

The products of radical decomposition observed in the spectra are also consistent with isomerization by 1,4-, 1,5-, and/or 1,6-H shift. Propylene was observed in the spectra of pyrolyzed 1-hexyl, 1-heptyl, and 1-octyl nitrites, but definite propylene bands were not seen in the spectrum of pyrolyzed 1-pentyl nitrite. Propylene can be produced through the well-known β scission of 2-pentyl, 2-hexyl, or 2-heptyl radicals,[5,17b] but it is not a decomposition product of primary *n*-alkyl radicals which do not have low-energy isomerization pathways to secondary alkyl radicals. In the photoelectron spectra of both propyl and butyl radicals, for instance, no definite propylene bands are evident.[20] Propylene has, however, been observed as a decomposition product of *n*-alkyl radicals which have the unpaired electron localized on the second carbon, such as 2-butyl.[20] The prominence of propylene in the spectra of pentyl, hexyl, and heptyl radicals presented here seems to indicate that isomerization of the radical center to the 2-position is important in each of these cases; i.e., that isomerization through the largest possible cyclic transition state is important in each case. Finally, the observation of propylene also pertains to the question of the A factor for radical isomerization. Its presence indicates that secondary radical decomposition occurs at a rate comparable to that of 1,4-H shift isomerization and that decomposition must be taken into account when determining isomerization rate constants. The larger, theoretically consistent A factors,[14] therefore, gain additional credibility.

The competition between isomerization and decomposition of the radicals is evident when the high- and low-temperature pyrolysis spectra are compared. Particularly interesting is the fact that the secondary radical band disappears at high temperatures while the primary radical band remains. The main reason for the persistance of the primary radical band at high temperatures is that the β scission decomposition processes for both primary and secondary radicals result in fragment primary radicals. This is clearly illustrated in Figure 4, a and b, which are spectra of pyrolyzed 2-methyl-1-pentyl nitrite, the precursor to 2-pentyl radical. Isomerization of the 2-pentyl radical through 1,4-H shift to yield the 1-pentyl radical is thermodynamically unfavorable; the equilibrium constant for isomerization is on the order of 0.01 for the conditions of the present experiment. Hence, isomerization is not expected to be a significant source of primary radicals; the observed primary radical band, which is consistent with spectra

(31) Fossey, J.; Nedelec, J. Y. *Tetrahedron* **1981**, *37*, 2967–2976.
(32) Lin, M. C.; Back, M. H. *Can. J. Chem.* **1966**, *44*, 2369–2380.
(33) Tardy, D. C. *Int. J. Chem. Kinet.* **1974**, *6*, 291–294.
(34) Gordon, A. S.; McNesby, J. R. *J. Chem. Phys.* **1960**, *33*, 1882–1883.
(35) Rudat, M. A.; McEwen, C. N. *J. Am. Chem. Soc.* **1981**, *103*, 4349–4354.

TABLE I: Thermochemical Data[a]

radical	IP_a, eV	$\Delta H_f°(R)$	$\Delta H_f°(R^+)$ this work	$\Delta H_f°(R^+)$ ref 38[b]	$D(R^+-H^-)$[c]
1-C_5H_{11}	8.13	10.9	198	194	268
1-C_6H_{13}	8.10	6.0	193	189	268
1-C_7H_{15}	8.10	1.0	188	183	268
2-C_5H_{11}	7.22	7.4	174	179	244
2-C_6H_{13}	7.17	3.0	168	173	243
2-C_7H_{15}	7.17	−2.0	163	168	243

[a] All values except IP_a's in kcal/mol. [b] Values of ref 38 are estimated. [c] Hydride affinities calculated by using alkane heat of formation values from ref 39 and H electron affinity data from ref 40.

previously obtained for ethyl radical,[21] can only be due to decomposition of the 2-pentyl radical. As was noted above, at high pyrolysis temperatures the 2-pentyl radical band virtually disappears due to rapid β C–C cleavage.

Distinguishing between 1,4-, 1,5-, and 1,6-H shift reactions is a problem in studies of alkyl radical isomerization. Since each of these processes results in a secondary radical with an adiabatic IP in the range 7.00–7.25 eV, the reactions cannot be distinguished on the basis of the resulting secondary radical. As Scheme I shows, however, the secondary radicals produced through the different isomerization processes do have distinct decomposition products, some of which should be distinguishable by PES. In particular, 1-butene and 1-pentene have sharp bands which do not overlap each other, although larger 1-alkenes probably will overlap the first band of 1-pentene. As was noted above, the bands characteristic of 1-butene and 1-pentene lie in a spectral region congested by the presence of NO among the decomposition products of the nitrite precursor. There is some indication of the presence of both 1-butene and 1-pentene in the spectra of 1-heptyl and 1-octyl nitrites pyrolyzed at high temperatures. Both of these alkenes are expected decomposition products of the 3-hexyl radical, the result of a 1,4-H shift from 1-hexyl radical. Likewise, 1,4-H shift isomerization of the 1-heptyl radical results in the 4-heptyl radical, which decomposes by β scission to 1-pentene and ethyl radical, while the 1,5-H shift isomerization product, 3-heptyl radical, decomposes to produce either 1-butene or 1-hexene (which cannot be resolved in the present work from 1-pentene). Although these isomerizations are supported by evidence for the presence of 1-butene and 1-pentene in the spectra, the poor resolution of the alkene bands renders the conclusions tentative.

Thermochemistry. Radical ionization potentials can be combined with data for radical heats of formation to calculate heats of formation for the corresponding carbocations. Previous attempts to measure the IP's of large primary *n*-alkyl radicals by electron impact mass spectrometry were unsuccessful because the onset of *n*-alkyl radical ionization was obscured by the presence of *sec*-alkyl radicals resulting from isomerization.[36,37] In the PES experiment this problem is avoided since the bands arising from primary and secondary alkyl radicals are well-resolved. Although significant amounts of decomposition product primary radicals probably contriute to the primary radical band, as Figure 1 shows, these smaller primary radicals have higher adiabatic IP's than the large primary radicals which are initially formed.

Another potential problem associated with the use of high-temperature pyrolysis for radical production is the possible presence of "hot bands" arising from the ionization of vibrationally excited radicals. If hot bands were present, the reported adiabatic IP's, as well as the derived cation heats of formation, would be low, while the calculated hydride affinities would be high. Hot bands are not likely to be significant in the present work. No evidence for hot bands has been found in the spectra of smaller hydrocarbons studied by the same techniques as those employed here, even though the pyrolysis temperatures used were generally higher than those used in the present work.[19-25] In addition, the IP's obtained in those studies agreed well with IP's measured by independent techniques.

If it is assumed that band onsets correspond to the adiabatic IP's of the nascent large radicals, an assumption which seems justified on the basis of the above arguments and the relatively small change in geometry upon ionization from radical to carbocation,[20] the photoelectron spectroscopic data can be used to calculate carbocation heats of formation. This has been done to produce the data of Table I. The uncertainty in the measured IP's is about 0.05 eV. The values of Lossing for radical heats of formation, estimated from group additivity rules, were used, and Lossing's estimated carbocation heats of formation are also reproduced for comparison.[36] The PES values are all within 5 kcal/mol of those of Lossing. The relative stabilities of the various carbocations are probably best reflected in their hydride affinities, $D(R^+-H^-)$, also calculated in Table I. The values indicate that little or no further stabilization of alkyl carbocations is achieved by increasing the chain length to greater than five carbons. This result contrasts with that observed for smaller alkyl carbocations, where $D(R^+-H^-)$ is a linear function of the logarithm of the number of atoms in R^+.[37]

Acknowledgment. This work was supported by the National Science Foundation under Grant CHE-8407857. D. V. Dearden expresses thanks to the National Science Foundation for support through a graduate fellowship. We are also grateful to ARCO for providing funds to support PES studies of free radicals.

Registry No. 1-C_5H_{11}•, 2672-01-7; 1-C_6H_{13}•, 2679-29-0; 1-C_7H_{15}•, 3356-67-0; 2-C_5H_{11}•, 2492-34-4; 2-C_6H_{13}•, 2493-44-9; 2-C_7H_{15}•, 3474-30-4; 1-$C_5H_{11}^+$, 25453-92-3; 1-$C_6H_{13}^+$, 39749-96-7; 1-$C_7H_{15}^+$, 52187-33-4; 2-$C_5H_{11}^+$, 25453-93-4; 2-$C_6H_{13}^+$, 79097-00-0; 2-$C_7H_{15}^+$, 79096-98-3; 1-pentyl nitrite, 463-04-7; 1-hexyl nitrite, 638-51-7; 2-methyl-1-pentyl nitrite, 98858-44-7; 1-heptyl nitrite, 629-43-6; 1-octyl nitrite, 629-46-9.

(36) Lossing, F. P.; Maccoll, A. *Can. J. Chem.* **1976**, *54*, 990–992.
(37) Lossing, F. P.; Holmes, J. L. *J. Am. Chem. Soc.* **1984**, *106*, 6917–6920.
(38) Maccoll, A. *Org. Mass Spectrom.* **1982**, *17*, 1–9.
(39) Cox, J. D.; Pilcher, G. "Thermochemistry of Organic and Organometallic Compounds"; Academic Press: New York, 1970.
(40) Franklin, J. L.; Dillard, J. G.; Rosenstock, H. M.; Herron, J. T.; Draxl, K.; Field, F. H. *Natl. Stand. Ref. Data Ser., Natl. Bur. Stand.* **1969**, *No. 26*.
(41) Barrier heights estimated from the data in ref 10, 38, and 39 and Batt, L.; McCulloch, R. D.; Milne, R. T. *Int. J. Chem. Kinet., First Symp.* **1975**, 441.